



**University of
Nottingham**

UK | CHINA | MALAYSIA

Department of Chemical and Environmental
Engineering

Investigation into the Improvement of Recycled Polypropylene for Use in Automobile Manufacturing

Yitao Zheng BEng (Hons)

Thesis submitted to the University of Nottingham for the
degree of Doctor of Philosophy

August 2020

Abstract

The increasingly strict legislation on plastic recycling and the public concerns about environmental protection have driven the waste plastics recycling industry and the development of recycled plastics applications. However, recycled plastics are rarely used in high-value-added applications, especially in the automobile industry.

This thesis aimed to investigate the feasibility of utilising recycled plastics for auto parts manufacturing. It started with the background study focused on the use of plastics in automobiles and the status of waste plastic recycling in China. Recycled polypropylene (RPP) was selected as the focused material because it is widely used for the manufacturing of automobiles parts. A literature review of recycled plastics was conducted to understand the degradation mechanism and reinforcing techniques in detail.

The experimental study consists of four sections: 1) Development and characterisation of the RPP/Talc composites for the manufacturing of the armrest box. The prepared formula processed the industrial trial, the products meet all the mechanical requirements of the armrest box, and it can save 35.2% of material cost.

2) Preparation of RPP-based blends for automobile bumper. With the addition of 20 wt% of maleic anhydride grafted linear low-density polyethylene (LLDPE-g-MA), the notched impact strength of the RPP composites improved by 252.6%. And 10 wt% LLDPE-g-MA filled RPP3 meet the mechanical requirements for the middle-end bumper.

3) Process development for the use of recycled short milled carbon fibre (rSMCF) as a filler and investigation of its effects on the mechanical properties of the composite. By adding 5 wt% rSMCF, the tensile modulus and flexural modulus of RPP composites increased by 52.3% and 47.3%, respectively. And the coupling agent maleic anhydride grafted polypropylene (MAPP) significantly improved the interfacial adhesion between rSMCF and PP matrix. At 5 wt% MAPP loading, The tensile strength and flexural strength of 5 wt% RSMCF filled PP composites was increased from 21.8 MPa to 24.3 MPa and 27.2 MPa to 31.7 MPa, respectively. This study shows that only a small amount of rSMCF addition will contribute to significant improvement of polypropylene (PP) based composites in tensile and flexural properties.

4) Evaluating the effects of hollow glass bead (HGB) on weight reduction, mechanical behaviours and flame retardancy. The effects of MAPP on compatilising RPP and fillers were analysed, the interfacial effects were studied by the microscale observation. By addition 10 wt% of HGB, the total weight of VPP and RPP composites have a reduction of around 4%. The reduction of impact properties is the major drawback of HGB. By adding 10 wt% of HGB in RPP3 and RPP4, the un-notched impact strength reduced by 54.1% and 48.5%. The processed cone calorimeter test shows by adding 10 wt% HGB to VPP, the heat release rate decrease from 766.6 kW/m² to 536.6 kW/m². The mechanism of the flame retardancy of HGB was further analysed by scanning electron microscopy, during the burning HGB can form an effective protection layer floating on the melted plastics to suppress the flame and thus improve the flame retardancy of PP composites.

This study found that it is possible to partially replace virgin polypropylene (VPP) with RPP in some specific automobile applications.

The novelty of this research is the utilisation of well-developed techniques (filler addition, polymer blending) to develop recycled composite to meet the requirement from manufacturers and evaluate its performance in real automobile parts. It presented a crucial step from the lab-scale study to the large-scale industrial use of recycled plastics in the automobile industry. This study developed a process for manufacturing rSMCF filled PP composites. By only using a small amount (<5 wt%) of rSMCF, the mechanical properties of PP composites significantly improved. The use of recycled carbon fibre (rCF) in recycled plastics provide a cost-effective way for both resource-saving and properties reinforcement. In order to reduce the environmental impact on the automobile industry, HGB was introduced as a lightweight material into the PP matrix for weight reduction. The mechanical and flammability results of HGB filled PP composites were investigated and discussed. The developed process for utilising rCF and HGBs showed the potential of a more sustainable and lower environmental impact pathway for the automobile industry.

This page is intentionally left blank.

Affirmation

I hereby declared that all the work contained in this research is my own work (unless acknowledged otherwise) and has not been previously submitted for any other degree. The following research article has been published based on the research:

- ZHENG, Y., GU, F., REN, Y., HALL, P. & MILES, N. J. 2017. Improving Mechanical Properties of RPP-based Composites Using Taguchi and ANOVA Techniques. *Procedia CIRP*, 61, 287-292.
- GU, F., ZHENG, Y., ZHANG, W., YAO, X., PAN, D., WONG, A. S. M., GUO, J., HALL, P. & SHARMIN, N. 2018. Can bamboo fibres be an alternative to flax fibres as materials for plastic reinforcement? A comparative life cycle study on polypropylene/flax/bamboo laminates. *Industrial Crops and Products*, 121, 372-387.

The following patents have been applied:

- Philip Hall, Yitao ZHENG, Fu Gu (2018) A short recycled carbon fibre/polypropylene composite and its preparation method. Invention Patent (201811539159.5)

This page is intentionally left blank.

Acknowledgements

I would like to thank my supervisors Dr. Philip Hall, Dr. Peter Summers and Prof. Michael George for giving me this opportunity to undertake this PhD research at the University of Nottingham, Ningbo, China.

Many thanks to Dr. Fu GU, without his help and suggestions, much of the work would not be possibly finished. And I am grateful to Dr. Nusrat Sharmin for her advice and recommendations in my research. I also wish to thank Bin Wang for his help on FTIR tests. Further many thanks to Dr. Zheng Wang for his help and care during my study period.

I would also like to thank my colleagues and friends, Julian Zhu, Helen Xu, Karey Shan, Jane ZHANG, Kate YUAN and Jason WANG from the technical service group at the University of Nottingham, Ningbo, China for their continuous support to complete this work.

Finally, I would like to thank my parents for their understanding, and support throughout my study.

This page is intentionally left blank.

Table of contents

Abstract.....	i
Affirmation.....	v
Acknowledgements	vii
Chapter 1 Introduction.....	1
1.1 Introduction	1
1.2 Background	3
1.2.1 The use of plastics in automobiles.....	3
1.2.2 Plastic recycling in China	8
1.2.3 Advantages of using recycled plastics.....	13
1.2.4 Barriers for recycled plastic applications ...	16
1.3 Objectives and aims	18
1.4 Research Strategy	19
Chapter 2 Literature review	21
2.1 Introduction	21
2.2 Overview of recycled plastics in the automobile industry	22
2.3 Degradation of plastics.....	26
2.3.1 Thermal degradation.....	26
2.3.2 Thermo-oxidative degradation.....	29
2.3.3 Photo-oxidative degradation.....	32
2.3.4 Biological degradation	35
2.3.5 Conclusion.....	37
2.4 Modification and improvement	39
2.4.1 Fillers.....	39
2.4.2 Polymer blending.....	50
2.4.3 Compatibilisers and Coupling agents	53
2.4.4 Conclusion.....	55
2.5 Mathematical tools for prediction and optimisation ..	57
2.5.1 Taguchi method.....	58
2.5.2 Principal component analysis (PCA)	63
2.5.3 Conclusion.....	65

2.6	Summary.....	66
2.7	Outlook	69
Chapter 3	Experimental fundamentals	71
3.1	Introduction	71
3.2	Materials.....	72
3.2.1	Plastics	72
3.2.2	Fillers	73
3.2.3	Coupling agent and compabilisers	74
3.2.4	Others	75
3.3	Fabrication of composites.....	75
3.3.1	Plastic characterisation and Talc-filled RPP composites	75
3.3.2	RPP/PE and RPP/Elastomer blended composites	78
3.3.3	Recycled short milled carbon fibre filled PP/RPP composites.	81
3.3.4	Hollow glass beads filled PP/RPP composites	86
3.4	Characterisation methods	89
3.4.1	Tensile properties	89
3.4.2	Flexural properties	90
3.4.3	Impact properties.....	91
3.4.4	Rheological properties.....	92
3.4.5	Thermal properties	93
3.4.6	Flammability properties.....	93
3.4.7	Fourier transform infrared spectroscopy (FTIR) analysis	95
3.4.8	Morphology study.....	95
3.4.9	Outsourced tests:.....	96
3.5	Industrial requirement.....	99
Chapter 4	Plastics characterisation and talc-filled RPP composites	101
4.1	Introduction	101
4.2	Plastic characterisation	104
4.2.1	Materials	104

4.2.2	Characterisation Results	104
4.3	Talc reinforced RPP composites	109
4.3.1	Results and discussions	111
4.3.2	Conclusion	125
4.4	Industrial trial	126
4.4.1	Application selection	126
4.4.2	Products and evaluation	128
4.5	Summary	136
Chapter 5	RPP/PE and RPP/Elastomer blended composites..	139
5.1	Introduction	139
5.2	The effects of elastomer on PP composites.	140
5.2.1	Raw Materials.....	140
5.2.2	Results and discussion	142
5.2.3	Conclusion.....	159
5.3	The effects of elastomer on mineral filler filled	161
5.3.1	Results and discussion	162
5.3.2	Conclusion.....	175
5.4	Summary	176
Chapter 6	Comparison of the recycled short carbon fibre	177
6.1	Introduction	177
6.2	Results and discussions.....	178
6.2.1	Effects of surfactant.....	178
6.2.2	Effects of the fibre content.....	179
6.2.3	Effects of coupling agent	204
6.3	Conclusion.....	216
Chapter 7	Comparison of the hollow glass bead filled virgin	219
7.1	Introduction	219
7.2	Effects of HGBs content.....	220
7.2.1	Density reduction	220
7.2.2	Mechanical properties	222

7.2.3	Morphological studies	240
7.2.4	Conclusions	244
7.3	Flammability tests for VPP/HGB composites.....	245
7.3.1	Cone calorimeter test	246
7.3.2	Morphological study of char residue.....	253
7.3.3	UL94 horizontal burning	255
7.3.4	Thermal properties	256
7.3.5	Conclusion.....	259
7.4	Summary.....	260
Chapter 8	Conclusion and further work.....	263
8.1	Conclusion	263
8.1.1	Plastic characterisation and Talc-filled RPP composites	263
8.1.2	RPP/PE and RPP/Elastomer blended composites	264
8.1.3	Recycled short carbon fibre filled PP/RPP composites.	265
8.1.4	Hollow glass beads filled PP/RPP composites	266
8.2	Further work	267
Reference	271

List of Figures

Figure 1-1 Use of plastics in the automotive sector (PlasticsEurope, 2013)	5
Figure 1-2 Various approaches for recycling of PSW (Singh et al., 2017).....	11
Figure 1-3 Producer price index for virgin plastics and recycled plastics (FRED, 2019)	15
Figure 2-1 Plastic parts in Mercedes-Benz car (Sattler, 2019)	23
Figure 2-2 Used Bumper recycling (Honda, 2020).....	24
Figure 2-3 Decomposition of polymethyl methacrylate (PMMA) (Hu and Chen, 2003).....	27
Figure 2-4 Hydrogen atom abstraction (Billingham, 2002)	27
Figure 2-5 Dehydrochlorination of PVC (Billingham, 2002)	28
Figure 2-6 Three steps of thermo-oxidative degradation (Zeus, 2005).....	30
Figure 2-7 Process for photooxidation in polymers (Polymer Properties Database, n.d.-c).....	34
Figure 2-8 Mechanism of enzymatic catalysed hydrolytic polymer degradation (Rydz et al., 2015)	36
Figure 2-9 Photo of talc minerals and talcum powder (SERIA TRADING, n.d.)	39
Figure 2-10 Carbon fibre recycled from the fluidised bed recycling process for the use of automobile parts (Meng et al., 2017).....	46
Figure 2-11 3M HGB and other fillers (3M, 2013).....	48
Figure 3-1 KRSHJ-20 co-rotating twin-screw extruder ...	76
Figure 3-2 Haitian MA1200/370 injection moulding machine	76
Figure 3-3 Injection moulding machine in Shuanglin group co., LTD	78
Figure 3-4 Process of rSMCF dispersion	83
Figure 3-5 Zhenggong ZG-201 flat vulcanising machine	84
Figure 3-6 Retsch SM2000 cutting mill	84
Figure 3-7 (a) rCFRP sheet before shredding (b) rCFRP	

pellets after shredding	85
Figure 3-8 Photo of the universal test machine	89
Figure 3-9 Photo of a tensile test specimen	90
Figure 3-10 Photo of a flexural test specimen	90
Figure 3-11 Photo of impact test machine	91
Figure 3-12 Photo of notched specimen for impact test.	91
Figure 3-13 Photo of melt flow index tester	92
Figure 3-14 Photo of TG/DTA 6300	93
Figure 3-15 Photo of flame chamber.....	94
Figure 3-16 Photo of UL94 test specimen	94
Figure 3-17 Photo of Fourier transform infrared spectroscope.....	95
Figure 3-18 Photo of scanning electron microscope	96
Figure 4-1 The flow chart of Chapter 3.....	102
Figure 4-2 a) Internal view of the injection moulding machine; b) top view of the manufactured armrest box	103
Figure 4-3 Potential applications of RPP and VPP	107
Figure 4-4 Plot of S/N ratios against the selected components for TM.....	113
Figure 4-5 Plot of S/N ratios against the selected components for TS	113
Figure 4-6 Plot of S/N ratios against the selected components for FM	114
Figure 4-7 Plot of S/N ratios against the selected components for FS	114
Figure 4-8 SEM image of the tensile fracture surface of the specimen with 20 wt%VPP, 10 wt% talc and 2.5 wt% of MAPP.....	115
Figure 4-9 Interaction plots of (a) talc × MAPP, (b) VPP × MAPP, (c) VPP × talc, for TM	116
Figure 4-10 Interaction plots of (a) talc × MAPP, (b) VPP × MAPP, (c) VPP × talc, for TS.....	118
Figure 4-11 Interaction plots of (a) talc × MAPP, (b) VPP × MAPP, (c) VPP × talc, for FM	119
Figure 4-12 Interaction plots of (a) talc × MAPP, (b) VPP × MAPP, (c) VPP × talc, for FS.....	120

Figure 4-13 Plot of S/N ratios against the selected components for PCA scores	122
Figure 4-14 the process for industrial trial	126
Figure 4-15 Injection moulding machine for industrial trial from Shuanglin group co., LTD.....	129
Figure 4-16 Front views of the VPP based armrest box	130
Figure 4-17 Bottom views of the armrest box	130
Figure 4-18 the photo of sample a) before, b) after 700 hours thermal ageing test at 150 °C	132
Figure 4-19 heat resistance test after a) 1hour, b) 3hours, c)9 hours, d) 27 hours	133
Figure 4-20 Low-temperature resistance test after a) 1 hour, b) 3 hours, c) 9 hours, d) 27 hours	134
Figure 5-1 FTIR spectra of VPP, RPP and PET.....	142
Figure 5-2 Correlations of tensile strength with LLDPE, LLDPE-g-MA and SEBS-g-MA loading	145
Figure 5-3 Correlations of elongation at break with LLDPE, LLDPE-g-MA and SEBS-g-MA loading	146
Figure 5-4 Correlations of flexural modulus with LLDPE, LLDPE-g-MA and SEBS-g-MA loading	147
Figure 5-5 Correlations between flexural strength with LLDPE, LLDPE-g-MA and SEBS-g-MA loading	147
Figure 5-6 Correlations between unnotched impact strength with LLDPE, LLDPE-g-MA and SEBS-g-MA loading	149
Figure 5-7 Correlations between notched impact strength with LLDPE, LLDPE-g-MA and SEBS-g-MA loading .	150
Figure 5-8 Correlations between notched impact strength at -30°C with LLDPE, LLDPE-g-MA and SEBS-g-MA loading	151
Figure 5-9 SEM micrograph of the fracture surface of composite with: (a) 100% RPP, (b) 100%VPP.....	152
Figure 5-10 SEM micrograph of the fracture surface of composite with 80%RPP+20%LLDPE.....	153
Figure 5-11 SEM micrograph of the fracture surface of composite with 80%RPP+20%LLDPE-g-MA	154
Figure 5-12 SEM micrograph of the fracture surface of composite with 80%RPP+20%SEBS-g-MA	155

Figure 5-13 SEM micrograph of the fracture surface of composite with 80%RPP+10%LLDPE-g-MA+10%VPP	157
Figure 5-14 SEM micrograph of the fracture surface of composite with 70%RPP+10%LLDPE-g-MA+20%VPP	158
Figure 5-15 SEM micrograph of the fracture surface of composite with 60%RPP+10%LLDPE-g-MA+30%VPP	158
Figure 5-16 SEM micrograph of the fracture surface of composite with 50%RPP+10%LLDPE-g-MA+40%VPP	159
Figure 5-17 The correlation between tensile strength and filler loading.....	163
Figure 5-18 The correlation between elongation at break and filler loading	163
Figure 5-19 The correlation of flexural modulus and filler loading.....	164
Figure 5-20 The correlation of flexural strength and filler loading.....	165
Figure 5-21 The correlation of notched impact strength and filler loading.....	166
Figure 5-22 The correlation of notched impact strength at -30°C and filler loading	167
Figure 5-23 The correlation of unnotched impact strength and filler loading	168
Figure 5-24 The correlation between tensile strength and SEBS-g-MA loading.....	169
Figure 5-25 The correlation between elongation at break and SEBS-g-MA loading.....	169
Figure 5-26 The correlation of flexural modulus and SEBS-g-MA loading	170
Figure 5-27 The correlation of flexural strength and SEBS-g-MA loading	171
Figure 5-28 The correlation of notched impact strength and SEBS-g-MA loading.....	172
Figure 5-29 The correlation of notched impact strength at -30 °C and SEBS-g-MA loading	173
Figure 5-30 The correlation of unnotched impact strength	

and SEBS-g-MA loading	174
Figure 6-1 (a) RCF before shredding and (b) RCF after shredding	178
Figure 6-2 SEM micrographs of the tensile-facture surface of, recorded at (a) SF _{2.5} /PP/rSMCF ₅ at low magnification (b) SF _{2.5} /PP/rSMCF ₅ at high magnification	184
Figure 6-3 SEM micrographs of the tensile-facture surface of, recorded at (c) SF _{2.5} /RPP/rSMCF ₅ at low magnification (d) SF _{2.5} /RPP/rSMCF ₅ at high magnification	186
Figure 6-4 SEM micrographs of the impact-facture surface of (a) SF _{2.5} /PP/rSMCF ₅ at low magnification (b) SF _{2.5} /PP/rSMCF ₅ at high magnification	188
Figure 6-5 SEM micrographs of the impact-facture surface of (a) SF _{2.5} /RPP/rSMCF ₅ at low magnification (b) SF _{2.5} /RPP/rSMCF ₅ at high magnification	190
Figure 6-6 (a) Optical image of SF ₁ /PP/rSMCF ₂ . (b) FTIR spectra of (i) PP (ii) averaged spectra in SF ₁ /PP (iii) averaged SF/PP spectra in SF ₁ /PP/rSMCF ₂ (iv) averaged rSMCF spectra in SF ₁ /PP/rSMCF ₂ (v) SF. (c) Chemical image based on the integrated band area (1067-1123 cm ⁻¹) of SF ₁ /PP/rSMCF ₂ . (d) Integrated band area histogram for the SF _{2.5} /PP/rSMCF ₅ chemical image shown in (c) excluding regions of rSMCF (black line) and SF _{2.5} /PP (yellow line).....	192
Figure 6-7 MFI results (g/10 min under load of 2.16 kg at 230 °C) for increasing surfactant and surfactant/rSMCF concentrations in the RPP/rSMCF composites	194
Figure 6-8 MFI results (g/10 min under load of 2.16 kg at 230°C) for increasing surfactant and surfactant/rSMCF concentrations in the PP/rSMCF composites	194
Figure 6-9 SEM micrographs of the fracture surface (a) SF ₁ /PP/rSMCF ₂ (b) SF _{2.5} /PP/rSMCF ₅	197
Figure 6-10 SEM micrographs of the fracture surface (a) SF ₁ /RPP/rSMCF ₂ (b) SF _{2.5} /RPP/rSMCF ₅	198
Figure 6-11 DSC heating curves of (a) surfactant added PP samples (b) rSMCF reinforced PP samples.....	199
Figure 6-12 DSC heating curves of (a) surfactant added RPP samples (b) rSMCF reinforced RPP samples.....	200

Figure 6-13 FTIR spectra of PP, PE and RPP	203
Figure 6-14 Tensile and flexural modulus of the SF _{2.5} /PP/MAPP/rSMCF ₅ and SF _{2.5} /RPP/MAPP/rSMCF ₅ composites with 0-20 wt% MAPP	208
Figure 6-15 Tensile and flexural strength of the SF _{2.5} /PP/MAPP/rSMCF ₅ and SF _{2.5} /RPP/MAPP/rSMCF ₅ composites with 0-20 wt% MAPP	209
Figure 6-16 SEM micrographs of the pull-out rSMCF on the impact-facture surfaces of SF _{2.5} /PP/MAPP/rSMCF ₅ with (a) 2.5 wt%, (b) 5 wt%	211
Figure 6-17 SEM micrographs of the pull-out rSMCF on the impact-facture surfaces of SF _{2.5} /PP/MAPP/rSMCF ₅ with (a) 10 wt%, and (b) 20 wt% MAPP	212
Figure 6-18 SEM micrographs of the pull-out rSMCF on the impact-facture surfaces of SF _{2.5} /RPP/MAPP/rSMCF ₅ with (a) 2.5 wt%, (b) 5 wt%	214
Figure 6-19 SEM micrographs of the pull-out rSMCF on the impact-facture surfaces of SF _{2.5} /RPP/MAPP/rSMCF ₅ with (a) 10 wt%, and (b) 20 wt% MAPP	215
Figure 7-1 Correlations of tensile modulus of VPP based composites at different iM30K, S60HS, Al(OH) ₃ loading	224
Figure 7-2 Correlations of the tensile strength of VPP based composites at different iM30K, S60HS, Al(OH) ₃ loading	225
Figure 7-3 Correlations of iM30K content of the tensile modulus of RPP3 and RPP4 based composites	227
Figure 7-4 Correlations of iM30K content of the tensile modulus of RPP3 and RPP4 based composites	228
Figure 7-5 Correlations of the flexural modulus of VPP based composites at different iM30K, S60HS, Al(OH) ₃ loading	231
Figure 7-6 Correlations of flexural strength of VPP based composites at different iM30K, S60HS, Al(OH) ₃ loading	232
Figure 7-7 Correlations of iM30K content of the flexural modulus of RPP3 and RPP4 based composites	234
Figure 7-8 Correlations of iM30K content of the strength of RPP3 and RPP4 based composites	235
Figure 7-9 Correlations of un-notched impact strength of	

VPP based composites at different iM30K, S60HS, Al(OH) ₃ loading	237
Figure 7-10 Correlations of iM30K content of the strength of RPP3 and RPP4 based composites	240
Figure 7-11 SEM images of the fracture surface of PP-5S60HS	241
Figure 7-12 SEM images of the fracture surface of (a) PP-2.5S60HS (b) PP-5S60HS (c) PP-10S60HS	242
Figure 7-13 SEM images of the fracture surface of PP-10S60HS+5MAPP	243
Figure 7-14 HRR results of the hollow glass beads and Al(OH) ₃ filled PP composites	246
Figure 7-15 SPR results of (a) S60HS filled PP composites (b) iM30k filled PP composites (c) Al(OH) ₃ filled composites	248
Figure 7-16 Mass curves of the hollow glass beads and Al(OH) ₃ filled PP composites in cone calorimeter test	250
Figure 7-17 THR results of the hollow glass beads and Al(OH) ₃ filled PP composites	251
Figure 7-18 TTI results of the HGBs and Al(OH) ₃ filled PP composites	252
Figure 7-19. SEM images of the char residue of (a) PP-10S60HS (b) PP-10iM30K (c) PP-10Al(OH) ₃	254
Figure 7-20 Relationship between burning velocity and filler loading	255
Figure 7-21 TGA curves of PP/HGB, PP/Al(OH) ₃ composites, containing different wt% filler content	257

List of Tables

Table 1-1 Amount of polymers used in automobile parts (Bechtold, 2006)	4
Table 2-1 Wavelength of UV radiation when polymers have the maximum sensitivity	33
Table 2-2 L9 Orthogonal array example	60
Table 3-1 List of the plastics used in this section	75
Table 3-2 Selected components (VPP, talc and MAPP) and their levels	77
Table 3-3 Designed compositions based upon Taguchi L9 (3 ³) OA.....	77
Table 3-4 RPP/(LLDPE, or LLDPE-g-MA, or SEBS-g-MA) formulations	79
Table 3-5 RPP/LLDPE-g-MA/VPP formulations.....	80
Table 3-6 RPP, Al(OH) ₃ , Talc and SEBS-g-MA blending ratio	81
Table 3-7 Weight fraction of the PP, RSMCF, SF and MAPP blends.....	82
Table 3-8 Weight fraction of the RPP, RCF, SF and MAPP blends (wt%).....	86
Table 3-9 VPP based composite formulation (wt%)	87
Table 3-10 The designed formula for glass bubble filled RPP	88
Table 3-11 Mechanical properties requirements for the automobile parts	99
Table 4-1 List of the plastics used in the experiments ..	104
Table 4-2 Experiment results of the plastic characterisation	105
Table 4-3 The comparison of the mechanical properties of RPP with VPP	105
Table 4-4 Designed compositions based upon Taguchi L9 (3 ³) OA.....	110
Table 4-5 Mechanical results and the corresponding S/N ratio based upon Taguchi L9 (3 ³) OA	112
Table 4-6 Contributions for S/N ratios of tested mechanical properties obtained by ANOVA	121
Table 4-7 PCA scores for the S/N ratios of the RPP/talc	

composites	122
Table 4-8 ANOVA results for PCA scores	123
Table 4-9 Experimental results and S/N ratios of the optimal	124
Table 4-10 The comparison of the shell of air conditioner formula results and industrial requirements	127
Table 4-11 The average price of the raw materials, information obtained during 2018	135
Table 5-1 Mechanical properties requirements for the automobile parts	140
Table 5-2 Properties of Plastic materials used in this study	141
Table 5-3 RPP/LLDPE, RPP/LLDPE-g-MA and RPP/SEBS-g-MA formulations	141
Table 5-4 Results of RPP/LLDPE composites	143
Table 5-5 Results of RPP/LLDPE-g-MA composites.....	144
Table 5-6 Results of RPP/SEBS-g-MA composites	144
Table 5-7 RPP/LLDPE-g-MA/VPP formulations	156
Table 5-8 Results of RPP/LLDPE-g-MA/VPP formulations	156
Table 5-9 RPP, Al(OH) ₃ , Talc and SEBS-g-MA blending ratio	162
Table 6-1 Mechanical results of VPP/RPP with different loading of surfactant	179
Table 6-2 Mechanical results of PP/RPP with different loading of rSMCF	180
Table 6-3 DSC results of PP/SF and SF/PP/rSMCF composites	201
Table 6-4 DSC results of RPP/SF and SF/RPP/rSMCF composites	202
Table 6-5 Mechanical results of RPP based composites with different loading of RCF and MAPP	204
Table 6-6 Mechanical results of RPP based composites with different loading of RCF and MAPP	205
Table 6-7 Mechanical results of 5%rCF filled composites with different MAPP content	207
Table 7-1 Density results of virgin PP, HGB filled and Al(OH) ₃ filled PP composites	220

Table 7-2 Density results of RPP and HGB filled RPP composites	222
Table 7-3 Tensile properties of virgin PP, HGB filled and Al(OH) ₃ filled composites	223
Table 7-4 Tensile properties of HGBs filled RPP composites	226
Table 7-5 Flexural properties of virgin PP, HGB filled and Al(OH) ₃ filled composites	230
Table 7-6 Flexural properties of HGBs filled RPP composites	233
Table 7-7 Impact properties of virgin PP, HGB filled and Al(OH) ₃ filled composites	236
Table 7-8 Unnotched impact strength of HGB filled RPP composites	239
Table 7-9 Temperature at 5% weight loss, the temperature at the maximum degradation rate of PP/HGBs, PP/Al(OH) ₃ composites	258

Abbreviations

ABS	Acrylonitrile butadiene styrene
AEV	Accumulative explained variation
ANOVA	Analysis of variance
ASA	Acrylonitrile styrene acrylate
CCT	Cone calorimeter test
CF	Carbon fibre
CFRP	Carbon fibre reinforced plastics
CNT	Carbon nanotube
DCP	Dicumyl peroxide
DSC	Differential scanning calorimetry
EPDM	Ethylene-propylene-diene monomer
EV	Explained variation
FM	Flexural modulus
FS	Flexural strength
	Fourier transform infrared spectroscopy
FTIR	
GFRP	Glass fibre reinforced plastics
HDPE	High-density polyethylene
HE	High-end
HGB	Hollow glass bead
HRR	Heat release rate
IS	Un-notched impact strength
L/D	Length to diameter ratio
LD	Low-end
LDPE	Low-density polyethylene
LLDPE	Linear low-density polyethylene
LOI	Limiting oxygen index
	Maleic anhydride grafted polyethylene
MAPE	
	Maleic anhydride grafted polypropylene
MAPP	
MDPE	Medium-density polyethylene
ME	Middle-end
MFI	Melt flow index
NIS	Notched impact strength
OA	Orthogonal arrays
OBS	Olefin block copolymer
PA	Polyamide
PC	Principle component
PCA	Principle component analysis
PE	Polyethylene
PET	Polyethylene terephthalate

PHRR	Peak of heat release rate
PI	Polyimide
PLA	Polylactic acid
PMMA	Polymethyl methacrylate
PP	Polypropylene
PUR	Polyurethane
PVC	Polyvinylchloride
rCF	Recycled carbon fibre
RPP	Recycled polypropylene
rSMCF	Recycled short milled carbon fibre
S/N	Signal to noise ratio
SAN	Styrene-acrylonitrile resin
SEBS-g-MA	Maleic anhydride grafted styrene ethylene butylene styrene
SEM	Scanning electron microscope
SF	Surfactant
SPR	Smoke production rate
TGA	Thermogravimetric analysis
TM	Tensile modulus
TPU	Thermoplastic polyurethane
TS	Tensile strength
TTI	Time to ignition
UV	Ultraviolet
VPP	Virgin polypropylene

Chapter 1 Introduction

1.1 Introduction

Today, plastic plays a vital role in the global economy, and it is widely applied in packaging, building, construction, automobile manufacturing, electronics, agriculture and many other applications. In 2017, the world's plastic production was more than 348 million tons, and China is the largest plastic producer which accounts for 29.4% of the world's plastic production (PlasticsEurope, 2018).

The increasing production and consumption of plastics have led to waste plastic management becoming a global challenge. The common waste plastics treatment methods include recycling, energy recovery and landfill. The landfill is regarded as the least desired option due to the long term consequences of environmental protection and resource-saving. In Europe, the council directive 1999/31/EC on the landfill of waste, strict landfill restrictions have been implemented for the reduction of landfilling of waste. This will encourage recycling and recovery of waste and obviate wasteful use of land. From 2006 to 2016, the volumes for recycling in the UK increased by 230% (525 to 1210 kilotons), energy recovery increased by 620% (231 to 1441 kilotons) and landfill decreased by 57% (2590 to 1116 kilotons)(PlasticsEurope, 2018). From 2006 to 2012, the imports of plastic to China increased from 5.9 million tonnes to 8.9 million tonnes (Velis, 2014). In the meantime, the Chinese domestic production of plastic products increased from 28.0 million tons to 57.8 million tons (ChinaIRN, 2018). Because of

the poor waste management systems, the dramatic increase in waste plastics led to severe environmental problems and raised unprecedented public concerns. In 2017, the China state council brought in legislation to strictly control solid waste imported into China. Nonindustrial plastic waste was banned to be imported to China.

The recycling of plastics is a more sustainable waste management option compared to landfill. As a valuable non-renewable resource, utilisation of recycled plastics will not only contribute to environmental protection but also can be economically profitable.

Most of the recycled plastics are used in low value-added applications. The limited applications of recycled plastics have hindered the development of the plastic recycling industry. The question is whether these recycled plastics can be applied in high value-added products. An example is the automobile industry, which consumes a large amount of advanced plastics materials. The average modern car weighting 1500 kg and contains 12% to 15% of plastics (PlasticsEurope, 2013). In 2018, China produced more than 23 million cars and require at least 4.14 million tons of plastics (OICA, 2018). If recycled plastics can be applied in the automobile industry, it will significantly extend the recycled plastics market, promote the waste recycling industry, and bring enormous environmental and economic benefits.

This thesis is an investigation of the potential of utilising recycled plastics in the manufacture of high-value automobile parts manufacturing thereby adding value to the waste material. In order to achieve this goal, it is essential to understand the barriers between recycled plastics and automotive applications.

This background will include 1) plastics in automobile applications, 2) current plastic recycling situation in China and plastics recycling technologies, 3) advantages and barriers to the reuse of recycled plastic in automobile production. This chapter also provides the objectives, aims and research strategy of this study.

1.2 Background

1.2.1 The use of plastics in automobiles

The use of plastics in automobile parts can be dated back to the 1900s (Pradeep et al., 2017). In 1941, a plastic prototype car which applied the hemp, sisal and cellulose-based plastics in the car body was invented by Henry Ford (Henry and Gregorie, 1942). From the 1970s to the 2000s, the average use of plastics in a car increased from approximately 50kg to 150kg (Patil et al., 2017). In 1999, the amount and type of plastics used in automobiles were summarised in Table 1-1 (Bechtold, 2006).

Table 1-1 Amount of polymers used in automobile parts
(Bechtold, 2006)

Part	Main Plastic Type	Weight in Average Car (Kg)
Bumpers	PP,ABS,PC	10.0
Seats	PUR,PP,PVC,ABS,PA	13.0
Dashboard	PP,ABS,PA,PC,PE	15.0
Fuel Systems	PE.POM,PA,PP	7.0
Body(Including body panels)	PP,PPE,PBT	6.0
Under the Hood Components	PA,PP,PBT	9.0
Interior Trim	PP,ABS,PET,POM,PVC	20.0
Electrical Components	PP,PE,PBT,POM,PVC	7.0
Exterior Trim	ABS,PA,PBT,PA,PVC	4.0
Lighting	PP,PC,ABS,PMMA,UP	5.0
Upholstery	PVC,PUR,PP,PE	8.0
Other Reservoirs	PP,PE,PA	1.0
Total		105.0

Table 1-1 shows that polypropylene (PP) is extensively applied in most automobile parts. Dashboard, seats and Bumpers are the heaviest components in a car made from plastic.

Today plastics make up about 50% of a modern car's volume, but only approximately 10% of its weight (SPI, 2016). The average weight of plastics in a 1500 kg modern car in Europe is between 180-225 kg (PlasticsEurope, 2013). It is also predicted that by 2020, the average plastic's weight in automobiles will increase to 350 kg (Plasticstoday, 2015).

The extensive use of plastics in the modern automobile industry is attributed to the demands for improving fuel economy and meeting the legislative and regulatory requirements (Pradeep et al., 2017). Patil et al. (2017) stated that every 10% of vehicle weight reduction can save 5%-7% of fuel consumption (Patil et al., 2017). The increasing amount of plastics used in automobiles is closely related to fuel efficiency. From 2004 to 2017, the fuel economy of automobiles in the US has improved 29% and the CO₂ emissions have a 23% reduction (EPA, 2019). Although fuel efficiency is the main reason for applying high-performance applications in automobile, plastics have many other advantages including (Patil et al., 2017): 1) minimisation of corrosion and extending the working life of the automobile parts; 2) allow design freedom and advanced creativity and innovation; 3) flexibility in integrating components; 4) recyclability.

In 2013, there are 3.8 million tons of plastics used in automobile applications, Figure 1-1 indicates the types of the plastics used in automobiles (PlasticsEurope, 2013).

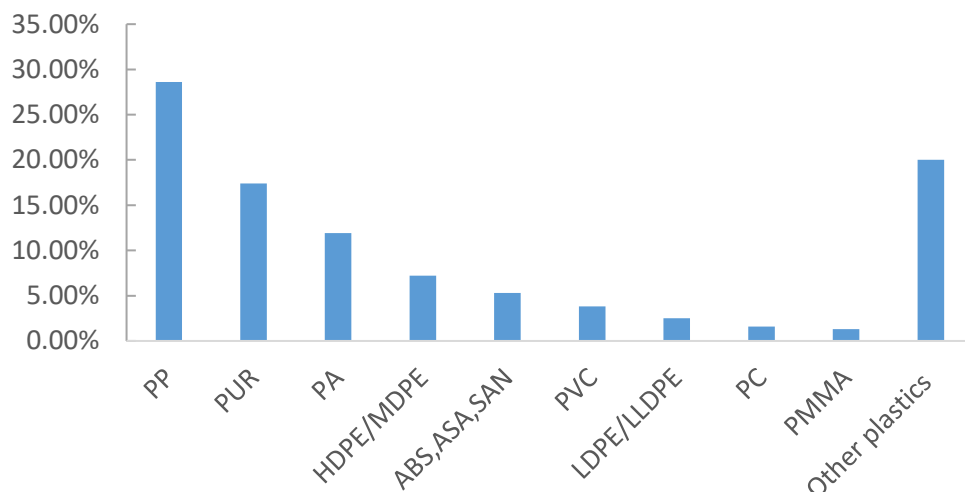


Figure 1-1 Use of plastics in the automotive sector (PlasticsEurope, 2013)

Polypropylene (PP), polyurethane (PUR) and polyamide (PA) are the top 3 high-performance plastics used in automobile manufacturing. These three plastics account for 57.9% of the total plastics used in a car. PP accounts for the highest share, 28.6%. PP has the advantages of low cost, good strength and stiffness and chemical (acid or alkaline) resistance (Lyu and Choi, 2015). And it is commonly applied for bumpers, air filters, battery boxes, containers, door panels, cup holders and many other applications (Pradeep et al., 2017). PUR is the second-largest type of thermoplastics used in automobiles. Solid PUR is an elastomeric material that has some outstanding properties include toughness, flexibility, high load-bearing capacity, resistance to abrasion and temperature (Power plastic recycling, N.A.). It is widely applied in automotive instrument panels, drive belts, seat foams, airbag covers, window encapsulation, sound and vibration absorption applications (Veejay plastic, 2016). PA has low cost, high mechanical strength, rigidity, temperature stability, low gas permeability, permanently solid and ageing resistant properties (Lyu and Choi, 2015). The major applications of PA are the parts under the engine hood, the application examples include motor coverings, suction elbows, wheel panels, plugs, mirror housings and connector housings (Lyu and Choi, 2015).

Other thermoplastics such as polyvinylchloride (PVC), polyethylene (PE) and acrylonitrile butadiene styrene (ABS) also play an important role in the automobile parts manufacturing. PVC has good flexibility, good thermal stability, high gloss and is flame retardant (Power plastic recycling, N.A.). It can be applied in protective coatings for underbodies and rocker panels, instrument panels, synthetic leather seat covers, seals, headliners, mud flaps and floor coverings (Veejay plastic,

2016). PE has the features of toughness, low water absorption, excellent chemical inertness, ease of processing and low coefficient of friction (Khanam and AlMaadeed, 2015). The applications of PE include glass fibre reinforced car bodies and electrical insulations (Patil et al., 2017).

The acrylonitrile in ABS improves the chemical and thermal stability of the polymer, and butadiene increase the toughness and strength, styrene gives a glossy finish to the polymer (Adreco Plastic, 2018). ABS has the advantages of low cost, low heat and electricity conductivity, high impact resistance, ease of painting and high-quality finish (Adreco Plastic, 2018). As a result, ABS is commonly applied in wheel covers, reflectors, car bodies, instrument panels/dashboards and seatbacks (Pradeep et al., 2017).

Besides, other plastics such as polycarbonate (PC), thermoplastic polyolefin (TPO), polyoxymethylene (POM), polybutylene terephthalate (PBT), polymethylmethacrylate (PMMA), upholstery (UP) and other engineering plastics are developed and applied in automobiles. These plastics not only have competitive mechanical, thermal, electrical properties but also maintain the lightweight and low cost as comparing the metals.

For further investigation of recycled plastics for automobile applications, PP is the most promising material. Not only does it has the highest weight fraction among all the automobile plastics, but also can be applied to most automotive plastic parts. The research on RPP will bring more potential economic benefits and have more flexibility in applicable parts selection.

1.2.2 Plastic recycling in China

Section 1.2.1 has briefly introduced the various kinds of plastics for automobile applications. But it remains unknown whether the recycled plastics can be applied for the same purpose as virgin plastics. To have a better understanding of recycled plastics, it is essential to study the background of plastic recycling in China (The purpose of this is to answer the following two question:

- Where are the recycled plastics coming from?
- What are the technologies applied for waste plastics management?

1.2.2.1 Source of the recycled plastics

Domestic source

The domestic sources are the major source of recycled plastics in China, which accounts for 60% to 70% of the total recycled amount from 2011 to 2016 (China plastics processing industry association, 2017). The amount of recycled domestic plastics continuously increased from 13.5 million tons in 2011 to 18.78 million tons in 2016 (China plastics processing industry association, 2017). In 2016 and 2017, the amount reduced by 9.9%, from 18.78 to 16.93 million tons (Ministry of Commerce P.R.C., 2018). However, the value of recycled plastics increased by 12.9% from 95.78 billion RMB to 108.13 billion RMB (Ministry of Commerce P.R.C., 2018). It means the value/quality of the recycled plastics is noticeably improved.

The recycling rate of plastics in China is remained at 25% to 30% from 2011 to 2016, the maximum recycling rate of 29.98% was reached in 2013 (China plastics processing industry

association, 2017). The low recycling rate and high amount of waste plastics generation lead to severe environmental problems, demands for landfill space and public concerns in China, which enforced the Chinese government to establish stricter environmental policies.

Foreign source

Imported recycled plastics increased rapidly during the past decades. In 2000, 2.0 million tons of recycled plastics were imported, and this value increased to 7.3 million tons in 2016 (China plastics processing industry association, 2017). In 2012, the waste plastics imported to China reached the maximum value of 8.9 million tons, but most of the reprocessors/manufacturers are still using low-tech equipment and pollution practices (Velis, 2014).

China was the major destination of waste plastics, which accounts for 56% of the global market, Hong Kong, Japan, Germany, the USA and Thailand are the top 5 import partners for China, accounts for 36.0%, 18.8%, 17.0%, 15.1% and 13.2% share, respectively (Velis, 2014). The amount of imported recycled plastics has a significant increase from 2000 to 2007, the average increase rate is over 10% every year, and from 2003 to 2004, the increase rate is 35.44% (China plastics processing industry association, 2017).

Since 2013, this situation has changed because of continuous public concern about environmental protection and the industrial requirement for high-quality raw materials. The Chinese government started the Green Fence operation in 2013, which strictly stipulated the quality of the imported waste resources (Velis, 2014). In 2017, the Chinese government established a new regulation on imported recycled plastics. In

2017, the amount of imported recycled plastics reduced to 5.8 million tons, which is about 35% lower than in 2012.

These kinds of policies will have a great impact on the global recycling market. For example, the exporters have to invest in more material recycling facilities to improve the quality of the recycled plastics, and more waste plastics will go to energy recovery. The strict plastic import policy of China has led to other countries rethinking their strategy of sustainable development. In the future, it is important to improve the quality of the recyclable and establish local close loops.

1.2.2.2 Plastic waste recycling technologies

The waste recycling (WR) in China has made considerable progress following the development in the last decade, in 2016, 246 million tons of waste were recycled (Xiao et al., 2018). Among these recyclable wastes, the recycling rate of waste plastics ranged from 20% to 30% (Xiao et al., 2018).

Plastic waste recycling in China can be classified into three groups: Industrial recycling, agricultural recycling and municipal recycling (Velis, 2014). Industrial recycling is predominately managed by plastic producers or recycling companies, usually, the kind of plastic scrap handled by these companies are from stable sources and of reliable quality. Agricultural recycling has the lowest recycling rate and is mainly based on manual recycling of plastic packaging and protective plastic films. Municipal recycling relies on householders sorting plastics from the waste stream and sold to private collectors.

Al-Salem et al. (2009) estimated four routes for plastic waste recycling: primary (re-extrusion), secondary (mechanical),

tertiary (chemical) and quaternary (energy-recovery). Figure 1-2 shows the detailed approaches for the recycling process for the plastic solid wastes (PSW) (Singh et al., 2017).

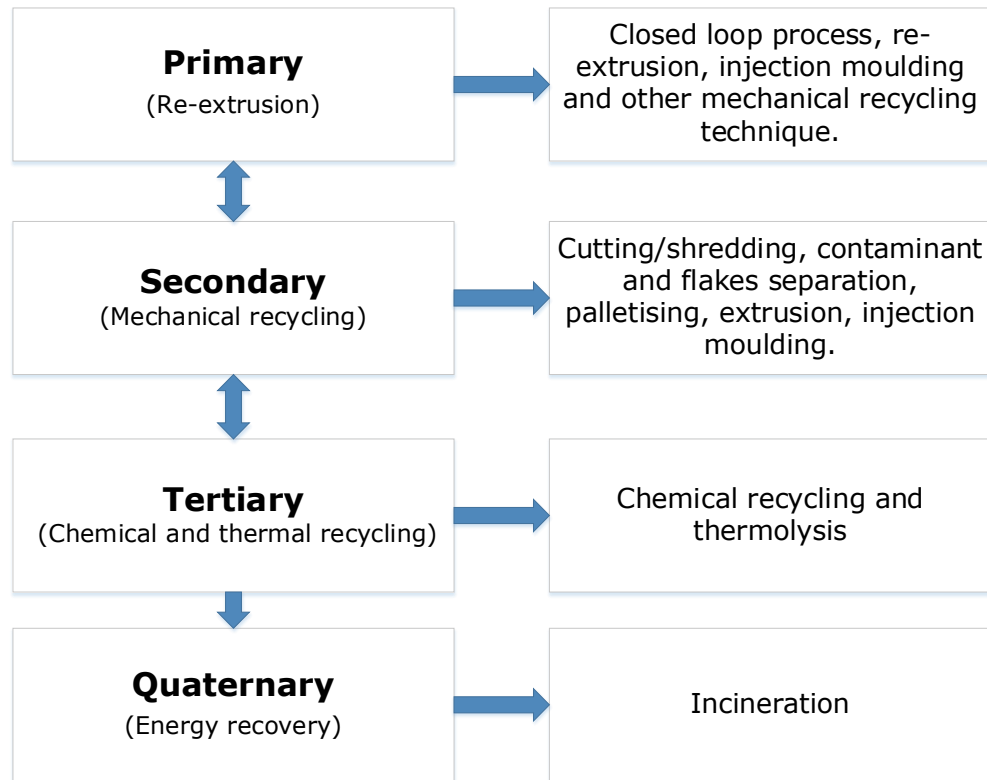


Figure 1-2 Various approaches for recycling of PSW (Singh et al., 2017)

- Primary recycling

Primary recycling is also known as re-extrusion, it utilises plastics scraps to produce materials that have similar features to the original products (Al-Salem et al., 2009). However, the plastics recycled from municipal waste are usually not suitable for re-extrusion due to the contamination (Yu et al., 2016). Primary recycling has to ensure the materials in the process are clean single-type material, so these kinds of materials are usually carried out by manufactures of plastic products within their own premises. (Kumar et al., 2011). After the primary recycling, the recycled materials can be reused directly for the

original product, reducing the use of virgin materials (Sadat-Shojai and Bakhshandeh, 2011). This type of recycling does not require a new market, and the controlled history of the materials ensure the quality of the final products.

- Secondary recycling

Secondary recycling is also a mechanical recycling process. It involves two main approaches: 1) separation of the waste plastics with contaminants and then segregation of the plastics into generic types before processing; 2) separation of plastics and contaminants then re-melted without plastic segregation (Kumar et al., 2011). The steps involved in this process usually include cutting, shredding, containment separation and flakes separation (Singh et al., 2017). Secondary recycling is the desired option only when sufficient quantities of source-separated homogeneous plastic waste can be supplied (Yu et al., 2016).

Waste plastics should be separated into different plastic types before secondary recycling. Municipal sourced waste plastics are not a good option for secondary recycling due to the inhomogeneity unless the plastics are separated into different types (Sadat-Shojai and Bakhshandeh, 2011). Single-polymers such as PP, PE and PS are preferred for secondary recycling, the complex contents of the polymer will cause difficulties in recycling if mixed (Al-Salem et al., 2009).

- Tertiary Recycling

In many cases, the recycled municipal solid waste (MSW) are heterogeneous, which make primary and secondary recycling becomes difficult (Singh et al., 2017). Tertiary recycling includes chemical recycling, in this process, the polymers are converted into smaller molecules, and it can be used as

feedstocks for manufacturing new plastic products or as a fuel-like energy source (Kumar et al., 2011). Tertiary recycling involves various technologies including chemolysis/solvolysis, gasification or partial oxidation and cracking (Kumar et al., 2011). The main advantages of tertiary recycling are that it may apply to the contaminated mixed-type polymers and only require limited pre-treatment (Al-Salem et al., 2009).

- Quaternary recycling

Quaternary recycling is classed as energy recovery processes from plastic solid waste (PSW). Energy recovery is an important method for MSW treatment, which burns MSW in waste-to-energy facilities for energy generation. Polyolefin from the packaging waste can generate almost the same amount of energy as fuel oil (Subramanian, 2000). The incineration of the PSW reduces the consumption of fossil fuels, so it lowers the greenhouse gases emission of the whole system (Scott, 2000). However, during the combustion of the PSW, it will also generate volatile organic compounds, smoke, heavy metals, dioxins and other undesirable compounds (Al-Salem et al., 2009). In modern facilities, the incineration temperature is high enough to decompose this hazardous chemical and prevent them into the ecosystem (Kumar et al., 2011).

1.2.3 Advantages of using recycled plastics

Section 1.2.2 has discussed the source and amount of recycled plastics in China, four types of waste plastics treatment options were also introduced in section 1.2.2. There is no doubt that the number of recycled plastics will keep increasing although the imported recycled plastics will reduce.

The performance of recycled plastics may not perfectly match

the requirements for industrial plastics. However, the advantages of recycled plastics are discussed below. By replacing virgin plastics with recycled plastics, the advantages can be classified into two categories: environmental benefits and cost-saving.

1.2.3.1 Environmental benefits

The major environmental benefits of plastic recycling come from the energy saved compared to the production of virgin plastics and the resources saved other than incineration and landfill (WRAP, 2016). It is reported that in Hangzhou, the provincial capital of Zhejiang, near 60% of the municipal solid wastes are landfilled (Zhou et al., 2018).

Due to the degradation during the manufacturing and during its lifecycle, the performance of the recycled plastics may not meet the specific requirements for some applications, especially some high-value-added uses. However, some automotive plastics parts do not require a specialist grade of polymer (WRAP, 2014). Recycled plastics have the potential to replace some of the virgin plastics based parts and reduce the overall carbon footprint of the automotive parts manufacturing process. Slătineanu et al. (2017) produced a life cycle assessment based on a Danish cleantech company called Plastix A/Sand and found that based on their scenario, recycled plastics have at least 5 times lower carbon footprint than virgin plastics.

Siddique et al. (2008) also reported other environmental benefits utilising waste/recycled plastics. These include conservation of non-renewable fossil fuels, reduction of energy consumption, reduction in the need for landfill space and the reduction of the emissions of CO₂, NO_x and SO₂. If the use of

recycled plastics in high added value products can be expanded while the economic benefits are increased, plastics recycling increase.

1.2.3.2 Cost-saving

Another important factor is the low price of recycled plastics. FRED (2019) established the producer price indexes of plastics material and recyclable plastics from 2009 to 2019, which is shown in Figure 1-3.

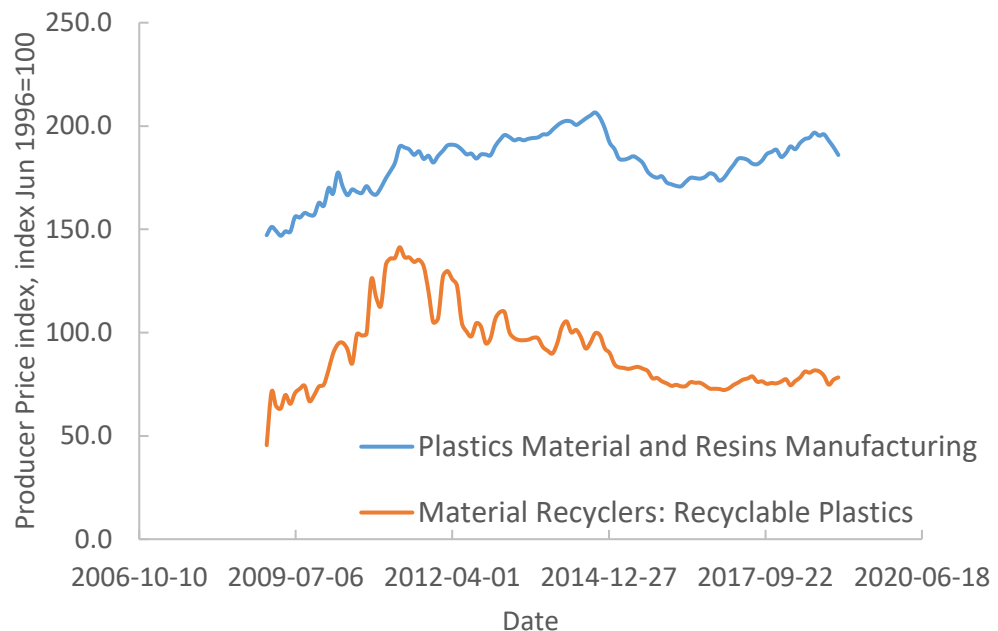


Figure 1-3 Producer price index for virgin plastics and recycled plastics (FRED, 2019)

As is shown in Figure 1-3, the gap of the price index increases from 2011 to 2018, which means the recycled plastics become much cheaper than virgin plastics.

However, it is necessary to note that the price of recycled plastics is not always more competitive than virgin plastics. The price of plastics are closely correlated to the oil price, the price of plastics will fluctuate with the change of the oil price (Mitte,

2018). Besides, unlike metals, the properties of recycled plastics may degrade each time they're processed. The processing of waste plastics recycling also requires other operation costs. This, therefore, makes the calculation of the economic benefits of recycled plastics complicated. When the oil price is low, the cost benefits of recycled plastics may be limited.

Due to the advantages of recycled plastics, some world's leading automobile manufacturers have started to investigate the feasibility of recycled plastics in automobiles. Volkswagen (2019) evaluated secondary raw materials, which are made from production residues or waste material. Maccarrone (2018) investigated the E-class Mercedes Benz and found that there are 72 components (around 54.4 kg in total) that can be produced partially from the high-quality recycled plastics. Volvo Car Group announced that from 2025, more than a quarter of plastics in the newly manufactured cars will use recycled material (VOLVO, 2018). In the future, recycled plastics may play a vital role in automobiles.

1.2.4 Barriers for recycled plastic applications

Post-consumer plastic is a valuable resource, however, the application of recycled plastics are limited because of various barriers.

McKinnon et al. (2018) summarised the four major barriers that hinder the market for recycled plastics:

- Low market demand for recycled plastics

The current low price of crude oil and virgin plastics reduces the investment for recycling plastics. Recycled plastics do not

have a high enough price advantage over virgin plastics. The low demand is also related to the uncertainties about the plastics quality and supply security, which mainly depends on the waste plastics management system.

- Low market information exchange

The waste recycling industry contains a long value chain, but the producer cannot find the optimal end-use because of the limited market communication.

- Limitation of technology

The technology barriers come from logistics, plastic separation and processing to gain reliable good quality products. Also, the quality of recycled plastics may degrade with processing. The degradation mechanism of the plastics and reinforcement technologies will be detailed in the literature review.

- Limitation of legislation.

The current recycling strategy is weight-based while plastics are relatively lighter than glass, metal and paper. This means that the recycling of plastics will have less contribution to meeting the targets of increasing the total recycling rates. And the diverse waste policy and implementation is another barrier for the cooperation of waste management in different nations.

Besides the cost of recycled plastics, which mainly depends on global crude prices, it is vital to provide a technically feasible pathway for extending the application of recycled plastics. Recycled plastics must have a stable source with stable quality. Otherwise, the impurities or the inconsistency of the quality of the recycled plastic will damage market trust. Although some of the recycled plastics can achieve desired properties in the lab, the source of the material has to be well controlled to

guarantee quality and supply consistency. As stated in section 1.2.2.2, the industrial/primary recycled plastic waste has stable sources and quality.

1.3 Objectives and aims

This research aimed to adapt recycled plastics so they are suitable for auto production. To achieve this goal, recycled plastics have to meet the requirements for industrial-scale production. The optimised formula should be both practically and economically available.

The primary objectives include:

- 1) To investigate the detailed mechanical and rheological properties of the recycled plastics and the requirement of the plastics for industrial-scale production;
- 2) To evaluate the effects of fillers on recycled plastic-based composites, include the commonly used mineral fillers, talcum, aluminium hydroxide and advanced fillers such as recycled carbon fibre and hollow glass beads;
- 3) To set up mathematical models to predict the performance of the recycled plastics with modifications of composition.
- 4) To evaluate the weakness of the recycled plastics based on the industrial requirements and provide possible formula, produce industrial parts.

1.4 Research Strategy

In order to achieve the goal of the utilisation of recycled plastics in automotive applications, this research has to identify (1) the knowledge gap between recycled plastics properties and industrial requirements; (2) the methods for improving the specific properties; (3) the tools for predicting the performance of the recycled plastics.

As is stated in section 1.2.1, based on the background study of the use of plastics in automobiles and plastic recycling in China, the industrial RPP is selected as the primary material for this study. The structure of this research can be classified as the following chapters:

Chapter 1. Introduce the situation of plastics recycling and the plastics in automobiles, identify the objectives, aims and research strategy of this research.

Chapter 2. This chapter provides the literature review focus on (1) the degradation of the plastics to understand the deterioration mechanism; (2) the reinforcement methods; (3) the mathematical tools for experiment design and properties optimisation.

Chapter 3. This chapter introduces the experiment procedures, details of the equipment, material, standards, sample preparation and tests.

Chapter 4. The mechanical properties characterisation of the virgin and recycled plastics were performed in this chapter. Talcum was studied in this chapter to improve the tensile and flexural properties of the composites. The improved formulas were prepared for the industrial trials.

Chapter 5. This chapter focus on improving the impact properties of the composites. PP was blended with PE, and the effects of the elastomer were also investigated.

Chapter 6. This chapter examines the effects of recycled carbon fibre and coupling agent content on the mechanical performance of the composites.

Chapter 7. Hollow glass beads have been used as the filler to achieve composites with desirable mechanical performance and lightweight. The flammability tests were also performed.

Chapter 8. This chapter concludes the present work and provides suggestions for further study.

Chapter 2 Literature review

2.1 Introduction

The increasing concern about environmental protection and resource conservation has accelerated the development of waste plastics recycling technologies and practices. Although various techniques have been used for plastic recycling, most recycled plastics have very limited applications due to the partial deterioration of mechanical properties. Based on the background study in Chapter 1, PP was selected as the focused polymer in this study. This chapter will also give a brief overview of the recycled plastics in the automobile. The current situation and problems of recycled plastics in the automobile industry are discussed.

Understanding of the following topics is a prerequisite for investigating the feasibility of recycled plastics for the automobile industry:

- The polymer degradation mechanisms and key factors;
- The techniques for improving the properties of recycled plastics based composites;
- The mathematical tools for experimental design and performance evaluation.

The degradation of plastics occurs during the manufacturing process and working periods. The mechanism for thermal, thermal-oxidative, photo-oxidative and biological degradation is discussed as well as the corresponding effects. The methodology for mechanical property reinforcement of recycled plastic is introduced. These methods include the addition of

fillers, polymer blending and the addition of compatibilizers and coupling agents. The final section of this chapter focuses on the mathematical tools for experimental design and optimisation. The mathematical tools include the Taguchi method, analysis of variance (ANOVA) and principal component analysis (PCA).

2.2 Overview of recycled plastics in the automobile industry

In recent years, China's domestic market demands drive a rapid increase in plastic recycling capacities. These recycled plastics are reported to be used in many sectors, the major destination of these plastics are non-food grade packaging (31 wt%), agricultural sectors (13 wt%), textile sectors (13 wt%) and construction sectors (10 wt%)(WRAP, 2010). Only a limited amount of recycled plastics used in high-value-added applications, such as the automobile industry.

It is reported that 10 years ago, the recycled plastics used in automobile sectors are only 1 wt% in China (WRAP, 2010). In 2017, 8.45 wt% of recycled plastics are reported being used in automotive applications globally (Locock, 2017). It was believed the increased consumer acceptance and the effects of the EU legislature increase the use of recycled plastics in the automobile industry. Figure 2-1 shows an A-Class Mercedes-Benz car which contains 118 components partly made of resource-conserving materials, including recycled plastics.



Figure 2-1 Plastic parts in Mercedes-Benz car (Sattler, 2019)

In Nissan Leaf, the manufacturer uses old PET bottles to make the seats, and use recycled fabric as the raw material for the sound insulator pads (Schmidt, 2018). Toyota announced that 20 wt% of recycled plastics are used in its vehicles (SPI, 2016). In 2019, the Fiat Chrysler automobile group manufactured the gasoline tanks, which use up to 39 wt% of recycled plastic for certain European applications (FCA, 2019). Since the policymaker tried to move the recycling rate of the vehicle from 85% to 95%, more shredding companies will increase the capture of plastics from this stream (MBA Polymers, 2014). Honda collected the bumpers with defects from the production process and end-of-life vehicles, and use the recycled plastics as raw materials for new auto parts (Honda, 2020).



Figure 2-2 Used Bumper recycling (Honda, 2020)

To improve competitiveness, different methods have been developed to improve the mechanical properties of recycled plastics close to virgin plastics. Commonly used methods include filler addition (Giannadakis et al., 2011, Inácio et al., 2017, Wang et al., 2014), compatibilisation (Song et al., 2010, Zheng et al., 2017), formula design (Gu et al., 2016b, Gu et al., 2016a) and process optimisation (Gu et al., 2014, Bhattacharya and Bepari, 2014, Mehat and Kamaruddin, 2011). Although the reinforcement technologies for plastics have been widely investigated, the industrial use of recycled plastics in automobiles is still very limited. In academic studies, only a few reported producing real auto parts with the evaluation of the comprehensive performance (Gu et al., 2016a). To bridge the knowledge gap between academic study and industrial use, it is necessary to build cooperation with industry and seek improvement methods.

Other than technical difficulties, the cost is another predominant factor. Recycled plastics are only preferred when the price is lower than virgin plastics, even they perform the same (Gallone and Zeni-Guido, 2019, Recycling today, 2017). It means that the price of recycled plastics is indexed against

the price of virgin plastics rather than reflecting the technical reality (cost in recycling and reprocessing recycled plastics) (Gallone and Zeni-Guido, 2019). As a result, the adoption of the reinforcement methods will be much depended on the cost of the proposed technology. In this case, some methods may not be realistic for the high yield automobile parts applications. Carbon nanotube (CNT) is one typical example, it has been proved effective in improving the mechanical and electrical properties of PP (Gamze Karsli et al., 2014, Shazed et al., 2014). Currently, the cheapest carbon nanotubes in the market are around \$100-200/kg (ScienceDaily, 2018), while the average price of non-aerospace grade carbon fibre is \$21.5/kg (Shama Rao et al., 2015). A small amount of CNT will dramatically increase the price of the composites, so CNT may be only feasible in a lab-scale study at the current stage. The same is true for other expensive materials, the price and usage amount should be carefully considered.

Except for low cost and competitive mechanical properties, recycled plastics should also meet the internal requirements of automobile manufactures. For example, the density of recycled plastics products. Connell from Toyota said that the company decide not to use recycled plastics in an interior part because the products will have a 7% increase in weight, increasing of the mass is against Toyota's policy (Recycling today, 2017). Now and in the future, there is no doubt that lightweight plastic materials will be preferred in the automobile industry, which means density is an important factor in the evaluation of the performance of composites.

Another problem is that the perception of recycled plastics has unsatisfactory properties (Recycling today, 2017). However, the

quality and the consistency of the recycled plastics are mainly dependent on the recycling processes and the stability of the source of the waste plastics as mentioned in Chapter 1. To avoid the variation of the quality of raw materials, this study selects the scaled and specialised company, which can assure the quality and quantity of the products.

2.3 Degradation of plastics

During the manufacturing process, service life and recycling process, both virgin and recycled plastics are subjected to a variety of degradation influences. Unlike virgin plastics, recycled plastics tend to suffer more degradations after service and during reprocessing, which results in varying degrees of deterioration of the mechanical properties (Kazemi Najafi, 2013). Understanding of the degradation mechanism is the prerequisite for polymer reprocessing and formulation design. This section will introduce the major categories of degradation mechanisms and effects of thermal, thermo-oxidative, photo-oxidative and biological degradations.

2.3.1 Thermal degradation

The thermal degradation of plastics is a result of the chemical reactions occurring in the polymers matrix at elevated temperature in absence of air or radiation (Billingham, 2002, Hawkins, 1984, Samperi et al., 2004, La Mantia et al., 2017). Thermal degradation has three distinct mechanisms (Billingham, 2002):

- Chain scission with de-propagation: when the polymer is heated to a temperature that the chain scission occurs and produces free radicals, causing rapid radical

- Thermal reaction without chain scission: At a given temperature, the reactions of substituent groups occur before scission, or compete with it. A typical example is the dehydrochlorination of poly(vinyl chloride)(PVC) as is shown in Figure 2-5.

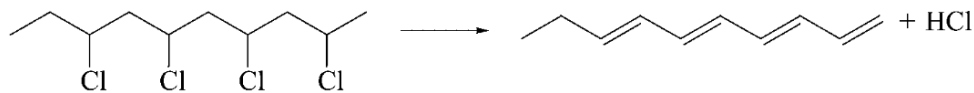


Figure 2-5 Dehydrochlorination of PVC (Billingham, 2002)

The thermal degradation can take place in the manufacturing processes, including extrusion, injection moulding, hot pressing and other heat treatment processes (Mendes et al., 2011).

A large number of thermal degradation investigations of PP and PE have been carried out in past decades, to study the impacts of processing parameters and polymer compositions (Mourad, 2010, da Costa et al., 2007, Qian et al., 2011, Fang et al., 2013, Mendes et al., 2011, Santos et al., 2002). In most heat treatment processes, the temperature is the crucial parameters that influence the level of thermal degradation. The variation in molecular weight of the polymers is one evidence for the degradation of plastics under high processing temperatures (Capone et al., 2007). Santos et al. (2002) studied the effects of multiple extrusions on the thermal stability of PP and high-density polyethylene (HDPE), high temperature (250°C onward) will lead to noticeable thermal degradation. Also, other factors such as the shear rate may play an important role in thermal degradation depending on the processing techniques. da Costa et al. (2007) found that a decrease of molecular weight in the PP matrix at a high shear rate level during the multiple extrusion process.

Other than processing parameters, polymer composition also has a major impact on its thermal performance. Mourad et al. (2009) investigated the thermal stabilities of PP/PE blend after the thermal ageing process, the addition of PE into PP caused the decline of the melting temperature, the heat of fusion and crystallinity content of PP. The presence of the fillers in PP based composites may lead to better thermal stability. Wang et al. (2013) studied the impacts of the talc content on the thermo-mechanical degradation of re-extruded PP/talc composites. Observation suggested that the rigidity of PP decreased because of thermal degradation, however, the reduced particle size caused by the re-extrusion process compensated the rigidity loss. Canetti et al. (2006) investigated the thermal degradation performance of PP/lignin composites, 5 wt% and 15 wt% of lignin were added into the PP matrix, the results indicated that the thermal degradation temperature was increased with increasing lignin content. Furthermore, the coupling agent can also contribute to the better thermal stability of PP composites. Kim et al. (2007) examined five different maleic anhydride grafted polypropylene (MAPP), and found that high M_w MAPP filled PP composites showed better thermal stability than low M_w MAPP filled ones. For improving the thermal stability of RPP composites, the addition of mineral filler, natural fibre and coupling agents may be considered in future study.

2.3.2 Thermo-oxidative degradation

Thermo-oxidative degradation of polymers can be defined as a thermally-activated diffusion and reaction process which occurred on the surface of composites under an oxidative environment (Hussein, 2018). Degradation due to various

reactions with oxygen is the most important mechanism of the deterioration of polymer properties (Hawkins, 1984). The majority of polymers degrade because of thermo-oxidation degradation during the processing and service life (Gijssman, 2008):

- In many cases, the processing of the polymers involves high temperature (usually higher than the melting and glass transition temperature), shear force, oxygen and water, which leads to degradation.
- During service life, the reaction of the polymer with oxygen in the air plays a major role, and the oxidation reaction is highly depended on the molecular structure of the polymer, structure defects, impurities and the exposed environment.

The thermal-oxidative degradation usually consists of three steps: initiation, propagation and termination steps (Kutz, 2012). Figure 2-6 shows the schematic of the thermal-oxidative degradation process (Zeus, 2005).

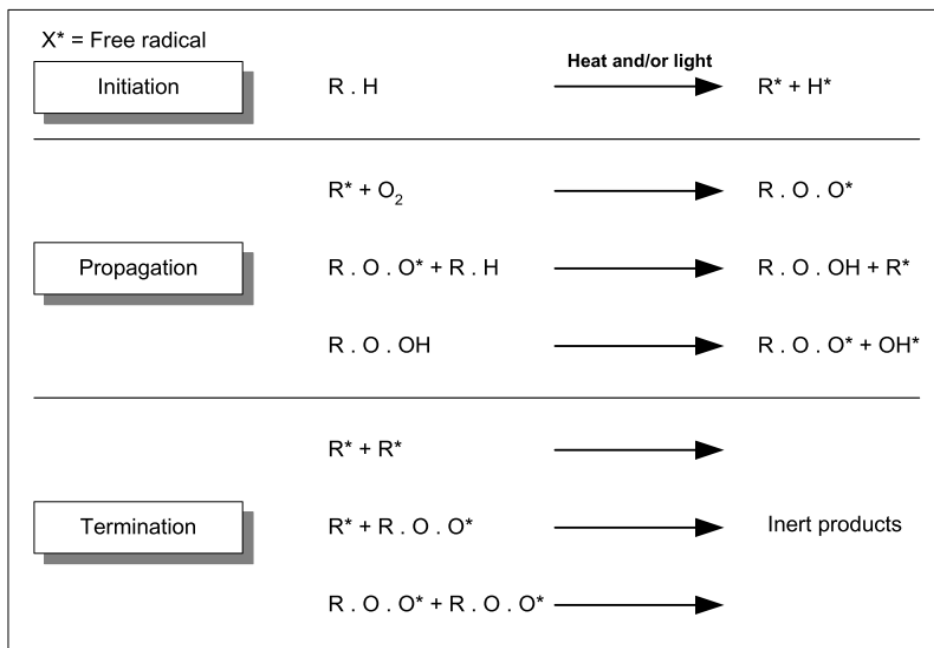


Figure 2-6 Three steps of thermo-oxidative degradation (Zeus, 2005)

In the initiation step, free radicals are formed when the backbone chain breakdown into small molecules. This process creates high reactive and unstable polymer 'free radical' (R^*) and a hydrogen atom with an unpaired electron (H^*) (Zeus, 2005). Then, in the propagation step, the decomposition reactions lead to crosslinking, main-chain unsaturation, intramolecular or intermolecular hydrogen transfer along the degradation of the main chain (Kutz, 2012, Gijsman, 2008). The free radical (R^*) reacts with oxygen (O_2) to form a peroxy radical (ROO^*). The peroxy radical (ROO^*) can react with another polymer (RH) to form a hydroperoxide ($ROOH$) and then regenerate the free radical (R^*). The $ROOH$ will then split into alkoxy radical (RO^*) and hydroxyl radical (*OH), which will continue the reactions with other polymers. In the termination step, the free radicals react with each other to form inert products.

All polymers are essentially susceptible to oxidation, the thermal-oxidative degradation of polymers is the focus of studying polymer degradation and stability (Celina, 2013). It was found that during the extrusion process of PP, the degradation rate at less than 230°C is negligible and it has a significant increment when the temperature is elevated from 230°C to 250°C , then the degradation rate remains constant with increasing temperature (González-González et al., 1998).

The multiple-extrusion process will accelerate the thermal-oxidative degradation, the molecular weight of PP decreased with increasing cycle number or temperature (Gijsman, 2008). As this study focus on PP, the recommended processing temperature for twin-screw extrusion and injection moulding is less than 230°C , and should not be higher than 250°C . On the

other hand, if the processing temperature has to be higher than 250°C in some special circumstances, the vacuum or inert gas atmosphere condition may be possible for the reduction of thermos-oxidative degradation effects.

The blending of different kinds of thermoplastics may lead to a change in the stability of the composites. The blend composition significantly influenced the degradative behaviour of polymer blends due to the interactions among different constituent in the blends (La Mantia et al., 2017). For example, the initial degradation temperature of PP increased when blending with nitrile rubber (George et al., 2000). Kaynak et al. (2017) studied the thermal and flammability performance of PP containing sepiolite-ammonium polyphosphate combinations, the incorporation of 5 wt% MAPP slightly increased the onset decomposition temperature, but the limiting oxygen index (LOI) value decreased from 32.2% to 27.8%. Nasir et al. (2011) simulated the thermo-oxidative degradation of PP, the increasing peak of carbonyl indicated the oxidation of the PP, the stabilizers (antioxidants) are effective in controlling the thermal-oxidative degradation. Besides, thermo-oxidative degradation may greatly affect the long-term stability of PP.

2.3.3 Photo-oxidative degradation

Given a certain amount of exposure to UV radiation, photodegradation may occur in the polymers which break the polymer chains, reduce the molecular weight and produce free radicals, meanwhile, the mechanical properties of the composite may deteriorate (Yousif and Haddad, 2013b).

Under normal conditions, most of the polymers expose to light with a wavelength higher than 290 to 300 nm during service

time. Light with a wavelength of less than 200 nm could break the C-C, C-H, and C-Cl bonds (Feldman, 2002). The polymers with intrinsic chromophores, such as carbonyl group (C=O), are sensitive to photoreaction, at an absorption wavelength of between 200 and 300 nm (Billingham, 2002).

Table 2-1 showed the wavelength of UV radiation when polymers have maximum sensitivity (Kelen, 1983).

Table 2-1 Wavelength of UV radiation when polymers have the maximum sensitivity

Polymer	Wavelength (nm)
Styrene-acrylonitrile copolymer	290,325
Polycarbonate	295,345
Polyethylene	300
Polystyrene	318
Poly(vinyl chloride)	320
Polyester	325
Vinyl chloride-vinyl acetate copolymer	327,364
Polypropylene	370

Three conditions are essential for the occurrence of photoinitiated chemical reactions (Billingham, 2002):

- The reacting molecule or impurity absorb the energy from light;
- The absorbed photons have enough energy to break the molecular bonds;
- The energy leads to the molecule reaction.

The degradation occurring in an outdoor environment may involve complex reaction mechanisms. Once the reaction is initiated by light, the subsequent reactions will be affected by oxygen, moisture and pollutants (Feldman, 2002). As recycled plastics may contain a certain amount of impurities, these impurities may also lead to photo-oxidative degradation. The Photo-oxidation will form embrittlement at the surface of the polymer, which leads to the surface craze and fracture in

polymers (Feldman, 2002). Figure 2-7 showed the general and photooxidation that occurred in polymers.

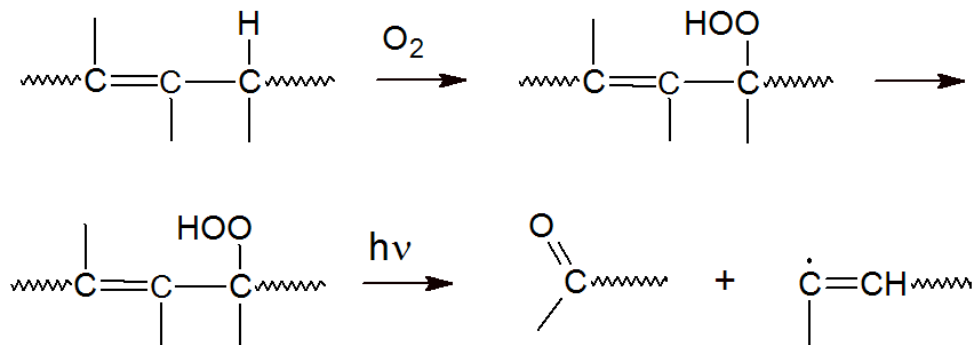


Figure 2-7 Process for photooxidation in polymers (Polymer Properties Database, n.d.-c)

Fillers may have an impact on the photo-degradation of PP-based composites (Rabello and White, 1996, Soccalingame et al., 2015, Waldman and De Paoli, 2008). Rabello and White (1996) experimented on the photodegradation of talc-filled PP, after exposure to ultraviolet (UV) radiation, the talc-filled PP maintained the tensile properties while the unfilled PP suffered significant deterioration. Soccalingame et al. (2015) assessed the effects of UV radiation on the PP/wood flour composites, the composites obtained better stability at higher content of the wood. The possible reason is that the lignin has the function of stabilization and anti-oxidation of the intransparent feature of the material limit the UV light scattering.

A coupling agent may also reduce the photo-oxidation degradation of PP composites. Adhikary et al. (2009) found MAPP significantly decreased the water absorption of the PP composites and enhanced the UV resistance of PP at light-water spray weather. After weathering, the composites containing MAPP showed less colour change as compared to unfilled

composites (Adhikary et al., 2009).

Waldman and De Paoli (2008) studied the PP and PS blends, due to the interaction of these two constituents, the blends show faster photo-degradation compared with their components. stabilizers can be used to stabilize the system, as a role of (1) light screeners, (2) UV absorbers, (3) excited-state quenchers, (4) peroxide decomposers, (5) free radical scavengers (Yousif and Haddad, 2013b).

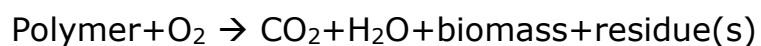
It can be found that there are a series of methods for improving the photo-oxidative resistance of plastic composites. The selection of the additives should be based on the overall performance of technical requirements.

2.3.4 Biological degradation

According to ASTM D-5488-94d "Standard Terminology of Environmental Labeling of Packaging Material and Packages", biodegradation is defined as the decomposition of the material into CO₂, CH₄, H₂O, inorganic compounds or biomass, the major mechanism is the enzymatic action of micro-organisms, and it can be measured by standardised tests (Singh and Sharma, 2008).

The biodegradation process can be classified into two categories - aerobic and anaerobic degradation (Leja and Lewandowicz, 2010):

- Aerobic biodegradation:



- Anaerobic biodegradation:

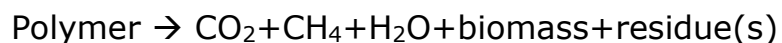


Figure 2-8 is a schematic diagram of the biodegradation that occurred in polymers.

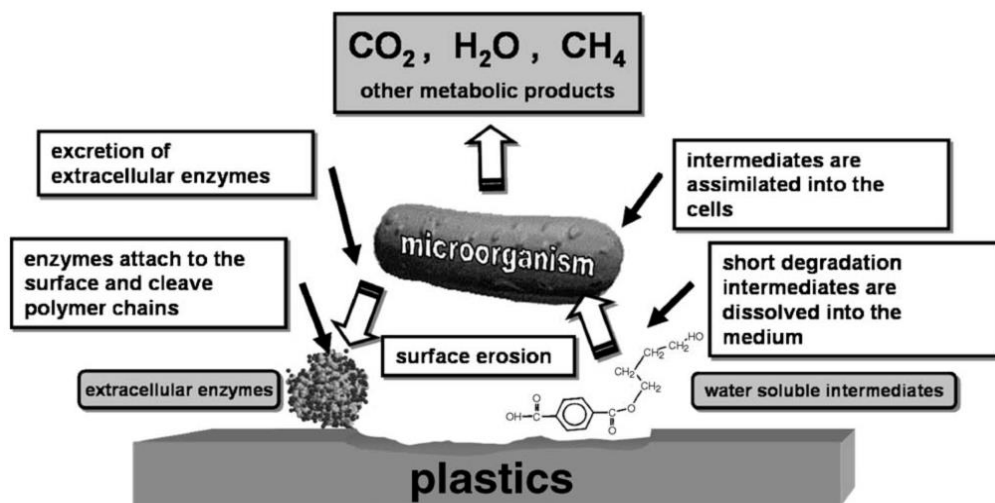


Figure 2-8 Mechanism of enzymatic catalysed hydrolytic polymer degradation (Rydz et al., 2015)

The biodegradation of the polymers includes four major processes: the attachment of microorganism to the polymer surface, the utilisation of the polymer as a carbon source, then the primary degradation and ultimate degradation (Arutchelvi et al., 2008). The primary mechanism for biodegradation is that the oxidation or hydrolysis of the high-molecular-weight polymers by enzymes, resulting in the degradation of the main chain into low-molecular-weight groups (Shah et al., 2008). Hydrolysis can occur only if the polymer has functional groups which can react with water and the polymer can attach water during the service life (Billingham, 2002). Since CH₂ is the main groups that consisted in PP, the surface of PP is hydrophobic, the initial degradation starts from the insertion of hydrophilic groups on the PP surface (Arutchelvi et al., 2008). Then the microorganism attached to the PP surface start to utilise it as the carbon source, the primary degradation step will create low-molecular-weight fragments, dimers or monomers, then

the ultimate degradation produces CO₂, H₂O and biomass.

The biodegradation of PP and PE leads to the reduction of molecular weight, tensile strength and viscosity (Arutchelvi et al., 2008). Strömberg and Karlsson (2009) studied the effects of biodegradation on surface and bulk properties changes of PP, recycled PP and polylactide biocomposites. They found that although PP is inert to biodegradation, the biofilm which is a mixture of microorganisms in an extracellular polysaccharide gel was still formed, and it imposed significant effects on the surface properties of the composite. As the target application of RPP in this study is automobile parts, the effects of biodegradation on the properties of the composites might be negligible.

2.3.5 Conclusion

This section introduced thermal, thermal-oxidative, photo-oxidative and biological degradations of polymers. The purpose of this section is to help to 1) understand the degradation mechanisms of plastics, especially PP; 2) give guidance to avoid degradation in this study, the processing temperature should not be higher than °C, and the preferred temperature is less than 230 °C.

Thermal degradation may occur during the reprocessing of RPP composites under an airless and high-temperature condition. Temperature and processing time are the key factors in thermal degradation and should be carefully controlled. The presence of the fillers such as talc and lignin are reported to improve the thermal stability of the PP composites. Based on the literature review and the processing condition of equipment used in this study, the preferred processing temperature of PP based

composites should not be higher than 250 °C. For RPP, which may contain a certain amount of other plastic blends, the processing temperature should be further controlled to prevent severe properties degradation.

Thermo-oxidative degradation may occur during the processing and service life of most of the polymers. The high temperature, shear force, oxygen and water may lead to thermo-oxidative degradation. It was suggested the processing temperature should be set lower than 230°C. And in service life, the degradation is highly depended on the molecular structure of the polymer, structure defects, impurities and exposed environment. It is suggested to blend PP with other polymers, rubbers or antioxidants to improve thermal stability.

During service time, when the polymer exposed to light, it may initiate a complex reaction which leads to photo-oxidative degradation. It will break the polymer chains, reduce molecular weight and may deteriorate the mechanical properties. Talc is reported to able to maintain certain mechanical properties. Some stabilizers may be added to the polymer matrix depending on the service condition of the composites.

Biodegradation may also happen in the service life of the composites. It consists of aerobic biodegradation and anaerobic biodegradation. The biodegradation may also cause adverse effects on the surface properties of the PP composites. Since PP is usually regarded as inert to biodegradation, biodegradation will not be considered as the major cause of the properties deterioration in this study.

2.4 Modification and improvement

2.4.1 Fillers

2.4.1.1 Mineral fillers

Mineral fillers are commonly used in thermoplastics for reducing the overall costs and improve the mechanical properties (Stricker et al., 1997). Talcum, calcium carbonate, kaolin, titanium dioxide and many other mineral fillers have proved as cost-effective materials for industrial applications (Leong et al., 2004, Weon and Sue, 2006, Ayaz et al., 2016).

Talc is one of the most commonly used fillers for reinforcing the properties of PP (Gu et al., 2016b, Wang et al., 2013, Wang et al., 2014).



Figure 2-9 Photo of talc minerals and talcum powder (Seria trading, N.A.)

Talc is effective in improving the tensile and flexural properties of the PP based composites (Leong et al., 2004, Weon and Sue, 2006). However, at high filler loading, the agglomeration of the particles may reduce the strength and toughness of the composites (Leong et al., 2004). Wang et al. (2013) studied the

thermal and mechanical properties of 0, 10 wt% and 20 wt% talc-filled PP composites after re-extrusion. The addition of talc leads to higher thermal stability, higher tensile modulus and yield stress. The significant increase of tensile modulus is closely related to the improved stiffness by addition of talc and the performance was highly affected by the aspect ratio and flow alignment of talc particles (Weon and Sue, 2006). Premalal et al. (2002) compared the mechanical performance of PP/rice husk powder and PP/talc composites, the talc-filled composites exhibited better yield strength, tensile modulus and flexural modulus. However, the impact strength reduces with the increase of the filler content. At high talc content, due to the poor interfacial adhesion between talc and PP matrix, cracks propagate more easily (Premalal et al., 2002). MAPP was reported to be effective in improving the interfacial adhesion between talc and PP (Ashenai Ghasemi et al., 2016, Gu et al., 2016b). Ashenai Ghasemi et al. (2016) obtained the maximum tensile strength, tensile modulus and impact resistance at 27.01 wt% talc and 4 wt% of MAPP. Furthermore, Gu et al. (2016a) added talc in RPP based composites with MAPP, by blending with a small amount of VPP, the optimal formula meet the technical requirements of engine cover and fender. Monti et al. (2020) used styrene-ethylene/butylene-styrene (SEBS) and a PP-based olefin block copolymer (OBS) significantly improve the impact strength of RPP composites. It is reported that the further addition of 10 wt% of talc in the RPP/SEBS or RPP/OBS matrix was effective in compensating the stiffness loss due to the addition of SEBS or OBS (Monti et al., 2020).

To apply talc into the RPP composites and improve the mechanical properties, it is also important to study the microstructure of the talc and PP matrix. The mechanical

performance of the composites was illustrated to be closely correlated to the size, shape and dispersion of talc in the matrix (McGenity et al., 1992, Weon and Sue, 2006, Monti et al., 2020).

Another commonly used inorganic filler is calcium carbonate (CaCO_3) (Chan et al., 2002). At first, calcium carbonate was only used to reduce the overall cost of the composites (Leong et al., 2004). Later, various studies investigated the filler content, particle size and dispersion, in attempting to reinforce the calcium carbonate filled composites. Zuiderduin et al. (2003) studied the effects of particle size (0.07-1.9 μm) and the content of calcium carbonate (0-32 wt%) on the tensile and impact properties of CaCO_3 /PP composites. The results showed the content of CaCO_3 is the dominant factor influencing the tensile modulus while particle size has little effect. The impact strength of the composites at 20°C increase with increasing CaCO_3 content, and the 0.7 μm filled CaCO_3 /PP composites obtained the highest impact strength (Zuiderduin et al., 2003).

Other researchers focused on particle size and further studied the nano-sized calcium carbonate. Eiras and Pessan (2009) studied 3 wt% of nano-sized calcium carbonate at a size range of 70-90 nm can lead to a rapid increase of elastic modulus and yield stress. The nanosized CaCO_3 can act as the nucleation sites for CaCO_3 /PP composites and improve the modulus and toughness (Weon and Sue, 2006).

The dispersion of CaCO_3 is another important factor that affects the mechanical performance of the composites. Zhu et al. (2014) studied the dispersion of CaCO_3 in PP/ CaCO_3 composites and showed small size CaCO_3 particles may agglomerate. The size smaller than 15 μm particles may form stress-concentrated points and lead to impact strength deterioration. The dispersion

of particles could be a dominant factor influencing the impact properties, and it is difficult to avoid the aggregation of the high content of un-treated CaCO_3 (Zuiderduin et al., 2003).

Aluminium hydroxide is an effective filler for improving the flame retardancy of the composites (Liang et al., 2010, Su et al., 2005, Ramazani et al., 2008, Liang et al., 2015a). It was reported that the limiting oxygen index (LOI) of PP/ $\text{Al}(\text{OH})_3$ increased linearly with the addition of $\text{Al}(\text{OH})_3$ in the PP matrix (Su et al., 2005). The reduction of LOI may be attributed to two factors: the crystal water in $\text{Al}(\text{OH})_3$, the released steam gas dilutes the combustible gases; and Al_2O_3 formed a protective layer to prevent further combustion (Ramazani et al., 2008). However, the introduction of $\text{Al}(\text{OH})_3$ to the matrix may lead to the deterioration of mechanical properties. With the addition of 5 wt% to 50 wt% of $\text{Al}(\text{OH})_3$ into PP, it was found that the tensile and flexural strength of the composite decreased with increasing level of filler (Shah et al., 2014). One possible explanation is that due to the poor adhesion between the filler and PP matrix, the agglomeration of $\text{Al}(\text{OH})_3$ act as defects and stress raisers (Su et al., 2005). By toughening with zinc neutralised sulfated ethylene-propylene-diene monomer (EPDM) ionomer, the tensile properties of the PP/ $\text{Al}(\text{OH})_3$ composites significantly improved, which is attributed to better dispersion and adhesion of $\text{Al}(\text{OH})_3$ in PP matrix (Su et al., 2005). Mai et al. (2001) also found the reduction of impact strength, flexural strength and tensile strength of the PP/ $\text{Al}(\text{OH})_3$ with adding $\text{Al}(\text{OH})_3$, the incorporation of acrylic acid grafted polypropylene improved the interfacial interaction between filler and matrix, which overcome adverse effects on mechanical properties.

2.4.1.2 Glass fibre

Glass fibre is widely applied in aerospace, leisure, automobile, construction and sports industries because of its low cost and relatively good mechanical properties (Wambua et al., 2003). The glass fibre reinforced plastics (GFRPs) suits many applications and in some cases are better options than carbon fibre reinforced plastics (CFRPs) because of the lower manufacturing cost (Sims and Broughton, 2000). GFRPs have the following characteristics (Sims and Broughton, 2000):

- Good corrosion resistance extends the fields of application for GFRPs.
- Lightweight, GFRPs can replace some of the metal automotive components with much less weight.
- Good toughness, suitable for high energy absorption applications.
- Good electrical insulation properties.
- High specific strength values, meet wide application requirements.
- Ease of processing, provides manufacturing flexibility.
- Ease of shaping, provides design flexibility.

Valente et al. (2011) studied the mechanical characterisation of recycled glass fibre/wood flour thermoplastic composites. The presence of glass fibre improves the flexural modulus and reduces the ability to absorb water. It was reported that 15 wt% glass fibre filled polylactic acid (PLA) composites achieved between a 32% and 21% increase in tensile and flexural strength (Varsavas and Kaynak, 2018). Bajracharya et al. (2017) investigated the durability of the 0-30 wt% of glass fibre

filled HDPE, LDPE and PP. With the addition of glass fibre, the composites showed reduced surface degradation under UV radiation and had better tensile strength and modulus retention than unfilled plastics. With the increasing content of glass fibre, PP/glass fibre composites achieved higher impact strength (Thomason and Vlug, 1997, Thomason, 2002). Except for the weight fraction, the interfacial adhesion between glass fibre and the base matrix is a key factor influencing the mechanical performance of the products (Etcheverry and Barbosa, 2012, Lin et al., 2015a). With the incorporation of coupling agents MAPP, the GFRP composites showed superior tensile, flexural and impact properties, while the coupling agent SEBS-g-MA provides the deterioration of tensile and flexural properties and improvement of impact properties (Lin et al., 2015a).

2.4.1.3 Recycled Carbon fibre

Today carbon fibre reinforced polymers (CFRP) are extensively used. In automobiles, a 30% reduction in life cycle energy use can be achieved by replacing conventional materials with CFRP (Das, 2011). During the past decade, the demand for carbon fibre (CF) has undergone a rapid increase with an average annual growth rate of over 15% p.a. The overall demand for CF worldwide is expected to reach 290,000 tonnes by 2024 (Kraus et al., 2014, Mraz, 2018).

The rapid increase in production and consumption of CFRP leads to the continuous concern for the disposal of waste CFRP. Polymers are generally difficult to recycle, and landfill is a common waste treatment method especially when the landfill is cheaper than other treatment options (Pickering, 2006). However, for the consideration of environmental impact,

legislation, production cost, resource management and economic opportunity, CFRP should be recycled (Pimenta and Pinho, 2011). Meng et al. (2018) assessed the financial viability of recycled carbon fibre for the automotive industry, it showed that the cost related to the recovery of CF is about 15% of the cost of producing virgin CF. The price of recycled carbon fibre (rCF) is typically 20% to 40% less than virgin carbon fibre, making the rCF reinforced composites more affordable (Jacob, 2019, Gardiner, 2014). However, due to the short fibre length and deterioration of mechanical properties, recycled carbon fibre is usually used for non-critical applications (Verma et al., 2018). The structural applications require both improved interfaces adhesion and a more uniform mesostructure (Giannadakis et al., 2011).

Recycled carbon fibre (rCF) might be a feasible option for the reinforcement of recycled plastics. The technical limitations of CFRP waste recycling process are the major constraint for the application of rCF (Witik et al., 2013). Wong et al. (2012) exploited the fluidised bed recycling process to produce recycled carbon fibres. Figure 2-10 showed the recycling of carbon fibre from aerospace waste to reuse in automotive parts.

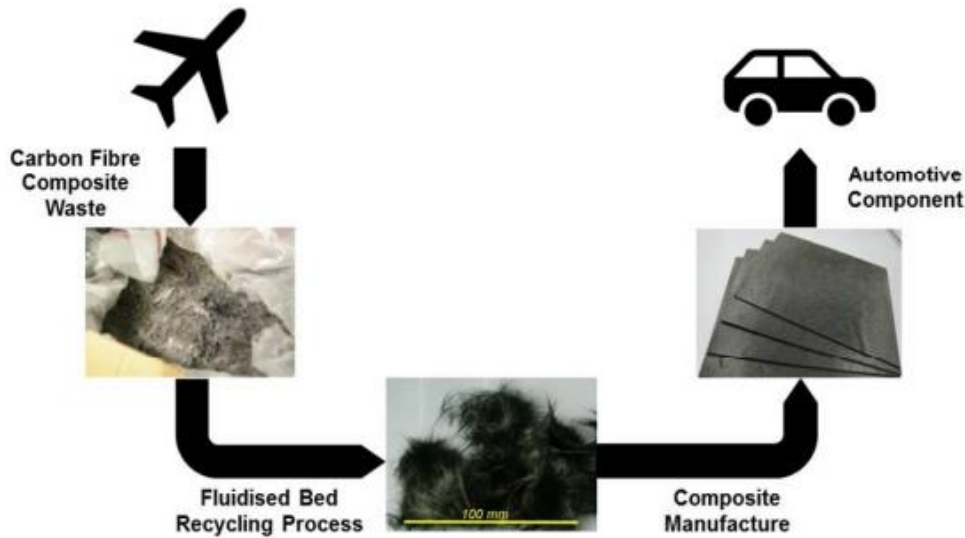


Figure 2-10 Carbon fibre recycled from the fluidised bed recycling process for the use of automobile parts (Meng et al., 2017)

With the addition of 30 wt% rCF in the composites, the tensile and flexural modulus can increase 768% and 872% as compared to neat PP (Wong et al., 2012). To further improve the rCF reinforced PP composites, many researchers have tried to improve the interfacial adhesion between rCF and PP (Cai et al., 2019, Unterweger et al., 2015, Wong et al., 2012, Lee et al., 2015). It was observed that the MAPP significantly improved the impact strength. And molecular weight and anhydride groups in the coupling agent played a major role in the compatibility of fibres and the polymers (Wong et al., 2012). The increment in the carbon fibre content and the compatibilizer levels can enhance the tensile strength at break and tensile modulus values of the short-carbon-fibre reinforced composites, and the fibre loading plays an important role in the performance of the carbon fibre reinforced composites (Karsli and Aytac, 2011). Interfacial adhesion of carbon fibre and base material is one of the key factors that influence the mechanical

performance of the composites (Unterweger et al., 2015). Liu et al. (2015) used ethylene-methyl acrylate-glycidyl methacrylate terpolymer to treat the surface of CF, with the incorporation of MAPP in PP matrix, the flexural strength, impact energy and tensile strength achieved 139.33%, 233.9% and 126.1% improvement. Another research hotspot is the fibre alignment, Akonda et al. (2012) and Xiao et al. (2019) use the carding process to obtain highly aligned rCF with satisfying mechanical properties. Pimenta and Pinho (2011) predicted the potential structural applications for recycled CFRP, including automotive, construction, aircraft interiors, wind turbine structures, leisure and sports goods.

Based on the present study, very few studies have investigated using rCF filled composites to improve recycled plastics as the base matrix. The performance of the techniques used in virgin plastics may be affected by the complex content and service history of recycled plastics. The effects of rCF on recycled plastics are not fully investigated. Another problem is that recycled plastics based composites are expected to be cheap. Recycled plastics with a high amount of rCF require a more developed recycled carbon fibre market and higher cost of the final product. At the current stage, it would be impractical for large scale production. So, this study will only consider using a small amount of short recycled carbon fibre, which is usually regarded as a low valued material, to reinforce RPP.

2.4.1.4 Hollow glass beads

Hollow glass beads have received a lot of interest from researchers as a potential filler for producing lightweight composites without comprising the mechanical performance

(Liang, 2005, Kumar et al., 2017). Considering the environmental effects and energy efficiency, it is desirable to develop lightweight materials for different applications (Hufenbach et al., 2011). Hollow glass beads (HGBs) consist of a rigid spherical glass shell and the hollow inside is filled with inert gas (argon). The average size range of the HGBs provided by 3M is 16 to 65 microns, and the density ranges from 0.125 to 0.60 g/cm³.

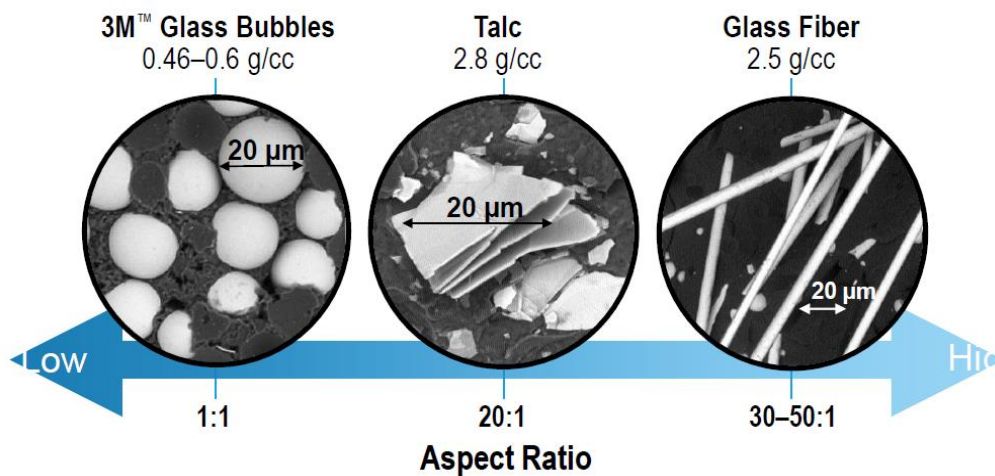


Figure 2-11 3M HGB and other fillers (3M, 2013)

Due to the structure of HGBs, they have low bulk density and relatively low thermal conductivity (Liang and Li, 2007, Liang and Li, 2006). Therefore, the addition of hollow glass beads to different polymers can potentially improve the mechanical properties while maintaining the lightweight structure (Liang, 2006, Liang, 2005, Li et al., 2013). Kumar et al. (2017) studied the effect of the addition of HGBs on natural fibre reinforced composites. They reported that it was possible to achieve both high strength and lighter weight with the addition of both HGBs and bamboo fibres to the PP matrix (Kumar et al., 2017). Hollow glass beads also have thermal insulation properties, and it has been reported that the addition of 20 vol% HGB can

reduce the effective thermal conductivity of PP composite by around 20% (Liang and Li, 2007, Liang and Li, 2006). HGB can also dramatically reduce the formation of smoke and thermal transmission of the TPU during combustion, which can eventually reduce the potential risk of it being a fire hazard (Jiao et al., 2017).

When PP burns, it can form molten drops and propagate the flame more easily which accelerates the burning rate. Therefore flame retardants have to be added to improve the flame-retardant properties of PP-based composites for specific applications (Liang and Zhang, 2010). A common practice is to add halogen-based compounds, this is an economical option for achieving both good flame retardancy and mechanical properties. However, the combustion of halogens will lead to the production of toxic dioxins and furans, which have adverse effects on human health and the environment (Kiliaris and Papaspyrides, 2010). Today halogen-free flame retardants are preferred due to environmental concerns (Schirp and Su, 2016). Therefore, HGBs have the potential for improving the mechanical properties of the plastics composites while maintaining a lightweight. As HGBs can be regarded as a novel material developed and applied in recent decades, the performance of HGBs on VPP and RPP has not been fully investigated. This study will evaluate the flame retardancy performance of HGBs based on VPP rather than RPP, to reduce the variables that may affect the flammability results. This study will both characterize the mechanical performance and density of HGBs filled VPP and RPP composites.

2.4.2 Polymer blending

Polymer blending is the mixing of two or more macromolecular substances, polymers or copolymers with the content more than 2 wt%, to form a new material with different physical properties (Utracki, 1999). Polymer blending is an important technique for overcoming the high separation cost of commingled plastic wastes (Horák et al., 2005). And it is usually a cost-effective way to develop the material with specific requirements in the composite manufacturing industry (Horák et al., 2005). One of the main drawbacks of PP is the low impact strength (Lin et al., 2015b). This study focuses on PP/PE blending and PP/Rubber blending to achieve good mechanical properties, especially the reinforced impact strength of the RPP composites.

There is extensive research concerning the blending of PP with low-density polyethylene (LDPE), linear low-density polyethylene (LLDPE) and high-density polyethylene (HDPE) (Tai et al., 2000, Strapasson et al., 2005, Mourad, 2010). The blending ratio is the key factor influencing the mechanical properties of the PP/PE blends. Strapasson et al. (2005) studied the tensile properties of the PP/LDPE blends, the content ratio of the PP/LDPE was controlled at 0/100, 25/75, 50/50, 75/25 and 100/0 by weight fraction. The results show the stress-strain tensile curves are very dependent on the blending ratio of PP and LDPE, the increment of LDPE content leads to tensile strength reduction (Strapasson et al., 2005). A similar tendency was observed in PP/HDPE blends. Madi (2013) blends the recycled HDPE with up to 30 wt% of virgin PP, the tensile strength of the blends increased linearly with the addition of PP content. Mourad (2010) strongly recommended the PE content

of PP/PE blend should not higher than 25 wt% because of the dramatical deterioration of tensile behaviours. The morphological effects include spherulite sizes, intercrystalline links between lamellae, the interaction between HDPE and PP phases, were regarded as the main reasons for the change of tensile performance (Lovinger and Williams, 1980). However, when higher PP content added to the LDPE matrix, the corresponding impact strength decreased significantly (Strapasson et al., 2005). Madi (2013) also found that the impact strength of the blends decreased linearly with increasing PP content. In other words, the existence of PE in PP/PE blends has a positive effect on the impact properties. Tai et al. (2000) observed that the PP/LDPE blends with the weight ratio of 4:1 exhibits a similar impact strength as PP homopolymer. Furthermore, Yang et al. (2003) found that the sharp decrease of impact strength occurred when PP content is higher than 30 wt%. The fracture surface of impact specimens suggested that small voids were formed at low content of PE because of the poor interfacial adhesion between PE and PP (Yang et al., 2003). Ayaz et al. (2016) studied the mechanical properties of PP/LLDPE/TiO₂/SEBS nanocomposites, and find the content of LLDPE is the most significant factor that influencing the impact properties. The above studies indicated that the PP/PE blends may be an effective way to improve mechanical performance when the PP/PE blending ratio is carefully controlled. As most of the materials used in the literature are virgin plastics, it is essential to establish the correlation of recycled PP/PE blends composition and mechanical performance before applying them in any automobile applications.

Another important factor of the polymer blends is phase behaviour, because of the incompatibility of PP and PE, the low

interfacial adhesion may lead to severe mechanical properties deterioration (Robeson, 2007). Some researchers used different kinds of compatibilisers to improve the dispersion and adhesion of PP/PE blends (Chiu et al., 2010, Gao et al., 2012, Fang et al., 2013). Fang et al. (2013) blended PP/PE with two compatibilisers, maleic anhydride grafted polyethylene (MAPE) and ethylene-propylene-diene monomer (EPDM), the presence of the compatibilisers decrease the tensile strength significantly. The possible explanation is that although the compatibilisers enhanced the miscibility of PP and PE, the stiffness of the composite can hardly be improved (Chiu et al., 2010). On the other hand, due to the improved interfacial adhesion between PP and PE interaction layers, the impact strength was dramatically increased with the incorporation of the compatibilisers (Fang et al., 2013).

PP/Rubber blends are commercially important polymer blends (Horák et al., 2005). Many studies have proved that the elastomer SEBS is effective in improving the impact properties of the PP composite (Plawky et al., 1996, Abreu et al., 2005, Tjong et al., 2005, Liao and Tjong, 2011). Abreu et al. (2005) use SEBS as an impact modifier, which significantly improved the impact properties of the PP composites and SEBS acted as a nucleating agent which reduced the crystallisation temperature. Denac et al. (2005) studied the mechanical performance of PP/Talc/SEBS or PP/Talc/Maleic anhydride grafted SEBS (SEBS-g-MA) composites. When the loading of SEBS/SEBS-g-MA increase from 0 wt% to 20 wt%, the tensile modulus and tensile strength of the composite decreased, but the decrease was compensated by the addition of talc. On the other hand, the elongation at break and notched impact strength was significantly improved with a high content of

SEBS/SEBS-g-MA. Liu et al. (2009) observed a similar notched impact strength trend in PP/Mg(OH)₂/SEBS-g-MA composites. It is explained that SEBS-g-MA enhanced the interfacial interaction between PP and the mineral fillers, which promote the energy absorption ability when the impact occurs (Liu et al., 2009).

2.4.3 Compatibilisers and Coupling agents

Compatibilisation can be defined as the modification of the interface of immiscible or partially miscible polymers by forming physical or chemical bonds (Horák et al., 2005). The compatibilisers are commonly used as additives for improving the compatibility of different polymers.

Inuwa et al. (2017) investigated the compatibility effects of SEBS-g-MA on the PET/PP blends, 10 phr SEBS-g-MA filled blends achieved a 300% increase of impact strength. Papadopoulou and Kalfoglou (2000) also studied three compatibilisers LLDPE-g-MA, PP-g-MA and SEBS-g-MA on the PET/PP blends, the results indicated SEBS-g-MA has the highest compatibility efficiency, and the elastomeric compatibilisers absorbed more stress developed on PET/PP interface. Fang et al. (2013) blended waste PP and PE with compatibilisers MAPE and EPDM, the compatibilisers only plays a major role in improving impact properties and EPDM showed a better compatibility effect than MAPE via the morphological study of the microsurface.

Coupling agents are mainly used to improve the interfacial adhesion between polymers and the mineral fillers or fibres (Lin et al., 2015a, Franco-Marquès et al., 2011, Leong et al., 2004). Maleic anhydride grafted polypropylene (MAPP), is an effective

coupling agent used in PP based matrix and improving the interaction between the talc and PP/RPP matrix (Gu et al., 2016b, Gu et al., 2016a, Ashenai Ghasemi et al., 2016). Wong et al. (2012) use three different MAPP with different molecular weight and maleic anhydride contents to reinforce the PP/rCF composites, it was found MAPP improves the interfacial adhesion, result in higher tensile, flexural and impact strength. The incorporation of MAPP in PP/HGB composites also achieved good results. Kumar et al. (2017) combined MAPP with PP at a weight ratio of 1:9, in the SEM images of the surface of PP/HGB/Bamboo fibre samples, good dispersion of HGB and sufficient interfacial adhesion between HGB and PP matrix was observed.

Except for the amount of MAPP filled in the matrix, the molecular weight of MAPP may also cause a wide difference in the macro performance of the composites. Franco-Marquès et al. (2011) experimented to estimate the influence of MAPP on the mechanical properties of the PP composites, the study concentrated on the acid number and molecular weight of the MAPP. The lower molecular weight of the coupling agent contributed to higher ultimate tensile strength, flexural strength and notched impact strength. (Franco-Marquès et al., 2011). The dispersion of high molecular weight MAPP in PP matrix was at a low level during mixing, which keeps microdomains that help to reduce crack propagation and contribute to the higher unnotched Charpy Impact strength (Franco-Marquès et al., 2011).

Some coupling agents may cause the deterioration of tensile and flexural strength. Song et al. (2010) compared the mechanical performance of the plastic blends (PP, HDPE and PS)

with SEBS-g-MA, Maleic anhydride (MA) and dicumyl peroxide (DCP), the results show SEBS-g-MA significantly improved the impact strength. However, the flexural and tensile strength reduced. The similar effects of SEBS-g-MA on the impact performance of PP/talc composites are also reported (Denac et al., 2005). MAPP is effective in improving the tensile, flexural and impact properties of the short glass fibre filled PP composites, while SEBS-g-MA only improves the impact strength (Lin et al., 2015a). The application of coupling agent in some natural fibre filled composites has been reported to help to achieve desired mechanical properties (Gobi Kannan et al., 2014, Franco-Marquès et al., 2011, Kumar et al., 2017).

2.4.4 Conclusion

This section introduced the modification and improvement methods include the addition of fillers, polymer blending and use of compatibilisers and coupling agent.

The introduction of fillers starts with three commonly used fillers talc, calcium carbonate and aluminium hydroxide. These three mineral fillers have shown strong evidence on improving the mechanical properties of PP composites. The content of the fillers is a critical factor and will be further studied in the recycled PP based composites. Other important factors include the filler size, shape, dispersion, and surface adhesion with the polymer matrix. It is worth mentioning that these fillers may have opposite effects on the tensile and impact properties of PP composites, so the composite formula may need to be tailored for the specific requirements. This section also introduced glass fibre and recycled carbon fibre. Both two fibres have shown the potential to improve the mechanical properties of PP

composites. The fibre content and fibre-polymer matrix interfacial interaction are the crucial factors that influence the macroscale properties of the PP composites. A knowledge gap exists between short recycled carbon fibre and the performance of PP or RPP composites, where short recycled carbon fibre may be a cost-effective and eco-friendly way to significantly improve the recycled PP performance. HGB was introduced as another novel material, it seems to be effective in reducing density, improving flame retardancy and maintaining desired mechanical properties.

Polymer blending is a cost-effective way to develop a material with specific requirements. As the use of mineral fillers may cause the deterioration of impact properties, this study investigates PP/PE and PP/Rubber blends aimed to reinforce the mechanical properties of the RPP composites, especially the impact properties. In PP/PE blends, the content ratio of PP and PE should be carefully controlled to balance the tensile and impact behaviours. Compatibilisers are recommended to improve the interfacial adhesion of PP and PE to achieve high impact strength. PP/SEBS (SEBS-g-MA) blends were also reported effective in improving the impact properties. In RPP base composites, the effects of PE and SEBS (SEBS-g-MA) require further investigation.

As mentioned in the study of fillers and polymer blending, the compatibilisation of polymers and the interfacial adhesion between fillers and polymer matrix are the critical factors need to be considered. LLDPE-g-MA, PP-g-MA and SEBS-g-MA have shown great improvement in specific properties of PP composites. However, due to the complex processing, service history and recycling techniques, the recycled PP may have

some unexcepted impurities or constituents. It is unclear whether the selected compatibilisers and coupling agent can achieve the desired performance.

2.5 Mathematical tools for prediction and optimisation

Since the selected reinforcement technique tends to have diverse effects on different properties of the composites, our study has to investigate the correlations of resulting performance and influencing parameters. And it is crucial to find an effective method to decipher all of the key factors (Mehat and Kamaruddin, 2011). For example, for improving the manufacturing process, Taguchi method and principal component analysis (PCA) method can be used to improve the processing parameters. It has been reported that the Taguchi method and PCA can be very powerful tools used in the optimisation of the injection moulding condition of recycled plastic (Gu et al., 2014, Oktem et al., 2007, Kumar et al., 2015, Ayaz et al., 2016). Mehat and Kamaruddin (2011) used Taguchi method with the controlling factors including melt temperature, packing pressure, injection time and packing time to optimise the mechanical properties of recycled plastics, the results indicated that the flexural modulus of the part produced from recycled plastics can be optimised by adjusting the operating parameters, which is more economical than using additives. Parida et al. (2015) estimated the machining parameters for GFRP composite, Taguchi and response surface methods were applied to optimise the surface roughness. The result showed the feed rate has less impact on the surface roughness of the composite, and Taguchi method can be used to optimise the

drilling condition to minimise the surface roughness (Parida et al., 2015). Taguchi method is a cost-effective method for estimate an optimum setting for a product/process, based on the experimental design factors and their levels. The response surface method will develop a quadratic function to describe the performance of a product/process, and use the equation to find the optimum condition. To start a study, Taguchi method is a good tool for reducing the list of potential factors in a cost-effective and time-effective way and find the key factors that influence the performance of a product/process.

As the Taguchi method has been proved highly effective in processing procedure development, it may be also practical to improve the formula, especially for the dependent parameters. Taguchi design only uses a limited amount of trial to find the interactions between selected factors while the full factorial design is a design that every set of every factor appears with every set of every other factor (NIST, 2012a). At this stage, both the full factorial design and Taguchi method were applied in the experiment design. However, in the future, when the amounts of additives increases and the more dependent factors are introduced, it is crucial to use a highly effective method such as multi objectives algorithm, to optimise the formula, and both save cost and time.

2.5.1 Taguchi method

Taguchi method is a statistical method developed by Genichi Taguchi, it is widely applied in quality control, engineering, manufacturing etc. (Taguchi et al., 2007). And it is an important tool used for robust design and produces the products in a short time and relatively low cost (Kumar et al., 2015). In other

words, it is an experiment design tool that can reduce the variation of the product without eliminating the causes of the variation, and control both time and cost at a low level (Katie and Scott, 2000). Kumar et al. (2015) found that Taguchi optimisation method successfully helped to optimise the design parameters of the PP/corn fibre composites to obtain the tensile, flexural and impact properties. Some other research also proved the effectiveness of Taguchi method for optimising the composition and processing parameters in PP-based composites preparation (Ravi Kumar et al., 2017, Şahin et al., 2018, Ozcelik, 2011, Ayaz et al., 2016, Gu et al., 2014).

Yang and Tarnng (1998) summarise the steps for the parameter design based on Taguchi method:

- 1) identify the parameters that need to be evaluated;
- 2) choose the levels for the design parameters and potential interaction between these parameters;
- 3) select appropriate orthogonal arrays (OA) for the designed parameters;
- 4) process the experiment based on the designed formula;
- 5) analyse the results using S/N ratio and ANOVA;
- 6) select the optimal parameters;
- 7) verify the optimal parameter by the confirmation test.

2.5.1.1 Orthogonal arrays

An orthogonal array is a matrix that the columns of the arrays are balanced and orthogonal, which means every pair of columns, all factor combination occurs the same of times (Minitab.com, 2019a). And in the Taguchi method, it doesn't

contain any repeated rows. Orthogonal arrays are suggested to be used to check the existence of interactions and the reasons for non-reproducibility (Taguchi et al., 2007). The expression of the Taguchi orthogonal arrays is usually like the following formula (Taguchi et al., 2007):

$$L_a(b^c)$$

In which a is the number of runs, b is the number of levels and c is the number of factors.

For example, $L_9(3^4)$ stands for 9 runs, 4 factors at 3 levels design.

And Table 2-2 shows an example of L9 orthogonal array.

Table 2-2 L9 Orthogonal array example

Run \ Factor	1	2	3	4
1	1	1	1	1
2	1	2	2	2
3	1	3	3	3
4	2	1	2	3
5	2	2	3	1
6	2	3	1	2
7	3	1	3	2
8	3	2	1	3
9	3	3	2	1

2.5.1.2 S/N ratio

S/N ratio is short for the signal to noise ratio, which is a logarithmic function mainly aimed to optimise the design of the product, or improve the process, and minimise the noise

(variability) during the process (Rosa et al., 2009). For the Taguchi method design, the S/N function has to be chosen first. Minitab.com (2019b) provides three commonly used signal-to-noise ratios:

1. S/N ratio - larger is better (for example, agricultural production)

$$\frac{S}{N} = -10 \times \left(\frac{\log\left(\frac{1}{\sum Y^2}\right)}{n} \right) \quad (2.1)$$

2. S/N ratio - nominal is best, on-target, minimum variation (for example, the bodyweight)

$$\frac{S}{N} = -10 \times \log(\sigma^2) \quad (2.2)$$

3. S/N ratio - smaller is better (for example, pollution emission)

$$\frac{S}{N} = -10 \times (\log(\sum Y^2)/n) \quad (2.3)$$

Where Y is the experiment result at the test, n is the total number of experiment trials, σ is the standard deviation.

2.5.1.3 Analysis of variance (ANOVA)

Analysis of variance of a technique used to compare the means of samples (Hess and Hess, 2018). In the multi-factor model, it has a response variable (dependent) and one or more factor variables (independent) (NIST, 2012b). It is aimed to test the equality of some means and find statistically significant parameters. ANOVA has been widely used for the research of polymers. da Costa et al. (2007) used ANOVA as a tool to select and determine the best conditions for PP recycling. Altan (2010) applied the ANOVA methods for investigating the effects of melt temperature, injection pressure, packing pressure, packing time on the shrinkage of PP and PS composites (Altan, 2010). And ANOVA has been proved by other researchers as a powerful

technique for determining the dominant factors in influencing different properties of the polymers (Zheng et al., 2017, Ashenai Ghasemi et al., 2016, Daneshpayeh et al., 2016).

The analysis of variance consists of several factors (Minitab.com, 2021):

Sum of squares (SS)

SS_{total} is the total variation in the data.

$$SS_{\text{total}} = \sum_i \sum_j (y_{ij} - \bar{y}_{..})^2 \quad (2.4)$$

SS_{factor} is the estimated factor level mean around the overall mean

$$SS_{\text{factor}} = \sum_{i=1}^n (\bar{y}_i - \bar{y}_{..})^2 \quad (2.5)$$

SS_{error} is the deviation of the observation within its corresponding factor level.

$$SS_{\text{error}} = \sum_i \sum_j (y_{ij} - \bar{y}_i)^2 \quad (2.6)$$

Where y_{ij} is the value of jth observation at the ith factor level;

$\bar{y}_{..}$ is the mean of the observation at the ith factor level;

\bar{y}_i is the mean of all observations.

Degree of freedom (DF)

DF indicated the number of independent element in the sum of squares.

$$DF_{\text{factor}} = r - 1 \quad (2.7)$$

$$DF_{\text{error}} = n_T - r \quad (2.8)$$

$$DF_{\text{Total}} = n_T - 1 \quad (2.9)$$

Where n_T is the total number of observations;

r is the number of factor levels.

Means of squares (MS)

The calculation of mean square for the factor MS_{factor} :

$$MS_{factor} = \frac{SS_{factor}}{DF_{factor}} \quad (2.10)$$

The calculation of the mean square for error MS_{error} :

$$MS_{error} = \frac{SS_{error}}{DF_{error}} \quad (2.11)$$

F-value

F : the ratio between the mean of squares effect and the mean of squares error.

$$F = \frac{MS_{factor}}{MS_{error}} \quad (2.12)$$

F-test is used to see the significance of each factor (or interaction) on the response variable or signal-to-noise ratio.

P : p is the probability value that gives the degree of confidence at which the factor (or interaction) is significant. It was applied to check the F distribution table, in this study, $P < 0.05$.

2.5.2 Principal component analysis (PCA)

The principal component analysis was initially developed by Pearson in 1901, and the modern instantiation was formalised by Hotelling, who also developed the term of principal component (Pearson, 1901, Hotelling, 1933, Abdi and Williams, 2010).

PCA is one of the most important and powerful statistical technique for almost all scientific disciplines (Bro and Smilde, 2014, Abdi and Williams, 2010). It is a multivariate statistical method use orthogonal transformation to convert some variable which may have potential relations into linearly

uncorrelated variables to account for the variance of the original response (Fung and Kang, 2005). PCA was also extensively used for evaluating the performance of polymers (Song et al., 2014, Gu et al., 2016b, Gu et al., 2016a, Gu et al., 2014, Zheng et al., 2017). Abdi and Williams (2010) listed the goals of PCA,

- 1) extract the most important information from the data table;
- 2) compress the size of the data via only keep the most important information;
- 3) simplify the description of the data set;
- 4) analyze the structure of the observations and the variables.

The procedure for PCA is shown below:

1. Set up the original multiple response array:

$$X^0 = \begin{bmatrix} x_{11} & \cdots & x_{1n} \\ \vdots & \ddots & \vdots \\ x_{m1} & \cdots & x_{mn} \end{bmatrix} \quad (2.13)$$

where m is the number of trials and n is the number of the response.

2. Normalise the response

$$X = \begin{bmatrix} \tilde{x}_{11} & \cdots & \tilde{x}_{1n} \\ \vdots & \ddots & \vdots \\ \tilde{x}_{m1} & \cdots & \tilde{x}_{mn} \end{bmatrix} \quad (2.14)$$

3. Calculate the correlation coefficient array

$$R = \begin{bmatrix} r_{11} & \cdots & r_{1n} \\ \vdots & \ddots & \vdots \\ r_{m1} & \cdots & r_{mn} \end{bmatrix} \quad (2.15)$$

In which,

$$r_{jk} = \frac{\sum_{i=1}^n (x_{ij} - \bar{x}_j)(x_{jk} - \bar{x}_k)}{\sqrt{\sum_{i=1}^n (x_{ij} - \bar{x}_j)^2 \sum_{i=1}^n (x_{jk} - \bar{x}_k)^2}} \quad (2.16)$$

And \bar{x}_j, \bar{x}_k are the mean values of x_j and x_k .

4. Determine the eigenvalues and eigenvectors

The eigenvalues and eigenvectors are determined from the correlation coefficient array,

$$(R - \lambda_j)V_j = 0 \quad (2.17)$$

Where λ_j eigenvalues, $\sum_{j=1}^n \lambda_j = n$, $j=1, 2, \dots, m$; $V_j=(a_{j1}, a_{j2}, \dots, a_{jn})^T$ are the eigenvectors corresponding to the eigenvalues.

5. Calculate explained variations (EV)

$$b_j = \frac{\lambda_j}{\sum_{i=1}^n \lambda_i} \quad (2.18)$$

6. Calculate accumulative explained variations (AEV)

$$a_p = \frac{\sum_{j=1}^p \lambda_j}{\sum_{i=1}^n \lambda_i} \quad (2.19)$$

in which, b_j represents the explained variations (EV) of the j^{th} eigenvalue, and a_p represents the accumulative explained variations (AEV) of the p^{th} eigenvalue. Each eigenvalue has an associated eigenvector.

7. Calculate the final data

$$Y_{mj} = \sum_{i=1}^n x_m(i)V_{ij} \quad (2.20)$$

in which Y_{mj} is the j^{th} final data formulated from eigenvector V_{ij} of principal components in the analysis.

2.5.3 Conclusion

This section introduced the mathematical methods for experimental design, result analysis and formula optimisation. Taguchi method is used to simplify the multivariable experiment design, and to analyse the connections between selected factors and properties via ANOVA. Principle component analysis is a multivariate statistical method can be used for the formula

optimisation. These tools are used to serve the multivariable problems. Especially in some cases, the full factorial design method becomes extremely time-consuming or impossible.

2.6 Summary

In order to overcome the technical barriers of utilising recycled plastics in the automotive industry, this chapter first studied the degradation mechanism of the plastics. It helps to understand the weakness of recycled plastics and provides background knowledge for reducing properties deterioration.

The degradation of plastics can be roughly divided into two categories: degradation during plastic processing and during the service time. The thermal and thermo-oxidative degradation mainly occurs during the processing, such as extrusion, injection moulding, high processing temperature may deteriorate the end-product properties. During the service time, photo-oxidative degradation plays an important role. When the composite exposes to UV radiation, the specific molecular structure of the composites and the existence of impurities may accelerate the photodegradation. The review of the degradation will help to avoid inappropriate setting of heat temperature and processing time in further investigation. And it also provides the background information for the formula design of the composite in the aspect of reducing degradation during service life.

This chapter also reviewed the methods for improving the properties of plastics. The modification section studied the following sections:

- Fillers. Mineral fillers, include talc, calcium carbonate, mica and aluminium hydroxide etc., are commonly used for

reinforcing plastics. These traditional fillers are proved to be cost-effective and efficient. Glass fibre reinforced plastics (GFRP) and carbon fibre reinforced plastics (CFRP) are another two types of composites with superior mechanical performance. The high cost of CFRP limits the application area, the recycled carbon fibres showed a promising outlook in polymer manufacturing. Hollow glass beads (HGB) have the advantage of lightweight, and it has the potential to achieve good flame retardancy and mechanical properties. In this study, talcum and recycled carbon fibre were selected mainly aimed to improve the tensile and flexural properties of the composites. $\text{Al}(\text{OH})_3$ and HGBs were selected to increase the flame retardancy of the composites, $\text{Al}(\text{OH})_3$ and HGBs filled composites were also compared in terms of mechanical properties, densities and thermal properties.

- Polymer blending. It is a cost-effective way to get the desired properties, however, for some immiscible or partially miscible polymers, compatibilisers may be required to improve the phase adherence. PP blend with PE and rubber are mainly discussed aimed to improve the mechanical properties, especially the impact properties of the PP composites.
- Compatibilisers and coupling agent. Compatibilisers and coupling agent are effective additives to enhance the phase adherence of the polymers and improve the surface adhesion between plastics and fillers. PP-g-MA is reported efficient in improving the tensile, flexural and impact properties of the PP based composites. SEBS-g-MA might be a good option if high impact performance is required. In

this study, the effects of the selected coupling agent and compatibiliser on the tensile, flexural and impact properties of RPP based composites was investigated.

There are varieties of variables that influence the properties of the final product, and the product should meet a series of requirements to achieve the real industrial application. The mathematical method Taguchi method is proved as an effective tool to simplify the experimental design and optimise the performance of the PP-based composites. The principal component analysis is also used to evaluate the performance of the optimised formula. This study will investigate the effectiveness of these mathematical tools and simplify the experiment design with multi-variables.

2.7 Outlook

Chapter 1 introduced the reason why recycled plastics are rarely used in automotive applications, based on the analysis of the automotive plastics and plastics recycling market situation in China, the industrial RPP is set as the target polymer for further research.

Chapter 2 focus on the degradation mechanism of the polymers and the reinforcement method mainly focuses on the PP. The polymer blending, filler addition and the incorporation of compatibilisers and coupling agent may be feasible ways.

For different parts of the automotive applications, it is a big challenge to assess the feasibility of recycled plastics for certain automotive applications. The improved plastics should have reliable mechanical, thermal, rheological and flammability properties. There are several steps that have to be done:

1. Characterisation of recycled plastics. This part will identify the gaps between recycled plastics and industrial requirements, and also the weakness of recycled plastics.
2. Assessment of the performance of different fillers and additives. The effects of fillers and additives on selected properties will be evaluated.
3. Industrial trial. Provide a suitable formula for industrial trial and assess the performance.

This page is intentionally left blank.

Chapter 3 Experimental fundamentals

3.1 Introduction

The experimental parts can be divided into four sections in terms of the reinforcement of recycled plastics focusing on different properties.

Section 1: The raw material (VPP and RPP) was characterised and compared to the industrial requirements of different automobile parts. RPP/talc/MAPP/VPP composites were studied to achieve high tensile and flexural properties. The results were compared to the industrial requirements and the industrial trial was processed to make automobile armrest boxes.

Section 2: Polymer blending (RPP/LLDPE, RPP/LLDPE-g-MA) and elastomers (SEBS-g-MAH) were employed to compensate for the impact strength loss. RPP/LLDPE-g-MA/VPP, RPP/SEBS-g-MAH/talc and RPP/SEBS-g-MAH/Al(OH)₃ was studied to satisfy the requirements of automobile bumper.

Section 3: Short recycled carbon fibre (rCF) was usually regarded as a waste material, and it was applied as a novel filler for enhancing the comprehensive properties. MAPP was employed to improve the interfacial adhesion between rCF and PP matrix.

Section 4: Hollow glass bead (HGB) was selected as the lightweight filler for achieving lightweight, desirable mechanical properties and flame retardancy. Al(OH)₃ was selected as the flame retardant mineral filler for comparison with HGB.

The characterisation tests include the physical, mechanical, thermal and morphological properties. This chapter will give a

brief description of the selected materials, sample preparation process and characterisation tests.

3.2 Materials

3.2.1 Plastics

Virgin polypropylene (VPP):

VPP1: An injection grade of PP block copolymer produced by Dushanzi Sinopec, denoted EPS30R. VPP1 has a density of 0.89 g/cm³ and a melt flow index (MFI) of 2.01 g/10 min at 230°C under a load of 2.16 kg following ISO1133-1:2011.

VPP2: An injection grade of PP homopolymer with a trademark of H1500, produced by LG Chem Co., Ltd., Republic of Korea. The density and MFI of VPP2 are 0.9 g/cm³ and 10.97 g/10 min, respectively.

VPP3: An injection grade PP block copolymer with a trademark of PPB-M02D, was produced by Sinopec Maoming Co., Ltd., Guangdong, China. The density and MFI are 0.9 g/cm³ and 2.60 g/10 min, respectively.

LLDPE: An injection grade linear low-density polyethylene (LDPE) with a trademark of DFDA2001, was produced by Sinopec Guangzhou Co., Ltd., Guangdong, China. The density and MFI are 0.92 g/cm³ and 2.00 g/10 min, respectively.

RPP (RPP):

RPP1: The RPP pellets with a trademark of JC-PP-5A used in this study were purchased from Tianqiang Recycling Co., Ltd., Shanghai, China. It was recycled from post-customer storage bags. The density of RPP1 is 0.90 g/cm³, and the melt flow index is 11.0 g/10 min at 230°C under a load of 2.16 kg in accordance with ISO1133-1:2011.

RPP2: The RPP pellets with a trademark of PP-1003 used in this study were purchased from Tianqiang Recycling Co., Ltd., Shanghai, China. It was industrial recycled plastic. The density of RPP2 is 0.90 g/cm³, and the melt flow index is 1.70 g/10 min at 230°C under a load of 2.16 kg in accordance with ISO1133-1:2011.

RPP3: The RPP pellets with a trademark of PP-535 were purchased from Tianqiang Recycling Co., Ltd., Shanghai, China, and have a density of 0.91 g/cm³ and a melt flow index (MFI, at 230°C under a load of 2.16 kg according to ISO1133-1:2011) of 2.47 g/10 min. It was recycled from industrial production scraps.

RPP4: The RPP pellets with a trademark of PP-197 were obtained from Tianqiang Recycling Co., Ltd., Shanghai, China. The density of RPP3 is 0.89 g/cm³, and the melt flow index is 45.0 g/10 min at 230°C under a load of 2.16 kg in accordance with ISO1133-1:2011. The source of RPP4 is unspecified.

RPP5: The RPP pellets with a trademark of TQ-1006 were obtained from Tianqiang Recycling Co., Ltd., Shanghai, China. The density of RPP5 is 0.90 g/cm³, and the melt flow index is 7.96 g/10 min at 230°C under a load of 2.16 kg in accordance with ISO1133-1:2011. It was recycled from beverage caps.

3.2.2 Fillers

Talc: Talc used in this study was purchased from Ningbo Haike, a local supplier, has an average particle size of 12.5 μm and a density of 2.75 g/cm³.

Al(OH)₃: The Al(OH)₃ was supplied by Tonglai Chemicals CO., Ltd., Guangzhou, China. It has a density of 2.40 g/cm³ and a

median size of 13 μm .

Hollow glass bead (HGB): Two kinds of HGBs with the trademark of S60HS and iM30K were purchased from 3M™ Co., Ltd., USA. S60HS has a density of 0.6 g/cm^3 , and an average size of 30 μm . iM30K has a density of 0.6 g/cm^3 and an average size of 18 μm .

Recycled carbon fibre (RCF): The rCF material was kindly provided by Professor Steve J Pickering at the University of Nottingham, UK. The short carbon fibre was recovered in a fluidised bed process. The rCF has a density of 1.78 g/cm^3 .

3.2.3 Coupling agent and compabilisers

Maleic anhydride grafted polypropylene (MAPP): MAPP used in this study is bought from Nanjing Deba Chemical Co.,Ltd, has a density of 0.9 g/cm^3 and an MFI of 88.67 g/10 min at 230 °C under a load of 2.16 kg.

Maleic anhydride grafted linear low density polyethylene (LLDPE-g-MA): The LLDPE-g-MA with a trademark of 18350P was purchased from Arkema Co., Ltd., Paris, France. It has a density of 0.931 g/cm^3 , and the melt flow index is 3.8 g/10 min at 230 °C under a load of 2.16 kg.

Maleic anhydride grafted styrene ethylene butylene Styrene (SEBS-g-MA): SEBS-g-MA with a trademark of 1901 was purchased from Kraton Co., Ltd., US. It has a density of 0.91 g/cm^3 , and the melt flow index is 3.8 g/10 min at 230 °C under a load of 2.16 kg.

3.2.4 Others

Surfactant (SF): Polyoxyethylene (20)oleyl ether [guaranteed reagent grade] was purchased from xiya, Reagent CO., Ltd., China, with a density of 1.07 g/cm³.

3.3 Fabrication of composites

3.3.1 Plastic characterisation and Talc-filled RPP composites

3.3.1.1 RPP and VPP characterisation

The VPP and RPP were characterised and compared to the industrial requirements of different automobile parts. Table 3-1 listed the plastics characterised in this section.

Table 3-1 List of the plastics used in this section

Plastic	Source	Trade code
VPP1	Dushanzi Petrochemical Co., Ltd.	EPS30R
VPP2	LG Chem Co., Ltd.	H1500
rPP1	Post-customer storage bags	JC-PP-5A
rPP2	Industrial recycled plastics	TQ-1003
rPP3	Industrial production scraps	PP-535

After drying in an oven at 75°C for 12 h and manually well-mixed, all materials were compounded by a KRSHJ-20 co-rotating twin-screw extruder (as is shown in Figure 3-1), whose screw diameter is 20 mm and L/D=44, with processing temperatures profile was set at 170-180-185-190-190-190-185°C. The screw rotating speed was set at 150 rpm. The

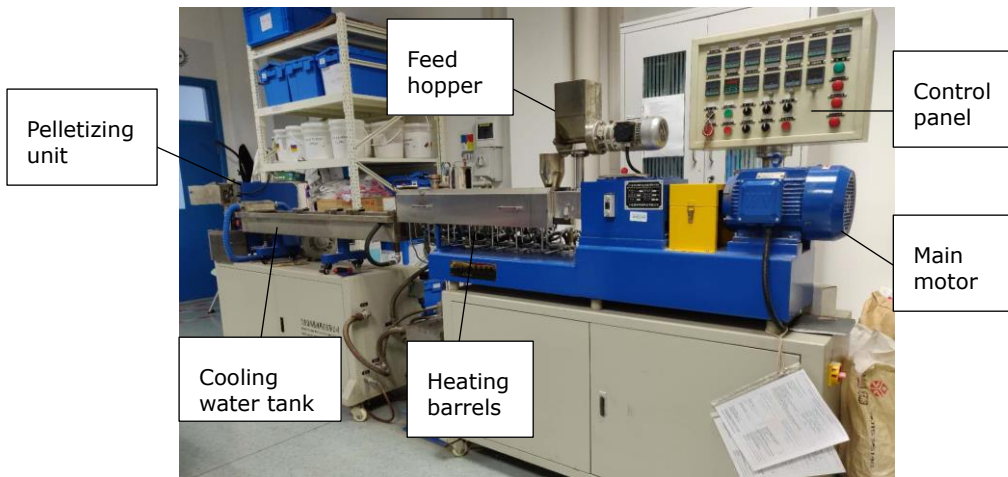


Figure 3-1 KRSJ-20 co-rotating twin-screw extruder

The pellets were dried at 75°C for 12 h before being injection moulded into ISO specimens using a Haitian MA1200/370 injection moulding machine (as is shown in Figure 3-2) in a temperature profile of 190-195-200-200-200°C.



Figure 3-2 Haitian MA1200/370 injection moulding machine

3.3.1.2 RPP/Talc/MAPP/VPP composites

Talc, MAPP, VPP2 and RPP1 were used to produce PP composites. MAPP was employed to improve the interfacial adhesion between talc and PP matrix to enhance the mechanical performance of the composites. The levels of selected

components are shown in Table 3-2.

Table 3-2 Selected components (VPP, talc and MAPP) and their levels

Components	Level 1	Level 2	Level 3
VPP2 (wt%)	20	40	60
talc (wt%)	5	10	20
MAPP (wt%)	0	2.5	5

The composition design employed the Taguchi method, which is shown in Table 3-3. If using the full factorial design, it needs $3^3=27$ series of experiments, while it only needs 9 groups in Taguchi L9(3^3) OA.

Table 3-3 Designed compositions based upon Taguchi L9 (3^3) OA

Trial No	VPP2 (wt%)	Talc (wt%)	MAPP (wt%)
1	20	5	0
2	20	10	2.5
3	20	20	5
4	40	5	2.5
5	40	10	5
6	40	20	0
7	60	5	5
8	60	10	0
9	60	20	2.5

The sample preparation procedure is the same as Section 3.3.1.1.

3.3.1.3 Industrial trial (Armrest box)

Two formulas were selected for making an automobile armrest box:

1. 52.5 wt% RPP3, 40 wt% VPP2, 5 wt%Talc and 2.5 wt%MAPP.

2. 30 wt% RPP3, 60 wt% VPP2, 5 wt%Talc and 5 wt%MAPP.
The sample preparation procedure and parameters are the same as in Section 3.3.1.1. The trial equipment was supplied by our industrial partner Shuanglin group co., LTD. Figure 3-3 shows the photo of the injection moulding machine used in Shuanglin group co., LTD.



Figure 3-3 Injection moulding machine in Shuanglin group co., LTD

3.3.2 RPP/PE and RPP/Elastomer blended composites

3.3.2.1 RPP/LLDPE, RPP/LLDPE-g-MA and RPP/SEBS-g-MA blending

LLDPE, LLDPE-g-MA and SEBS-g-MA were selected for improving the impact properties of the RPP composites. The RPP used here is RPP3. The compositions of LLDPE, LLDPE-g-MA and SEBS-g-MA were controlled at 5 wt%-20 wt%. Table 3-4 shows the composition of the samples in this study.

Table 3-4 RPP/(LLDPE, or LLDPE-g-MA, or SEBS-g-MA) formulations

NO.	RPP3(wt%)	LLDPE (wt%)	LLDPE-g-MA (wt%)	SEBS-g-MA (wt%)
1	100	-	-	-
2	95	5	-	-
3	90	10	-	-
4	80	20	-	-
5	95	-	5	-
6	90	-	10	-
7	80	-	20	-
8	95	-	-	5
9	90	-	-	10
10	80	-	-	20

After prepared by the designed composition, these samples are mixed and blended by a co-rotating twin-screw extruder. The twin-screw extruder used in this study was KRSHJ-20 from Kangrun machinery co. LTD, China, which has a 20 mm screw diameter and L/D of 44. The processing temperature profile was set at 175-185-195-200-200-200-195°C, from the first heating barrel beneath the feeding hopper to the die. Water cooling is used in this process and the cooled strands are subsequently pelletised. Then the pellets were oven-dried at 80°C for 10 h before the further injection moulding.

An MA1200/370 injection moulding equipment from Ningbo Haitian Precision Machinery Co., Ltd, China, was used to prepare the test specimen following the ISO standard for tensile, flexural and impact properties tests. The temperature profile of heating barrels was: 190-195-200-200-200°C. The injection pressure, injection speed, packing pressure and holding time was controlled at 40 MPa, 50 g/s, 40 MPa and 10 s, respectively. These parameters are controlled as the same for all the sample preparation and each test, at least 5 samples were prepared

for testing.

3.3.2.2 RPP/LLDPE-g-MA/VPP composites

Based on the results in Section 3.3.2, 10 wt% of LLDPE-g-MA was set as constant. The content of VPP3 was set as 10 wt% to 40 wt%. Table 3-5 shows the composition of the RPP/LLDPE-g-MA/VPP samples.

Table 3-5 RPP/LLDPE-g-MA/VPP formulations

NO.	RPP3 (wt%)	LLDPE-g-MA (wt%)	VPP3 (wt%)
11	80	10	10
12	70	10	20
13	60	10	30
14	50	10	40

The sample preparation process is consistent with the samples in Section 3.3.2.

3.3.2.3 RPP/SEBS-g-MAH/Al(OH)₃, RPP/SEBS-g-MA/Talc composites

Al(OH)₃ and Talc was selected to balance the reduction of tensile and flexural properties of RPP/SEBS-g-MA composites. The formulation and the sample designations were presented in Table 3-6.

Table 3-6 RPP, Al(OH)₃, Talc and SEBS-g-MA blending ratio

NO.	RPP3 (wt%)	Al(OH) ₃ (wt%)	Talc (wt%)	SEBS-g-MA (wt%)
1	95	5	-	-
2	90	10	-	-
3	80	20	-	-
4	95	-	5	-
5	90	-	10	-
6	80	-	20	-
7	85	10	-	5
8	80	10	-	10
9	70	10	-	20
10	85	-	10	5
11	80	-	10	10
12	70	-	10	20
13	75	20	-	5
14	70	20	-	10
15	60	20	-	20
16	75	-	20	5
17	70	-	20	10
18	60	-	20	20

The sample preparation process is consistent with the samples in Section 3.3.2.

3.3.3 Recycled short milled carbon fibre filled PP/RPP composites.

3.3.3.1 VPP/rSMCF/MAPP composites

VPP/rSMCF/MAPP composites use VPP1 as the base matrix. The short recycled carbon fibre, which is usually regarded as waste material, was used here to study the performance in VPP/rSMCF composites. MAPP was employed to improve the interfacial adhesion between the PP matrix and rSMCF surface. The composition of the blends was shown in Table 3-7.

Table 3-7 Weight fraction of the PP, RSMCF, SF and MAPP blends

Sample	PP	RCF	Surfactant	MAPP
1-1	PP	100	-	-
1-2	SF _{0.5} /PP	99.5	-	0.5
1-3	SF ₁ /PP	99	-	1
1-4	SF _{2.5} /PP	97.5	-	2.5
1-5	SF _{0.5} /PP/rSMCF ₁	98.5	1	0.5
1-6	SF ₁ /PP/rSMCF ₂	97	2	1
1-7	SF _{2.5} /PP/rSMCF ₅	92.5	5	2.5
1-8	SF _{0.5} /PP/MAPP ₁	98.5	-	0.5
1-9	SF ₁ /PP/MAPP ₂	97	-	1
1-10	SF _{2.5} /PP/MAPP ₅	92.5	-	2.5
1-11	SF _{0.5} /PP/rSMCF ₁ /MAPP ₁	97.5	1	0.5
1-12	SF ₁ /PP/rSMCF ₂ /MAPP ₂	95	2	1
1-13	SF _{2.5} /PP/rSMCF ₅ /MAPP ₅	87.5	5	2.5
1-14	SF _{2.5} /PP/rSMCF ₅ /MAPP _{2.5}	90	5	2.5
1-15	SF _{2.5} /PP/rSMCF ₅ /MAPP ₁₀	82.5	5	2.5
1-16	SF _{2.5} /PP/rSMCF ₅ /MAPP ₂₀	72.5	5	2.5

To ensure the dispersion performance of the recycled carbon fibre, the weight ratio of recycled carbon fibre and surfactant was controlled as 2:1. The content of recycled carbon fibre was controlled as 1 wt% to 5 wt%, the content of maleic anhydride was controlled as 1 wt% to 20 wt%. The sample preparation process consists of the dispersion of rSMCF, compounding PP/rSMCF and injection moulding process.

Dispersion of rSMCF

In this study, a combined process of the dispersion of rSMCF in the water and hot press to obtain well-dispersed recycled carbon fibre reinforced plastics (rCFRPs) were prepared. The process used in this study was adapted from the wet-laid process (Shah and J. Schubel, 2015). Firstly, the rSMCF and surfactant were mixed in the water with the mass ratio of 2:1. Then it was placed in an ultrasonic water bath for 1 hour at

room temperature and constantly stirred. Then the mixture was poured into a glass tray, which was covered with a 25 μ m PI film. The glass tray was dried in an oven at 90 °C for 24 hours with constant airflow to evaporate all the water content. Finally, a layer of well-dispersed rSMCF was obtained on the polyimide (PI) film. Figure 3-4 shows the dispersion process of rSMCF.

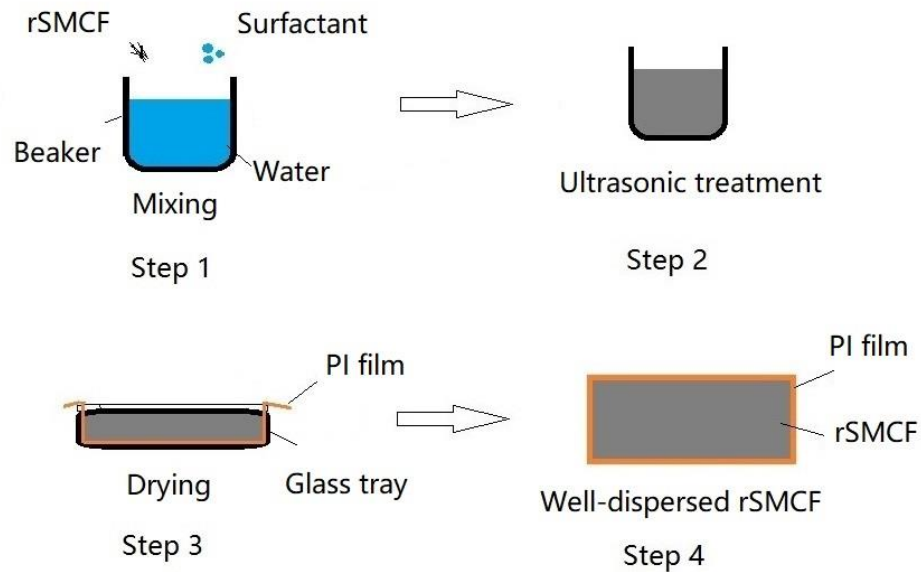


Figure 3-4 Process of rSMCF dispersion

Compounding PP and rSMCF

The dispersed rSMCF was then covered with evenly distributed PP pellets (and MAPP pellets where applicable) and compressed to obtain a plastic sheet by using a flat vulcanising machine from Dongguan Zhenggong Machinery Co., Ltd, China, Model ZG-201 (as is shown in Figure 3-5) at 180 °C and 80MPa for 3 min.



Figure 3-5 Zhengong ZG-201 flat vulcanising machine

Then the sheets were shredded by using a Retsch SM2000 cutting mill (as is shown in Figure 3-6) equipped with a 10 mm-by-10 mm square aperture sieve to get the shredded pellets.



Figure 3-6 Retsch SM2000 cutting mill

Figure 3-7 showed the example of the rCFRP sheet before and after shredding

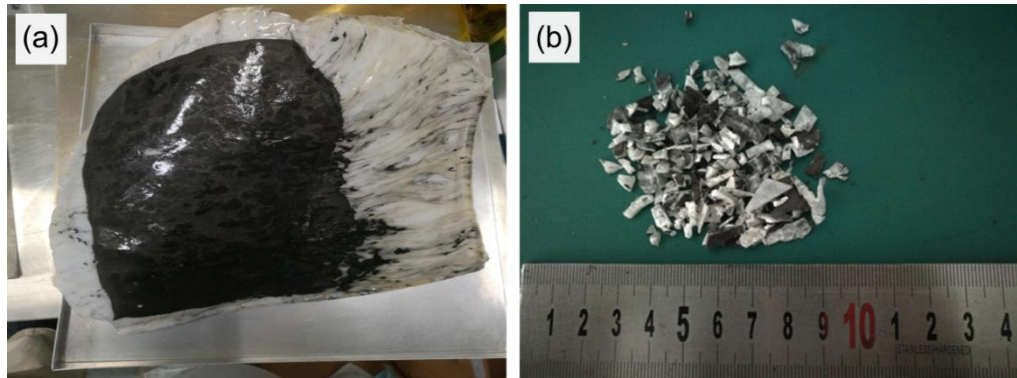


Figure 3-7 (a) rCFRP sheet before shredding (b) rCFRP pellets after shredding

After the shredding, the pellets were blended by using a twin-screw extrusion process. The processing temperature was set as 165-180-190-190-190-190-185°C, from the first heating barrel to the die. The screw rotation speed was set at 120rpm. The extruded plastics were air-cooled and then pelletised.

Injection moulding process

The PP/rCF pellets were then injection moulded to obtain the specimens according to ISO527-2:2012; ISO178:2010 and ISO180:2000. The temperature of the heating barrel was 190-195-200-200-200°C. The injection pressure was 50 MPa, injection speed was 60 g/s, packing pressure was at 60 MPa for 10 s, cooling time was 10 s and the mould temperature was 50°C.

3.3.3.2 RPP/rSMCF/MAPP composites

This part uses RPP5 as the base matrix to replace the VPP1 studied in section 3.3.3. The composition of the RPP/rSMCF/MAPP composites was shown in Table 3-8.

Table 3-8 Weight fraction of the RPP, RCF, SF and MAPP blends (wt%)

Sample		RPP5	RCF	Surfactant	MAPP
2-1	RPP	100	-	-	-
2-2	SF _{0.5} /RPP	99.5	-	0.5	-
2-3	SF ₁ /RPP	99	-	1	-
2-4	SF _{2.5} /RPP	97.5	-	2.5	-
2-5	SF _{0.5} /RPP/rSMCF ₁	98.5	1	0.5	-
2-6	SF ₁ /RPP/rSMCF ₂	97	2	1	-
2-7	SF _{2.5} /RPP/rSMCF ₅	92.5	5	2.5	-
2-8	SF _{0.5} /RPP/MAPP ₁	98.5	-	0.5	1
2-9	SF ₁ /RPP/MAPP ₂	97	-	1	2
2-10	SF _{2.5} /RPP/MAPP ₅	92.5	-	2.5	5
2-11	SF _{0.5} /RPP/rSMCF ₁ /MAPP ₁	97.5	1	0.5	1
2-12	SF ₁ /RPP/rSMCF ₂ /MAPP ₂	95	2	1	2
2-13	SF _{2.5} /RPP/rSMCF ₅ /MAPP ₅	87.5	5	2.5	5
2-14	SF _{2.5} /RPP/rSMCF ₅ /MAPP _{2.5}	90	5	2.5	2.5
2-15	SF _{2.5} /RPP/rSMCF ₅ /MAPP ₁₀	82.5	5	2.5	10
2-16	SF _{2.5} /RPP/rSMCF ₅ /MAPP ₂₀	72.5	5	2.5	20

The sample preparation process is the same as the process of preparing VPP/RCF/MAPP composites in section 3.3.3.

3.3.4 Hollow glass beads filled PP/RPP composites

3.3.4.1 VPP/HGB and VPP/Al(OH)₃ composites

VPP/HGB and VPP/Al(OH)₃ composites use VPP3 as the base matrix and by twin-screw extrusion and injection moulding process. The formulations were given in Table 3-9.

Table 3-9 VPP based composite formulation (wt%)

Sample code	VPP3	HGB(iM30K)	HGB(S60HS)	Al(OH) ₃
PP	100	-	-	-
PP-2.5iM30K	97.5	2.5	-	-
PP-5iM30K	95	5	-	-
PP-10iM30K	90	10	-	-
PP-2.5S60HS	97.5	-	2.5	-
PP-5S60HS	95	-	5	-
PP-10S60HS	90	-	10	-
PP-2.5Al(OH) ₃	97.5	-	-	2.5
PP-5Al(OH) ₃	95	-	-	5
PP-10Al(OH) ₃	90	-	-	10

After mixing, PP pellets and fillers were blended by a co-rotating twin-screw extruder (KRSHJ-20, China), which has a screw diameter of 20 mm and L/D of 44. The processing temperature was 175-185-195-200-200-200-195°C, from the first heating barrel beneath the feeding hopper to the die. Blended strands of the composites were quenched in a water bath and subsequently pelletised. The pellets were then dried in an oven at 80°C for 10 h before sampling.

The pellets were injection moulded into ISO standard tensile, flexural and Izod impact specimens by an injection moulding machine (Haitian MA1200/370, China). The temperature profile of heating barrels was: 190-195-200-200-200°C. For each composition, 5 specimens were prepared for the mechanical tests.

For flammability tests, samples were prepared using a vulcanising machine (or so-called hot compressor) model ZG-20T (Zhenggong™, Dongguan, Guangdong Province). This had an inner pressing space of 300 × 300 mm and a pressure capacity of 20 tons was used. The temperature of the hot process was set and maintained at 190°C. The sample

preparation procedure consisted of the following three phrases: (1). 70 MPa, kept for 200 s; (2). 75 MPa, kept for 100 s; (3). 80 MPa, kept for 60 s. 2 s decompression was used between any two phases to release the air within the pellets. After the hot press, the plates were applied to the cold press at room temperature which consisted of the same three phases: (1). 70 MPa, kept for 200 s; (2). 75 MPa, kept for 100 s; (3). 80 MPa, kept for 60 s. 2 s decompression was used between any two phases to release the air within the pellets. The dimensions of the specimen used for the flammability test was fixed to 125 × 12.5 × 3 mm.

3.3.4.2 RPP/HGB/MAPP composites

RPP/HGB/MAPP use RPP3 and RPP4 as the base matrix and the composites were prepared by twin-screw extrusion and injection moulding process. The formulations were given in Table 3-10.

Table 3-10 The designed formula for glass bubble filled RPP

Sample code	RPP wt%	iM30K wt%	MAPP wt%
RPP3	100	-	-
RPP3-2.5iM30K	97.5	2.5	-
RPP3-5iM30K	95	5	-
RPP3-10iM30K	90	10	-
RPP3-10iM30K-5MAPP	85	10	5
RPP4	100	-	-
RPP4-2.5iM30K	97.5	2.5	-
RPP4-5iM30K	95	5	-
RPP4-10iM30K	90	10	-
RPP4-10iM30K-5MAPP	85	10	5

The process of preparing RPP/HGB/MAPP composites was the same as the process described in section 3.3.4. This part only studied the mechanical properties of the RPP/HGB/MAPP

composites.

3.4 Characterisation methods

3.4.1 Tensile properties

The test of tensile properties followed the standard ISO 527-2:2012. The dimension of the injection moulded specimen follows type 1B. The tensile tests were performed on a Gotech TCS-2000NE universal testing machine with a full-scale load range of 20 kN at a fixed crosshead speed of 50 mm min⁻¹. The tensile modulus was obtained by an extensometer (Epsilon Technology Co.Ltd) at a tensile elongation of 1%.

Figure 3-8 shows a photo of the universal testing machine. Figure 3-9 shows an example of the standard tensile test specimen used in this study.



Figure 3-8 Photo of the universal test machine



Figure 3-9 Photo of a tensile test specimen

3.4.2 Flexural properties

The test of flexural properties followed the standard ISO 178-2010. Flexural tests were performed on a Gotech TCS-2000NE universal testing machine with a full-scale load range of 20 kN. The crosshead speed was 5 mm/min, and the span was 64 mm. The photo of the universal test machine was shown in Figure 3-8. Figure 3-10 shows an example of the standard flexural test specimen in this study.



Figure 3-10 Photo of a flexural test specimen

3.4.3 Impact properties

The test of impact properties followed the standard ISO 180-2001. The equipment used for testing is the impact test machine (Gotech GT-7045-NHR) shown in Figure 3-11. The impact test specimen for the un-notched test is the same as the flexural test specimen shown in Figure 3-10. The notched specimen is shown in Figure 3-12.



Figure 3-11 Photo of impact test machine



Figure 3-12 Photo of notched specimen for impact test

3.4.4 Rheological properties

The test of impact properties followed the standard ISO 1133. The equipment used for testing is the melt flow index tester (Gotech GT-7200-M1BH) shown in Figure 3-13. The nominal load used in this study is 2.16kg and the melt temperature is 230 °C.



Figure 3-13 Photo of melt flow index tester

3.4.5 Thermal properties

The thermal properties were carried out using the TG/DTA 6300 (Seiko, Japan). The photo of the TG/DTA 6300 was shown in Figure 3-14. In this study, samples with around 8 mg were heated from 40°C to 550°C with a heating rate of 10°C/min at the nitrogen gas condition, with a flow rate of 200 mL/min.



Figure 3-14 Photo of TG/DTA 6300

3.4.6 Flammability properties

The flammability properties were carried out using the FFT horizontal /vertical flame chamber shown in Figure 3-15 by following UL94 standard. The dimension of the specimen was 125 mm*13 mm*3 mm, the specimens were marked at 25 mm and 100 mm, as is shown in Figure 3-16. These specimens will be conditioned at 23°C for more than 48 hours. The flow rate of the methane gas was set as 105 ml/min. When the test started, the specimens were placed on clamps and ignited for 30 s. If the flame reached the 25 mm mark on the specimen within 30 s, the ignition device was removed. The time is taken for the flame to arrive 25 mm (denoted by ignition time) and

100 mm (denoted by end time) marks were recorded, and the burning rate (mm/min) between the marks was measured.



Figure 3-15 Photo of flame chamber



Figure 3-16 Photo of UL94 test specimen

3.4.7 Fourier transform infrared spectroscopy (FTIR) analysis

Fourier transform infrared spectroscopy (FTIR) study of the plastics were performed using a VTRTEX 70 (Bruker, Germany) at attenuated total reflectance (ATR) mode for 32 times and wavenumber resolution is 4 cm^{-1} . Figure 3-17 is the front photo of FTIR.



Figure 3-17 Photo of Fourier transform infrared spectroscope

3.4.8 Morphology study

The morphological study of the composites was carried out by scanning electron microscope using a Zeiss Sigma at an acceleration voltage of 3.00 kV as was shown in Figure 3-18. Before SEM observation, all samples were sputter-coated with a thin layer of gold to avoid electrical charging.

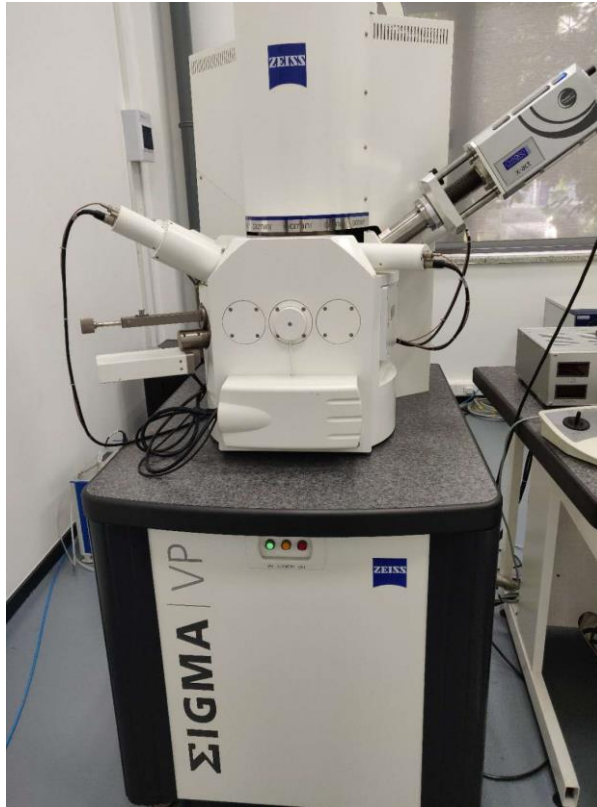


Figure 3-18 Photo of scanning electron microscope

3.4.9 Outsourced tests:

3.4.9.1 Differential Scanning Calorimetry

DSC was conducted to analyse the possible changes in crystallinity of the PP/rSMCF and RPP/rSMCF composites, using a Perkin Elmer, Pyris 7 thermal analyser. All DSC tests were carried out at constant heating and cooling rates of 10°C/min under an N₂ atmosphere. Specimens were initially heated to 200°C for 4 min before cooling to room temperature. The second heating cycles were performed to 180°C for 20 min. Melting temperature (T_m) and crystal content (χ_0) were obtained from the second heating cycle to elucidate the effects of previous thermal treatments (da Costa et al., 2007). T_m was determined at the maximum peak of the endothermic curve,

and χ_0 was calculated according to Equation 1, with respect to the crystallisation enthalpy and PP content (Al-Maadeed et al., 2014).

$$\chi_0 = \frac{\Delta H_{m1}}{f \cdot \Delta H_{m1}^0} \quad (3.1)$$

where ΔH_{m1} is the enthalpy of fusion, ΔH_{m1}^0 is the enthalpy of fusion of 100% crystalline isotactic PP which set at 209 J/g according to da Costa et al. (2007), and f is the effective PP weight fraction in the composite.

In this study, the selected RPP was found polluted by PE, the ratio of PP in PP/PE blends was measured by (Shimadzu, 2017):

$$f = \frac{\Delta H_{m1}}{\Delta H_{m1}^0} / \left(\frac{\Delta H_{m1}}{\Delta H_{m1}^0} + \frac{\Delta H_{m2}}{\Delta H_{m2}^0} \right) \quad (3.2)$$

Where ΔH_{m2} is the specific heat of melting of completely crystalline PE, ΔH_{m2}^0 is set as 293 J/g (Aumnate et al., 2019).

3.4.9.2 Cone calorimeter test

The cone calorimeter test (CCT) was performed for the PP/HGB composites by the cone calorimeter device (Fire Testing Technology, UK) according to the ISO 5660 standards. The dimension of the sample was controlled as 100*100*3 mm. The specimens were exposed to the external heat flux of 35 kW/m².

This page is intentionally left blank.

3.5 Industrial requirement

The industrial requirement of varies automotive applications were provided by Shuanglin group co., LTD. Table 3-11 indicates the details of the mechanical parameters, test standards and the required values.

Table 3-11 Mechanical properties requirements for the automobile parts (Part 1)

NO.	Parameters	Standard test conditions, Units	Material categories								
			PP-01#	PP-02#	PP-03#	PP-04#	PP-05#	PP-06#	PP-07#	PP-08#	PP-09#
1	Tensile strength	ISO 527-1/2:2012, MPa	≥13	≥15	≥20	≥20	≥20	≥22	≥18	≥30	≥27
2	Elongation at break ²	ISO 527-1/2:2012, %	/	≥50	≥30	≥20	≥25	≥15	≥20	/	/
3	Flexural strength	ISO 178:2010, MPa	/	≥20	≥35	≥30	≥27	≥30	≥26	≥40	≥38

Table 3-11 Mechanical properties requirements for the automobile parts (Part 2)

NO.	Parameters	Standard test conditions, Units	Material categories								
			PP-01#	PP-02#	PP-03#	PP-04#	PP-05#	PP-06#	PP-07#	PP-08#	PP-09#
4	Flexural modulus	ISO 178:2010, MPa	1300-1700	≥1100	≥2000	≥1800	≥1500	≥2000	≥1500	/	/
5	Unnotched impact strength	ISO 180:2000;kJ/m ²	NB/PB ¹	/	/	/	/	/	/	≥20	≥20
6	Notched impact strength	ISO 180:2000,kJ/m ²	≥35	≥15	≥15	≥10	≥10	≥10	≥8	≥2.5	≥2.3
7	Notched impact strength at -30°C	ISO 180:2000,kJ/m ²	≥5	≥3.5	≥4	≥2.8	≥3	≥3	≥2.8	/	/
Applicable products ²			Bumper (HE)	Bumper (ME)	Dashboard (ME)	Dashboard (LE)	Door panel (ME)	Column board (ME)	Door panel (LE)	shell of air conditioner /armrest box (ME)	shell of air conditioner/armrest box (LE)
Remark			1: NB/PB means no broken/partial broken. 2. Only for reference, not a strict requirement 2: HE means high-end, ME means middle-end, LE means lower-end								

Chapter 4 Plastics characterisation and talc-filled RPP composites

4.1 Introduction

As previously indicated recycled plastics' quality, quantity and consistency are the crucial factors for automobile manufacturers (Recycling today, 2017). The recycled plastics used in this study were provided by a Chinese listed enterprise, Tianqiang Recycling Co., Ltd., Shanghai, China. Both selected recycled plastics and virgin plastics were characterised at the start of this study, it allows the comparison between selected plastics and potential automobile applications. The main objective of this chapter is to assess the feasibility of talc-filled RPP composites for specific auto parts.

As mentioned previously in chapter 2, several important factors influence the performance of talc-filled PP/RPP composites: 1) content of talc; 2) interfacial adhesion between talc and PP matrix (Weon and Sue, 2006, Ashenai Ghasemi et al., 2016, Gu et al., 2016b). So in the experimental design, different concentration of talc filler (5 wt%, 10 wt%, 20 wt%) was added to the RPP matrix. The composition of talc is controlled lower than 20 wt% for the ease of extrusion (relatively higher MFI) and avoid severe impact deterioration (Leong et al., 2004). The compounding was performed using a twin-screw extrusion process to effectively mix the talc in the PP matrix (Nekhlaoui et al., 2015, Weon and Sue, 2006). Three levels (0, 2.5 wt%, 5 wt%) of coupling agent MAPP was also applied to improve the

interfacial adhesion between talc and RPP matrix. The talc-filled RPP composites are expected to have improved tensile and flexural properties, but the deterioration of impact properties may occur (Premalal et al., 2002, Wang et al., 2013). Three levels (20 wt%, 40 wt%, 60 wt%) of VPP was incorporated to balance the tensile and flexural performance of the talc-filled RPP composites.

An industrial trial was conducted aimed to produce a real automobile part. The use of the raw materials for the industrial trial was prepared in our lab, and the industrial partner provides technical support and instructions during the trial. The industrial trial was processed in the workshop of Shuanglin Group Co., Ltd. The performance and cost savings of the product were assessed.

So, there are three sections in this chapter, as is shown in Figure 4-1.

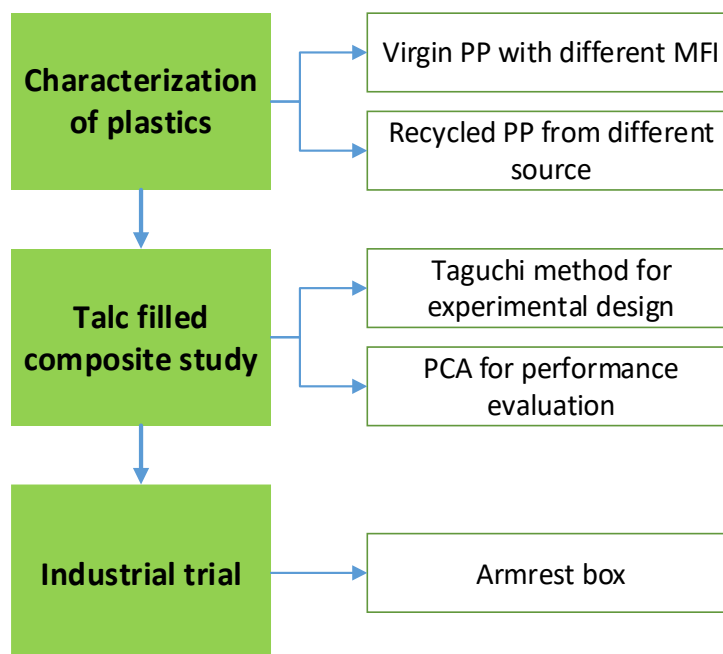


Figure 4-1 The flow chart of Chapter 3

- Section 1. Characterisation of plastics.

The mechanical properties of the obtained raw material - RPP and VPP pellets were characterised. These RPP pellets were mechanically recycled without any further modification, and the VPP pellets were pure PP. The results were compared with the industrial requirements of specific auto parts. The strengths and weaknesses of RPP and VPP were identified.

- Section 2. Talc filled RPP composites

This investigation aims to significantly improve the tensile and flexural properties of those automobile parts with high tensile and flexural requirements. The content of talc, MAPP and virgin PP was selected as the control parameters. Taguchi method, ANOVA and PCA techniques were applied for the optimisation and evaluation of the formula.

- Section 3. Industrial trial

This section is an industrial trial based on cooperation with our industrial partner. Due to the limitation of the mould, the plastic amount for trial and the properties requirements, the formulas for making automobile armrest box were selected for this industrial trial. An economic analysis was also given in this section. Figure 4-2 shows the photo of the injection moulding machine and the manufactured armrest box.



Figure 4-2 a) Internal view of the injection moulding machine;
b) top view of the manufactured armrest box

4.2 Plastic characterisation

4.2.1 Materials

Three kinds of RPP and two kinds of VPP were selected. The source and trade code of these plastics are shown in Table 4-1.

Table 4-1 List of the plastics used in the experiments

Virgin material	Source	Trade code
VPP1	Dushanzi Petrochemical Co., Ltd.	EPS30R
VPP2	LG Chem Co., Ltd.	H1500
RPP1	Recycled from post-customer storage bags by Tianqiang Recycling Co., Ltd.	JC-PP-5A
RPP2	Recycled from industrial recycled plastics by Tianqiang Recycling Co., Ltd.	TQ-1003
RPP3	Recycled from industrial production scraps by Tianqiang Recycling Co., Ltd.	PP-535

VPP1 is designed for the use of high load packages, pass boxes, and paint buckets. VPP2 is designed for houseware and toys. The applications of these plastics can be extended to other fields depending on the specific application requirements. The selected RPPs are provided by Tianqiang Recycling Co., Ltd., which is China's listed company, to ensure the quality and quantity stability of the plastics. The selected RPPs are recycled from different sources, the mechanical properties will be detailed characterised at the beginning of this study.

4.2.2 Characterisation Results

The RPP and VPP specimens were prepared by twin-screw extrusion and injection moulding followed the same processing parameters as mentioned in Chapter 3. The mechanical

properties of the selected VPP and RPP were shown in Table 4-2.

Table 4-2 Experiment results of the plastic characterisation

Properties	VPP1	VPP2	RPP1	RPP2	RPP3
Tensile modulus (MPa)	1206	1625	1239	1456	1430
Tensile strength (MPa)	27	35	25	26	25
Elongation at break %	92	20	25	50	55
Flexural modulus (MPa)	1233	1506	1162	1465	1293
Flexural Strength (MPa)	31	41	30	35	33
Notched impact strength (kJ/m ²)	46	3	4	8	12
Unnotched impact strength (kJ/m ²)	97	66	50	81	109
-30 °C, Notched impact strength (kJ/m ²)	8	2	2	3	3

It is shown in Table 4-2 that the mechanical properties of VPP with a different trademark can vary considerably. To have a better understanding, RPP1, RPP2 and RPP3 were compared with VPP1 and VPP2, which set the values of VPP1 and VPP2 as standard 100% value. The comparison results were shown in Table 4-3.

Table 4-3 The comparison of the mechanical properties of RPP with VPP

Plastic Samples	RPP1	RPP2	RPP3	RPP1	RPP2	RPP3
Properties	Set VPP1 as 100%			Set VPP2 as 100%		
Tensile modulus (MPa)	103%	121%	119%	76%	76%	88%
Tensile strength (MPa)	93%	96%	91%	73%	73%	72%
Elongation at break %	27%	55%	60%	127%	127%	276%
Flexural modulus (MPa)	94%	119%	105%	77%	77%	86%
Flexural Strength (MPa)	97%	115%	107%	73%	73%	81%
Notched impact strength (kJ/m ²)	9%	18%	25%	137%	137%	387%
Unnotched impact strength (kJ/m ²)	51%	83%	112%	75%	75%	166%
-30°C, Notched impact strength (kJ/m ²)	30%	36%	41%	115%	115%	158%

The results indicated that RPP1, RPP2 and RPP3 have close tensile modulus, tensile strength, flexural modulus and flexural strength to VPP1. The notched impact strength and notched impact strength at -30 °C are the key factors that could limit the RPPs being applied in the same field of VPP1. As for VPP2, due to the low base value, RPPs especially RPP3, showed better results in notched impact strength. However, VPP2 has the highest tensile modulus, tensile strength, flexural modulus and flexural strength among all of these selected PP. These mechanical properties were compared with the requirements in Table 3-11. By comparing the results in Table 4-2 and the requirements in Table 3-11, Figure 4-3 showed the potential of the raw materials for the listed industrial applications. Although these recycled plastics may have the potential for most of the applications, the connected applications in Figure 4-3 were more likely achieved at the early stage. As the properties may have inter-relations, the reinforcement method may have opposite effects on different applications.

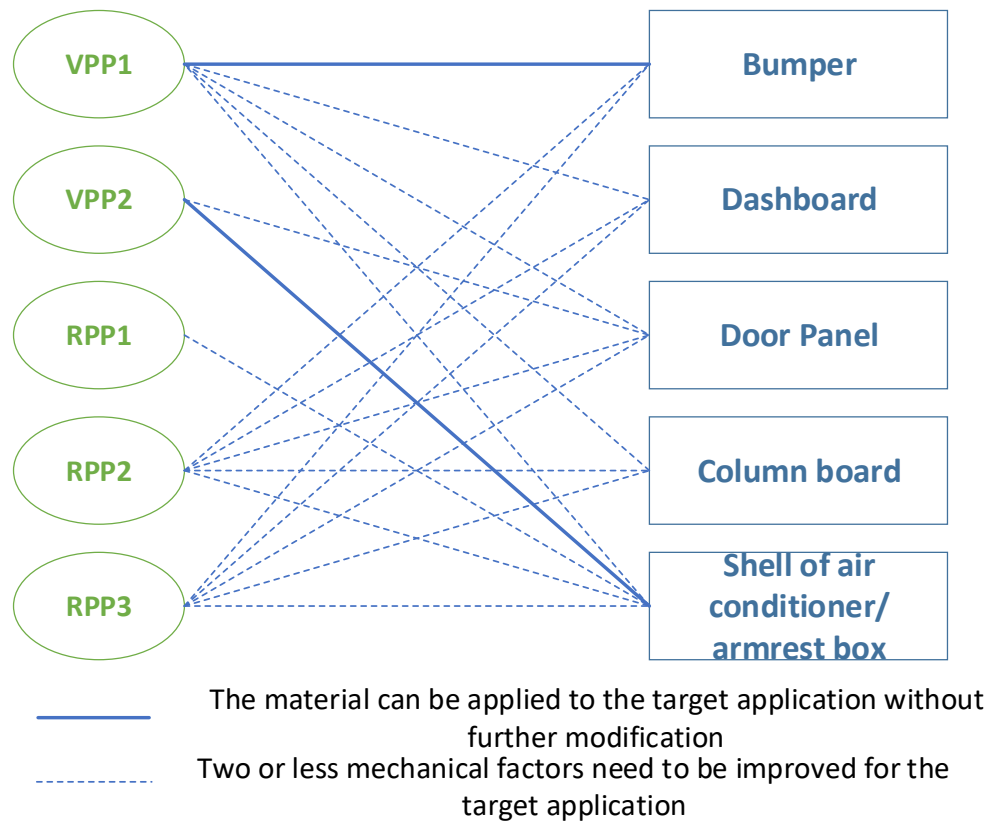


Figure 4-3 Potential applications of RPP and VPP

The features of these selected plastics were further discussed in the following sections:

4.2.2.1 VPP1

Feature: High impact properties, low flexural modulus

VPP1 was found to have the potential for making most of the automobile parts in Table 3-11 with modification. As shown in Figure 4-3, VPP1 meets all the mechanical requirements for the middle-end bumper. It may also be used for the high-end bumper following modification of the flexural modulus. For other applications like a dashboard, door panel and column board, the main weakness of VPP1 is the flexural modulus. Middle-end dashboard requires a flexural modulus of 2000 MPa, which is the highest among these applications. The tensile

strength and flexural strength of VPP1 is 10% and 22.5% lower than the middle-end shell of an air conditioner.

4.2.2.2 VPP2

Feature: High tensile strength, high flexural modulus and strength, low notched impact strength.

VPP2 can be directly used as the raw material for the shell of an air conditioner. As the shell of the air conditioner needs high tensile and flexural strength but low requirements on impact strength. The low notched impact of VPP2 is the major obstacle for extending to the other applications.

4.2.2.3 RPP1

Feature: low tensile strength, low flexural modulus and strength, low impact properties.

Figure 4-3 showed that RPP1 is could be applied to the shell of an air conditioner. To achieve this, improvements are needed to the tensile strength from 25 MPa to at least 27 MPa and the flexural strength from 30 MPa to 38 MPa. The notched impact strength has to be kept higher than 2.3 kJ/m². The notched impact strength is one of the major weaknesses of RPP1. It would be difficult for RPP1 to be applied in bumpers, for the middle-end and high-end bumpers, the notched impact strength has to be improved by 275% and 1033.3%, respectively. Even for the lower-end door panel, the notched impact strength has to achieve 100% improvement to reach the minimum requirement. Flexural modulus is another factor that hinders the application of RPP1. RPP1 has the lowest flexural modulus among these five plastics.

4.2.2.4 RPP2

Feature: High flexural modulus and flexural strength, relatively low impact properties.

Compared to VPP1, the flexural modulus and strength of RPP1 are 18.8% and 15.2% higher. The notched impact strength at room temperature and at -30 °C of RPP2 is 82% and 64% lower than VPP1. RPP2 may not be able to be applied in bumpers, but for most of the other automotive applications. RPP2 is as competitive as VPP1.

4.2.2.5 RPP3

Feature: Relatively high impact strength (among RPPs), Low tensile strength.

RPP3 has some properties that could make it more useful compared to VPP1. RPP3 has a relatively high impact strength, which meets the requirements of the low-end dashboard, door panel, column board and shell of an air conditioner. It might be a challenge for RPP3 to be applied for bumpers. But for the rest of the applications, the effort should be put on improving the tensile strength, flexural modulus and flexural strength.

4.3 Talc reinforced RPP composites

Based on the study in previous plastic characterisation, the mechanical properties of VPP1 meet the requirements of the bumper, and VPP2 can be applied to the shell of an air conditioner or armrest box. RPP2 and RPP3 have the potential for most of the provided automobile parts. Compared to RPP2, RPP3 maintained better flexural strength and notched impact strength. So RPP3 was selected for this section.

In this section, talc was incorporated to improve the tensile and flexural performance of the RPP composites. The Taguchi method was employed for the formulation design, the designed compositions were shown in Table 4-4.

Table 4-4 Designed compositions based upon Taguchi L9 (3³) OA.

Trial No	VPP2 (wt%)	Talc (wt%)	MAPP (wt%)
1	20	5	0
2	20	10	2.5
3	20	20	5
4	40	5	2.5
5	40	10	5
6	40	20	0
7	60	5	5
8	60	10	0
9	60	20	2.5

RPP3 was selected as the base material, the content of VPP2, talc, and MAPP was selected as the parameters to be evaluated. Formulas will be optimised to obtain the composite with the best tensile and flexural properties. Taguchi method and principal component analysis were applied for the design and optimisation of the composition formula.

It was reported that the optimal amount of MAPP for PP composites is 3.9 wt% (Homkhiew et al., 2014), 4 wt% (Ashenai Ghasemi et al., 2016). So in this study, the maximum content of MAPP was set as 5 wt%, which is slightly higher than 4 wt%. The maximum amount of Talc was set as 20 wt%, for the stable processing of twin-screw extrusion of the equipment. The maximum content of VPP was set as 60 wt%, as the industrial partner prefer high content of VPP.

4.3.1 Results and discussions

4.3.1.1 Analysis of S/N ratios

As mentioned in Chapter 2, Section 2.5.1, S/N ratio is a logarithmic function mainly aimed to optimise the design of the product, or improve the process, and minimise the noise (variability) during the process (Rosa et al., 2009). Equation 2.1, 2.2 and 2.3 in Section 2.5.1 are commonly used for calculating the S/N ratio.

In this study, as larger mechanical properties are preferred, the S/N ratio ratios of the tested mechanical properties were calculated using a 'larger is better' equation (Equation 2.1) as shown below:

$$S/N = -10 \log_{10} \left(\frac{1}{n} \sum_{i=1}^n \frac{1}{y_i^2} \right) \quad (2.1)$$

In which n is the total number of trials, y_i is the i th experiment at the test.

The results of the tensile modulus (TM), tensile strength (TS), flexural modulus (FM), flexural strength (FS) and their S/N ratio are shown in Table 4-5.

Table 4-5 Mechanical results and the corresponding S/N ratio
based upon Taguchi L9 (3³) OA

Trial No	TM	S/N of TM	TS	S/N of TS	FM	S/N of FM	FS	S/N of FS
1	1460	63.37	26.29	28.39	1575	63.95	36.43	31.23
2	1720	64.68	26.14	28.35	1707	64.63	37.43	31.46
3	1991	65.96	25.43	28.09	2041	66.19	38.56	31.72
4	1583	63.99	28.62	29.13	1644	64.32	38.83	31.78
5	1658	64.39	28.49	29.09	1808	65.14	40.03	32.05
6	1883	65.54	25.52	28.14	2000	66.02	38.8	31.78
7	1607	64.12	30.91	29.8	1694	64.57	41.12	32.28
8	1653	64.36	29.09	29.28	1783	65.02	40.38	32.12
9	2161	66.67	28.69	29.15	2130	66.56	42.97	32.66
Note: The unit for TM, TS, FM and FS is MPa								

The correlation of the weight fraction of VPP, talc, and MAPP on the S/N ratio of TM, TS, FM and FS are shown in Figure 4-4 to Figure 4-7.

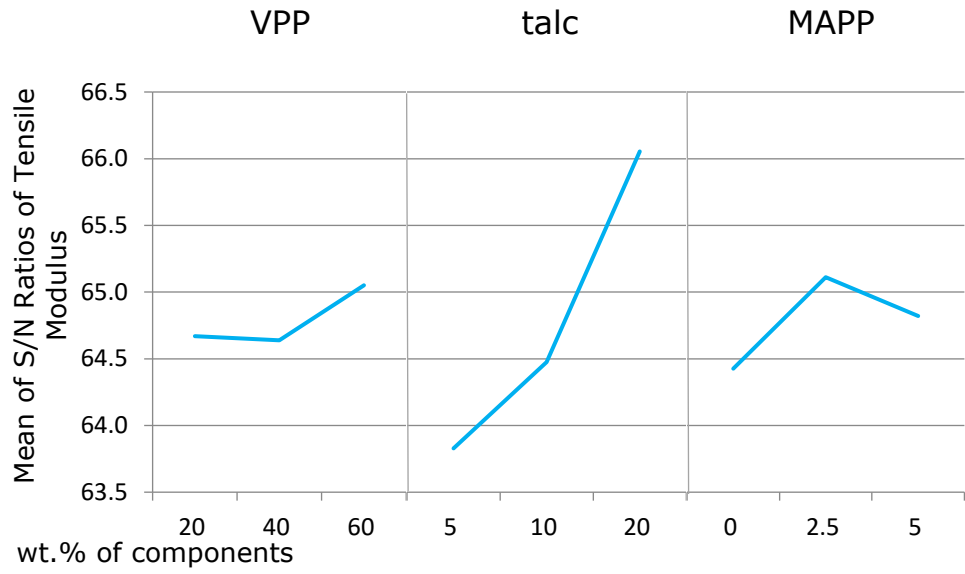


Figure 4-4 Plot of S/N ratios against the selected components for TM

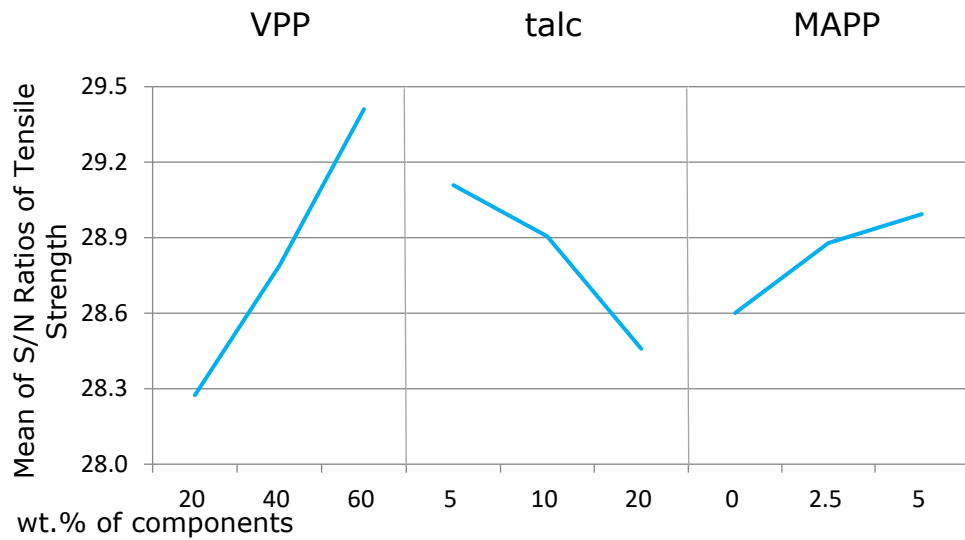


Figure 4-5 Plot of S/N ratios against the selected components for TS

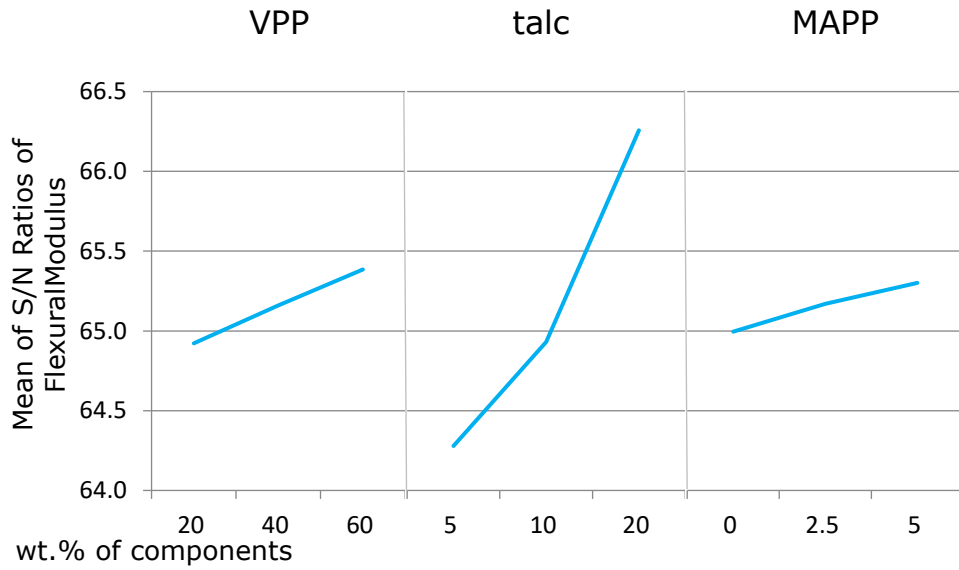


Figure 4-6 Plot of S/N ratios against the selected components for FM

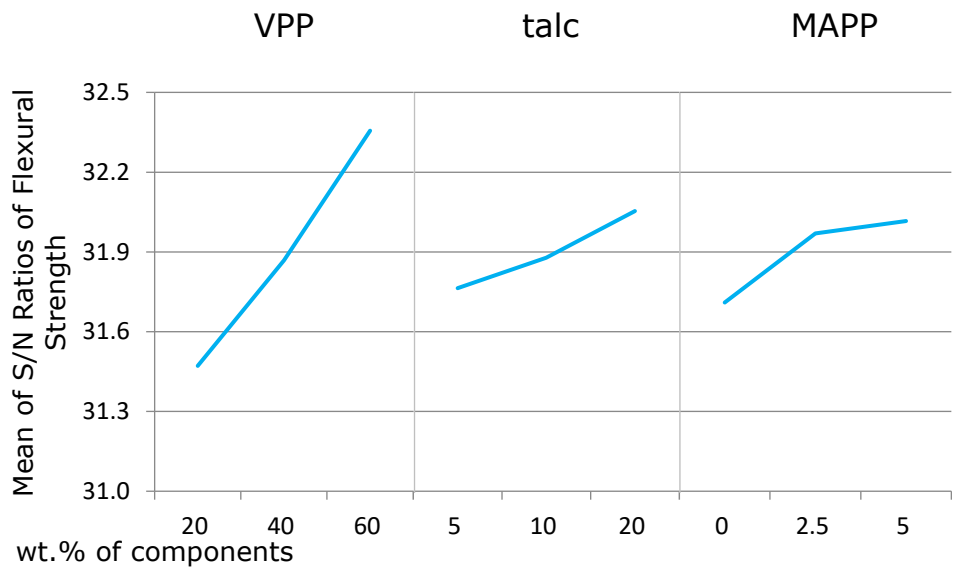


Figure 4-7 Plot of S/N ratios against the selected components for FS

Based on the S/N calculation equation, the high value of S/N ratio requires both high mechanical properties (TM, TS, FM, FS)

and low deviations of the tested values in the same group.

Figure 4-4 to Figure 4-7 indicated that VPP has positive effects on TM, TS, FM and FS. As is shown in Table 4-3, VPP2 has better performance of TM, TS, FM and FS than RPP3, so the addition of VPP content is expected to improve the performance of TM, TS, FM, and FS properties of the composites. The S/N ratio results showed that the content of VPP is the most significant factor in improving TS and FS.

Figure 4-4 and Figure 4-6 shows talc is the most influencing factor in controlling TM and FM. Figure 4-8 shows the talc is well dispersed in the RPP matrix. TM and FM increased by 29.79% and 25.57% when the talc content increased from 5 wt% to 20 wt%. This finding is in accordance with our previous findings (Gu et al., 2016a). As for the coupling agent MAPP, small content (2.5 to 5 wt%) can also have a high contribution to the TS and FS. At 5 wt% MAPP, the tensile modulus of the composite may deteriorate.

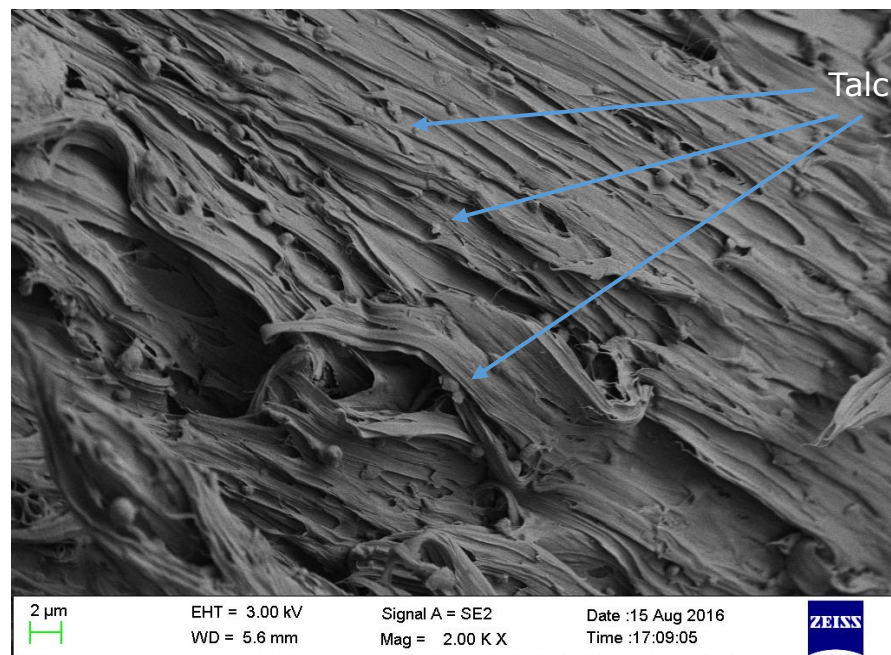


Figure 4-8 SEM image of the tensile fracture surface of the specimen with 20 wt%VPP, 10 wt% talc and 2.5 wt% of MAPP

An interaction plot is a graphical tool that shows the interactions or dependencies between variables (Lovie, 2005). The interaction plot of talc × MAPP, VPP × MAPP, and VPP × talc for tensile modulus was plot in Figure 4-9.

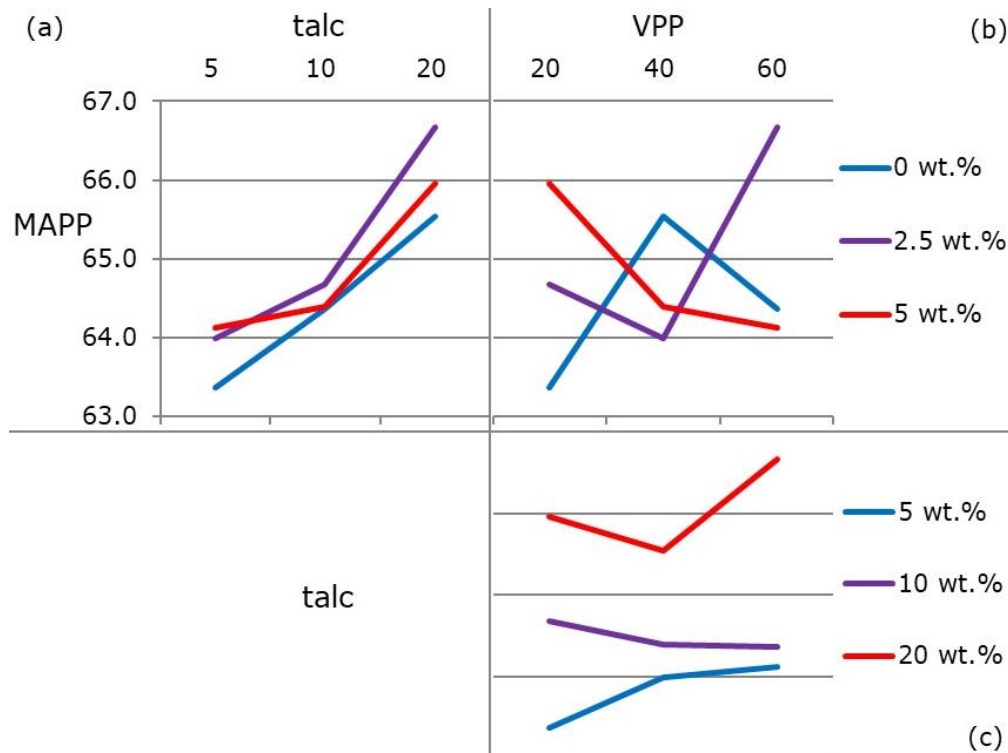


Figure 4-9 Interaction plots of (a) talc × MAPP, (b) VPP × MAPP, (c) VPP × talc, for TM

To draw the interaction plot, Figure 4-9 (a) was used as an example, the following line was plotted:

Blue line (MAPP at 0 wt%): S/N ratio of TM of trial No.1 (0 wt% MAPP, 5 wt% talc), No.8 (0 wt% MAPP, 10 wt% talc) and No.6 (0 wt% MAPP, 20 wt% talc).

Purple line (MAPP at 2.5 wt%): S/N ratio of TM of trial No.4(2.5 wt% MAPP, 5 wt% talc), No.2 (2.5 wt% MAPP, 10 wt% talc) and No.9 (2.5 wt% MAPP, 20 wt% talc).

Red line (MAPP at 5 wt%): S/N ratio of TM of trial No.7 (5 wt%

MAPP, 5 wt% talc), No.5 (5 wt% MAPP, 10 wt% talc) and No.3 (5 wt% MAPP, 20 wt% talc).

These interaction plot represent the S/N value when talc and MAPP, or VPP and MAPP, or VPP and talc composition were controlled. The average S/N ratios of the mechanical properties are shown in the vertical axis in the figures, while the variation of the components is shown in the horizontal axis.

In the interaction plots, the parallel lines mean no interaction occurs, while the nonparallel lines mean the interaction occurs (hp, 2019). In Figure 4-9 (a), the three lines are almost parallel, which means when the content of talc increase from 5 wt% to 20 wt%, whatever the value of MAPP is (0-5 wt%), the tendency of the corresponding S/N ratio is similar. So, the interaction of talc and MAPP on the S/N ratio of TM is insignificant in this study.

The interactions between VPP and MAPP on TM are most significant, followed by VPP and talc. In the VPP × MAPP interactions of TM (Figure 4-9 (b)), the S/N ratios of 0 wt% MAPP is initially increased with increasing VPP content and finally decreased, while the S/N ratios of 2.5 wt% MAPP show an opposite pattern, decreased initially and later increased with VPP content. The S/N ratios of 5 wt% MAPP are decreasing with VPP content. In the VPP × talc interactions of TM (Figure 4-9 (c)), the S/N ratios of 5 wt% talc and 10 wt% talc show little change with VPP content, while the S/N ratios of 20 wt% talc are initially decreased and eventually increased with VPP content.

The interaction plot of tensile strength was plot in Figure 4-10.

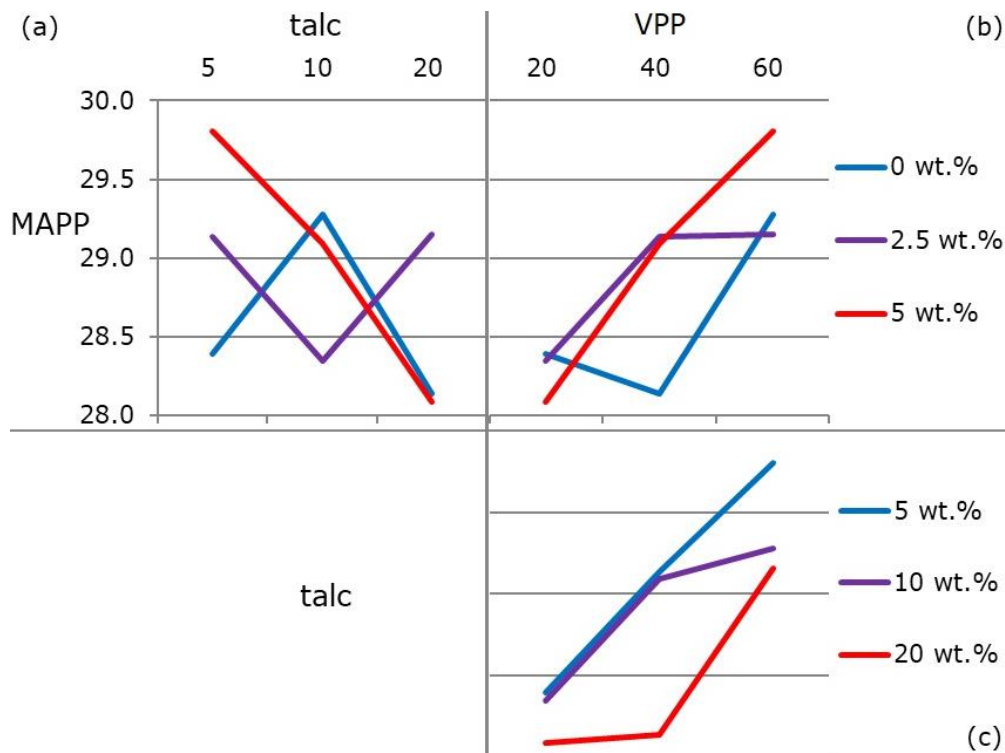


Figure 4-10 Interaction plots of (a) talc \times MAPP, (b) VPP \times MAPP, (c) VPP \times talc, for TS

For the S/N ratios of TS, the VPP \times talc and VPP \times MAPP interactions are insignificant since parallel lines shown in Figure 4-10(b) and (c), except for 0 wt% MAPP in VPP \times MAPP which is initially decreased and then eventually increased with VPP content. The interactions between talc and MAPP of TS (Figure 4-10(a)) are most significant.

The interaction plot of flexural modulus was plot in Figure 4-11.

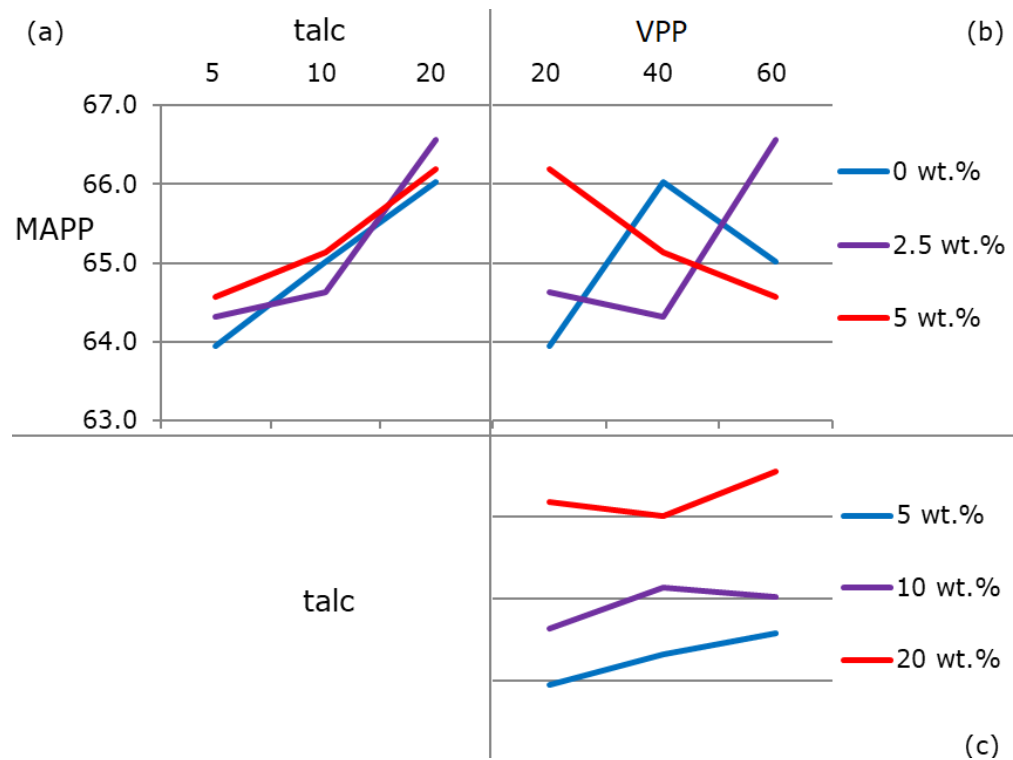


Figure 4-11 Interaction plots of (a) talc × MAPP, (b) VPP × MAPP, (c) VPP × talc, for FM

The VPP × MAPP interactions of FM are the same as that of TM, which are most significant as shown in Figure 4-9(b) and Figure 4-11(b). In the vPP × talc interactions of FM (Figure 4-11(c)), the S/N ratios of 5 wt% talc are increasing with VPP content, and the S/N ratios of 10 wt% talc are initially increased and eventually decreased with vPP content while the S/N ratios of 20 wt% talc have shown the opposite behaviour. For talc × MAPP, their interactions are most insignificant as all the S/N ratios are increased with talc content.

The interaction plot of flexural modulus was plot in Figure 4-12.

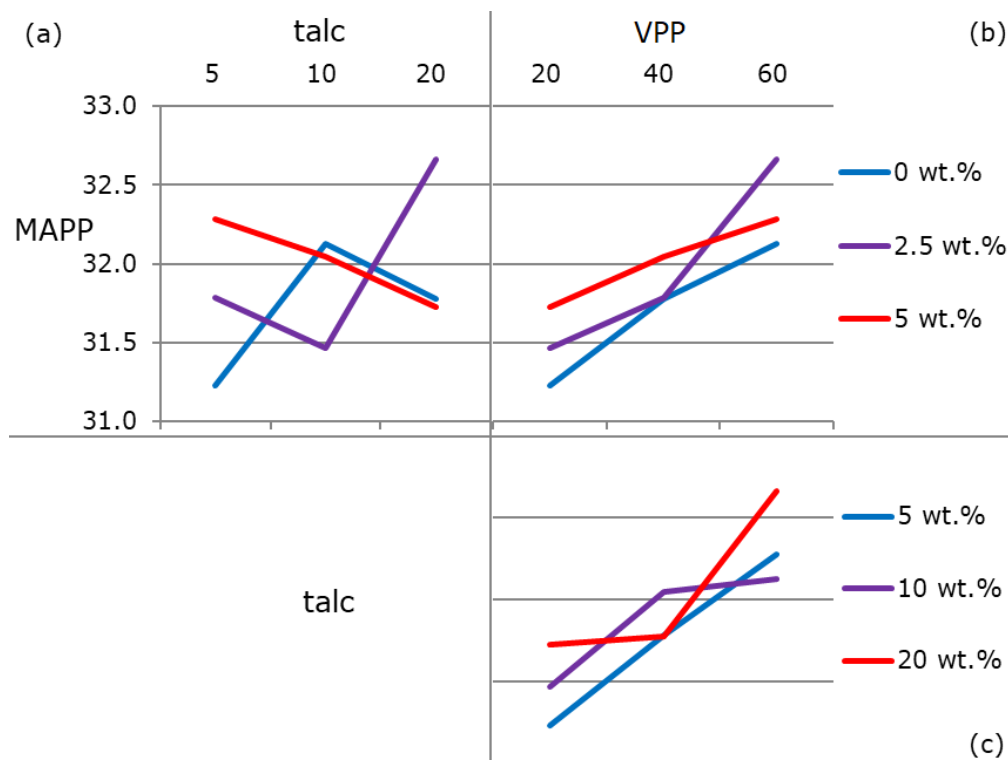


Figure 4-12 Interaction plots of (a) talc × MAPP, (b) VPP × MAPP, (c) VPP × talc, for FS

The generic pattern of interactions between the selected components of FS is similar to the interactions of TS. The vPP × talc and vPP × MAPP interactions were quite insignificant as shown in Figure 4-12 (b) and (c). The talc × MAPP interactions (Figure 4-12(a)) are the most significant.

Analysis of variance of a technique used to compare the means of samples (Hess and Hess, 2018). In this study, ANOVA was applied to estimate the error variance of the components' effects and to obtain their contributions. The results of ANOVA for the S/N ratios of tested mechanical properties are given in Table 4-6. The ANOVA results confirm the previous findings, as talc is the most influential factor in controlling TM and FM with

contributions of 88.43% and 92.51% respectively, while VPP is the most influential factor in controlling TS and FS with contributions of 67.63% and 78.50% respectively. The influences of an error on all tested mechanical properties are negligible since their contributions are less than 3%.

Table 4-6 Contributions for S/N ratios of tested mechanical properties obtained by ANOVA

Source	DF	Contribution (%) of TM	Contribution (%) of TS	Contribution (%) of FM	Contribution (%) of FS
VPP	2	3.55	67.63	4.87	78.5
talc	2	88.43	23.13	92.51	8.52
MAPP	2	7.99	8.51	2.14	10.92
Error	2	0.03	0.73	0.47	2.07
Total	8				

4.3.1.2 Reduction of Dimensionality

PCA can reduce the dimensionality of a data set consisting of a number of interrelated variables while retaining as much as possible of the variation present in the original data set (Jolliffe, 2003). Principal components (PC) are selected and ordered according to their explained variation (EV) (Jolliffe, 2003, Gu et al., 2016a). In this study, PCA was carried out in a generic correlation manner based on the method used in previous work (Gu et al., 2016a, Gu et al., 2014). Compared with the grey relational analysis method used in previous literature (Ayaz et al., 2016), employing PCA for reducing dimensionality can preserve most of the information when avoiding the impacts of related indicators. The first two PCs were selected since their accumulated explained variation (AEV) was over 99%. The

complete descending ranking of PCA scores is shown in Table 4-7.

Table 4-7 PCA scores for the S/N ratios of the RPP/talc composites

Rank	Score	Trial No
1	1.2538	9
2	0.8232	7
3	0.7361	8
4	0.6888	5
5	0.6243	3
6	0.6006	6
7	0.484	4
8	0.3129	2
9	0.0588	1

From Table 4-7, the main effects of the selected components on the PCA scores are plotted in Figure 4-13.

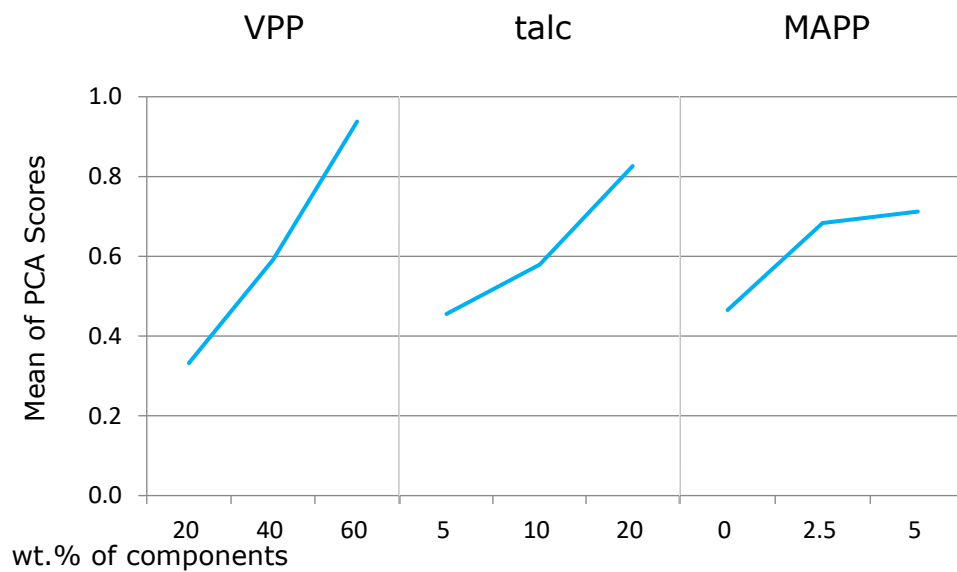


Figure 4-13 Plot of S/N ratios against the selected components for PCA scores

Since a larger PCA score indicates a better overall mechanical performance, the optimal conditions for the selected controllable factors were hereby obtained: 60 wt% VPP, 20 wt% talc and 5 wt% MAPP. This is compatible with previous research, as the content of RPP should be limited for yielding a better mechanical performance (Gu et al., 2014, Mehat and Kamaruddin, 2011). Table 4-8 showed the ANOVA results for PCA scores. When $P < 0.05$, it shows the results have statistical significance, so the composition of VPP and Talc is proven to affect the results of PCA scores statistically.

Table 4-8 ANOVA results for PCA scores

Source	DF	SS	MS	F	p	Contribution (%)
VPP	2	0.55	0.28	46.91	<0.05	62.31
talc	2	0.21	0.11	18.11	<0.05	24.06
MAPP	2	0.11	0.05	9.27	>0.05	12.3
Error	2	0.01	0.01			1.33
Total	8					

4.3.1.3 Confirmation tests

A set of confirmation tests was carried out to verify the obtained optimal conditions. The RPP based composite with 60 wt% VPP, 20 wt% talc and 5 wt% MAPP was processed and tested in the same manner as previous composites. An average of 10 specimens was tested for each property, and the experimental results and their S/N ratios were shown in Table 4-9.

Table 4-9 Experimental results and S/N ratios of the optimal composite

Property	Experimental	Δ * of Experimental	S/N Ratio	Δ * of S/N
TM	2484	42.24	67.9	4.81
TS	28.89	4.33	29.21	1.35
FM	2171	19.28	66.73	2.41
FS	43.78	11.14	32.83	2.91

* Δ is the variation expressed in % with respect to the average values presented in Table 4-4.

As shown in Table 4-9, tensile and flexural properties were enhanced at the optimal conditions when compared to the average performance of the initially designed composites. TM was the property with the most significant improvement of 42.24%, followed by 19.28% of FM and 11.14% of FS. Thus, all tested properties show an observable improvement, and the overall mechanical performance was optimised by the proposed approach. Although the optimal formula only contains 15 wt% RPP, the blend ratio is higher than the current usage of recycled materials in the manufacturing sector (e.g. less than 1% in the automobile industry) (WRAP, 2010).

4.3.2 Conclusion

In this study, Taguchi method coupled with ANOVA was employed to optimise the formula of RPP/talc composites for improving mechanical performance. Three components, VPP, talc and MAPP were selected as the controllable factors, and a Taguchi L9 (3^3) OA was used for experimental design as the number of initial trials was minimised. From the S/N ratio analysis, it was found that talc is the most influential factor in controlling TM and FM, while VPP has the most significant impact on TS and FS. The interactions between components were also investigated, as vPP \times MAPP has the most observable influences on TM and FM, while talc \times MAPP is the most influential interaction for TS and FS. The impacts of the three components were verified by ANOVA results. The multi-dimensional data was reduced to a single array of scores via PCA, and the optimal composition was hence obtained by analysing the PCA scores. The effectiveness of the Taguchi-ANOVA optimising approach has been successfully proven by confirmation tests on the composite of the optimal formula. Compared with current industrial practice, this approach extends the use of recycled plastics, and hence improves the sustainability of the plastic manufacturing sector.

4.4 Industrial trial

The industrial trial was based on the previous study of talc reinforced RPP composites, to find the formula for automotive products with high tensile and flexural requirements. The industrial trial was carried out with our industrial partner Shuanglin Group Co., Ltd. And the process of the industrial trial was shown in Figure 4-14.



Figure 4-14 the process for industrial trial

4.4.1 Application selection

Properties requirements

In the study of talc-filled RPP composites, the tensile and flexural properties of PP based composites have been improved via Taguchi and ANOVA techniques. The optimised formula showed the best tensile and flexural properties than any other formulas in this section. Unfortunately, due to the deterioration of the impact strength, the optimised formula cannot meet the requirements on impact properties. After comparing the mechanical results of the samples in Section 4.3 with industrial requirements, Table 4-10 showed the experimental results of the selected formula which meet the requirements for the shell of the air conditioner. As compared with the requirements provided by Shuanglin co. Ltd., two formulas meet the manufacturing standard, formula 1 and formula 2. Formula 1

consists 52.5 wt% RPP3, 40 wt% VPP (H1500), 5 wt% talc and 2.5 wt% MAPP. Formula 2 consists 30 wt% RPP3, 60 wt% VPP (H1500), 5 wt% Talc and 5 wt% MAPP. Formula 1 is designed for the lower end shell of an air conditioner. Formula 2 contains 20 wt% more VPP than formula 1, the tensile strength and flexural strength of the formula 2 based specimens meet the requirements for the middle-end shell of an air conditioner.

Table 4-10 The comparison of the shell of air conditioner formula results and industrial requirements

Properties	Formula 1	Formula 2	Low-end shell of air conditioner/ armrest box	Middle-end of shell of air conditioner/ armrest box	Unit
Tensile modulus	1583	1607	/	/	MPa
Tensile strength	29	31	≥27	≥30	MPa
Elongation at break	31	34	/	/	%
Flexural modulus	1644	1694	/	/	MPa
Flexural Strength	39	41	≥38	≥40	MPa
Notched impact strength	3.2	3.1	≥2.3	≥2.5	kJ/m ²
Unnotched impact strength	39	37	≥20	≥20	kJ/m ²
Notched impact strength at -30°C	/	/	/	/	kJ/m ²
Note: Formula 1: 52.5 wt% RPP3 40 wt% H1500 5 wt% Talc 2.5 wt% MAPP Formula 2: 30 wt% RPP3 60 wt% H1500 5wt% Talc 5 wt% MAPP					

Availability of mould

An industrial partner (Shuanglin group co., LTD.) provided the mould for the industrial trial. Unfortunately, the mould of a shell

of an air conditioner is not available at that time, so our partner suggested using the mould for the armrest box, which has almost the same mechanical properties requirements.

Sample preparation

Unlike lab-scale production, which only needs to make the specimens for testing various properties, the industrial application usually requires a much larger feedstock. The amount is dependant on the target applications.

The armrest box was selected for the industrial trial. 30 kg of the prepared PP formula were required for the production trial. The trial aimed to test whether the small scale testing of the blend can be used for industrial output.

4.4.2 Products and evaluation

Formula 2 (30 wt% RPP3, 60 wt% VPP (H1500), 5 wt%Talc and 5 wt% MAPP) was selected for this industrial trial. The processing parameters of twin-screw extrusion was followed by the parameters in section 2. After the twin-screw extrusion, the sample pellets were dried in the oven at 80 °C for 24 hours to remove the surface moisture. 30 kg of sample pellets were prepared in the lab. The industrial trial was processed in the mould manufacturing workshop in Shuanglin group co. Ltd.

These pellets were again dried on-site at 80 °C for 2 hours to ensure the removal of surface moisture. Then the pellets were fed into the injection moulding machine. Figure 4-15 is the photo of the Haitian MA1600/540 injection moulding machine in the mould workshop of Shuanglin.



Figure 4-15 Injection moulding machine for industrial trial from Shuanglin group co., LTD.

The industrial trial was processed by the engineers of our industrial partner. The plastic pellets were injected followed by the operating parameters provided in section 2. The temperature profile of the five heating zone was 190-195-200-200-200°C. The injection pressure was 50 MPa, injection speed was 60 g/s, packing pressure was at 60 MPa for 10s, cooling time was 10s and the mould temperature was 50°C. A control group use VPP based pellets to produce the armrest box using the same processing parameters. The formula of the VPP based pellets was unavailable due to commercial confidentiality.

Figure 4-16 and Figure 4-17 illustrated the top and bottom view of the armrest box based on VPP and RPP.

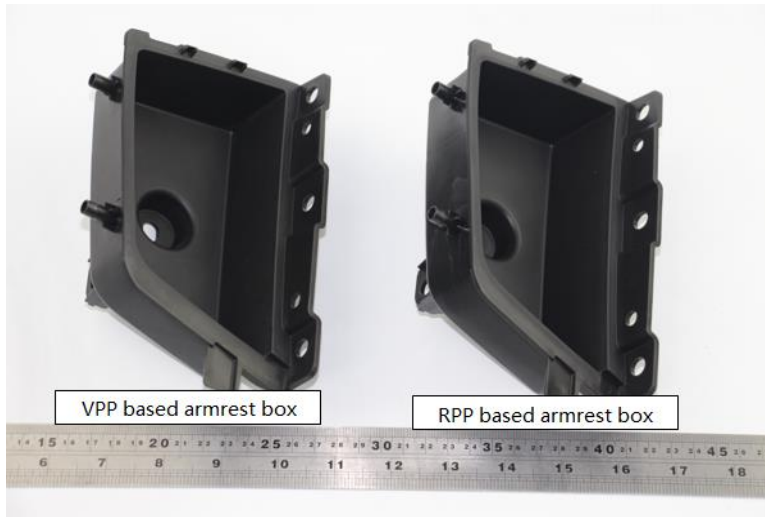


Figure 4-16 Front views of the VPP based armrest box

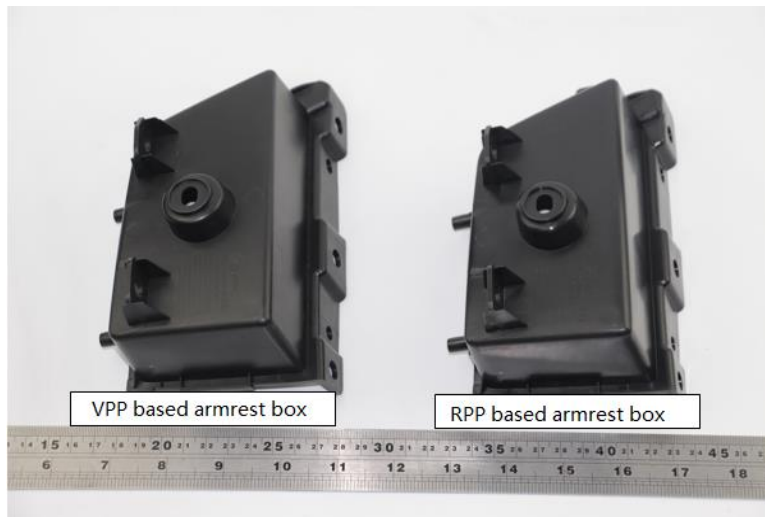


Figure 4-17 Bottom views of the armrest box

Based on the observation of the appearance of the two armrest box made by the plastics provided by Shuanglin and ourselves, the armrest box has no significant defect. The major difference between these two armrest boxes in the appearance is that the RPP based one has a reflective surface, while the VPP based one has a matt surface. This may be attributed to the fact that the VPP based formula contains 20 wt% of talc, which affects the surface finish. Due to the dispersion of the talc, there is some visible colour difference in the RPP based armrest box.

This problem is during the lab-scale preparation step, it is difficult to ensure the composition of the extruded pellets is consistent.

Except for the mechanical properties, there were some additional quality requirements, which is based on the raw material:

One point worth pointing out is that these factors are suggested value for the quality control and ensure the quality consistency of the VPP based pellets purchased by our industrial partner. Some parameters may not be suitable for the RPP based formula in this study.

1. Melt flow index (MFI), follow the standard of ISO 1133-1:2011, at a temperature of 230°C and load of 2.16 kg. There are no specific requirements for MFI. However, it should be as high as possible when all other parameters are satisfied, it was recommended by our industrial partner for the ease of processing. The MFI of RPP based pellets are 9.7 g/10 min.
2. Ash content, using the standard of ISO 3451-1:2008, at a temperature of 600°C. The ash content of the VPP based pellets is controlled at 22±2%. Due to the difference in the formula, the ash content of RPP based pellets is 8.9%. This is due to the fact there is only 5 wt% of talc added into the RPP based composites, while our partner discloses that the VPP based pellets contain 20 wt% talc.
3. Density, using the standard of ISO 1183-1:2012, method A. The suggested density value for VPP based pellets is 1.05±0.02 g/cm³. The density of RPP based pellets is

0.96 g/cm³. The difference also comes from the formula.

4. Fusion temperature, using the standard of ISO 11357-1:2009 ISO 11357-3:2011. The suggested value is higher than 158°C, the value for the RPP based pellets is 160.3°C.
5. Thermal ageing resistance, using the standard of GB/T 7141-2008. After 700 hours of thermal ageing at 150°C, it should have no surface chalking. The photos of the samples before and after the thermal ageing test were shown in Figure 4-18.

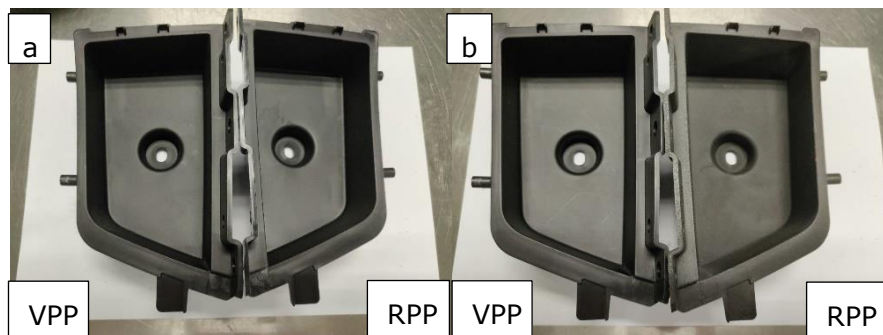


Figure 4-18 the photo of sample a) before, b) after 700 hours thermal ageing test at 150 °C

It is shown that after the thermal ageing test, the surface of the RPP based armrest box becomes more coarse, while the VPP based one has little difference. Limited surface chalking was observed in the specimen after the test.

1. Heat resistance, follow the standard of DIN EN ISO 53497. After 24 hours at 110°C. Figure 4-19 showed photos of the samples after the heat resistance test.

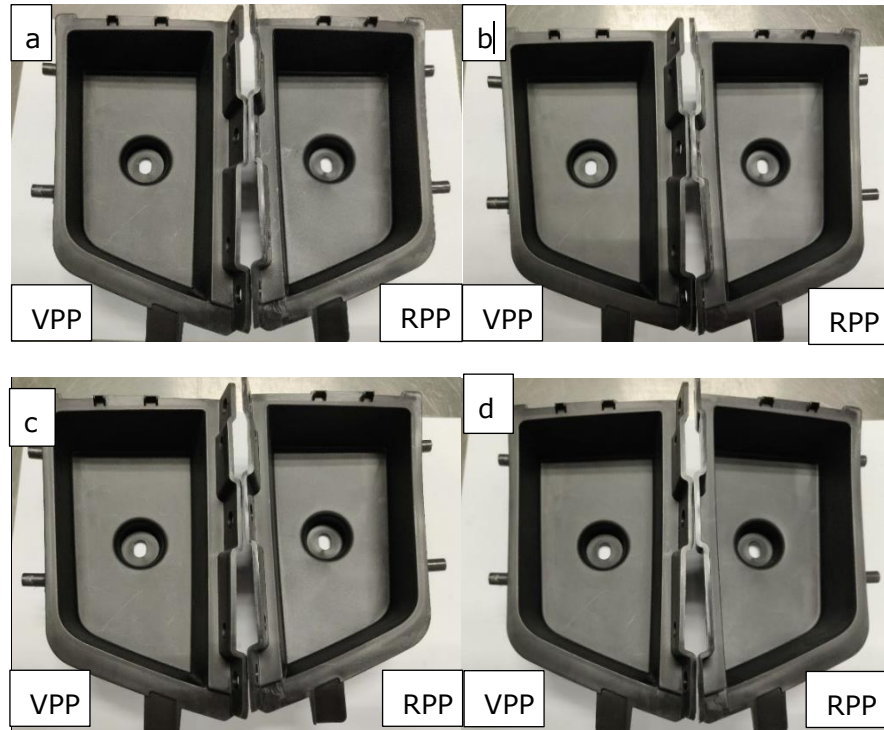


Figure 4-19 heat resistance test after a) 1hour, b) 3hours, c)9 hours, d) 27 hours

From the photo, the differences between these two parts are insignificant. And there is no embrittlement, shape change or surface change observed in both of the parts.

2. Low-temperature resistance. After 24 hours at -40°C , it should have no cracks or similar defects. Figure 4-20 showed the photos of the samples after the low-temperature resistance test.

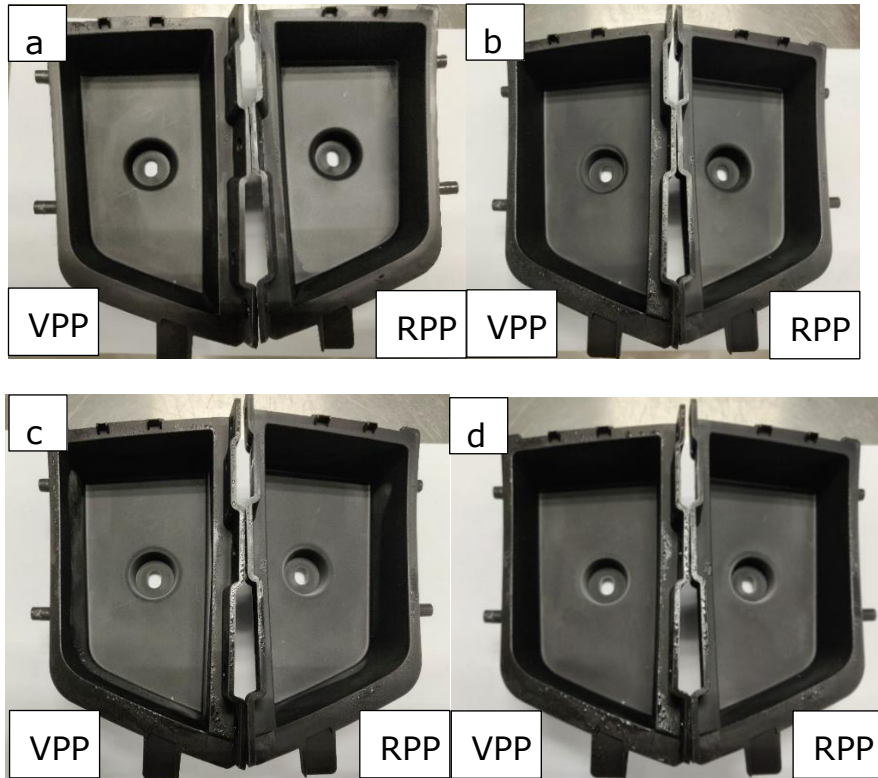


Figure 4-20 Low-temperature resistance test after a) 1 hour, b) 3 hours, c) 9 hours, d) 27 hours

After the temperature rose to room temperature, the surface difference of the VPP and RPP based armrest boxes is insignificant. And there are no cracks observed in any part of both of the armrest boxes. The cracks may be caused by the shrinkage of plastics during the cooling, if the regions of the part shrink unequally, the part may deform and change shape or form cracks.

Economic analysis

The utilisation of RPP in the automobile parts will bring considerable economic benefits to the automobile industry. The

detailed economic assessment may require the evaluation of the cost of the whole life cycle of the auto parts. However, the economic analysis was not the focus of this research. In this study, the economic analysis only consider the cost reduction in the raw material.

The calculation was based on the price of the raw materials in August 2018. Table 4-11 showed the information on the raw material prices.

Table 4-11 The average price of the raw materials, information obtained during 2018

Material	Price (RMB/ton)
VPP	10000
RPP	3500
Talc	1050
MAPP	13500
Partner's VPP based pellets	12000

According to the formula, 30 wt% RPP3, 60 wt% VPP (H1500), 5 wt%Talc and 5 wt% MAPP, the calculated material cost of the RPP based composites is 7.78 RMB/kg. Other costs such as storage, transportation, and manufacturing prices were not considered. Compared to VPP based plastics (12 RMB/kg), the RPP based formula showed a saving of 35.2% of the raw material cost.

The weight of an armrest box is about 85 g, a normal automobile has 4 armrest box. If this formula is applied to 300,000 cars, this formula could lead to a saving of 430,000 RMB. Although the cost-saving is very limited for this specific part, the reason is that the cost-saving is closely related to 1)

the cost gap between VPP and RPP based pellets, 2) the weight of the selected automobile parts, 3) the quantity of the replaced RPP based parts.

The armrest box is only a small component of the interior trim. When the recycled PP can be used for replacing other parts, the economic benefits will be much more significant. Assume the formula can be extended to 10 kg of other interior trim and applied to 300,000 cars. The cost-saving will reach 12.6 million RMB. For the 'heavy component', such as bumper and dashboard, the replacing of VPP by RPP will bring significant economic benefits.

4.5 Summary

By comparing to VPP and the requirements for automotive parts, the industrial RPP (RPP2 & RPP3) was found to have the potential for specific automobile parts. As compare to VPP1, RPPs have close tensile strength, tensile modulus, flexural strength and flexural modulus. The impact properties, especially the notched impact strength, are the major weakness that limited these RPPs to be applied in high impact properties required applications, such as the bumpers. On the other hand, some other parts may only require a low value of impact strength, such as the shell of air conditioner, armrest box.

The shell of air conditioner/ armrest box required high tensile strength and flexural strength. Taguchi method was applied for the experimental design and results analysis. The results of the VPP/RPP/Talc/MAPP composites show the content of VPP is the most influential factor for TS and FS, the content of Talc is the

most influential factor for TM and FM. By using the PCA technique, the optimised formula for achieving the best tensile and flexural properties of the composites was obtained. The effectiveness of the PCA method in this experiment was proved by the confirmation tests. Unfortunately, the deterioration of the impact strength of the optimised formula causes it unsuitable for use of the armrest box. In the real industrial case, more factors should be involved in the experimental design.

By comparing the results with the automobile requirements, after discussion with our industrial partner, the formula 30 wt% RPP3, 60 wt% VPP (H1500), 5 wt% Talc and 5 wt% MAPP was selected for the industrial trial. For the industrial trial, the prepared RPP based pellets successfully produced the required products following the same processing parameters in the lab. RPP based armrest box has a smooth surface while the visible colour difference was found. This means the dispersion of talc should be improved in the future. And for the additional technical requirements, RPP based composites meet most of the requirements. And for some specific parameter, such as ash content, density, its value is lower than the required value. However, this requirement is only for the VPP based pellets for quality control and to ensure quality consistency. In the future, if RPP based composites can be applied in large-scale automobile parts production, the customised technical requirements will be established. The RPP based composites meet the requirements of the heat and cold resistant test, while in the thermal ageing test, the formula may need further improvement. For the economic analysis, the RPP based material can have 35.2% of cost-saving as compared to the cost of the raw material provided by our partner. And if RPP applications can be extended to the heavier, more expensive

and higher amount of automobiles, the cost-saving will be much more significant.

Chapter 5 RPP/PE and RPP/Elastomer blended composites

5.1 Introduction

The incorporation of talcum and MAPP in the RPP matrix in the previous chapter showed significant improvement of the tensile and flexural performance. However, the reinforcement of the impact strength of these mineral fillers filled composites require further investigation. Automobile bumpers, which requires high impact properties, were chosen as the target applications. RPP/PE and RPP/Rubber blending were studied to improve the impact performance.

This chapter will use the same recycled plastic RPP3 as in chapter 4. Table 5-1 listed the industrial requirements of the bumpers provided by an industrial partner Shuanglin group co., LTD.

Table 5-1 Mechanical properties requirements for the automobile parts

Parameters	Standard testing conditions		Application		
	Testing standards	Testing parameters		High-end bumper	Middle-end bumper
Tensile strength (MPa)	ISO527	Gauge speed:	50 mm/min	≥13	≥15
Elongation at break (%)	ISO527	Gauge speed:	50 mm/min	/	≥50
Flexural modulus (MPa)	ISO178	Gauge speed:	5 mm/min	1300-1700	≥1100
Flexural strength (Mpa)	ISO178	Gauge speed:	5 mm/min	/	/
Unnotched impact strength (kJ/m ²)	ISO180	Hammer selection:	7.5J, 3.46m/s	No break /Partial break	/
Notched impact strength (kJ/m ²)	ISO180	Hammer selection:	7.5J, 3.46m/s	≥35	≥15
Notched impact strength at -30°C (kJ/m ²)	ISO180	Hammer selection:	7.5J, 3.46m/s	≥5	≥3.5

5.2 The effects of elastomer on PP composites.

5.2.1 Raw Materials

Polymer blending is a cost-effective method to develop the material with specific requirements (Horák et al., 2005). The RPP/PE and RPP/Rubber blends were selected in this chapter for improving the impact strength of RPP. To overcome the weakness of impact strength of RPP, some literature reported that PP/LLDPE blending and the addition of elastomer SEBS-g-MA was effective in improving the impact properties (Ayaz et al., 2016, Inuwa et al., 2017). Table 5-2 shows the density and

the melt flow index of the selected plastics and elastomer in this study.

Table 5-2 Properties of Plastic materials used in this study

	RPP3	VPP3	LLDPE	LLDPE-g-MA	SEBS-g-MA
True density (g/cm ³)	0.89	0.9	0.92	0.931	0.91
Melt flow index (g/10 min)	2.2	2.6	2	3.8	22

Table 5-3 shows the composition of the designed formula in this study. Mourad (2010) suggested the composition of PE content in PP/PE blends should be less than 25 wt% to avoid the deterioration of tensile behaviours. So in this study, three content levels (5 wt%, 10 wt%, 20 wt%) of LLDPE, LLDPE-g-MA and SEBS-g-MA was selected.

Table 5-3 RPP/LLDPE, RPP/LLDPE-g-MA and RPP/SEBS-g-MA formulations

NO.	RPP (wt%)	LLDPE (wt%)	LLDPE-g-MA (wt%)	SEBS-g-MA (wt%)
1	100	-	-	-
2	95	5	-	-
3	90	10	-	-
4	80	20	-	-
5	95	-	5	-
6	90	-	10	-
7	80	-	20	-
8	95	-	-	5
9	90	-	-	10
10	80	-	-	20

5.2.2 Results and discussion

5.2.2.1 FTIR analysis

Unlike VPP, RPP usually contains different kinds of additives during the manufacturing and impurities during the working lifetime and recycling process. In this study, the polymer blending technique was employed, and the PE was introduced into the RPP matrix. The impurities in RPP may greatly affect the compatibility of PP and PE, so the FTIR technique was employed for a better understanding of the RPP composition.

The FTIR analysis found the presence of polyethylene terephthalate (PET) in the RPP matrix. Figure 5-1 presents the FTIR spectra of VPP, RPP and PET.

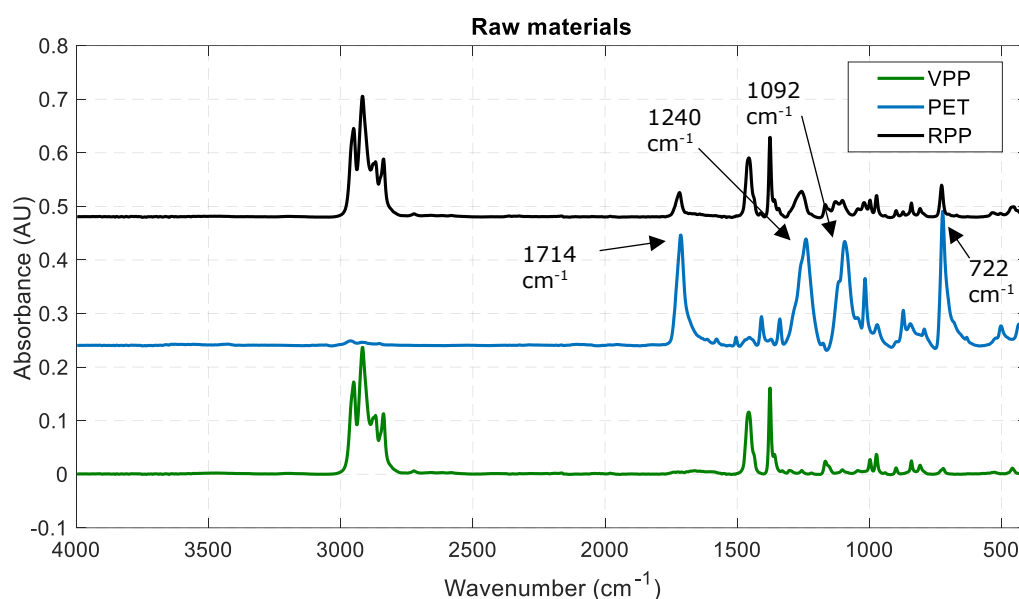


Figure 5-1 FTIR spectra of VPP, RPP and PET

The chemical bonds of the RPP contain several bands belonging to PET. In comparing with PET and PP, PET has several unique peaks at 1714 cm⁻¹ corresponding to terephthalic acid ester C=O group, the asymmetric C-C-O and the O-C-C stretching at

1240 cm^{-1} and 1092 cm^{-1} , respectively, and at 722 cm^{-1} is attributed to the C-H wagging vibrations from the aromatic structures (Strain et al., 2015).

The melting point of PET is 264°C, which is much higher than PP (179°C) and LLDPE (141°C) (Polymer Properties Database, n.d.-b). As the processing temperature of twin-screw extrusion and injection moulding in this study are controlled around 190°C, the small amount of PET in the RPP matrix was not melted and acted as a solid filler. However, as PET and PP are immiscible, the mechanical properties of the composites may be reduced by the poor interfacial adhesion between PET and PP matrix. The compatibility effects will be evaluated by the morphological study.

5.2.2.2 Mechanical properties

The experimental data of the tensile, flexural and impact tests are given in Table 5-4, Table 5-5, Table 5-6.

Table 5-4 Results of RPP/LLDPE composites

Sample ID	Tensile properties		Flexural Properties		Impact Properties		
	TS (MPa)	Elongation at break %	FM (MPa)	FS (MPa)	IS (kJ/m ²)	NIS (kJ/m ²)	NIS at -30°C (kJ/m ²)
1	24.8	54.9	1293.0	32.9	109.3	11.6	3.2
2	24.0	129.1	1227.0	30.7	102.9	12.7	2.7
3	22.9	247.0	1123.2	28.2	100.4	35.7	2.9
4	21.7	482.8	1008.5	24.9	92.3	33.0	3.3

Table 5-5 Results of RPP/LLDPE-g-MA composites

Sample ID	Tensile properties		Flexural Properties		Impact Properties		
	TS (MPa)	Elongation at break %	FM (MPa)	FS (MPa)	IS (kJ/m ²)	NIS (kJ/m ²)	NIS at -30°C (kJ/m ²)
1	24.8	54.9	1293	32.9	109.3	11.6	3.2
5	24.3	131.5	1062.7	29.7	106.3	12.4	3.9
6	23.4	92.3	1100.7	28.8	101.1	15.2	4.4
7	21.9	266.3	936.2	24.4	92.4	41	4.6

Table 5-6 Results of RPP/SEBS-g-MA composites

Sample ID	Tensile properties		Flexural Properties		Impact Properties		
	TS (MPa)	Elongation at break %	FM (MPa)	FS (MPa)	IS (kJ/m ²)	NIS (kJ/m ²)	NIS at -30°C (kJ/m ²)
1	24.8	54.9	1293	32.9	109.3	11.6	3.2
8	23.3	94.4	1114.5	28.7	102	12.1	4
9	22	199.2	933.1	25.6	96.4	45.8	4.7
10	19.3	321.5	818.5	21	84.4	53.6	6.8

By comparing to the bumper requirements in Table 5-1, the major weakness with the chosen RPP is the flexural modulus, notched impact strength and notched impact strength at -30 °C. The tensile strength, elongation at break and flexural strength were shown to have acceptable values. The detailed analysis of the effects of the RPP compositions on the mechanical properties is given in the following sections.

Tensile characterisation

Figure 5-2 shows the tensile strength of the base matrix (RPP), LLDPE, LLDPE-g-MA and SEBS-g-MA filled RPP based composites.

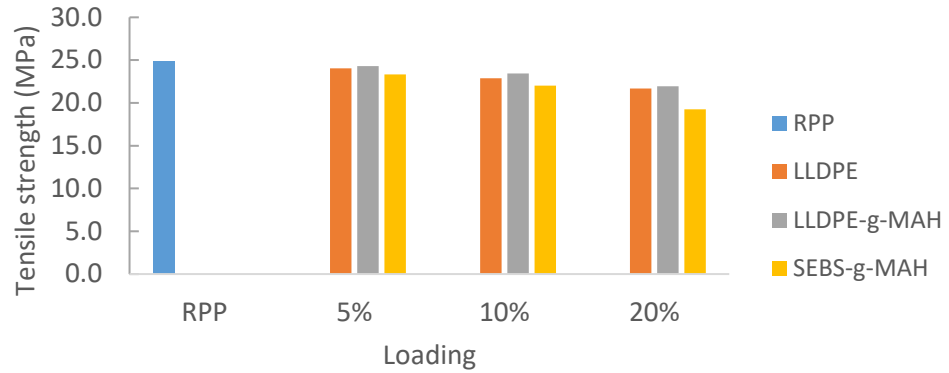


Figure 5-2 Correlations of tensile strength with LLDPE, LLDPE-g-MA and SEBS-g-MA loading

Compared to 100% RPP, the tensile strength of 5 wt%, 10 wt% and 20 wt% LLDPE filled RPP composites reduced from 24.8 MPa to 24.0, 22.9 and 21.7 MPa, respectively. The minimum requirements of tensile strength for high-end and middle-end bumpers is 15 MPa and 13 MPa, so all of the tested samples meet the tensile strength requirement. Daneshpayeh et al. (2016) evaluated the TS of PP/LLDPE/TiO₂ composites by using Taguchi method and reported that LLDPE has adverse effects on tensile strength and the reduction is attributed to poor interaction effects.

LLDPE-g-MA filled RPP composites showed the same tendency but slightly less deterioration of tensile strength. Compared to 100% RPP, the tensile strength shows an 11.7% reduction with 20% LLDPE-g-MA loading.

SEBS-g-MA filled RPP had the most severe deterioration of TS, with 20 wt% loading of the filler, the TS reduced by 22.5%. Similar results of TS of PP/SEBS-g-MA blends were reported show a linear decrease with the addition of the SEBS-g-MA content from 0 to 20 vol% (Denac et al., 2005, Jiang and Zhang,

2009). It was due to the incorporation of SEBS-g-MA which reduced the composite stiffness and ductility (Denac et al., 2005).

For the elongation at break, the results are shown in Figure 5-3.

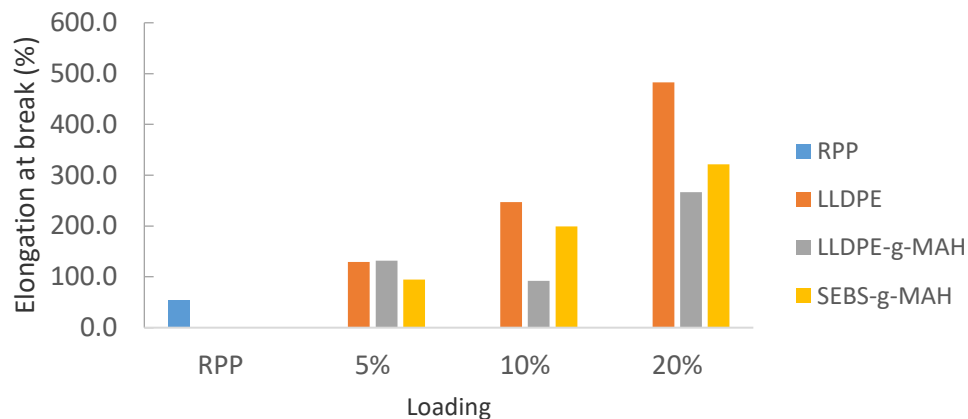


Figure 5-3 Correlations of elongation at break with LLDEP, LLDPE-g-MA and SEBS-g-MA loading

The RPP/LLDPE-g-MA blends exhibited scattered values while RPP/LLDPE and RPP/SEBS-g-MA blends showed a linear increase with increasing SEBS-g-MA content from 0 wt% to 20 wt%. Daneshpayeh et al. (2016) observed the same tendency of the elongation at break in LLDPE/PP composites. The ductility difference could be explained by the fact that the RPP used in this study contains a certain amount of PET, which can be observed from Figure 5-1.

A linear increase of the elongation at break of RPP/SEBS-g-MA blends with the increasing of SEBS-g-MA was observed in Figure 5-3. The addition of SEBS-g-MA improved the dispersion of PET in the PP matrix during the mixing. Papadopoulou and Kalfoglou (2000) studied the compatibility effectiveness of SEBS-g-MA for PET/PP blends, the addition of SEBS-g-MA

improve the tensile properties of PP/SEBS-g-MA/PET ternary blend. As RPP contains a certain amount of PET, the addition of SEBS-g-MA improved the dispersion of PET in PP based matrix. For the application of bumpers in this study, the TS and elongation at break of all the test samples meet the requirements of bumpers.

Flexural characterisation

Figure 5-4 and Figure 5-5 show the correlation between flexural modulus of RPP based composites with 0 wt% to 20 wt% LLDPE, LLDPE-g-MA and SEBS-g-MA loading.

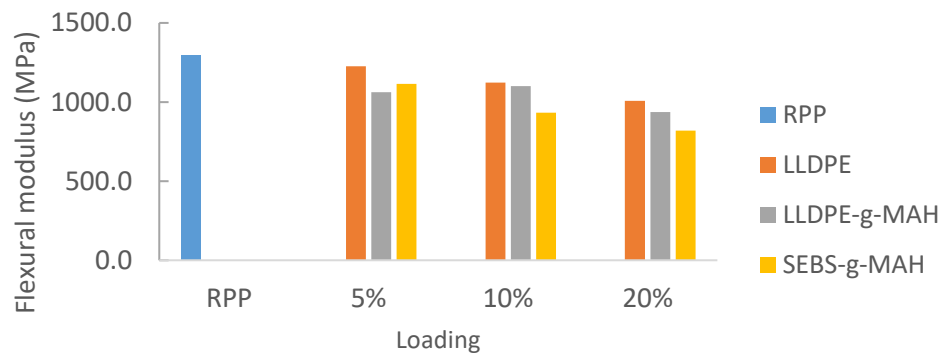


Figure 5-4 Correlations of flexural modulus with LLDPE, LLDPE-g-MA and SEBS-g-MA loading

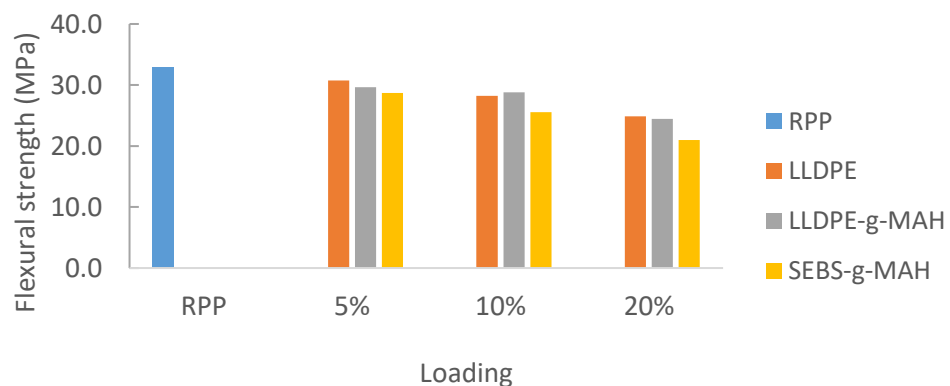


Figure 5-5 Correlations between flexural strength with LLDPE, LLDPE-g-MA and SEBS-g-MA loading

When the loading of LLDPE increased from 5 wt% to 20 wt%, FM decreased from 1227.0 MPa to 1008.5 MPa, FS decreased from 30.7 MPa to 24.9 MPa. With the increasing weight fraction of LLDPE-g-MA, both FM and FS of the composites decreased. A 27.6% and 25.7% of reduction in FM and FS was observed with 20 wt% of LLDPE-g-MA loading. Clemons (2010) studied the PP/HDPE blends and find that with the decreased PP ratio in HDPE-PP blends from 0:100 to 100:0, the flexural strength decreased from 50.1 MPa to 20.2 MPa. The results were also consistent with the findings by Ayaz et al. (2016). One possible explanation is that the PE and PP are immiscible (Chiu et al., 2010), and the PP used in the study has superior flexural performance than PE.

The SEBS-g-MA filled composites showed an even lower FS and FM as compared to the LLDPE-g-MA filled composites. The FM and FS reduced by 36.7% and 56.8% with 20% SEBS-g-MA loading as compared to 100% RPP. Ayaz et al. (2016) reported that SEBS has a beneficial effect on improving the flexural properties of PP/LLDPE/TiO₂/SEBS nano-composites. The conflicting results could be explained that in our current study no fillers were involved, so the SEBS-g-MA is not functionalised as a coupling agent for better dispersion of mineral fillers, and SEBS-g-MA is much more ductile than the base matrix.

As is shown in Table 5-1, for the automotive bumper, the flexural modulus of the composite has to be higher than 1100 MPa, in this study, except VPP and RPP, 5–10 wt% LLDPE, 10 wt% LLDPE-g-MA and 5 wt% SEBS-g-MA filled composite meet these requirements.

Impact strength characterisation

Figure 5-6 presents the correlation of un-notched impact

strength (IS) with the 0 to 20 wt% loading of LLDPE, LLDPE-g-MA and SEBS-g-MA.

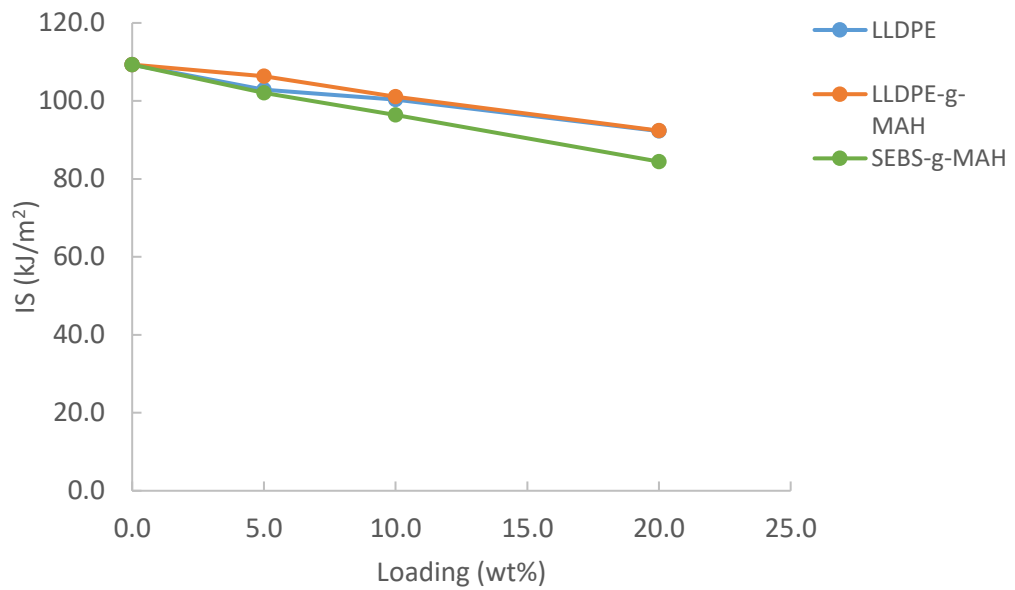


Figure 5-6 Correlations between un-notched impact strength with LLDPE, LLDPE-g-MA and SEBS-g-MA loading

At the same loading, the LLDPE, LLDPE-g-MA and SEBS-g-MA blended RPP have very close un-notched impact strength. It was observed from Figure 5-6 that when the content of LLDPE-g-MA increase from 0 wt% to 20 wt%, the un-notched Izod impact strength decreased from 109.3 to 92.4 kJ/m².

With an increasing amount of SEBS-g-MA 0 wt% to 20 wt%, the IS decreased from 102.0 to 84.4 kJ/m². One possible reason for such a trend could be the increased radical depolymerisation of the plastic molecules with increasing MA content, which makes the materials more brittle (Gao et al., 2012). Another possible reason is that these additives reduced the crack initiation energy or the propagation energy (Monti et al., 2020).

The results of the notched impact strength (NIS) are given in Figure 5-7.

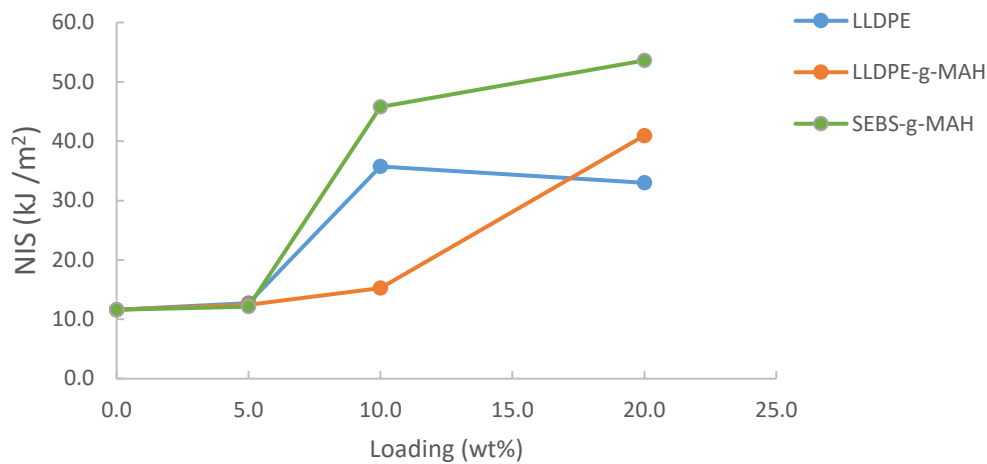


Figure 5-7 Correlations between notched impact strength with LLDPE, LLDPE-g-MA and SEBS-g-MA loading

Figure 5-7 indicates that as the LLDPE-g-MA content increased from 0 wt% to 20 wt%, the notched impact strength increased by 252.6% with respect to 100%RPP. These results are consistent with the literature (Younesi and Bahrololoom, 2009, Ayaz et al., 2016). It was also observed that when the loading is more than 5 wt%, SEBS-g-MA showed superior improvement in NIS than LLDPE-g-MA. The RPP/SEBS-g-MA based composites exhibited a maximum improvement of 42 kJ/m² in NIS at 20 wt% SEBS-g-MA loading. This increment could be due to the better interfacial filler/matrix adhesion, as phase separation or miscibility is a vital factor in influencing the impact resistance (Denac et al., 2005). As compared to the unnotched impact performance, the results showed the addition of LLDPE, LLDPE-g-MA and SEBS-g-MA significantly improve the resistance to crack propagation, but slightly reduced the crack initiation energy.

The results from notched impact strength at -30 °C are given in Figure 5-8.

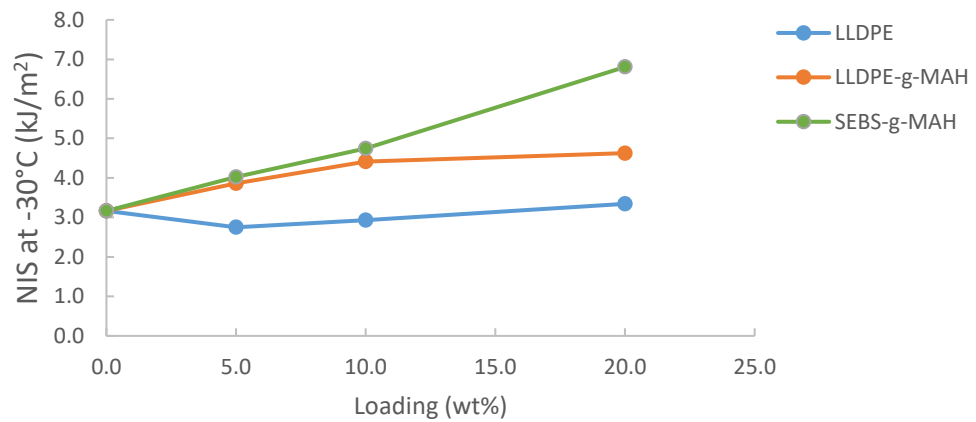


Figure 5-8 Correlations between notched impact strength at -30°C with LLDPE, LLDPE-g-MA and SEBS-g-MA loading

The performance of RPP/LLDPE composites was noticeably lower as compared to RPP/LLDPE-g-MA and RPP/SEBS-g-MA. RPP/LLDPE-g-MA composites showed 46.2% of increment in NIS at -30°C at 20 wt% LLDPE-g-MA loading as compared to 100% RPP. It was found that the NIS at -30°C reached a plateau when the loading of LLDPE-g-MA is between 10wt% and 20 wt%. A linear improvement of NIS at -30°C was observed with increasing the SEBS-g-MA loading, and it reached 6.8 kJ/m² when the SEBS-g-MA loading is 20wt%. The lower NIS values observed at lower temperature conditions could be attributed to the lower resistance to radical crack growth (Tai et al., 2000). At low temperature, the material becomes much more brittle and the interfacial adhesion becomes much more important for better impact stress propagation. For the middle-end bumper, 10-20% loading of LLDPE-g-MA or SEBS-g-MA can meet the requirement. However, for a high-end bumper, only 20 wt% SEBS-g-MA filled

composite can maintain the desired NIS at -30°C.

5.2.2.3 Morphology of fracture surface

The morphological study of the fractured surface of the notched impact strength specimens was conducted by SEM. The fracture surface of 100%RPP and 100%VPP are shown in Figure 5-9.

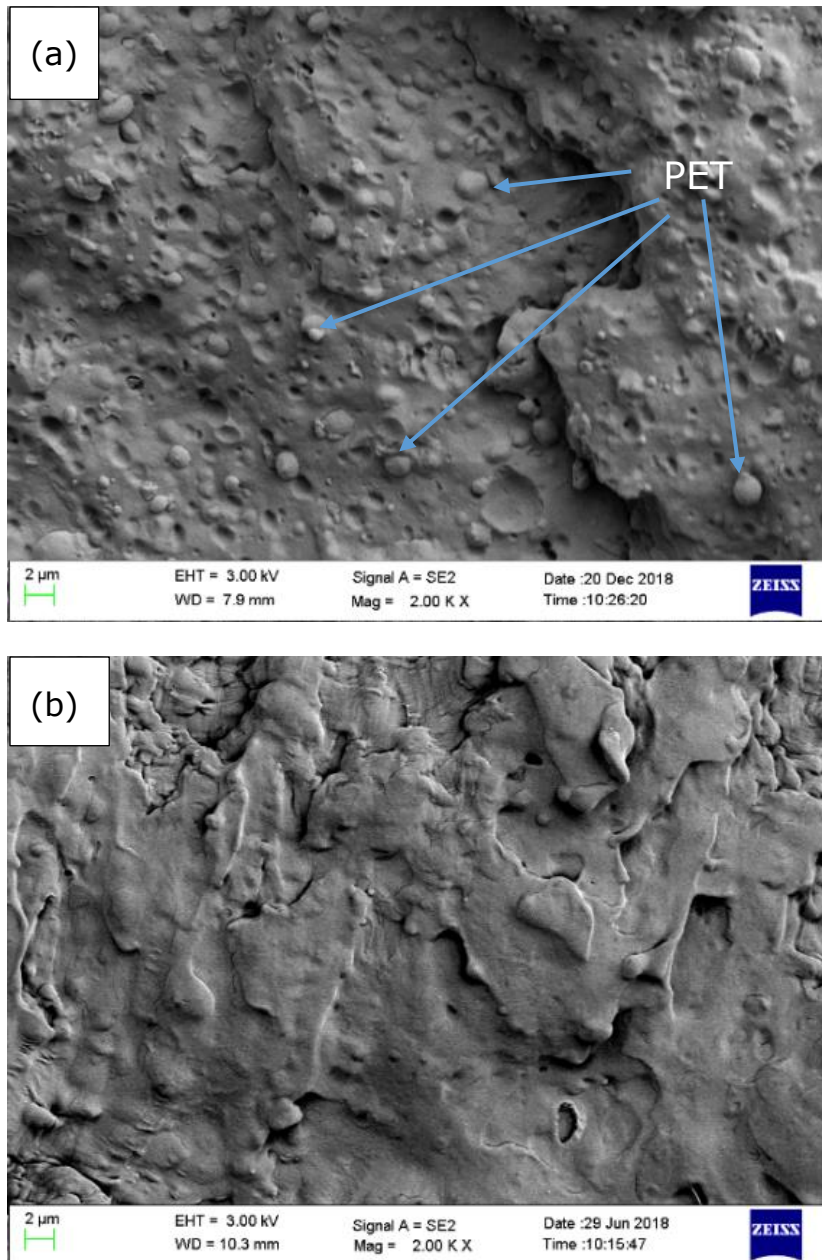


Figure 5-9 SEM micrograph of the fracture surface of composite with: (a) 100% RPP, (b) 100%VPP

It can be observed that the RPP contains many particles, and FTIR results confirmed that these particles are PET pellets. Moreover, the fractured surface of RPP exhibits many voids, indicating PP and PET are immiscible.

Figure 5-10 shows the fractured surface of the 80 wt%RPP+20 wt% LLDPE, fewer PET pellets were observed, but the interfacial adhesion between PET and base RPP matrix was very poor.

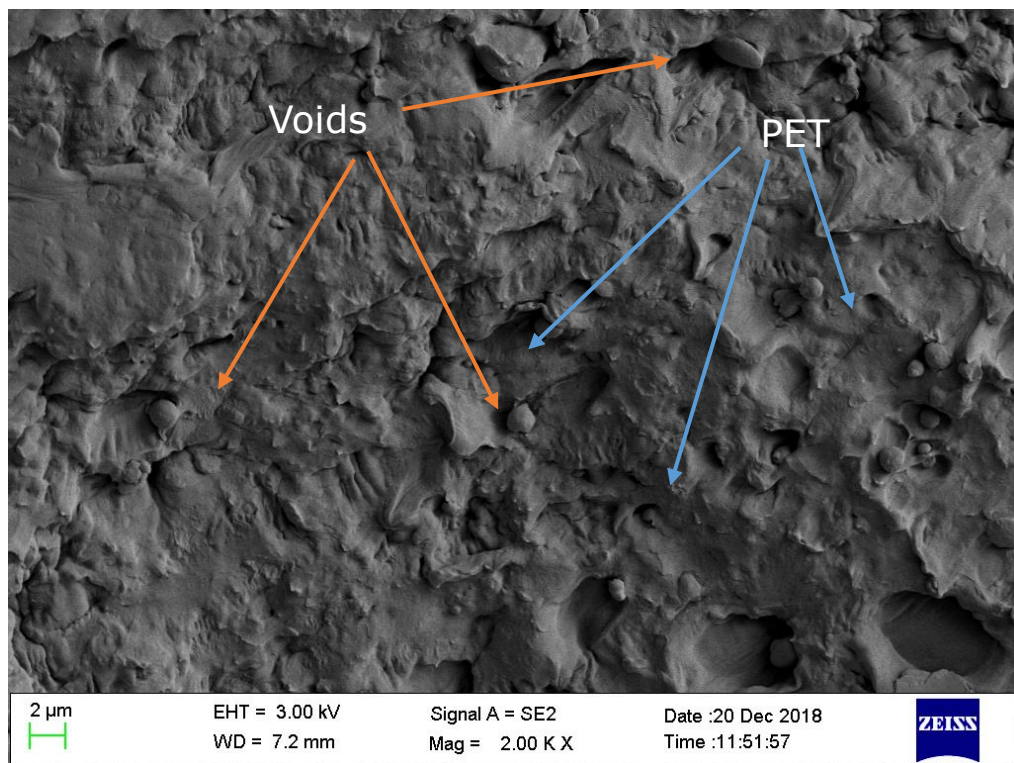


Figure 5-10 SEM micrograph of the fracture surface of composite with 80%RPP+20%LLDPE

It can be found in Figure 5-11 that PET becomes well dispersed at 20 wt% LLDPE-g-MA loading.

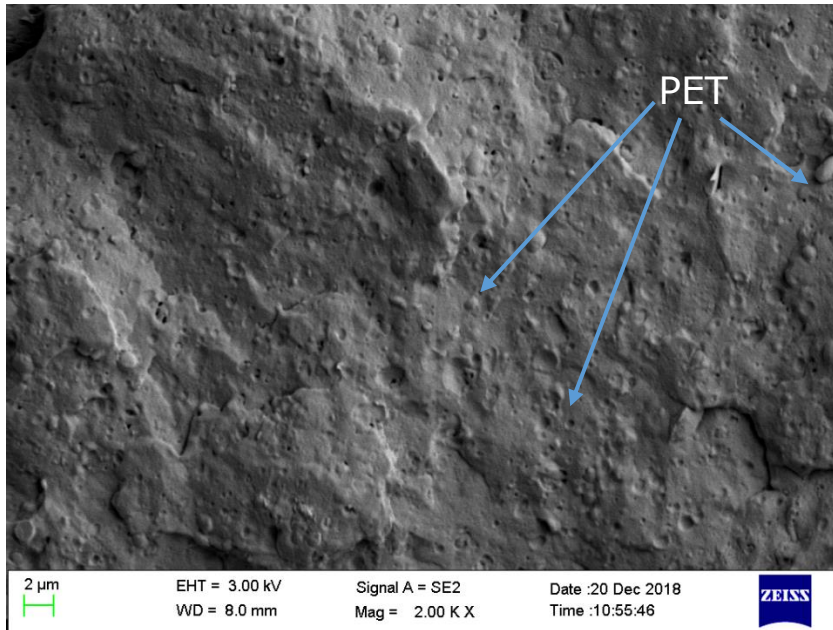


Figure 5-11 SEM micrograph of the fracture surface of composite with 80%RPP+20%LLDPE-g-MA

Fewer PET particles are pulled off from the matrix, indicating the interfacial adhesion between PET and PP matrix are improved.

Figure 5-12 shows the fractured surface of the RPP/SEBS-g-MA with adding SEBS-g-MA loading of 20 wt%.

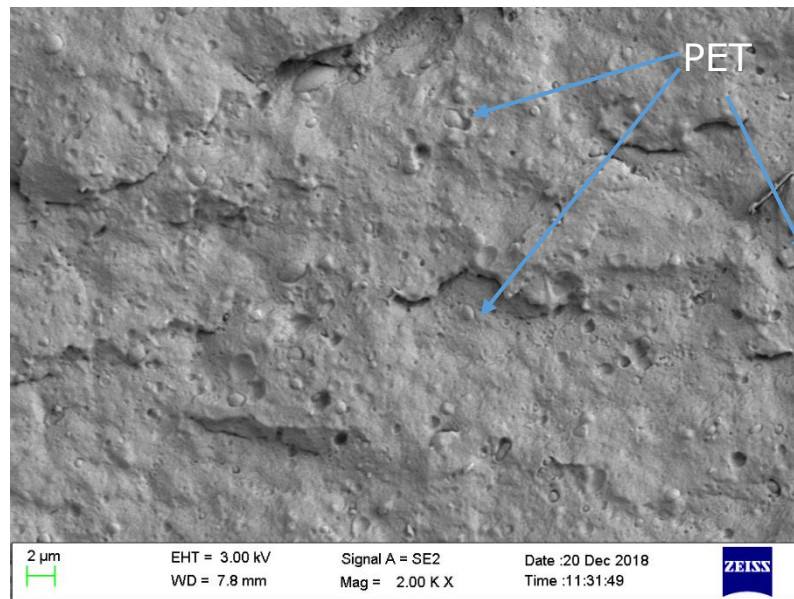


Figure 5-12 SEM micrograph of the fracture surface of composite with 80%RPP+20%SEBS-g-MA

In the pure RPP, there are considerable micro-cracks and small voids can be observed in the micrograph. It is evidence of poor adhesion. Papadopoulou and Kalfoglou (2000) observed when the SEBS-g-MA does not exceed 10 wt% level, the PP/SEBS-g-MA/PET ternary blends can have good component dispersion. In this study, when the SEBS-g-MA loading increased, Figure 5-12 suggests that the compatibility of PP and PET were improved. As a result, the impact properties of the SEBS-g-MA added blends were improved significantly.

5.2.2.4 Additional experiments (RPP/LLDPE-g-MA/VPP composites)

Based on the mechanical results in Table 5-4, Table 5-5 and Table 5-6.

it was found that only the formula 90 wt% RPP3+10 wt% LLDPE-g-MA met the requirements of the middle-end automotive bumper, while the flexural modulus 1100.7 MPa and

notched impact strength 15.2 kJ/m² is very close to the minimum requirements (>1100 MPa and >15 kJ/m²). To ensure the stable quality of the composites, RPP3 was partially replaced by VPP3, Table 5-7 the detailed formula in the additional experiments.

Table 5-7 RPP/LLDPE-g-MA/VPP formulations

NO.	RPP (wt%)	LLDPE-g-MA (wt%)	VPP3 (wt%)
11	80	10	10
12	70	10	20
13	60	10	30
14	50	10	40

The results were summarised in Table 5-8.

Table 5-8 Results of RPP/LLDPE-g-MA/VPP formulations

Sample ID	Tensile properties		Flexural Properties		Impact Properties		
	TS (MPa)	Elongation at break (%)	FM (MPa)	FS (MPa)	IS (kJ/m ²)	NIS (kJ/m ²)	NIS at -30°C (kJ/m ²)
VPP3	25.96	99.20	1107.80	30.94	113.28	40.25	4.00
11	24.92	65.94	1387.86	34.27	108.42	10.84	3.22
12	23.32	57.93	1180.00	29.45	97.34	34.97	3.98
13	23.39	72.65	1111.99	29.05	95.97	40.17	3.76
14	23.34	126.46	1138.60	29.01	96.26	42.20	3.84

TS and elongation at break of all the samples meet the requirements of the bumpers. When the content of VPP increases from 10 wt% to 40 wt%, FM decreased from 1387.86 MPa to 1138.6 MPa. Due to the high NIS of VPP, the value of NIS increased with the addition of VPP content, while the NIS at -30°C gained the highest value 3.98 kJ/m² at 20 wt% of VPP loading. Among these four formulas, sample 12, 13 and 14 meet the requirements for the middle-end bumpers. However,

for the high-end bumpers, FM and NIS at -30°C have to be further improved. As SEBS-g- has better performance in improving the impact properties than LLDPE-g-MA, the further study applied SEBS-g-MA and mineral fillers to achieve both high flexural properties and impact properties.

The fracture surface of the RPP/LLDPE-g-MA/VPP composites was presented from Figure 5-13 to Figure 5-16.

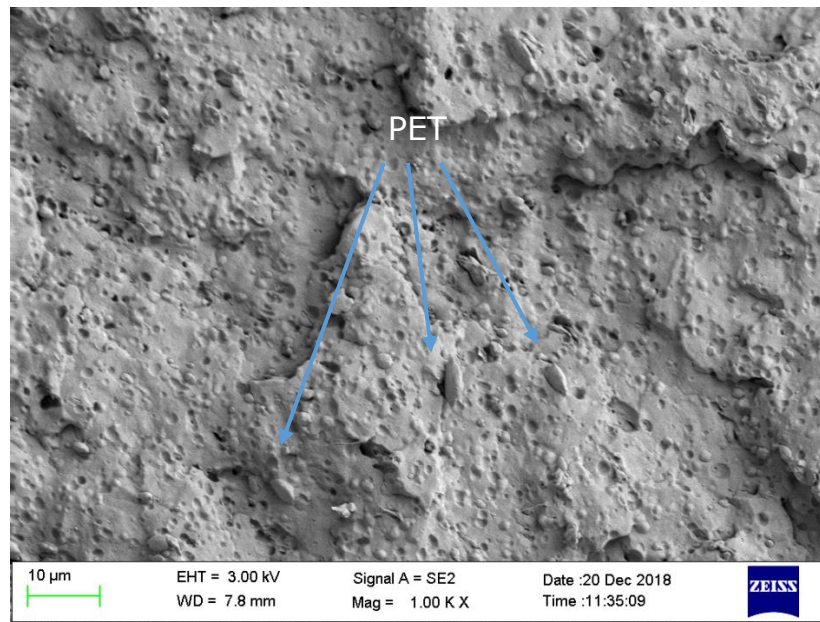


Figure 5-13 SEM micrograph of the fracture surface of composite with 80%RPP+10%LLDPE-g-MA+10%VPP

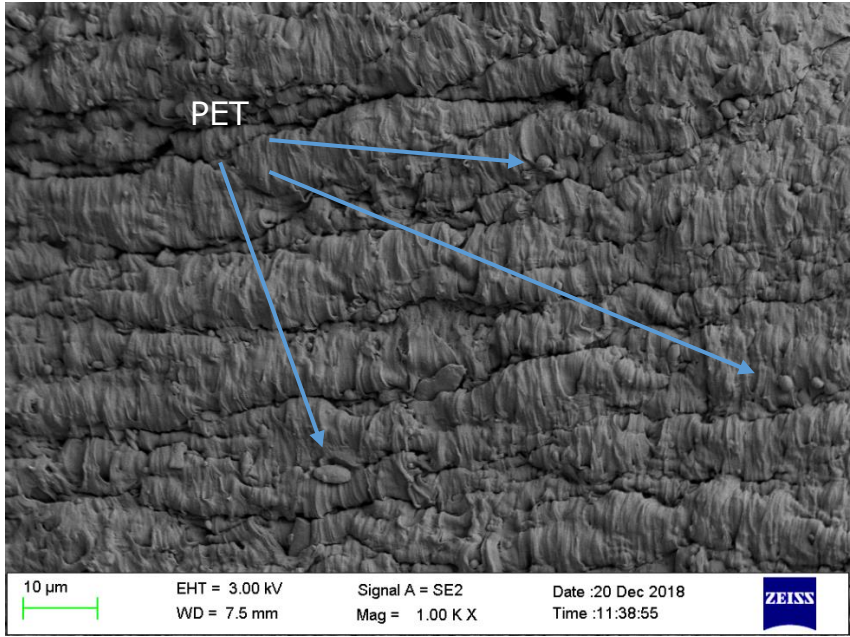


Figure 5-14 SEM micrograph of the fracture surface of composite with 70%RPP+10%LLDPE-g-MA+20%VPP

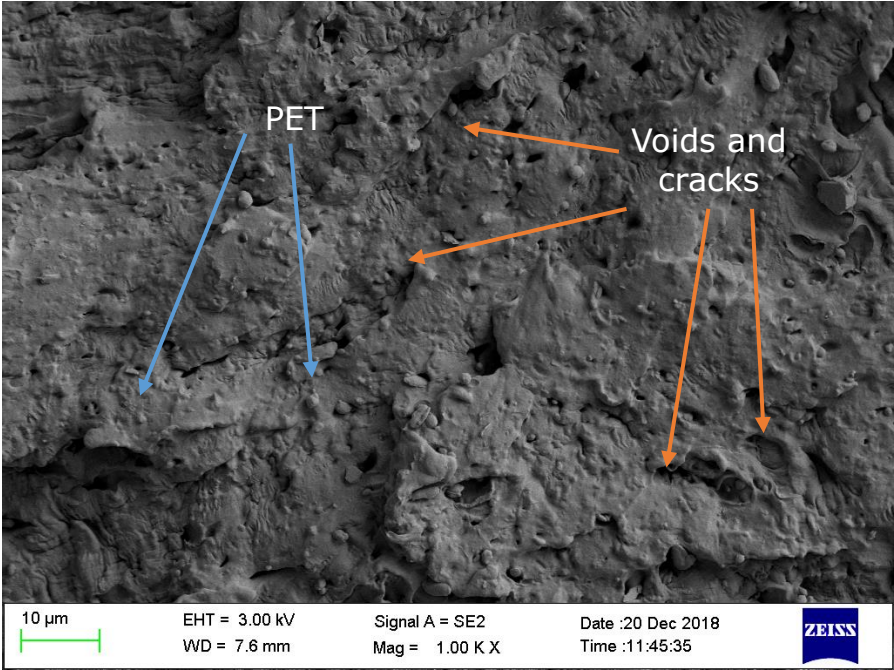


Figure 5-15 SEM micrograph of the fracture surface of composite with 60%RPP+10%LLDPE-g-MA+30%VPP

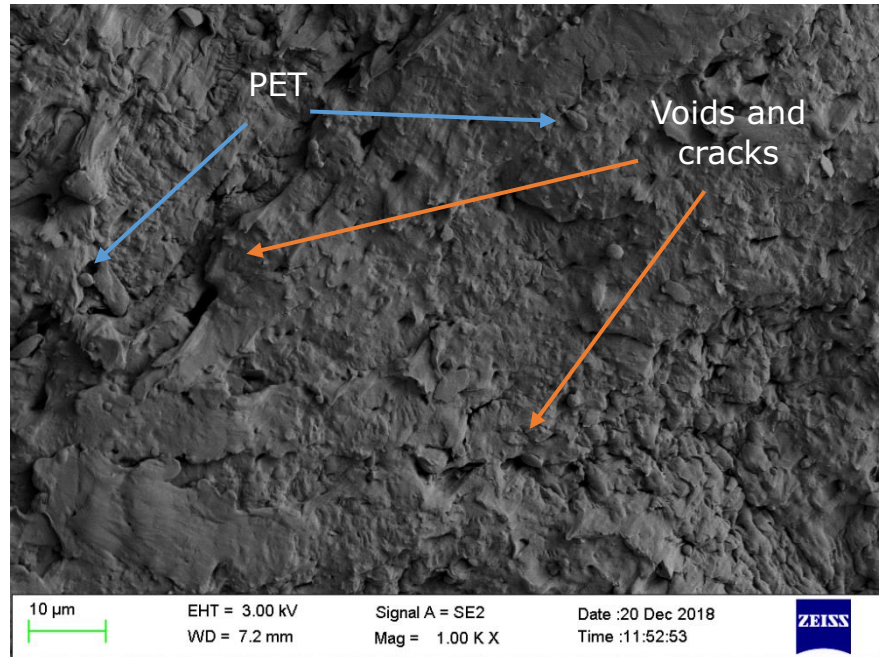


Figure 5-16 SEM micrograph of the fracture surface of composite with 50%RPP+10%LLDPE-g-MA+40%VPP

With the increasing VPP content, the number of immiscible PET pellets reduced. The decrease of RPP content 'diluted' the content of PET in the composites. However, the replacement of RPP with VPP have nearly no effects on the improvement of compatibility of PET and PP matrix.

5.2.3 Conclusion

The purpose of this section is to estimate the feasibility of utilising the RPP for the application of automobile bumpers. By comparing the mechanical performance of RPP and requirements of the automobile bumper, the weakness of the impact strength and flexural modulus is the major limitation for RPP. In the present study, 5 wt%, 10 wt% and 20 wt% of LLDPE, LLDPE-g-MA and SEBS-g-MA were estimated to achieve higher impact strength of the composites and at the same time, maintain the tensile and flexural properties. The results showed

that by adding LLDPE, LLDPE-g-MA and SEBS-g-MA, the TS, FM and FS decreased significantly. On the contrary, the elongation at break and impact strength increased dramatically. It was found in the RPP/LLDPE-g-MA composites, the maximum notched impact strength achieved 252.3% improvement with respect to 100%RPP when the weight fraction of LLDPE-g-MA was 20%. It was 17.1% and 173.3% higher than the minimum requirements of the high-end and middle-end bumper, respectively. Meanwhile, as compared to the base matrix, the tensile strength and flexural strength reduce 11.7% and 25.7%, respectively. SEBS-g-MA has more superior performance than LLDPE-g-MA in improving NIS and NIS at -30°C. The 80%RPP/20% SEBS-g-MA even reached the NIS at -30°C for the high-end bumper. However, the flexural modulus is 481.5MPa lower than the requirement, which limits its application. The morphology of the impact fracture surface further proved that the presence of LLDPE-g-MA and SEBS-g-MA improve the surface adhesion of PP and PET in the RPP based matrix, which contribute to the better impact performance of the blends. The sample 6 (90%RPP 10%LLDPE-g-MA) meet all of the mechanical requirements for the middle-end bumper, which may have the potential for industrial application. And the additional experiments use VPP to partially replace the RPP, the results indicated that the by replacing 20 wt%-40 wt% RPP with VPP, the composites can have a more balanced mechanical performance and meet the requirements for middle-end bumpers.

5.3 The effects of elastomer on mineral filler filled composites

In the previous section, the effects of the elastomer and polymer blending were studied. SEBS-g-MA showed superior improvement on the impact strength. However, the tensile modulus, flexural modulus and strength deteriorated significantly. This section aims to utilise the mineral fillers (talc and $\text{Al}(\text{OH})_3$) to improve the flexural modulus and use SEBS-g-MA to compensate for the impact properties loss. To investigate the feasibility of a more balanced stiffness and toughness of the RPP composites for the use of high-end bumpers.

Design of experiment

For the stable processing of twin-screw extrusion, the content of $\text{Al}(\text{OH})_3$ and talc was controlled at 5 wt%, 10 wt% and 20 wt%. And the amount of SEBS-g-MAH was controlled at 5 wt%, 10 wt%, 20 wt% based on the study in Section 5.2. The formulation and the sample designations were presented in Table 5-9.

Table 5-9 RPP, Al(OH)₃, Talc and SEBS-g-MA blending ratio

NO.	RPP3 (wt%)	Al(OH) ₃ (wt%)	Talc (wt%)	SEBS-g-MA (wt%)
1	95	5	-	-
2	90	10	-	-
3	80	20	-	-
4	95	-	5	-
5	90	-	10	-
6	80	-	20	-
7	85	10	-	5
8	80	10	-	10
9	70	10	-	20
10	85	-	10	5
11	80	-	10	10
12	70	-	10	20
13	75	20	-	5
14	70	20	-	10
15	60	20	-	20
16	75	-	20	5
17	70	-	20	10
18	60	-	20	20

5.3.1 Results and discussion

5.3.1.1 Results of RPP/Al(OH)₃ and RPP/Talc composites

Tensile properties

Figure 5-17 and Figure 5-18 illustrate the tensile strength and elongation at break of the Al(OH)₃ and Talc filled RPP.

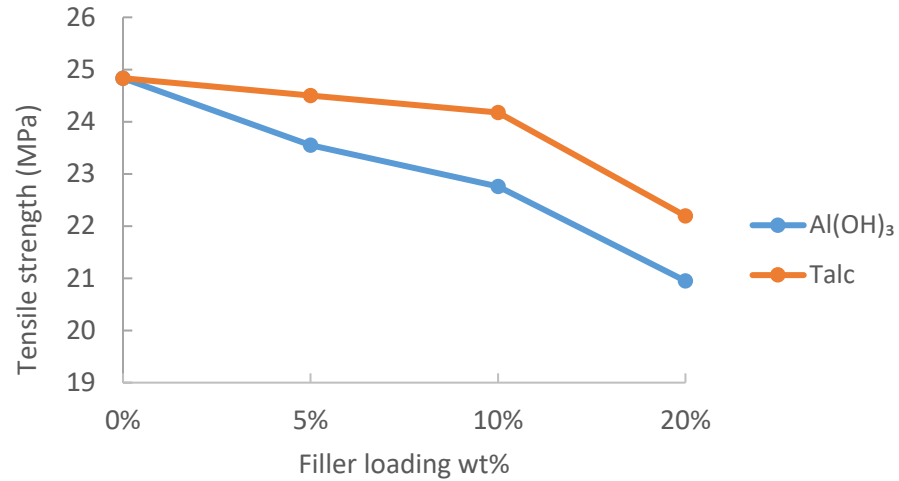


Figure 5-17 The correlation between tensile strength and filler loading

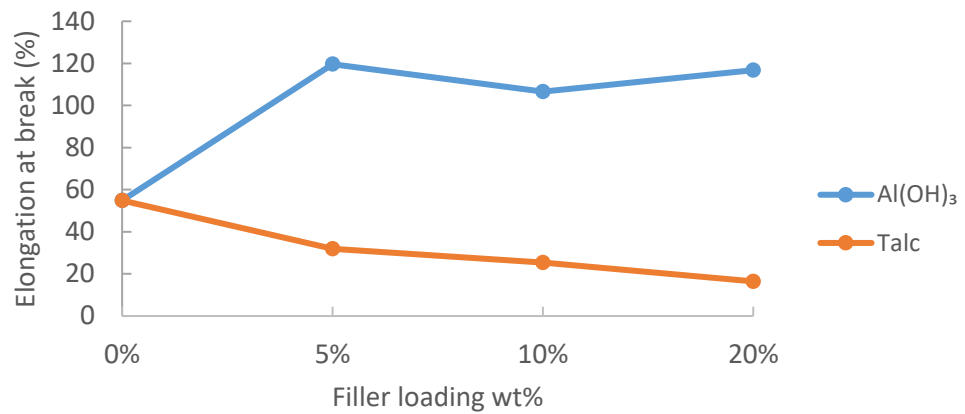


Figure 5-18 The correlation between elongation at break and filler loading

When the loading of talc increase from 0 wt% to 20 wt%, the tensile strength decrease from 24.8 MPa to 22.2 MPa. Leong et al. (2004) observed the increase of tensile strength of talc-filled PP when the volume fraction of talc is lower than 11%. The possible reason for this could be the inhomogeneous dispersion and agglomeration of talc particles. Another reason is the poor surface adhesion of talc and RPP. The talc particles create stress concentration zones under stress and cause the debonding and

frictional pullout (Nekhlaoui et al., 2015).

For $\text{Al}(\text{OH})_3$ filled RPP, the tensile strength decreased from 24.8 MPa to 20.9 MPa when the filler loading increased from 0 wt% to 20 wt%. Su et al. (2005) observed the same tendency for the $\text{Al}(\text{OH})_3$ filled PP, the main reason was the agglomeration of $\text{Al}(\text{OH})_3$, which act as defects and stress points due to the poor adhesion between filler and PP matrix.

As for the elongation at break, it continuous decrease with the increasing of talc content. The possible reason is that the talc particles cause cavitation because of the matrix/filler debonding (Wang et al., 2013). It can be observed that the elongation at break increase with increasing the content of $\text{Al}(\text{OH})_3$, indicating the $\text{Al}(\text{OH})_3$ particles improved the tensile fracture ductility of the RPP composites.

Flexural properties

Figure 5-19 and Figure 5-20 show the correlation between flexural modulus, flexural strength and filler loadings.

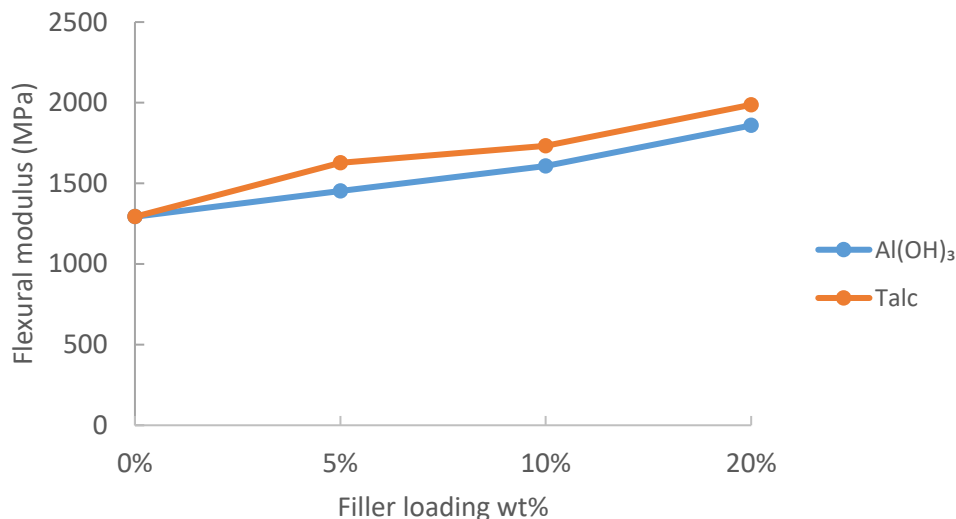


Figure 5-19 The correlation of flexural modulus and filler loading

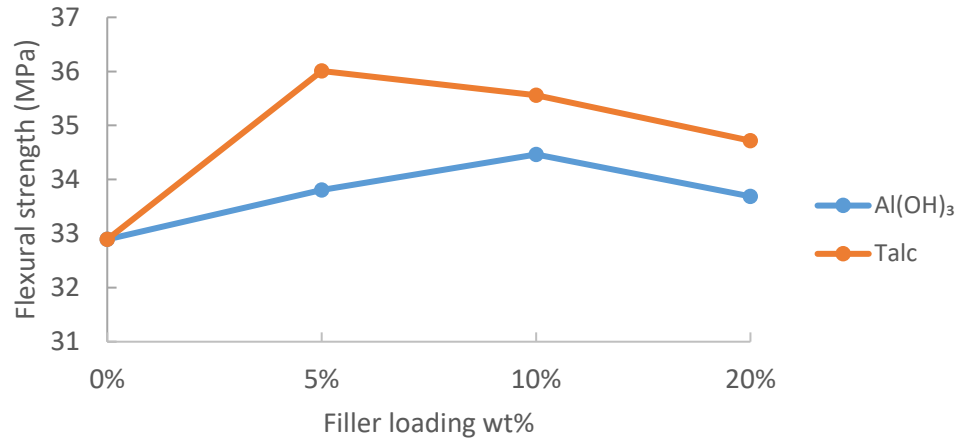


Figure 5-20 The correlation of flexural strength and filler loading

Both flexural modulus of the talc-filled and Al(OH)₃ filled RPP composites increased when the filler loading increases. The rigid particulate fillers improve the stiffness of the plastic matrix (Leong et al., 2004). Talc filled composites showed slightly better flexural modulus than the Al(OH)₃ filled composites. When the filler loading is 20 %, the flexural modulus of the talc and Al(OH)₃ filled composites were 1859 MPa and 1987 MPa, respectively.

For the flexural strength, the Al(OH)₃ filled PP gained the maximum value of 34.5 MPa when the filler loading is 10 wt%. The maximum flexural strength of talc-filled RPP is 36 MPa at 5 wt% talc loading. Then the flexural strength decreased with increasing the talc content.

Impact properties

The results of the notched impact properties (NIS) are illustrated in Figure 5-21.

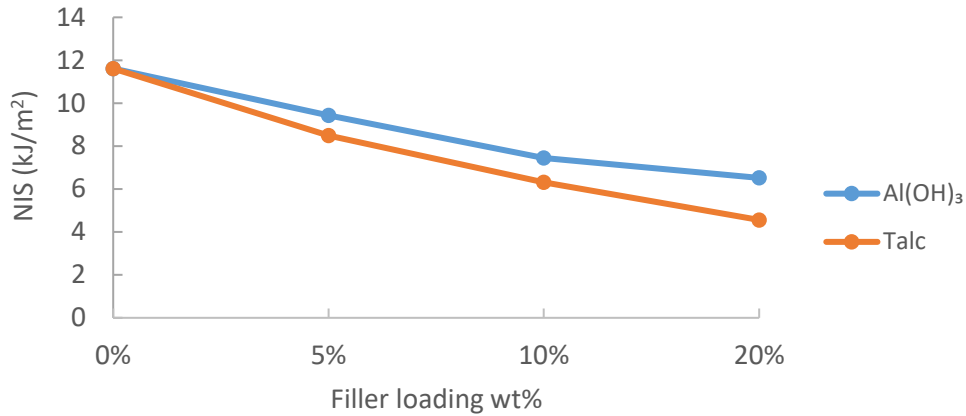


Figure 5-21 The correlation of notched impact strength and filler loading

The NIS of RPP composites deteriorated linearly with the addition of Al(OH)₃ and talc. The reduction of unnotched impact strength is a result of void formation and micro crazing due to the poor adhesion between filler and PP matrix (Lapcik Jr. et al., 2008). In 20 wt% filler loading, the NIS of Al(OH)₃ and talc-filled PP was 6.5 kJ/m² and 4.6 kJ/m², respectively. According to Table 3-11, the NIS only meets the requirements for the application of the shell of the air conditioner. So the NIS has to be improved for the bumper applications.

The results of NIS at -30°C are shown in Figure 5-22.

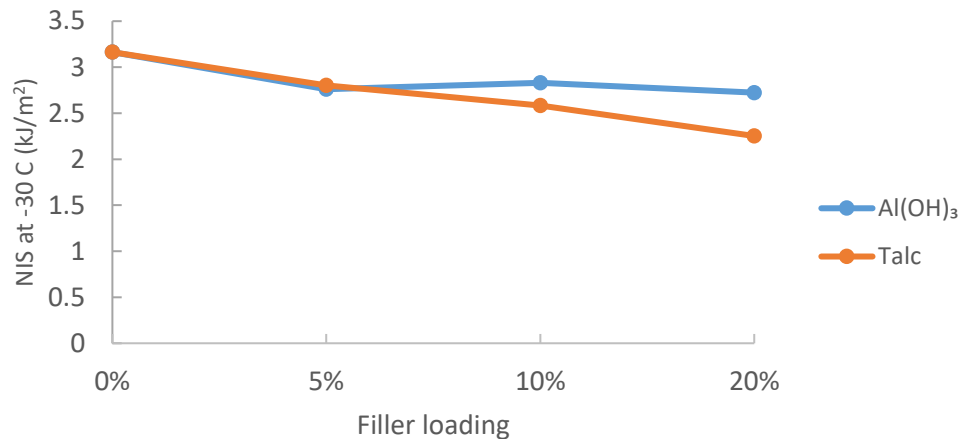


Figure 5-22 The correlation of notched impact strength at -30°C and filler loading

For the NIS at -30°C, the talc and Al(OH)₃ filled RPP decreased with the increasing of filler content. It was found the NIS at -30°C of talc-filled RPP decreased linearly with filler content. The findings are consistent with the results by Lapcik Jr. et al. (2008). The Al(OH)₃ filled RPP had a rapid decrease at 5 wt% Al(OH)₃ loading, which indicated a step-change in composite brittleness. At 10 wt% and 20 wt% loadings, the NIS at -30°C of Al(OH)₃ filled RPP is 0.2 kJ/m² and 0.4 kJ/m² higher than talc-filled PP.

Figure 5-23 presents the correlation between the unnotched impact strength (IS) and filler content.

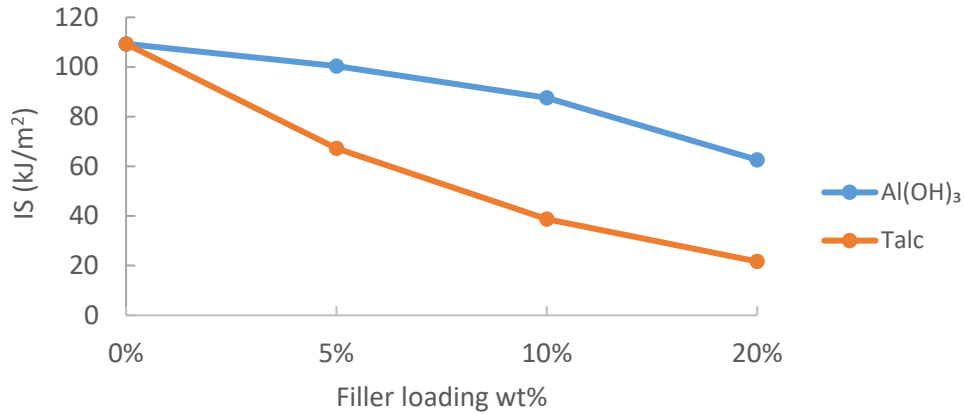


Figure 5-23 The correlation of unnotched impact strength and filler loading

For the IS, both Al(OH)₃ filled RPP and Talc filled PP decreased with the increasing of filler loading. At 5 wt%, 10 wt% and 20 wt% of filler content, the IS of Al(OH)₃ filled RPP was 49%, 126% and 189% higher than the talc-filled RPP. The reason is that the addition of Al(OH)₃ and talc improves the stiffness of the composites, but the high stiffness composites showed low impact properties due to the high stress transferred from the polymer matrix to the filler particulates (Premalal et al., 2002). The particulate reduced the crack initiation energy, and also cause the reduction of resistance to crack propagation.

5.3.1.2 Results of SEBS-g-MA filled RPP/Al(OH)₃ and RPP/Talc composites

Tensile properties

To improve the impact properties of the Al(OH)₃ and talc-filled PP, 5 wt%, 10 wt% and 20 wt% SEBS-g-MA were added into the composites. Figure 5-24 and Figure 5-25 illustrate the tensile strength and elongation at break of SEBS-g-MA filled RPP/Talc and RPP/Al(OH)₃ composites.

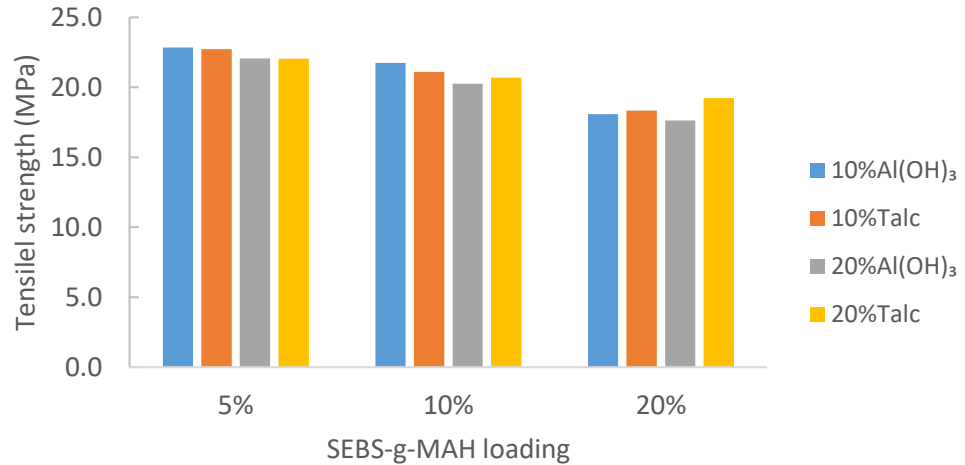


Figure 5-24 The correlation between tensile strength and SEBS-g-MA loading

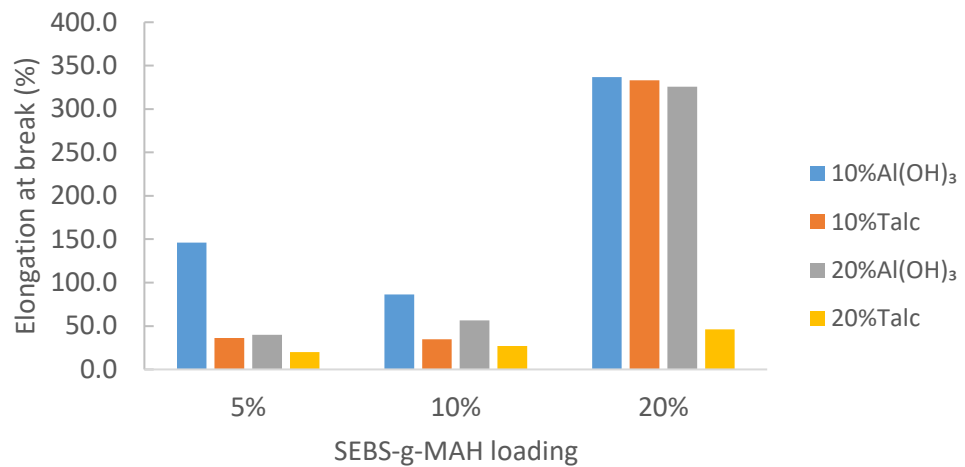


Figure 5-25 The correlation between elongation at break and SEBS-g-MA loading

It can be observed that the tensile strength decreased with increasing the SEBS-g-MA loading. Due to the elastomeric nature, the stiffness of the RPP composites reduced (Monti et al., 2020), and the elongation at break increased with the addition of SEBS-g-MA. A step change was observed when the SEBS-g-MA loading increase from 10 wt% to 20 wt%. The tensile strength of all the samples meet the minimum

requirements of both middle-end and high-end bumpers. The low elongation at break limited the talc-filled RPP to be applied in high-end bumpers.

Flexural properties

Figure 5-26 exhibits the flexural modulus against the SEBS-g-MA content.

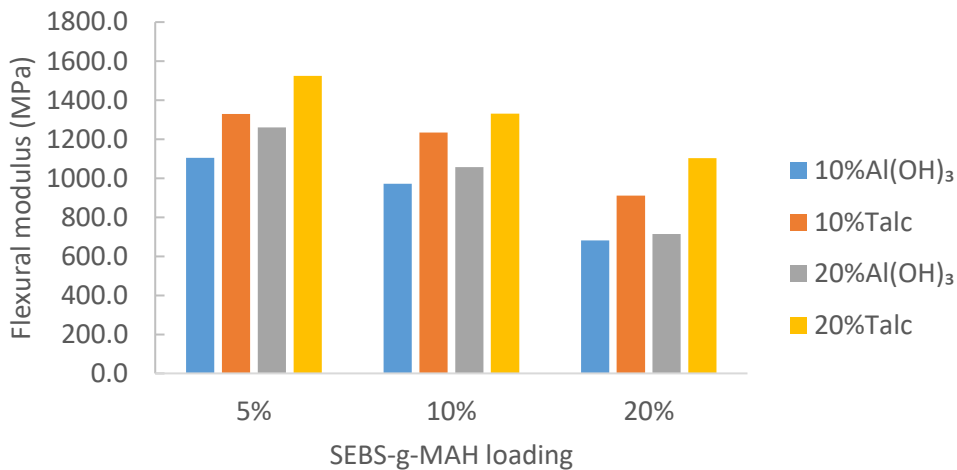


Figure 5-26 The correlation of flexural modulus and SEBS-g-MA loading

The incorporation of SEBS-g-MA also leads to the deterioration of flexural properties. Other researchers also obtained the same tendency (Jiang and Zhang, 2009). The reduction of the flexural modulus is because of the increasing content of SEBS-g-MA led to the decrease of the stiffness of the RPP composites (Abreu et al., 2005). The results showed that the flexural modulus can be enhanced by increasing the filler content when the SEBS-g-MA loading was kept constant. The highest flexural modulus 1329.0MPa was obtained by the 20 wt% talc filled RPP composites at SEBS-g-MA loading is 5 wt%. From the requirements of the industrial application, the minimum

requirement of the flexural modulus is 1100 MPa, among these formulae, when the SEBS-g-MA loading is 5%, the flexural modulus of all the samples is higher than 1100MPa. However, when the SEBS-g-MA loading increase to 10 wt%, all Al(OH)₃ filled PP failed the flexural modulus requirements. And at 20 wt%, the flexural modulus of 20 wt% talc-filled PP is 1102 MPa, which was very close to the minimum requirement.

The results of the flexural strength of Al(OH)₃ or Talc filled RPP composites at different SEBS-g-MA loading are illustrated in Figure 5-27.

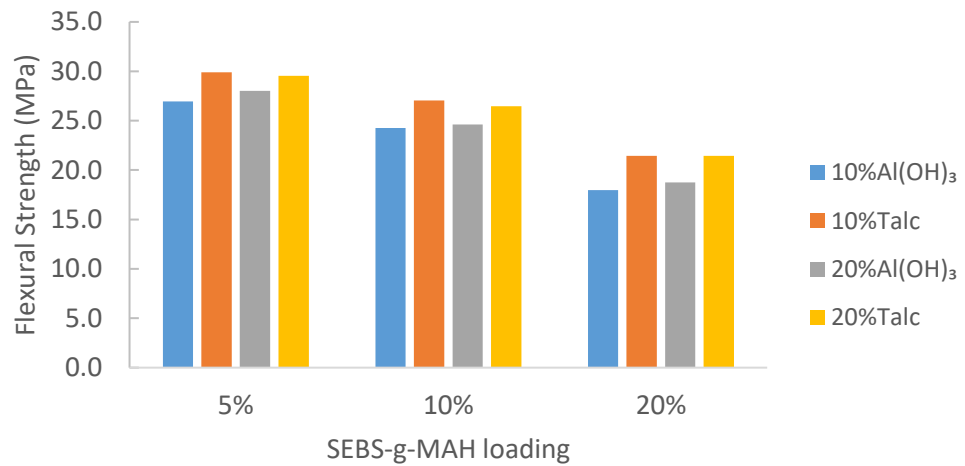


Figure 5-27 The correlation of flexural strength and SEBS-g-MA loading

The flexural strength obtained the highest value 29.9 MPa of 10 wt% of talc-filled RPP at the SEBS-g-MA loading of 5 wt%. Unlike the flexural modulus, the mineral filler content had limited effects on the flexural strength. A step change was observed when the SEBS-g-MA loading was increased from 10 wt% to 20 wt%, the flexural strength was significantly reduced.

Impact properties

The tendency of notched impact properties after the addition of SEBS-g-MA is given in Figure 5-28.

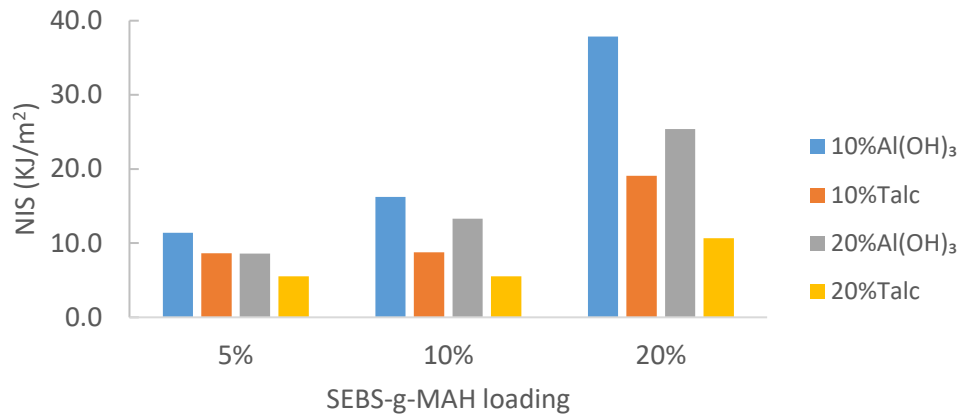


Figure 5-28 The correlation of notched impact strength and SEBS-g-MA loading

The NIS decreased with the increasing of Al(OH)₃ or talc content, but it was enhanced by the addition of SEBS-g-MA. At the same filler content and SEBS-g-MA loading, Al(OH)₃ filled RPP showed better impact performance than talc-filled RPP. It appears that talc embrittles the PP matrix and cause lower fracture toughness (Weon and Sue, 2006). When the SBES-g-MA loading is 20 wt%, the notched impact strength was dramatically increased. At 5 wt% SEBS-g-MA loading, the 10 wt% Al(OH)₃ filled PP showed the highest NIS among these four samples. And the value increases from 11.4 kJ/m² to 37.8 kJ/m² when the SEBS-g-MA increase from 5 wt% to 20 wt%. Denac et al. (2005) studied the PP/talc/SEBS (SEBS-g-MA) composites, the NIS of the composites slightly increase when the SEBS (SEBS-g-MA) content is less than 10 vol%, and when the SEBS (SEBS-g-MA) content is higher than 10 vol%, the NIS dramatically increased. Monti et al. (2020) also found SEBS has

a strong effect in increasing the NIS of PP/Talc composites. The results were consistent with the findings in this study. However, as compared to the industrial requirements, only 10 wt% $\text{Al}(\text{OH})_3$ and 20 wt% SEBS-g-MA filled RPP meet the notched impact requirements of the high-end bumpers, but as mentioned before, the flexural strength (681.3 MPa) of this sample was significantly lower than the required value (1300-1700 MPa).

The results of the NIS at -30°C are presented in Figure 5-29.

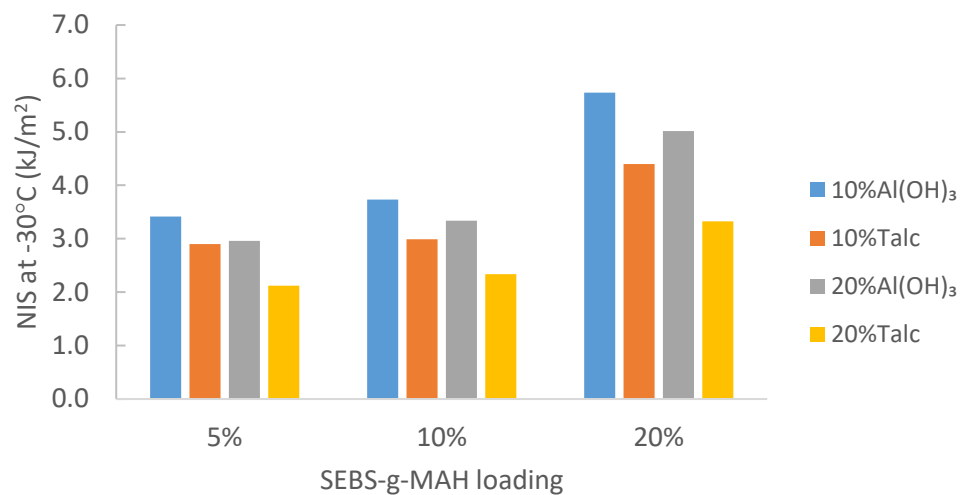


Figure 5-29 The correlation of notched impact strength at -30°C and SEBS-g-MA loading

Similar to the NIS at room temperature, the NIS at -30°C linearly increased with SEBS-g-MA loading. The incorporation of both talc and $\text{Al}(\text{OH})_3$ will contribute to the degradation of NIS at -30°C , and for the same filler content, $\text{Al}(\text{OH})_3$ filled PP has higher NIS at -30°C than talc-filled PP. The reason for the reduction of the notched impact strength is the high concentration of the stress at the edges of the talc and $\text{Al}(\text{OH})_3$ particles accelerate the crack growth (Ashenai Ghasemi et al., 2016). One noticeable point is that at -30°C , the NIS became

difficult to improve. For example, for the 10 wt% $\text{Al}(\text{OH})_3$, when the SEBS-g-MA loading increase from 10 wt% to 20 wt%, the NIS at room temperature improved 132.9% (see Figure 5-28), the notched impact strength at -30°C only improved 53.5% (see Figure 5-29).

Figure 5-30 illustrates the IS of the $\text{Al}(\text{OH})_3$ and talc-filled PP.

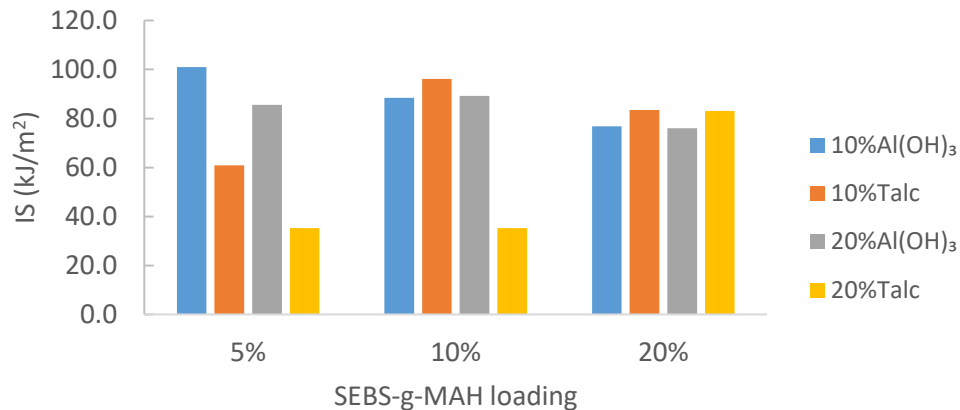


Figure 5-30 The correlation of unnotched impact strength and SEBS-g-MA loading

A slight decrease with the increase of SEBS-g-MA loading was observed in $\text{Al}(\text{OH})_3$ filled RPP composites. For the 10 wt% $\text{Al}(\text{OH})_3$ filled PP, the IS decrease from 101 kJ/m² to 76.8 kJ/m² when SEBS-g-MA content increase from 5 wt% to 20 wt%. And for 20 wt% $\text{Al}(\text{OH})_3$ filled PP, it gained the maximum value of 89.2 kJ/m² at 10 wt% SEBS-g-MA. The talc-filled RPP represents the opposite results. For the 10 wt% talc-filled PP, the maximum value of 96.1 kJ/m² also reached at 10 wt% SEBS-g-MA loading. For the 20 wt% talc-filled PP, the IS remained unchanged when the SEBS-g-MA loading is 5 wt% to 10 wt%. Then it dramatically increased from 35.2 kJ/m² to 83.1 kJ/m² with the SEBS-g-MA loading increase to 20 wt%. When compared to the NIS, these results indicated that talc-filled RPP has less impact resistance to crack propagation.

5.3.2 Conclusion

To overcome the weakness of the RPP blends in the previous section, the study of the RPP/Talc and RPP/Al(OH)₃ composites were processed to investigate the effects of these mineral fillers on the mechanical properties. The idea is to use mineral fillers to improve the flexural properties, especially the flexural modulus, and use SEBS-g-MA to compensate for the impact properties loss. The flexural modulus displayed an almost linear correlation with the mineral filler content. While the highest flexural strength of RPP/Al(OH)₃ and RPP/Talc reached the maximum value at 5 wt% and 10 wt% filler loading, respectively. The low elongation at break may limit the application of RPP/Talc composites being applied in middle-end bumpers. As expected, the NIS at both room temperature and -30°C decreased with increasing filler content. When SEBS-g-MA was incorporated into the mineral filler filled RPP, the NIS significantly improved especially when the loading of SEBS-g-MA is 20 wt%. However, it was found that the addition of both mineral fillers was insufficient to keep the desired flexural modulus. As a result, the stiffness and toughness of the RPP/Al(OH)₃/SEBS-g-MA and RPP/Talc/SEBS-g-MA cannot be well balanced to meet the requirements in this study.

5.4 Summary

To overcome the weakness of the impact properties, the effects of the LLDPE, LLDPE-g-MA, SEBS-g-MA on the mechanical properties of the RPP were studied in the first section. In the second section, the effects of SEBS-g-MA on talc and $\text{Al}(\text{OH})_3$ filled RPP were fully investigated.

SEBS-g-MA filled RPP maintained higher notched impact strength as compared to LLDPE and LLDPE-g-MA at the same loading. However, on the other hand, the deterioration of the flexural properties, especially the flexural modulus of the SEBS-g-MA filled PP hindered the application of the composites. According to the industrial requirements provided by the partner, the 90 wt%RPP and 10 wt%LLDPE-g-MA met the requirements for the middle-end bumper. Further use 20 wt% to 40 wt% of VPP to replace RPP can maintain a better balance of mechanical properties.

In the second section, the 10 wt% and 20 wt% of Talc and $\text{Al}(\text{OH})_3$ filled PP were added 5 wt%, 10 wt% and 20 wt% SEBS-g-MA to investigate the possibility of achieving high impact properties without compromising the tensile, flexural modulus and strength. However, the tensile and flexural properties have the opposite tendency with the notched impact properties. The stiffness and toughness of the mineral filler filled composites cannot be well balanced by using SEBS-g-MA.

Chapter 6 Comparison of the recycled short carbon fibre filled virgin and RPP composites

6.1 Introduction

In previous chapters, the focus has been on the performance of the commonly used mineral fillers (talc, $\text{Al}(\text{OH})_3$) reinforced RPP composites. Unlike the commercialised mineral fillers, recycled short carbon fibre is seen to have low value and usually regarded as waste. This chapter is an investigation of the potential of reinforcing RPP by using recycled short carbon fibre. Currently, the studies of recycled short carbon fibre on non-structural applications are very limited (Howarth et al., 2014). And there is no work where the author uses recycled polymers as the base matrix.

Due to the size of the obtained recycled carbon fibre, it cannot be directly processed using the twin-screw extrusion. This chapter develops the process for recycled short milled carbon fibre (rSMCF) filled VPP or RPP composites and investigates the effects of rSMCF on the corresponding mechanical and thermal performance. The coupling agent MAPP was introduced to improve the interfacial adhesion between rSMCF and VPP or RPP matrix. The microscale tests were processed to evaluate the fracture surface and the dispersion of rSMCF in VPP or RPP matrix.

6.2 Results and discussions

6.2.1 Effects of surfactant

In this study, the obtained RCF has an average length of 8.65mm, to prevent the possible instability in the twin-screw extrusion process, RCF was shredded into short size (average length 240 μm) named as recycled short milled carbon fibre (rSMCF). rSMCF was added into the PP/RPP matrix as a filler.

Figure 6-1 shows the appearance of the RCF and rSMCF.

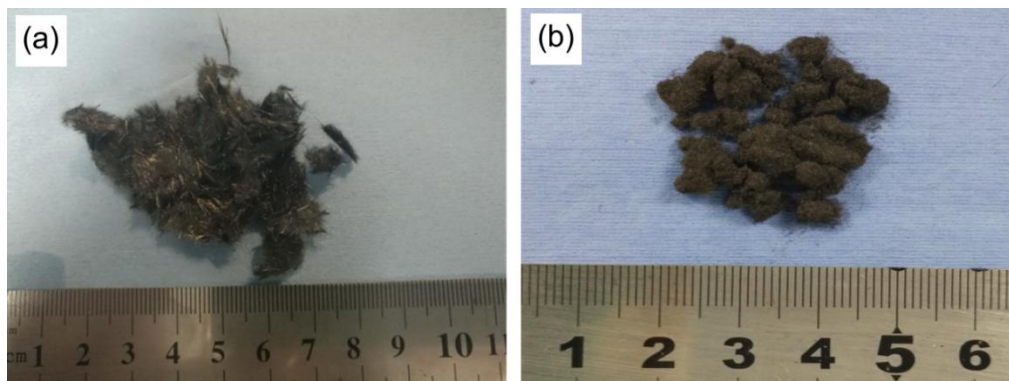


Figure 6-1 (a) RCF before shredding and (b) RCF after shredding

It can be observed that the agglomeration of the carbon fibres occurred before and after the shredding, which will cause the inhomogeneous dispersion of rSMCF in the plastic matrix after twin-screw extrusion. To overcome this problem, a process called 'Dispersion of rCF' was developed in this study. The surfactant Polyoxyethylene (20) oleyl ether was introduced into the process. The details of the process are described in Chapter 3, Section 3.3.3.

Due to the design of the process, the surfactant was used to ensure the dispersion of rSMCF, so the surfactant and rSMCF are to be added together. So, it is impossible to create a rSMCF

added group without surfactant. To estimate the effects of the surfactant, the control group 1-1 to 1-4 and 2-1 to 2-4 were prepared. The mechanical results of the surfactant added VPP and RPP polymers were shown in Table 6-1.

Table 6-1 Mechanical results of VPP/RPP with different loading of surfactant

Sample		Tensile Modulus	Tensile Strength	Flexural Modulus	Flexural Strength	Impact Strength
		(MPa)	(MPa)	(MPa)	(MPa)	(kJ/m ²)
1-1	PP	1304.9	23.10	1137.8	28.70	98.70
1-2	SF0.5/PP	1289.9	22.90	1121.7	28.60	100.10
1-3	SF1/PP	1331.3	23.20	1162.9	28.20	101.10
1-4	SF2.5/PP	1321.7	23.20	1164.2	29.00	102.40
2-1	RPP	1283.5	26.00	1099.2	28.20	98.80
2-2	SF0.5/RPP	1262.4	25.80	1080.8	27.40	101.90
2-3	SF1/RPP	1276.3	26.30	1076.8	27.40	100.80
2-4	SF2.5/RPP	1254.5	25.90	1079.7	26.80	101.30

Based on the results of the control groups, no significant effects of the surfactant on the tensile modulus, tensile strength, flexural modulus, flexural strength and impact strength were observed. The variation of the tested properties as compared to pure VPP and pure RPP are all within $\pm 5\%$. The maximum variation for VPP based composites come from the impact properties, the difference between the sample SF_{2.5}/PP and the sample PP is 3.7%. And for the RPP-based composites, the variation of flexural strength of the sample RPP and the sample SF_{2.5}/RPP is 4.9%.

6.2.2 Effects of the fibre content

The sample preparation process of rSMCF filled PP and RPP composites were given in Chapter 3, Section 3.3.3. The

designed compositions of the rSMCF filled PP and RPP composites were shown in Table 3-7 and Table 3-8 (In Chapter 3, Section 3.3.3.1 and Section 3.3.3.2).

The use of recycled carbon fibre has been extensively studied for the past decades. However, most of the study focus on recycled carbon fibre loading at more than 20 wt% (Wong et al., 2012, Giannadakis et al., 2011, Akonda et al., 2012). The high loading of recycled carbon fibre will increase the overall cost of the composites and limit industrial use. In this study, the weight fraction of rSMCF in this study was controlled as 1 wt%, 2 wt% and 5 wt%.

There is a very limited study of recycled short carbon fibre on non-structural applications (Howarth et al., 2014). The short recycled carbon fibre is seen to have low value and usually regarded as waste. And there is no work that the author realise to use recycled polymers as the base matrix. Our work will fulfil the knowledge gap in the mechanical and thermal performance of recycled short carbon fibre reinforced recycled PP composites. The results of 1 wt%, 2 wt% and 5 wt% rSMCF filled VPP and RPP composites were shown in Table 6-2.

Table 6-2 Mechanical results of PP/RPP with different loading of rSMCF

Sample		Tensile Modulus	Tensile Strength	Flexural Modulus	Flexural Strength	Impact Strength
		(MPa)	(MPa)	(MPa)	(MPa)	(kJ/m ²)
1-1	PP	1304.9	23.10	1137.8	28.70	98.70
1-5	SF _{0.5} /PP/rSMCF ₁	1395.9	22.80	1176.9	28.80	100.10
1-6	SF ₁ /PP/rSMCF ₂	1598.9	23.20	1245.8	29.30	103.10
1-7	SF _{2.5} /PP/rSMCF ₅	1790.1	21.80	1341.1	27.20	94.90
2-1	RPP	1283.5	26.00	1099.2	28.20	98.80
2-5	SF _{0.5} /RPP/rSMCF ₁	1390.3	25.93	1202.1	27.32	83.15
2-6	SF ₁ /RPP/rSMCF ₂	1511.8	25.62	1285.2	27.30	73.83
2-7	SF _{2.5} /RPP/rSMCF ₅	1954.4	26.43	1623.8	27.98	60.12

The tensile modulus and flexural modulus of the composites were significantly improved with the addition of rSMCF, with the greatest improvement at 5 wt%. At 5 wt% of rSMCF, the tensile modulus of VPP-based composites improved 37.7% while the RPP-based composites increased 52.3%. The compounding of VPP and rSMCF has increased the rigidity of the composites due to a transcrystalline layer (TCL) developing from the high strength carbon fibre which provides an improved surface stiffness (Wong et al., 2012). Compared to PE composites with the same loading of rSMCF (McNally et al., 2008), the improvements in tensile modulus of the PP/rSMCF composites in Table 6-2 are more significant (e.g. around 27% for PE and 37% for PP with 5 wt% rSMCF). The improvement of rSMCF on the tensile and flexural modulus of the RPP composites is even more significant than VPP composites. At 5 wt% of rSMCF, the tensile and flexural modulus improved 52.3% and 47.3% as compared to neat RPP. The improvement of tensile and flexural modulus was attributed to the incorporation of rigid carbon fibre (Wong et al., 2012). Hashemi (2008) argued that the elastic modulus (E_c), and tensile and flexural modulus of filled composites are not significantly affected by the fibre loading mode, thus the patterns of both modulus tend to be similar. Improvements to the tensile modulus were higher than those of flexural modulus, and the same phenomenon has been observed by Wong et al. (2012). This is potentially a result of fibre orientation within the composite matrix since it was demonstrated that CF in the injection moulded tensile specimens were preferentially oriented in the flow direction (Fu et al., 2000). The E_c of the PP/rSMCF composites can be predicted using Equation 2 (Fu et al., 2000, Shazed et al., 2014):

$$E_c = \lambda_E E_f V_f + E_m (1 - V_f) \quad (6.1)$$

where λ_E is the fibre (in this case rSMCF) efficiency factor for the composite modulus considering the effects of fibre length and orientation, V_f is the volume fraction of fibre in the composite, and E_c , E_f and E_m are the modulus of composite, fibre and polymer matrix, respectively. In this case, E_m refers to the modulus of the PP control group in Table 6-2 (sample 1-1). The efficiency factors (λ_E) for the tensile modulus of PP/rSMCF composites SF_{0.5}/PP/rSMCF₁, SF₁/PP/rSMCF₂, and SF_{2.5}/PP/rSMCF₅ can be calculated as 0.1126, 0.1428 and 0.0978, respectively, based on the densities and wt% of each component. The calculated efficiency factors (λ_E) for the tensile modulus of RPP/rSMCF composites SF_{0.5}/RPP/rSMCF₁, SF₁/RPP/rSMCF₂, and SF_{2.5}/RPP/rSMCF₅ are 0.1159, 0.1202 and 0.1367, respectively. The fibre efficiency results also proved that rSMCF has higher efficiency in RPP matrix than PP matrix at 5 wt% rSMCF content. The variance of the fibre efficiency in VPP and RPP composites at the same content may be attributed to the high MFI of RPP, indicating fibre has more consistent fibre orientation in RPP matrix. Fu et al. (2000) reported that a high volume fraction of fibre leads to the reduction of fibre length, which may lead to a decrease in fibre efficiency. However, the mean fibre length (240 μm) and mean fibre aspect ratio L/D (240:7.56) of the rSMCF used in this study are significantly lower than the CF materials used previously (mean fibre length and mean fibre aspect ratios of 300 μm and 300:7.5 (Fu et al., 2000), or 8.65 mm and 8650:7.56 (Wong et al., 2012), respectively. As fibre efficiency factors decrease with decreasing mean fibre length or mean fibre aspect ratio (Fu et al., 2000, Shazed et al., 2014, Fu and Lauke, 1996), the lower values observed in this study are in accordance with published results.

Unlike the continuous increments with rSMCF addition which have been reported previously (McNally et al., 2008, Han et al., 2012), both the tensile and flexural strength of the PP/rSMCF composites decrease with the increase of rSMCF content. Therefore, the modified rule of mixtures equation (Das, 2011, Fu and Lauke, 1996) is not applicable for predicting the strength of the uncompatibilised PP/rSMCF composites. In Table 6-2, the tensile and flexural strength of the RPP composites has a noticeable decrease at 1 wt% rSMCF loading. Then the tensile and flexural strength continuously increases and at 5 wt% rSMCF, the tensile strength is 1.6% higher than neat RPP, and the flexural strength is 0.8% lower. As the variation of both tensile and flexural strength of the control group was within $\pm 2\%$ (Table 6-1, sample 1-1 to 1-4, sample 2-1 to 2-4) the possibility of the surfactant's detrimental effect on the polymer can be ruled out. To investigate the reason for this reduction in tensile and flexural strength, SEM micrographs of the tensile fracture surface of SF_{2.5}/PP/rSMCF₅ were recorded (Figure 6-2).

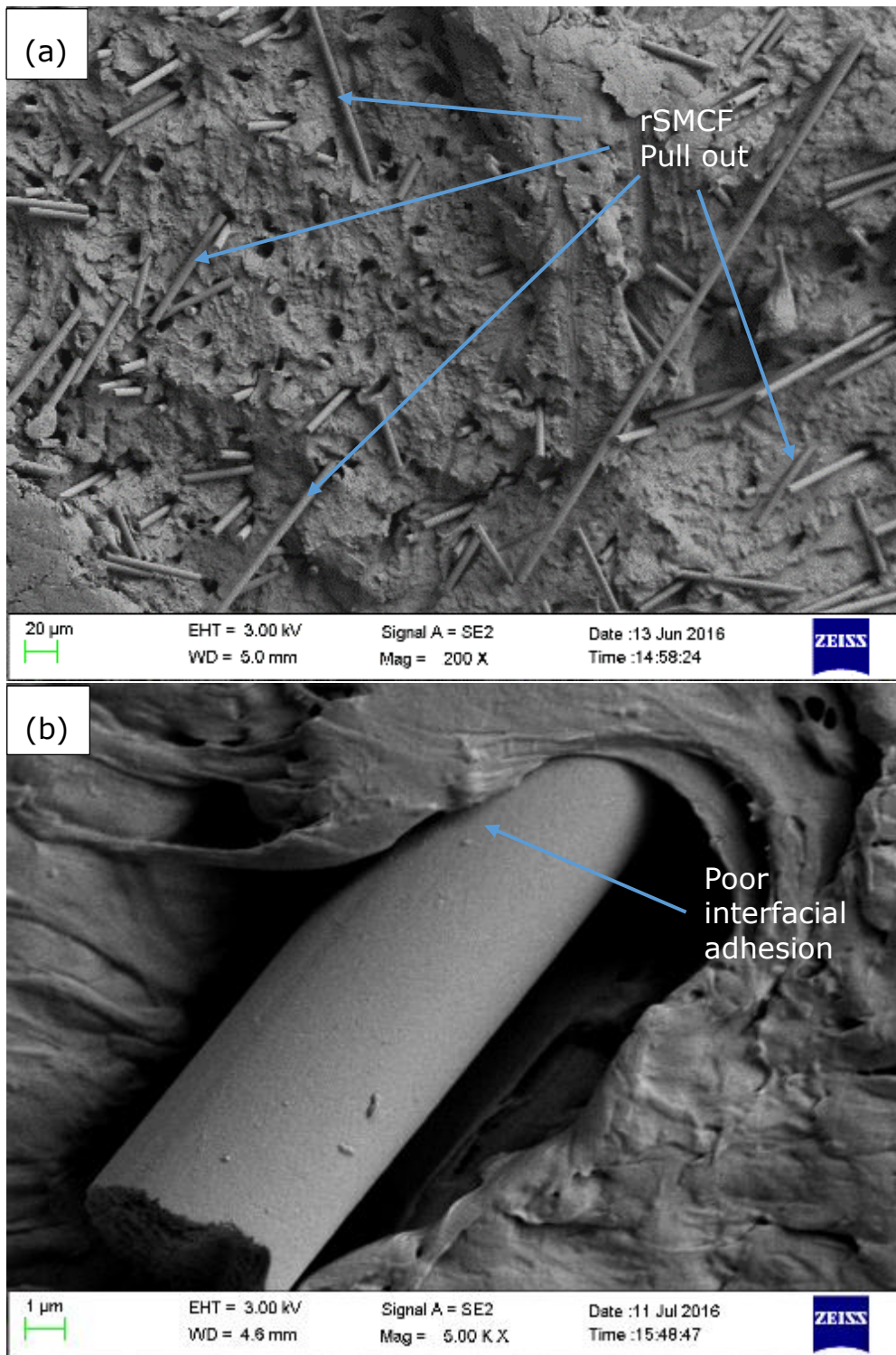


Figure 6-2 SEM micrographs of the tensile-facture surface of, recorded at (a) SF_{2.5}/PP/rSMCF₅ at low magnification (b) SF_{2.5}/PP/rSMCF₅ at high magnification

The SEM image Figure 6-2(a) shows voids where many fibres have been pulled from the composite matrix under tensile force. The surface of the rSMCF shows little adhesion to the VPP matrix, as shown in Figure 6-2 (b). Thus, the reduction in tensile and flexural strength for SF_{2.5}/PP/rSMCF₅ could be due to a lack of interfacial adhesion between VPP and rSMCF. The SEM photographs of tensile fracture surface of SF_{2.5}/RPP/rSMCF₅ were shown in Figure 6-3.

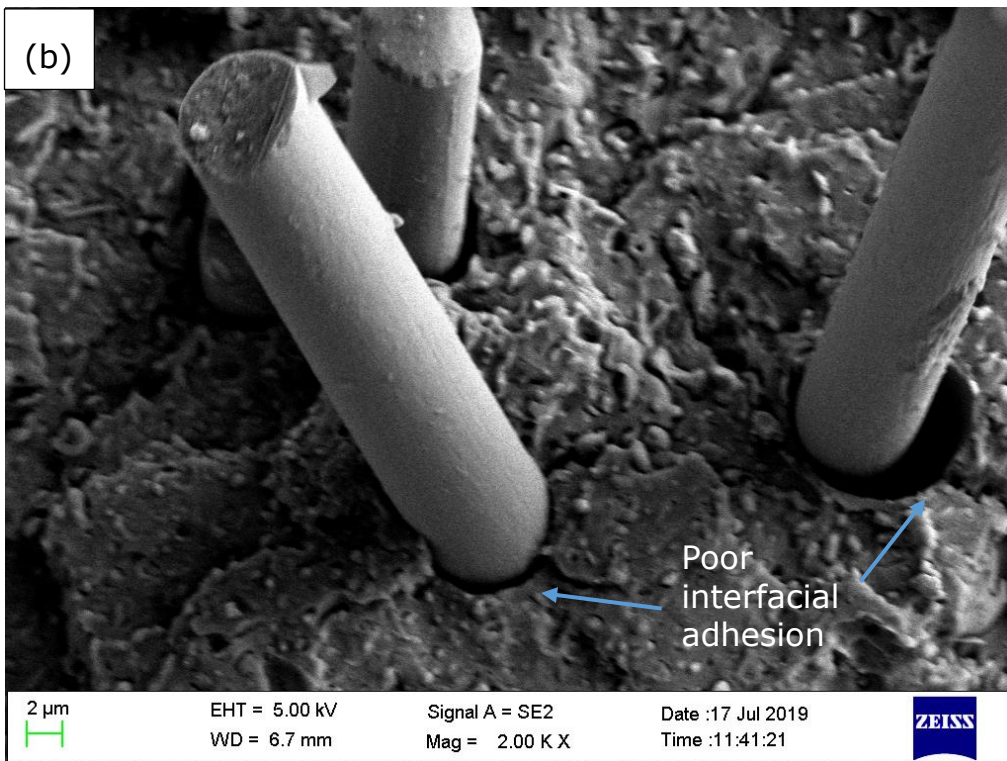
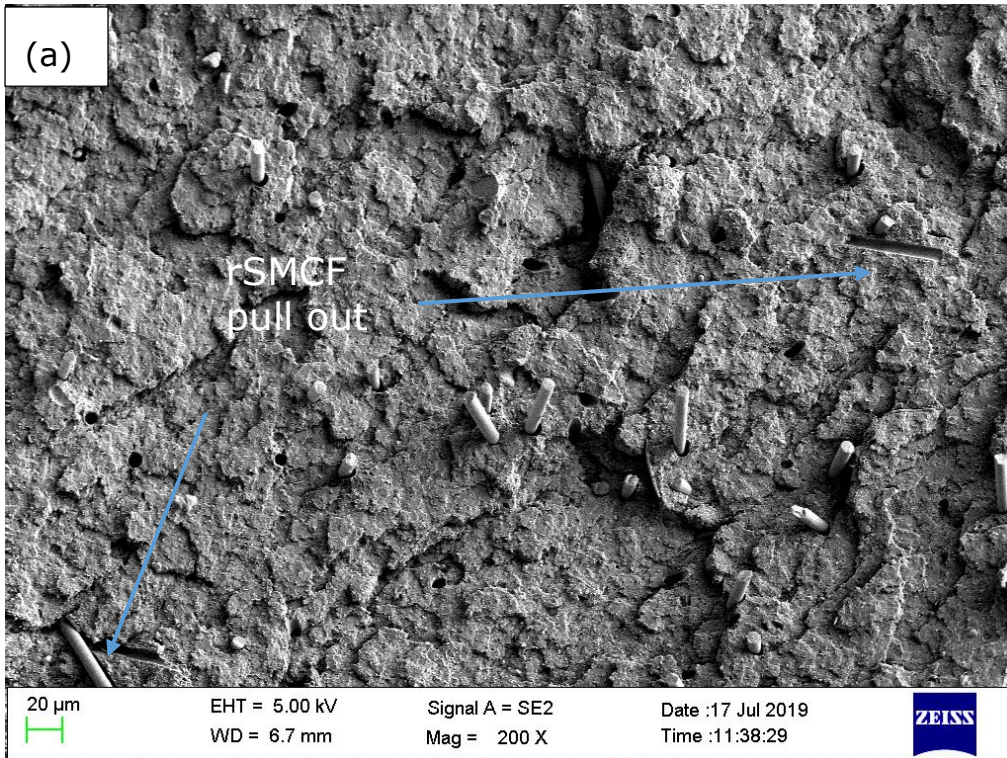


Figure 6-3 SEM micrographs of the tensile-facture surface of, recorded at (c) SF_{2.5}/RPP/rSMCF₅ at low magnification (d) SF_{2.5}/RPP/rSMCF₅ at high magnification

In the RPP based matrix, rSMCF was also pulled out and proved by the voids shown in Figure 6-3. However, as comparing Figure 6-2 (a) and Figure 6-3 (a), the interfacial adhesion of RPP/rSMCF is better than PP/rSMCF since the less pullet out rSMCF in RPP based matrix was observed.

The Izod impact results of the SF_{2.5}/PP/rSMCF composites are comparable to that of neat VPP, as shown in Table 6-2. The SEM micrographs of the impact-fracture surface of SF_{2.5}/PP/rSMCF₅ are shown in Figure 6-4, where the rSMCF can be seen as evenly dispersed in the VPP matrix.

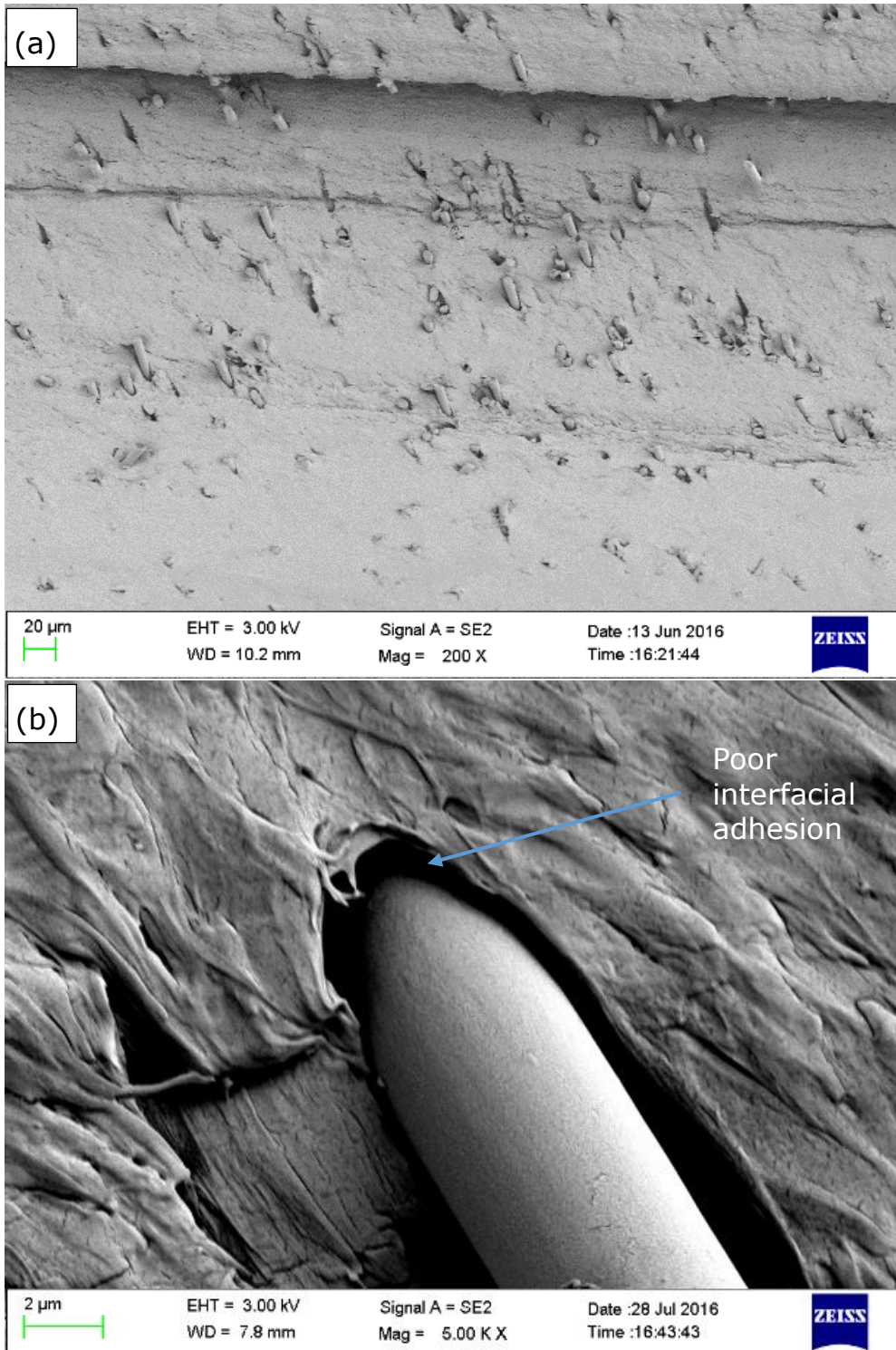


Figure 6-4 SEM micrographs of the impact-failure surface of (a) SF_{2.5}/PP/rSMCF₅ at low magnification (b) SF_{2.5}/PP/rSMCF₅ at high magnification

Despite there being minimal interfacial adhesion between the VPP matrix and rSMCF in the samples on the impact fracture [Figure 6-4 (b)], the impact strength of SF_{2.5}/PP/rSMCF₅ (94.9 ± 2.1 kJ/m²) is almost the same as neat VPP (98.7 ± 1.5 kJ/m²). Similar to the tensile and flexural strengths, the impact strength shows a slight decrease for SF_{2.5}/PP/rSMCF₅ compared to neat VPP, which can be explained through the lack of interfacial adhesion between the VPP matrix and rSMCF. Besides, Figure 6-4 (a) shows that the rSMCFs are aligned perpendicular to the impact fracture surface, thus, the fibres are preferentially oriented in the direction of injection melt flow as has been observed previously (Shazed et al., 2014). For the RPP based matrix, the un-notched impact strength has suffered a significant reduction with the addition of rSMCF. When the content of rSMCF increased from 1 wt% to 5 wt%, the un-notched impact strength reduced from 83.2 kJ/m² to 60.1 kJ/m². Figure 6-5 shows the fracture surface of the specimens after the impact test.

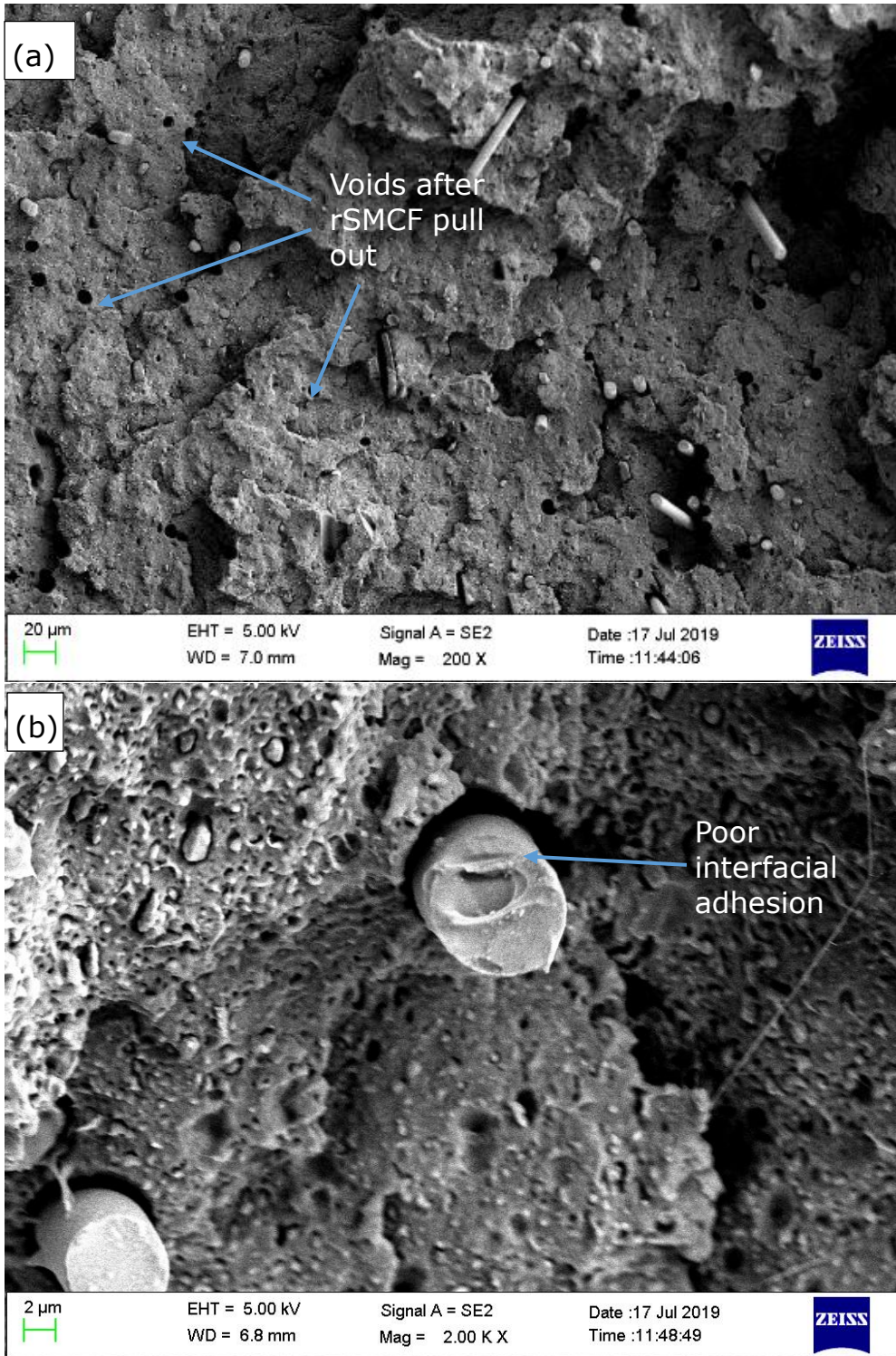


Figure 6-5 SEM micrographs of the impact-fracture surface of
 (a) SF_{2.5}/RPP/rSMCF₅ at low magnification (b)
 SF_{2.5}/RPP/rSMCF₅ at high magnification

It can be observed that the fracture surface of the PP

composites is smoother than the RPP composites. The large amounts of the holes presented in Figure 6-5(a) indicated rSMCF was pulled out during the impact, which is attributed to the poor interfacial adhesion between rSMCF and RPP matrix.

Using HD FTIR imaging to identify the chemical composition of the composite mixtures (Konevskikh et al., 2016) to understand the distribution of the surfactant. Mie scattering caused by the micrometre sized CF can be used to identify their location within the polymer matrix. The FTIR imaging results were shown in Figure 6-6.

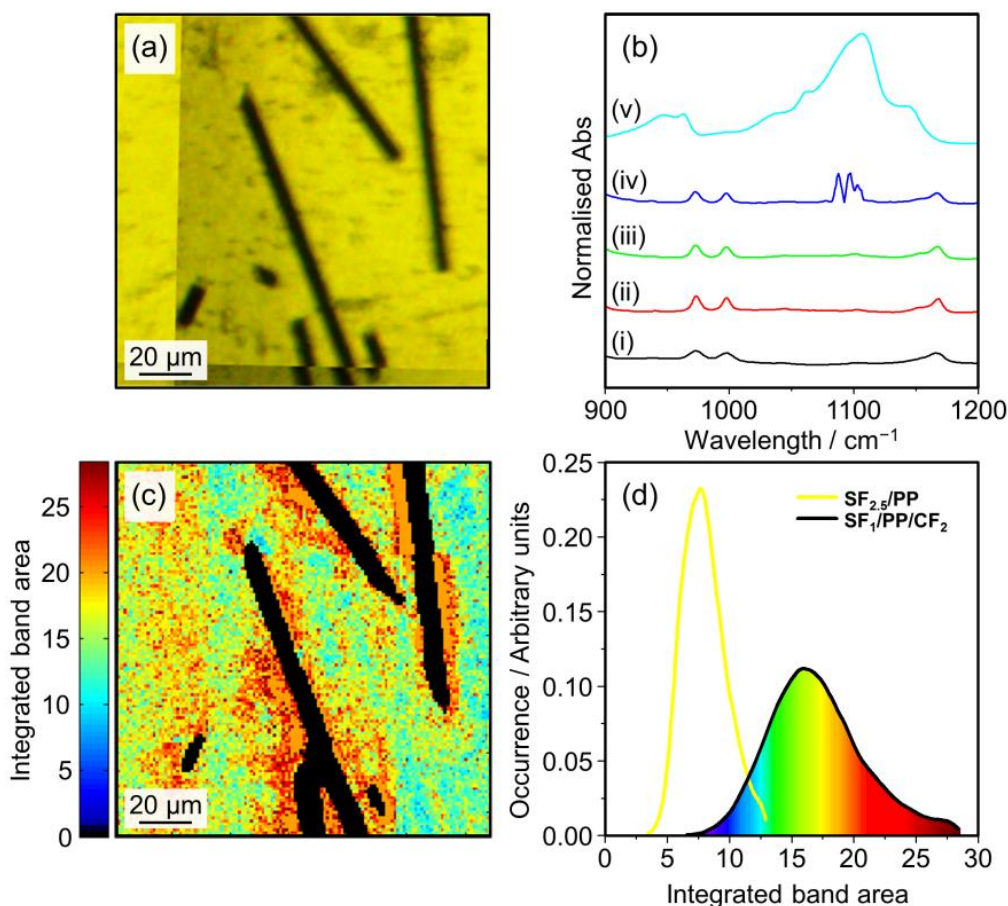


Figure 6-6 (a) Optical image of SF₁/PP/rSMCF₂. (b) FTIR spectra of (i) PP (ii) averaged spectra in SF₁/PP (iii) averaged SF/PP spectra in SF₁/PP/rSMCF₂ (iv) averaged rSMCF spectra in SF₁/PP/rSMCF₂ (v) SF. (c) Chemical image based on the integrated band area (1067-1123 cm⁻¹) of SF₁/PP/rSMCF₂. (d) Integrated band area histogram for the SF_{2.5}/PP/rSMCF₅ chemical image shown in (c) excluding regions of rSMCF (black line) and SF_{2.5}/PP (yellow line)

In Figure 6-6(b), the black pixels represent the mean absorbance (abs > 0.3818) in the range 1800 cm⁻¹ to 2000 cm⁻¹, a region in which there should be no peaks due to the surfactant or VPP. This accurately represents the CF and is easily distinguishable from the VPP/SF matrix through comparison with the optical image [Figure 6-6 (a)]. The

average IR spectrum of the rSMCF pixels corrected for scattering is shown in Figure 6-6, where the band of polyoxyethylene (20) oleyl ether is clearly visible. The chemical image of the VPP matrix, based the integral band area of the surfactant ($1067\text{-}1123\text{ cm}^{-1}$) is shown in Figure 6-6(c), where rSMCF pixels have been excluded (black) as the influence of scattering on the surfactant absorption could not be excluded, and outliers (pixels in the high and low range) are given the 25th and 75th percentiles respectively (see experimental section). As expected, the surfactant in the sample is not evenly distributed and has a higher concentration in regions close to the CF. The influence of the rSMCF on the distribution of the SF in the composite materials is more clearly observed from the band area histogram [Figure 6-6 (d)]. The distribution of the rSMCF sample ($\text{SF}_1/\text{PP}/\text{rSMCF}_2$, Figure 6-6(d), black line) has a mean ($\bar{x} = 17.06$) and standard deviation ($\sigma = 3.82$) that are not evenly distributed due to the influence of the rSMCF. However, the control sample ($\text{SF}_{2.5}/\text{PP}$, Figure 6-6(d), yellow line) has a normal distribution around the mean ($\bar{x} = 7.98$) and a lower standard deviation ($\sigma = 1.72$), indicating that the polyoxyethylene (20) oleyl ether is more evenly distributed in the PP matrix. The lower mean $\text{SF}_{2.5}/\text{PP}$ compared to $\text{SF}_1/\text{PP}/\text{rSMCF}_2$ is a result of poor mixing between VPP and the surfactant in the absence of rSMCF.

The MFI results of the PP/rSMCF and RPP/rSMCF composites are plotted in Figure 6-7 and Figure 6-8.

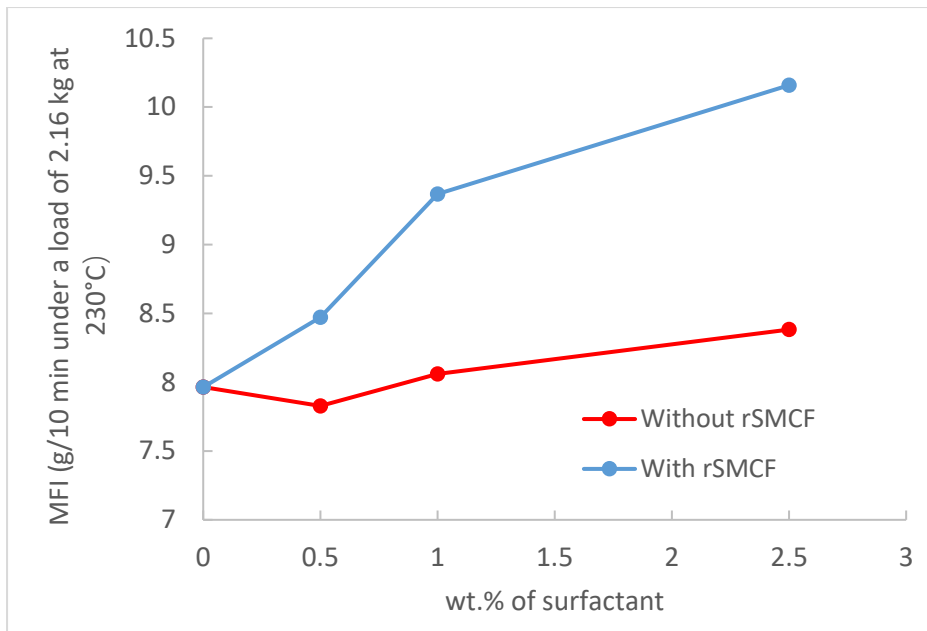


Figure 6-7 MFI results (g/10 min under load of 2.16 kg at 230 °C) for increasing surfactant and surfactant/rSMCF concentrations in the RPP/rSMCF composites

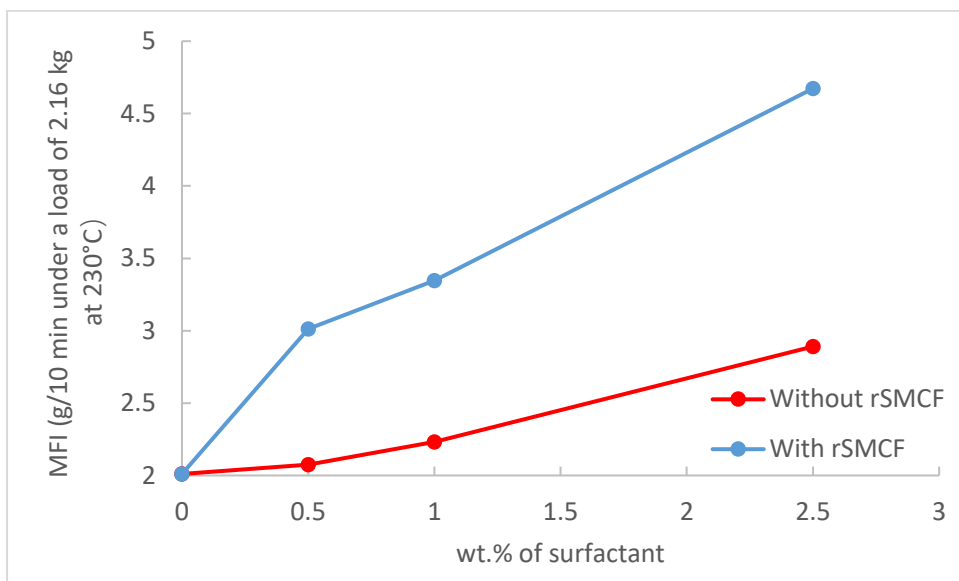


Figure 6-8 MFI results (g/10 min under load of 2.16 kg at 230°C) for increasing surfactant and surfactant/rSMCF concentrations in the PP/rSMCF composites

Both rSMCF and surfactant additions increase the MFI of the composites, with a greater increase observed for rSMCF. The MFI of SF_{2.5}/PP increased by 43.8% as compared to neat VPP, while SF_{2.5}/RPP increased 5.3% with respect to neat RPP. The addition of rSMCF further increase the MFI of the composites, when compared to the base material, SF_{2.5}/PP/rSMCF₅ increased 132.4% and SF_{2.5}/RPP/rSMCF₅ increased by 27.6%. The difference in MFI increment was due to the MFI of RPP is about 3 times higher than VPP, which make the change in MFI less significant. Since the MFI is a direct inverse measure of a polymeric material's viscosity, these results indicate that the presence of rSMCF and/or surfactant reduces the viscosity of the composites. The reduced melting viscosity with additions of the surfactant is presumably caused by the low molecular weight of polyoxyethylene (20) oleyl ether, as the molecular weight is inversely proportional to viscosity (Shaw and Tuminello, 1994). The increase of MFI caused by rSMCF addition requires further consideration. Roy and Gupta (1993) reported that the viscosity of a CF filled composite is mainly influenced by two competing mechanisms: (1) Interactions between fibre and matrix, which increases the viscosity, and (2) Wall-slip caused by the presence of longitudinally oriented fibres along the wall-melt interphase, which decreases the viscosity. At a lower fibre loading, the latter mechanism dominates the rheological behaviour of rSMCF filled composites (Roy and Gupta, 1993). However, this is contradictory to the observed increase in MFI in this study (Figure 6-7). The poor interfacial adhesion between the VPP or RPP matrix and rSMCF (Figure 6-2, Figure 6-3) results in delamination of the PP/rSMCF composites which is exacerbated with an increased number of particles or agglomerates in the VPP or RPP matrix. This

resulted from rSMCF addition, thereby the MFI values are increasing with rSMCF loading. This proposition is supported by comparing SEM images at 2 and 5 wt% rSMCF (Figure 6-9 and Figure 6-10) where the degree of exfoliation is increasing with increasing wt% rSMCF in the composite matrix.

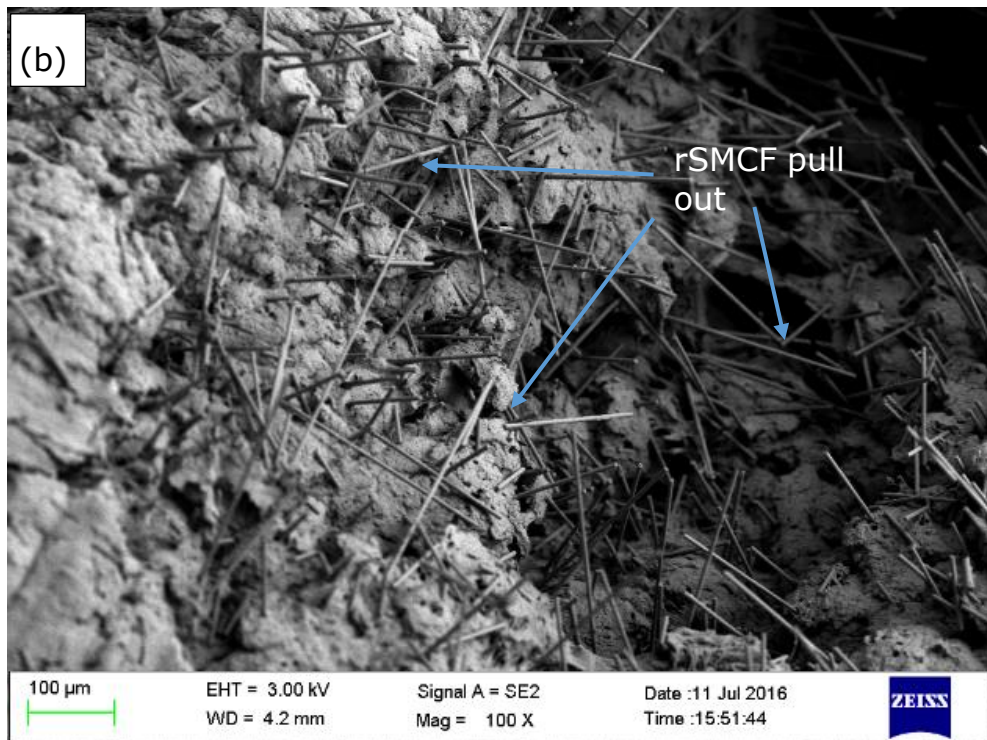
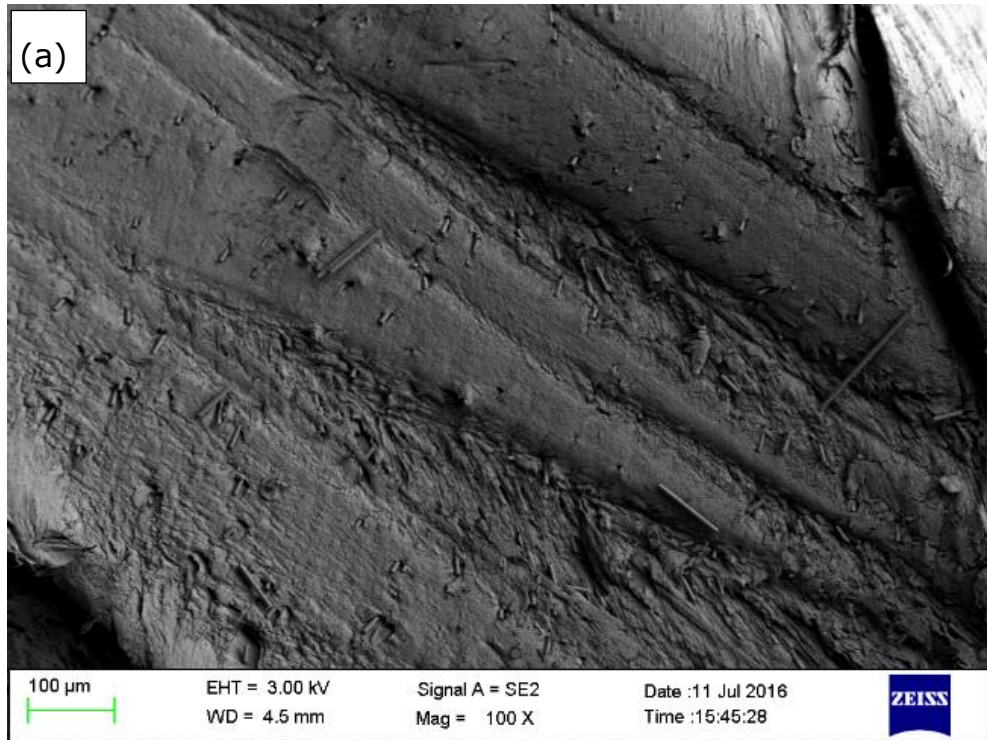


Figure 6-9 SEM micrographs of the fracture surface (a) $\text{SF}_1/\text{PP}/\text{rSMCF}_2$ (b) $\text{SF}_{2.5}/\text{PP}/\text{rSMCF}_5$

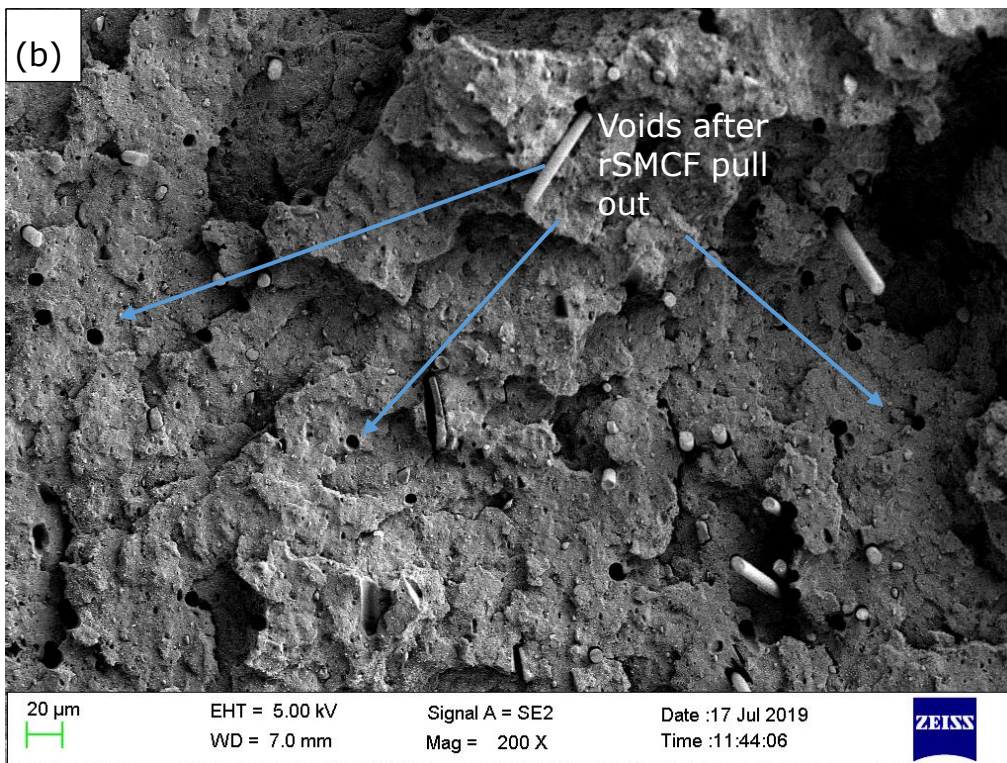
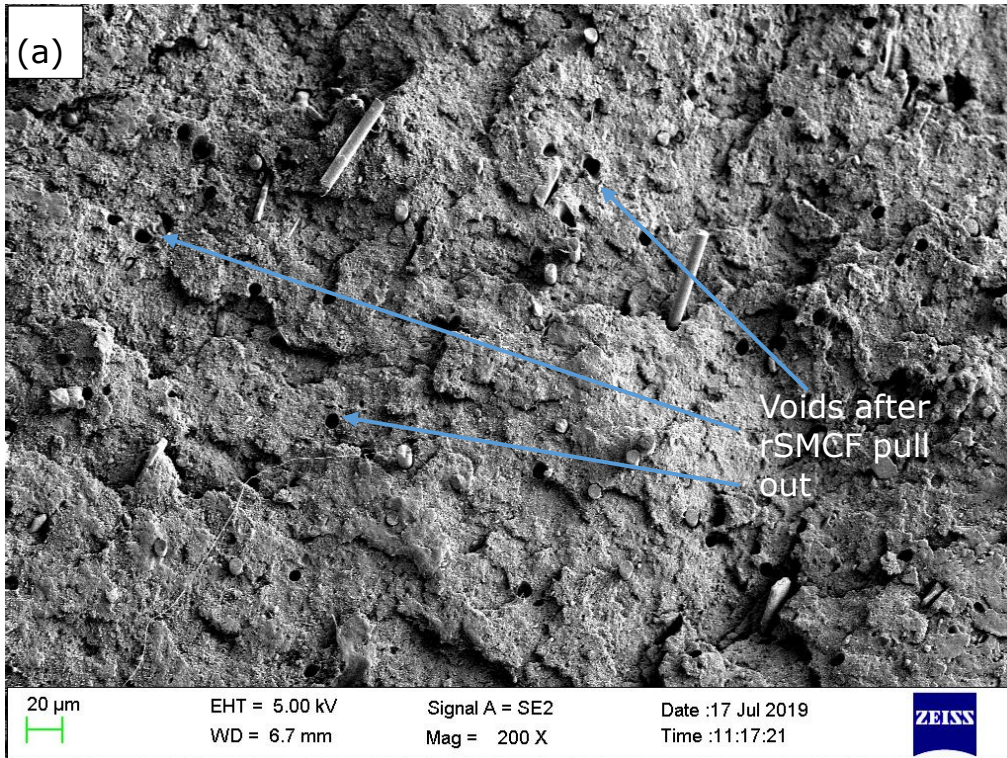


Figure 6-10 SEM micrographs of the fracture surface (a) SF₁/RPP/rSMCF₂ (b) SF_{2.5}/RPP/rSMCF₅

The differential scanning calorimeter (DSC) thermograms of the VPP-based and recycled PP-based composites are shown in Figure 6-11 and Figure 6-12.

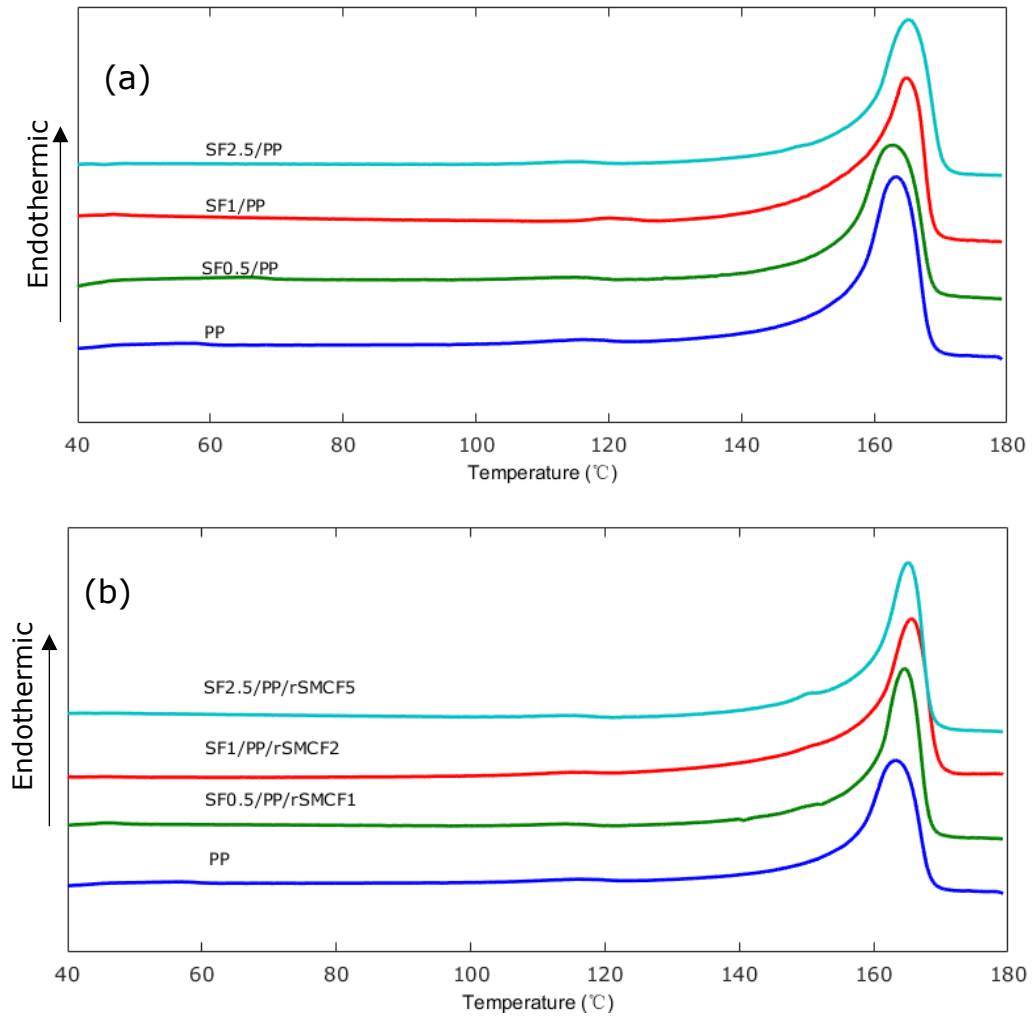


Figure 6-11 DSC heating curves of (a) surfactant added PP samples (b) rSMCF reinforced PP samples

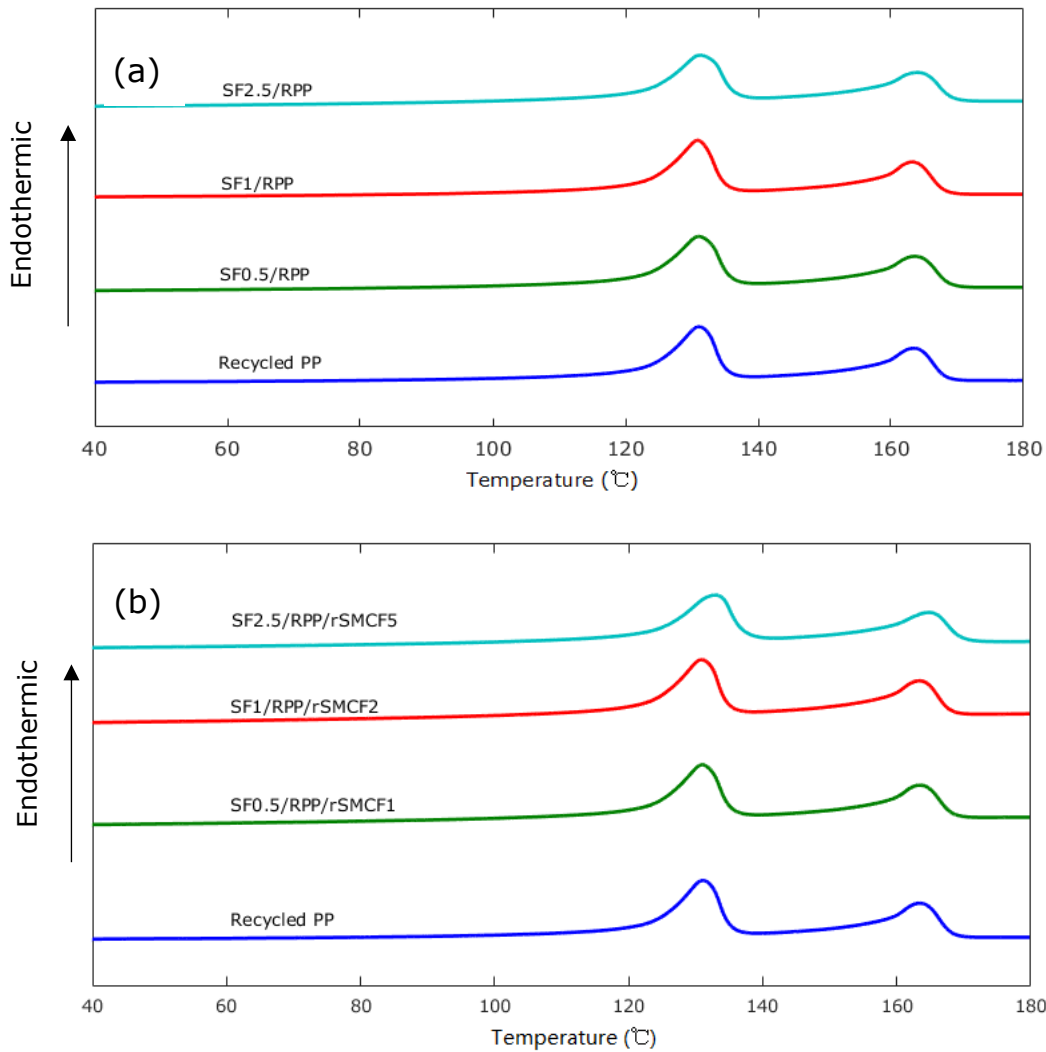


Figure 6-12 DSC heating curves of (a) surfactant added RPP samples (b) rSMCF reinforced RPP samples

These curves are taken from the second heating of the samples from the DSC. The addition of 0.5-2.5 wt% of surfactant to VPP and RPP composites slightly increase the melting temperature. In PP/SF composites, the melting temperature (T_m) increases from 154.6°C to 157.6°C when the surfactant content increase from 0.5 wt% to 2.5 wt%. Additionally, it is obvious that the RPP based matrix has two melting peaks in the heating process. The lower melting peak was attributed to the presence of PE in the RPP matrix.

For SF/PP/rSMCF composites, the T_m shifts to higher temperature with the addition of rSMCF. The T_m of neat RPP is 163.5°C, and the T_m of SF_{0.5}/RPP/rSMCF₁, SF₁/RPP/rSMCF₂ and SF_{2.5}/RPP/rSMCF₅ was 163.5, 163.4 and 164.7 °C, respectively. The presence of rSMCF has increased the T_m of VPP and RPP composites, which is consistent with the findings by Tan et al. (1990).

The crystallisation results are shown in Table 6-3 and Table 6-4.

Table 6-3 DSC results of PP/SF and SF/PP/rSMCF composites

	T_m (°C)	ΔH_{m1} (J/g)	X_c
PP	155.7	75.21	36.0%
SF _{0.5} /PP	154.6	71.44	34.2%
SF ₁ /PP	156.6	72.50	34.7%
SF _{2.5} /PP	157.6	67.89	32.5%
SF _{0.5} /PP/rSMCF ₁	157.8	80.29	38.4%
SF ₁ /PP/rSMCF ₂	158.9	60.52	29.0%
SF _{2.5} /PP/rSMCF ₅	158.7	64.11	30.7%

Table 6-4 DSC results of RPP/SF and SF/RPP/rSMCF composites

	T_m (°C)	ΔH_{m1} (J/g)	PP χ_0	ΔH_{m2} (J/g)	PE χ_0	Total χ_0
RPP	158.0	31.45	15.0%	51.99	17.7%	32.8%
SF _{0.5} /RPP	158.3	28.38	13.6%	48.38	16.5%	30.1%
SF ₁ /RPP	158.4	26.63	12.7%	50.43	17.2%	30.0%
SF _{2.5} /RPP	158.2	26.79	12.8%	52.84	18.0%	30.9%
SF _{0.5} /RPP/rSMCF ₁	158.6	24.13	11.5%	43.66	14.9%	26.4%
SF ₁ /RPP/rSMCF ₂	158.2	25.78	12.3%	48.21	16.5%	28.8%
SF _{2.5} /RPP/rSMCF ₅	158.0	25.07	12.0%	48.12	16.4%	28.4%

The H_m of the VPP and RPP composites decrease with the presence of surfactant in the system. The percentage of the crystallisation (χ_0) of PP, SF_{0.5}/PP, SF₁/PP and SF_{2.5}/PP can be calculated as 36.0%, 34.4%, 35.0% and 33.3%, respectively. χ_0 increased on addition of 1 wt% rSMCF (SF_{0.5}/PP/rSMCF₁) to the composite, then decreased at 2 wt% rSMCF (SF₁/PP/rSMCF₂), and increased again for SF_{2.5}/PP/rSMCF₅. It is reported that at low content, CF acts as the nucleation sites which accelerates the crystal growth of the polymers (Yan et al., 2014, Liu et al., 2015). This may explain the increase of χ_0 at 2 wt% rSMCF. However, as the content of fibres in the composites increase, fibres will prevent the mobility of the polymer matrix and reduce the crystallisation of the polymer (Karsli and Aytac, 2013, Ren et al., 2008). The changes in χ_0 are inversely correlated with the values of T_m , tensile strength, un-notched Izod impact strength and fibre efficiency factors for the tensile modulus (Table 6-2).

By using component measuring methods via DSC (Shimadzu,

2017), the content of PP and PE in the RPP was calculated as 45.9% and 54.1%. Table 6-4 presents the crystallisation results of PP/PE blends. For the RPP composites, a remarkable drop of χ_0 was observed for SF_{0.5}/RPP, with the increment of surfactant, the χ_0 of PP keeps decreasing, but χ_0 of PE keeps increasing. As a result, unlike VPP composites, the effects of the surfactant on the total χ_0 of RPP composites are very limited. The total χ_0 decreased on addition of 1 wt% rSMCF (SF_{0.5}/PP/rSMCF₁) to the composite, then increase at 2 wt% rSMCF (SF₁/PP/rSMCF₂), and decrease again for SF_{2.5}/PP/rSMCF₅. The total χ_0 of SF/RPP/rSMCF composites is positively related to the values of tensile strength, tensile modulus, flexural strength and flexural modulus. A FTIR analysis of pure PP, PE and RPP was studied to ensure the existence of PE in PP. The results were shown in Figure 6-13.

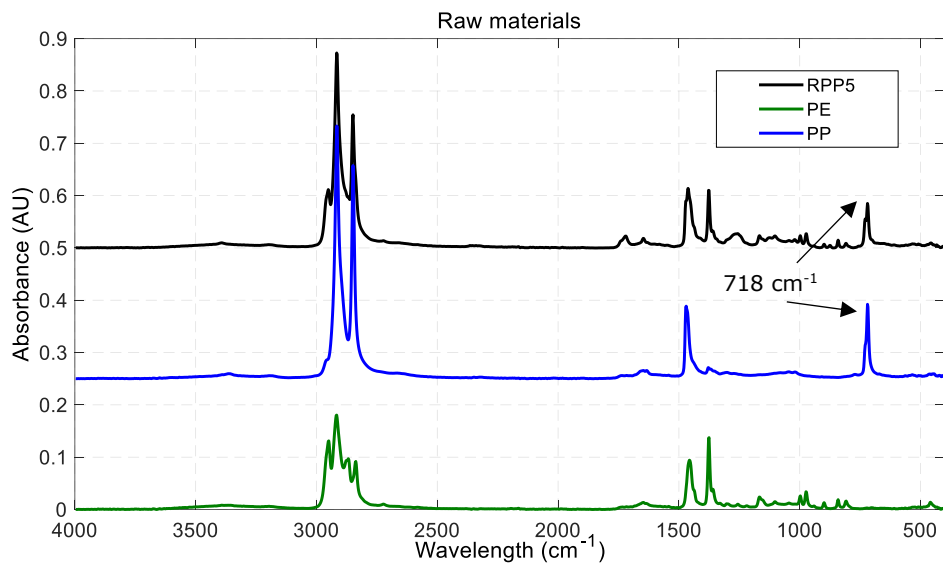


Figure 6-13 FTIR spectra of PP, PE and RPP

The distinct peak of PE at wave number 719 cm⁻¹ was correspond to the rocking deformation (Gulmine et al., 2002, Rajandas et al., 2012). The peak at 719 cm⁻¹ was observed both

in PE and RPP, which indicates the existence of PE in RPP.

6.2.3 Effects of coupling agent

Coupling agents play an important role in improving the mechanical properties of the carbon fibre added composites (Wong et al., 2012, Karsli and Aytac, 2011). To investigate the compatibilising effect of adding a coupling agent to the rSMCF composites, MAPP was initially added into the composite matrix at the same weight fraction as the rSMCF. The compositions and mechanical properties of SF/PP/MAPP/rSMCF and SF/RPP/MAPP/rSMCF composites were shown in Table 6-5 and Table 6-6.

Table 6-5 Mechanical results of RPP based composites with different loading of RCF and MAPP

Sample		Tensile Modulus	Tensile Strength	Flexural Modulus	Flexural Strength	Impact Strength
		(MPa)	(MPa)	(MPa)	(MPa)	(kJ/m ²)
1-8	SF _{0.5} /PP/MAPP ₁	1288.5	23.00	1145.0	29.30	99.50
1-9	SF ₁ /PP/MAPP ₂	1268.6	23.30	1163.2	29.60	100.60
1-10	SF _{2.5} /PP/MAPP ₅	1328.0	23.70	1161.1	29.20	95.70
1-11	SF _{0.5} /PP/MAPP ₁ /rSMCF ₁	1590.9	24.00	1235.1	29.80	103.10
1-12	SF ₁ /PP/MAPP ₂ /r SMCF ₂	1781.5	24.70	1524.9	34.00	107.20
1-13	SF _{2.5} /PP/MAPP ₅ /rSMCF ₅	2232.6	24.30	1738.7	31.70	110.00

Table 6-6 Mechanical results of RPP based composites with different loading of RCF and MAPP

Sample		Tensile Modulus	Tensile Strength	Flexural Modulus	Flexural Strength	Impact Strength
		(MPa)	(MPa)	(MPa)	(MPa)	(kJ/m ²)
2-8	SF _{0.5} /RPP/MAPP ₁	1258.1	24.99	1056.6	26.29	99.14
2-9	SF ₁ /RPP/MAPP ₂	1253.0	25.13	1046.0	26.30	94.78
2-10	SF _{2.5} /RPP/MAPP ₅	1276.0	25.27	1106.1	26.71	80.40
2-11	SF _{0.5} /RPP/MAPP ₁ /rSMCF ₁	1435.9	24.87	1204.1	26.62	62.66
2-12	SF ₁ /RPP/MAPP ₂ / rSMCF ₂	1479.5	24.31	1314.2	27.01	60.71
2-13	SF _{2.5} /RPP/MAPP ₅ /rSMCF ₅	1996.9	25.43	1770.6	28.82	44.04

As comparing the sample 1-8 to 1-10 in Table 6-5 and sample 1-1 to 1-4 in Table 6-1, the sole addition of MAPP has very limited effects on the mechanical properties. Since the variation when compared to unfilled PP are all within $\pm 3\%$. Compare to the PP/rSMCF composites in Table 6-2, the mechanical performance is increased through the addition of MAPP, as all tested properties showed improvement. The tensile and flexural modulus of the composites showed the largest increases at 5 wt% rSMCF loading, SF_{2.5}/PP/MAPP₅/rSMCF₅ (71.1% and 52.8% respectively) when compared to unfilled PP. The mechanical results of the SF/RPP/MAPP/rSMCF composites were shown in Table 6-6.

The sole addition of MAPP without carbon fibre has no significant effects on tensile modulus and flexural modulus, the maximum difference is within $\pm 5\%$ as compare to unfilled RPP. However, the synergistic effect of rSMCF and MAPP dramatically increase the tensile modulus and flexural modulus. The maximum value was obtained at 5 wt% rSMCF filled composites (SF_{2.5}/RPP/MAPP₅/rSMCF), the tensile modulus and flexural modulus were improved by 56.3% and 60.9%, as compared to

unfilled RPP.

The tensile, flexural strength and impact strength of SF_{2.5}/PP/rSMCF₅ composites in Table 6-2 showed a decrease compare to neat PP. However, with the addition of 5 wt% of MAPP, the SF_{2.5}/PP/MAPP₅/rSMCF₅ in Table 6-5, the tensile strength, flexural strength and impact strength improved 5.2%, 10.5% and 11.5% respectively, as compared to neat PP. However, for the RPP based composites, although the tensile strength increase with the increment of rSMCF and MAPP content, the tensile strength of SF_{2.5}/RPP/MAPP₅/rSMCF is still 0.57MPa less than unfilled RPP. And the impact strength of SF_{2.5}/RPP/MAPP₅/rSMCF has a 55.4% reduction compared to unfilled RPP.

With increasing the content of coupling agent, the filler-matrix interfacial adhesion can be improved, and therefore increase the mechanical performance of the composites (Wong et al., 2012, Qiu et al., 2003). While the 5 wt% rSMCF added composites showed superior mechanical properties, the loadings of MAPP varied from 0 wt% to 20 wt% was added to the SF_{2.5}/PP/rSMCF₅ and SF_{2.5}/RPP/rSMCF₅ to verifying the effects of MAPP. The results were shown in Table 6-7 and Figure 6-14.

Table 6-7 Mechanical results of 5%rCF filled composites with different MAPP content

Sample		Tensile Modulus	Tensile Strength	Flexural Modulus	Flexural Strength	Impact Strength
		(MPa)	(MPa)	(MPa)	(MPa)	(kJ/m ²)
1-7	SF _{2.5} /PP/rSMCF ₅	1790.1	21.80	1341.1	27.20	94.90
1-14	SF _{2.5} /PP/MAPP _{2.5} /rSMCF ₅	2226.1	24.10	1553.5	31.60	106.90
1-13	SF _{2.5} /PP/MAPP ₅ /rSMCF ₅	2232.6	24.30	1738.7	31.70	110.00
1-15	SF _{2.5} /PP/MAPP ₁₀ /rSMCF ₅	2485.0	25.20	1812.1	34.60	107.10
1-16	SF _{2.5} /PP/MAPP ₂₀ /rSMCF ₅	2515.0	28.20	1906.7	37.60	51.90
2-7	SF _{2.5} /RPP/rSMCF ₅	1954.4	26.43	1623.8	27.98	60.12
2-14	SF _{2.5} /RPP/MAPP _{2.5} /rSMCF ₅	1925.2	24.97	1705.7	28.11	44.65
2-13	SF _{2.5} /RPP/MAPP ₅ /rSMCF ₅	1996.9	25.43	1770.6	28.82	44.04
2-15	SF _{2.5} /RPP/MAPP ₁₀ /rSMCF ₅	2083.0	26.24	1866.0	30.23	40.55
2-16	SF _{2.5} /RPP/MAPP ₂₀ /rSMCF ₅	2140.4	27.29	1901.9	32.21	35.68

Figure 6-14 (a) illustrated all the tensile and flexural modulus of VPP based and RPP based composites improved with increasing MAPP content.

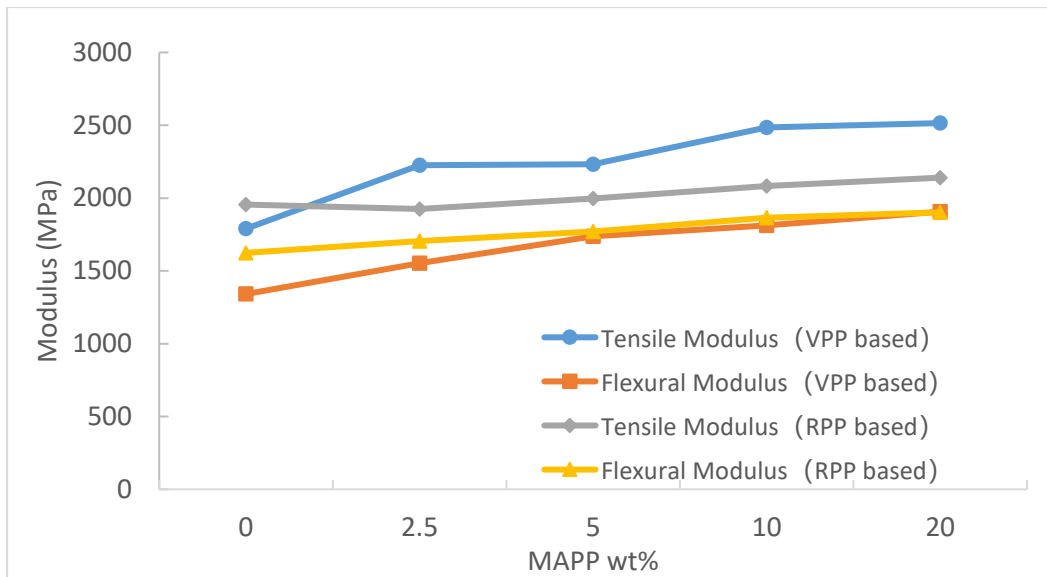


Figure 6-14 Tensile and flexural modulus of the SF_{2.5}/PP/MAPP/rSMCF₅ and SF_{2.5}/RPP/MAPP/rSMCF₅ composites with 0-20 wt% MAPP

At 20 wt% of MAPP, the tensile modulus and flexural modulus of SF_{2.5}/PP/MAPP₂₀/rSMCF₅ increased 40.8% and 42.5%, respectively, when compare to SF_{2.5}/PP/rSMCF₅. Also the tensile and flexural modulus of SF_{2.5}/RPP/MAPP₂₀/rSMCF₅ improved 9.7% and 72.7% as compare to SF_{2.5}/RPP/rSMCF₅.

The tensile and flexural strength of 5 wt% rSMCF filled PP and RPP composites at different MAPP loading is shown in Figure 6-15.

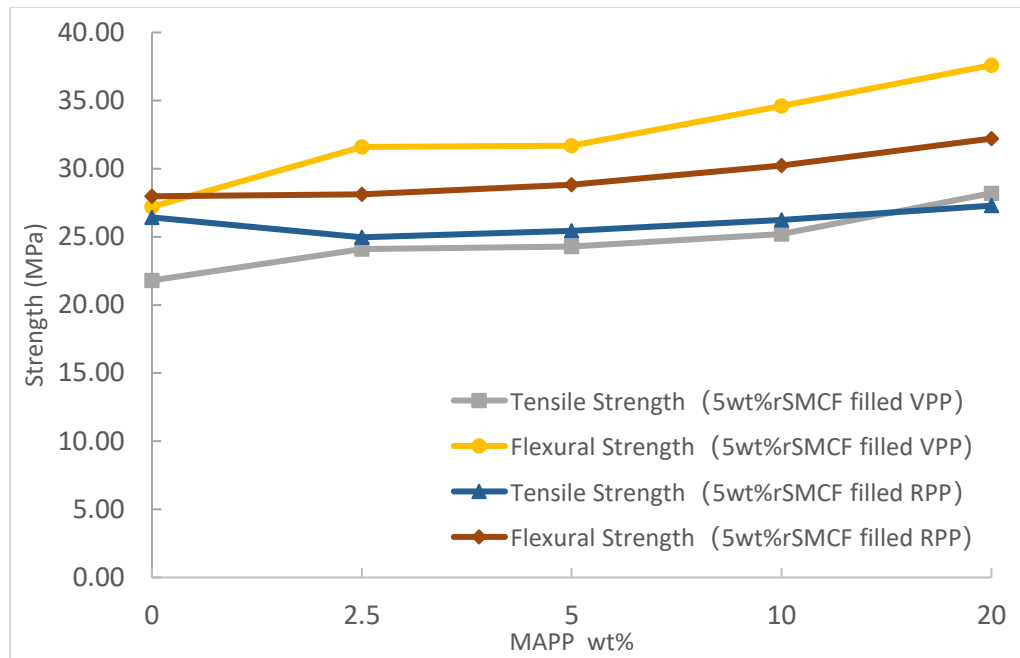


Figure 6-15 Tensile and flexural strength of the SF_{2.5}/PP/MAPP/rSMCF₅ and SF_{2.5}/RPP/MAPP/rSMCF₅ composites with 0-20 wt% MAPP

The tensile and flexural strength of the VPP based and RPP based composites were improved in the high content of MAPP. The MAPP was more effective in enhancing the tensile and flexural strength of the VPP based composites. Compare to SF_{2.5}/PP/rSMCF₅, the tensile and flexural strength of SF_{2.5}/PP/MAPP₂₀/rSMCF₅ improved 29.4% and 38.2%, respectively. In terms of SF_{2.5}/RPP/MAPP₂₀/rSMCF₅, the tensile and flexural strength increased 3.3% and 15.1%, when compare to SF_{2.5}/RPP/rSMCF₅. At low concentration of MAPP, the tensile strength of SF_{2.5}/PP/MAPP_{2.5}/rSMCF₅ enhanced 10.6% when compare to SF_{2.5}/PP/rSMCF₅, but the tensile strength of SF_{2.5}/RPP/MAPP_{2.5}/rSMCF₅ reduced 5.5% in respect to SF_{2.5}/RPP/rSMCF₅.

The impact strength peaked for SF_{2.5}/PP/MAPP₅/rSMCF₅, and suffered a loss of 45.3% at SF_{2.5}/PP/MAPP₂₀/rSMCF₅ compared

to SF_{2.5}/PP/rSMCF₅. And the impact strength of the RPP based composites continuous decrease with the addition of MAPP. At 20 wt% of MAPP, SF_{2.5}/RPP/MAPP₂₀/rSMCF₅ suffered 40.7% reduction in impact strength as compare to SF_{2.5}/RPP/rSMCF₅. Liu et al. (2015) indicated that MAPP and carbon fibre had an excellent synergistic effect in enhancing the interfacial interaction between the carbon fibre and PP matrix, which contribute to the significant improvement of flexural and impact properties. Figure 6-17 and Figure 6-17 showed the SEM micrograph of the impact fracture surface of SF_{2.5}/PP/MAPP/rSMCF₅ at the MAPP concentration of 2.5 wt% to 20 wt%.

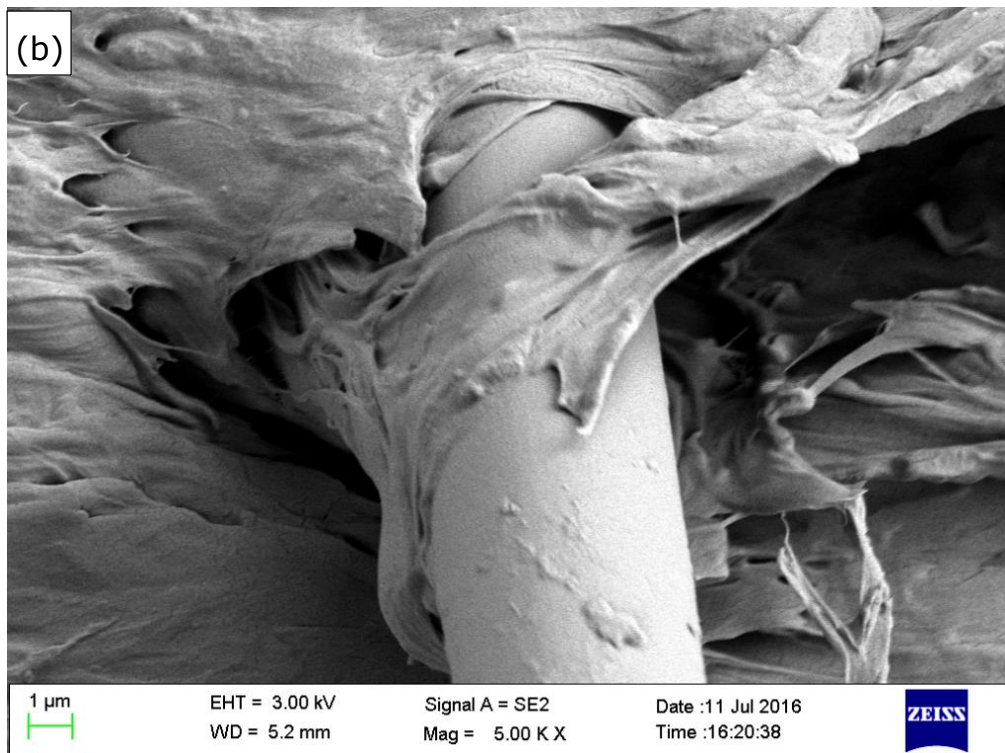
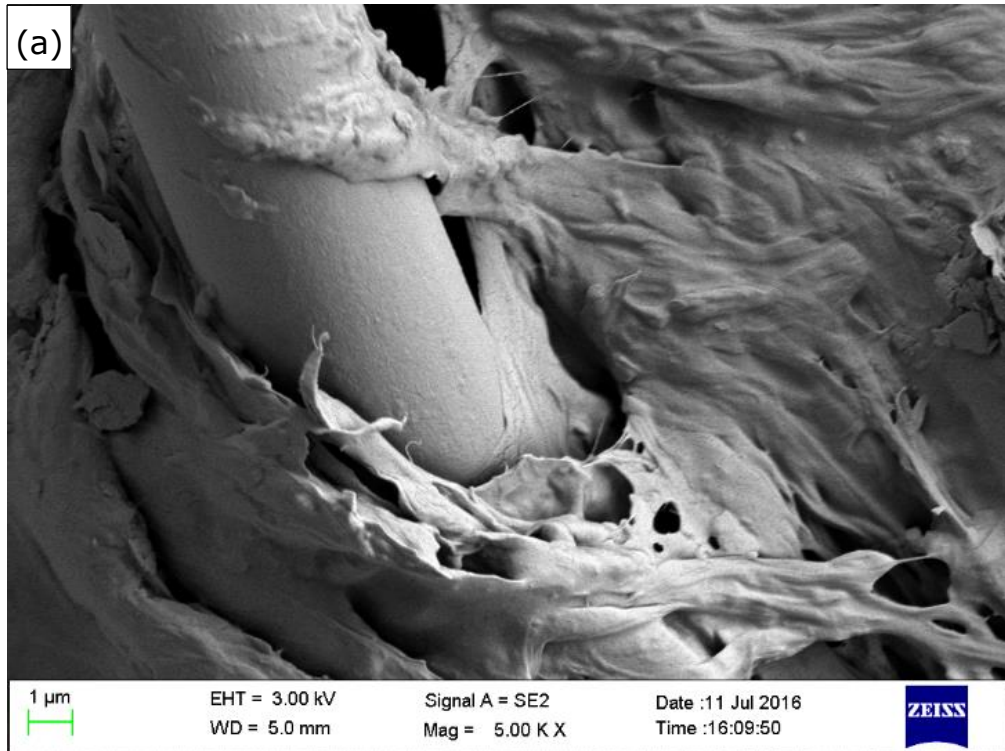


Figure 6-16 SEM micrographs of the pull-out rSMCF on the impact-facture surfaces of SF_{2.5}/PP/MAPP/rSMCF₅ with (a) 2.5 wt%, (b) 5 wt%

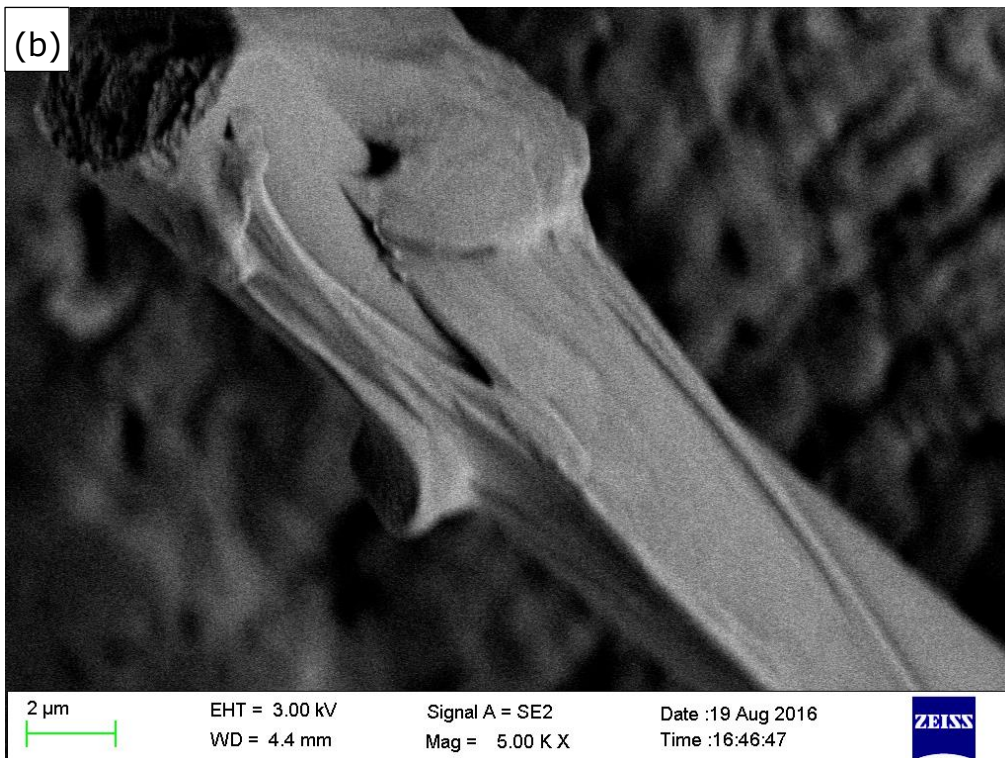
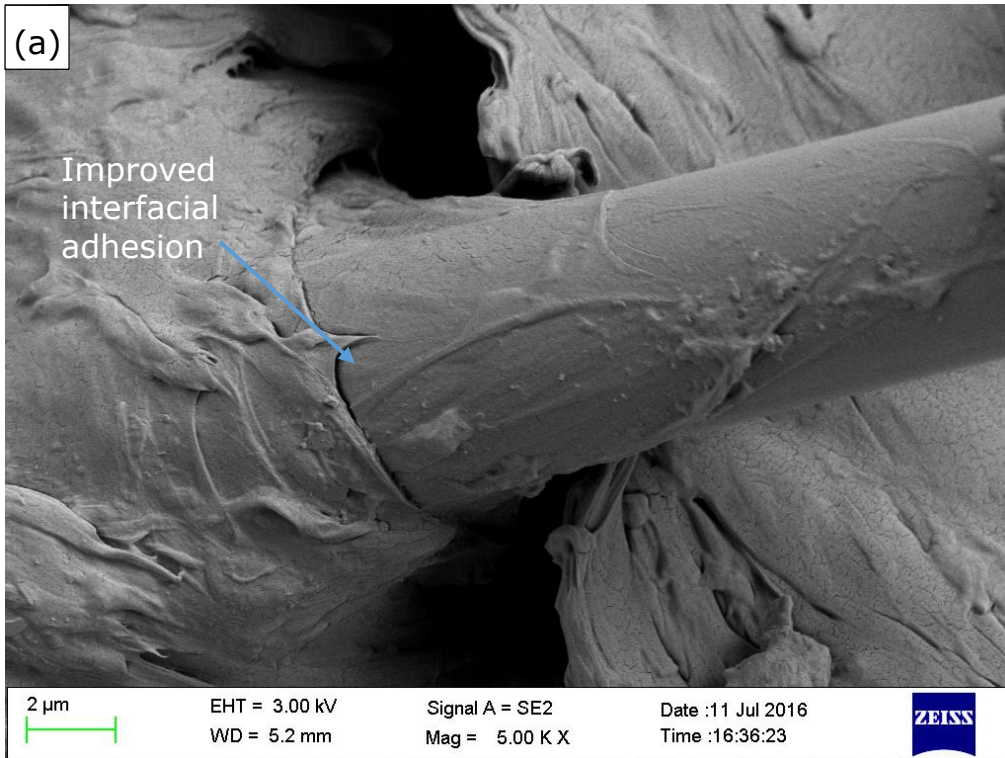


Figure 6-17 SEM micrographs of the pull-out rSMCF on the impact-fracture surfaces of SF_{2.5}/PP/MAPP/rSMCF₅ with (a) 10 wt%, and (b) 20 wt% MAPP

It can be observed that with increasing MAPP content, the VPP coverage on the pulled-out fibres and the adhesion with the composite matrix increases. However, the impact strength of the SF_{2.5}/PP/MAPP/rSMCF₅ decreased with additions of MAPP above 5 wt%. A similar trend was observed by Liu et al. (2015), when compounding PP and milled vCF with a high loading of MAPP (Qiu et al., 2006), which can also be explained through the low molecular weight of MAPP (Qiu et al., 2006, Liu et al., 2015).

The SEM micrograph of the impact fracture of SF_{2.5}/RPP/MAPP/rSMCF₅ composites was illustrated in Figure 6-18 and Figure 6-19 .

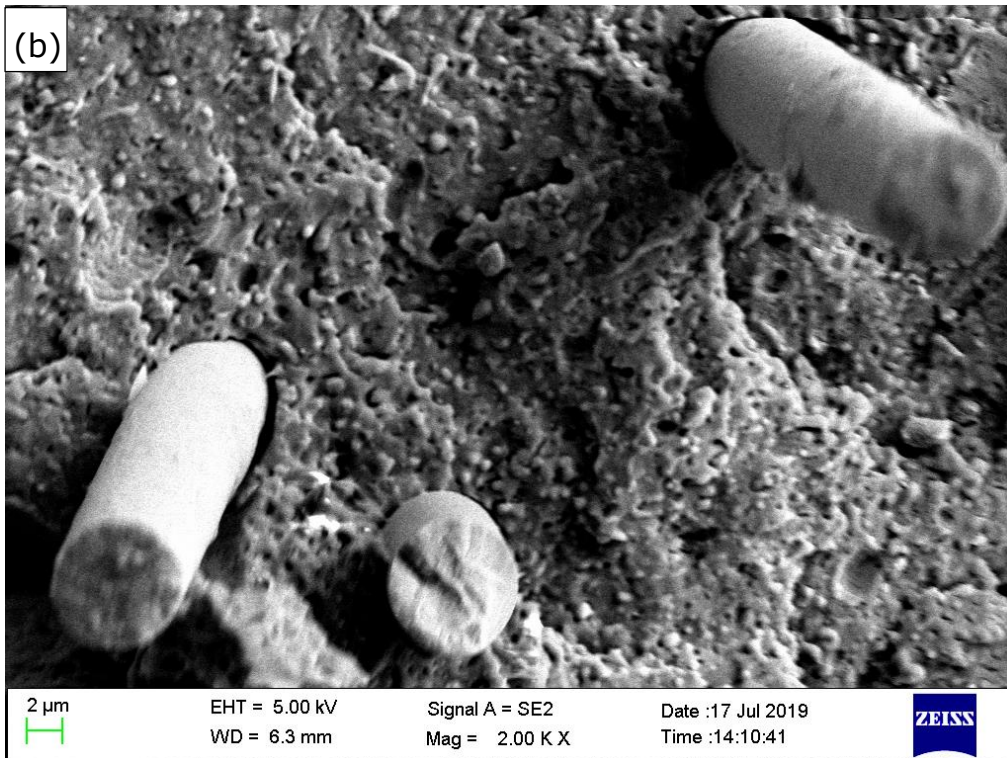
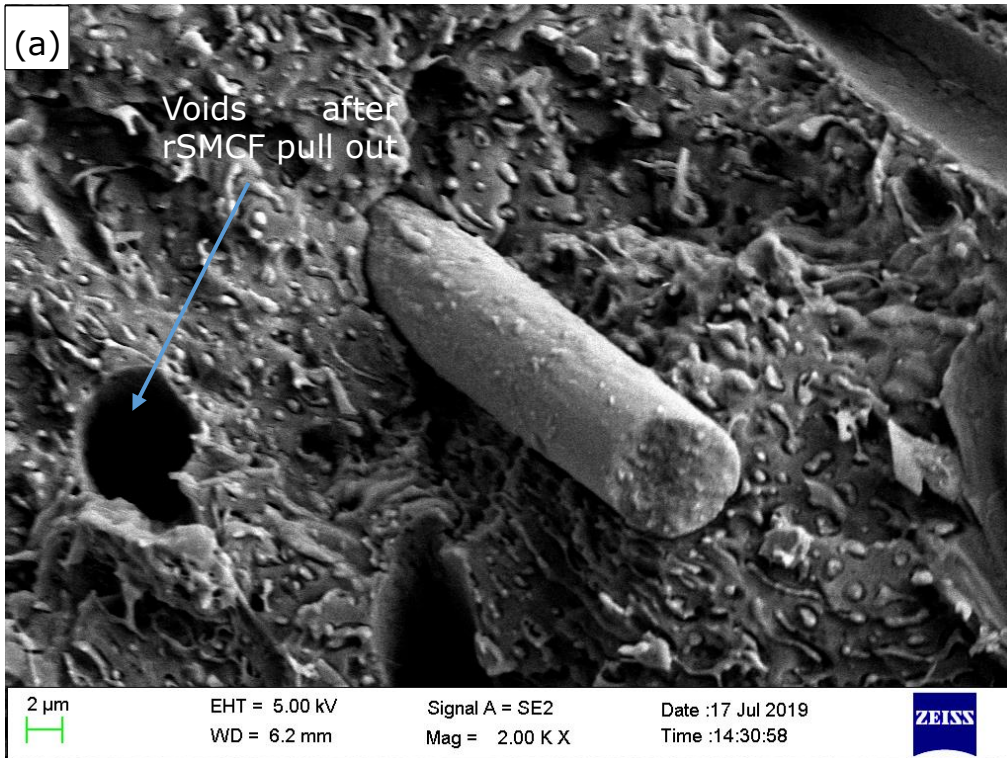


Figure 6-18 SEM micrographs of the pull-out rSMCF on the impact-facture surfaces of SF_{2.5}/RPP/MAPP/rSMCF₅ with (a) 2.5 wt%, (b) 5 wt%

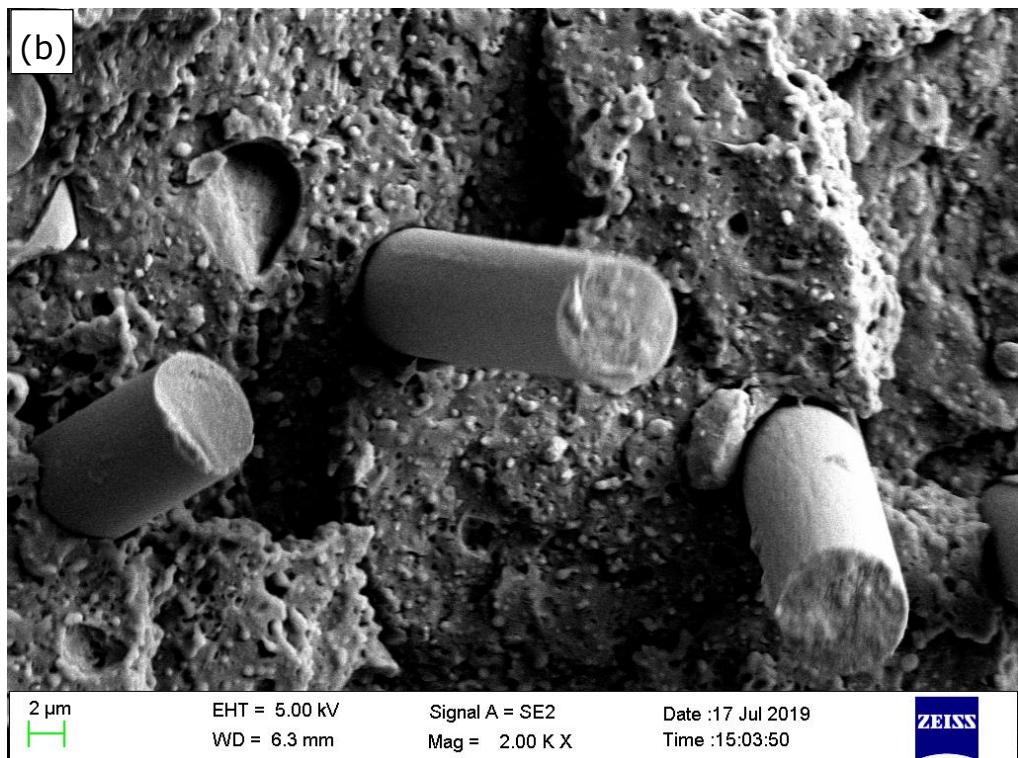
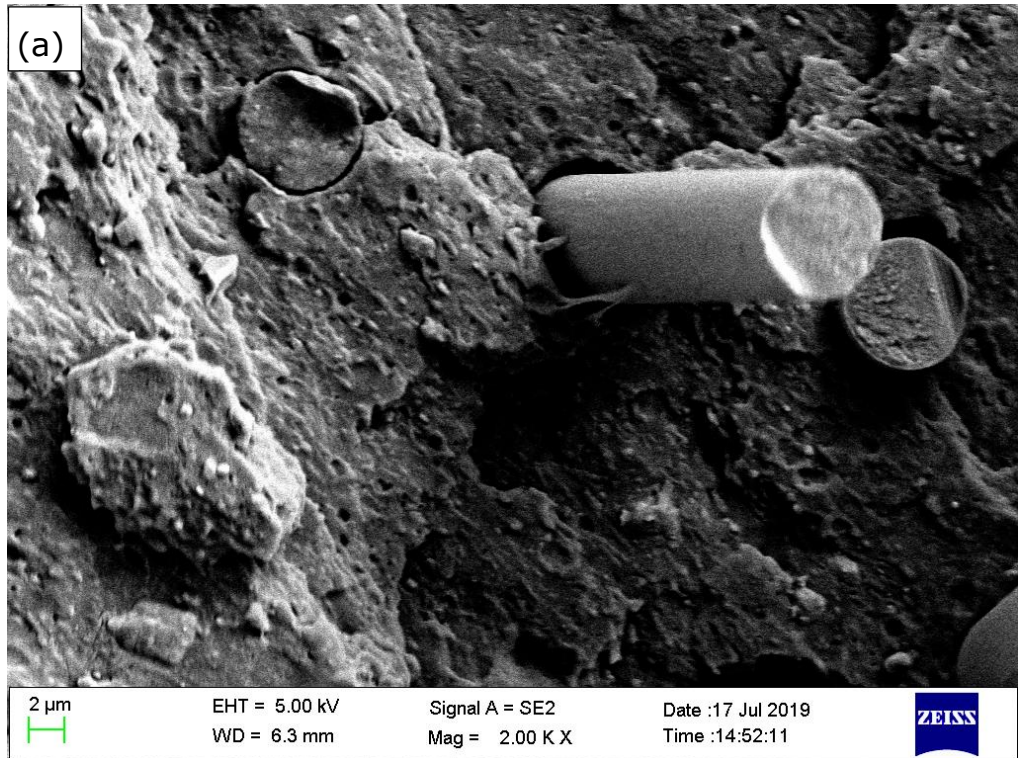


Figure 6-19 SEM micrographs of the pull-out rSMCF on the impact-fracture surfaces of SF_{2.5}/RPP/MAPP/rSMCF₅ with (a) 10 wt%, and (b) 20 wt% MAPP

Unlike the smooth fracture surface VPP based composites, the RPP based composites had a rough fracture surface. With the increment of MAPP concentration, no obvious cover of RPP on the rSMCF surface was observed. This could be attribute to the existence of PE in the RPP, because PE and PP are only partially miscible (Shanks et al., 2000). The existence of PE reduced the effectiveness of MAPP in improving the interfacial adhesion between RPP and rSMCF. Even so, with the increase of MAPP content, less recycled carbon fibres were pulled out, which indicate that the bonding strength of rSMCF/RPP was relatively strengthened. At high MAPP level, the low molecular weight of the MAPP limited the entanglement phenomenon thus reduce the impact performance (Wong et al., 2012).

6.3 Conclusion

In this study, rSMCF was used for reinforcing the PP-based composites in an attempt to improve the recycling and reuse of recycled short carbon fibre. One virgin PP and one recycled PP were selected as the base material for this study. Morphological and thermal characterisation has been carried out on new composite materials made with rSMCF to help explain the variations in mechanical performance. The rSMCF material recovered from a fluidised bed process was shredded into a smaller size, and then blended with PP and RPP at 1 wt%, 2 wt% and 5 wt% rSMCF through a novel procedure consisting of dispersion, compressing and extrusion.

The surfactant was proved to have nearly no effects on all the tested mechanical properties based on the results of the control groups. And the FTIR imaging results showed the surfactant was evenly dispersed in the PP matrix. The experimental results

showed that the low loadings of rSMCF were sufficient for improving the tensile and flexural modulus of the VPP based composites, while RPP-based composites obtained the same tendency. The tensile strength and flexural strength might slightly decrease with higher rSMCF content, but it can be overcome by adding the coupling agent MAPP. The addition of MAPP is effective in improving the fibre-matrix interfacial adhesion of both PP and RPP based composites. Although the existence of PE in the RPP may reduce the compatible effects of MAPP, the tensile and flexural properties were significantly improved with the increment of MAPP contents. However, the high content of MAPP contributes to the reduction of impact strength due to the low molecular weight of MAPP, which limited the entanglement of the polymer.

With a low loading of rSMCF and compatibiliser, the brittleness of the composites which has observed in previous literature can be avoided (McNally et al., 2008), while other mechanical properties can be improved significantly.

This study confirms the great potential of using rSMCF reclaimed from CFRP waste as a reinforcement for polymeric materials, and that PP/rSMCF composites can be applied in demanding industrial applications, including automobile part production. The proposed compounding procedure is scalable and of low cost, which has the potential to be adopted in the manufacturing sector.

This page is intentionally left blank.

Chapter 7 Comparison of the hollow glass bead filled virgin and RPP composites

7.1 Introduction

As mentioned in the literature review, weight reduction is an important criterion for evaluating the performance of plastic composites in a vehicle. The failure in weight reduction will hinder the use of recycled plastics in automobile parts (Recycling today, 2017).

The lightweight material hollow glass beads (HGBs), with the bulk density of 0.6g/cm^3 , were introduced in this study. An advantage of HGBs is that it also has the potential to be a halogen-free filler to improve the flame retardancy of PP composites.

The HGBs has a special structure, with a spherical rigid glass shell and the hollow inside is filled with inert gas (Argon). Resulting in low bulk density and relatively low thermal conductivity (Liang and Li, 2007, Liang and Li, 2006). $\text{Al}(\text{OH})_3$, which is a high-density flame resistant mineral filler, is selected for comparison, in the performance of weight reduction, mechanical properties and flame retardancy.

7.2 Effects of HGBs content

7.2.1 Density reduction

Table 7-1 shows the density results of virgin PP, HGBs filled and aluminium hydroxide filled PP-based composites in this study.

Table 7-1 Density results of virgin PP, HGB filled and Al(OH)₃ filled PP composites

Sample code	Experimental Density (g/cm ³)	Theoretical value (g/cm ³)
PP	0.913±0.005	0.9 ^a
PP-2.5iM30K	0.902±0.007	0.889
PP-5iM30K	0.894±0.009	0.878
PP-10iM30K	0.881±0.004	0.857
PP-2.5S60HS	0.902±0.004	0.889
PP-5S60HS	0.900±0.003	0.878
PP-10S60HS	0.889±0.007	0.857
PP-2.5Al(OH) ₃	0.917±0.002	0.914
PP-5Al(OH) ₃	0.928±0.004	0.929
PP-10Al(OH) ₃	0.962±0.007	0.960
^a Value obtained from the virgin PP supplier		

The volume fraction of filler and theoretical density of different composites were calculated by the following equations:

$$F_V = \frac{\frac{F_W}{\rho_F}}{\frac{F_W}{\rho_F} + \frac{P_W}{\rho_P}} \quad (7.1)$$

$$\rho_T = F_V \times \rho_F + (1 - F_V) \times \rho_P \quad (7.2)$$

where the filler is HGB or Al(OH)₃, F_v is the volume fraction of

filler, F_w and P_w are the weight fraction the weight fractions of filler and PP, ρ_T , ρ_P , ρ_F are the theoretical densities of PP composites, PP and filler.

It can be observed that with the same 10 wt% of filler loading, HGBs (iM30K) filled PP composites can achieve 3.5% of density reduction with respect to the base matrix. While the aluminium hydroxide filled composites have a 5.4% of density increase. Kumar et al. (2017) studied the density reduction effects of HGBs (trademark iM16K, 0.46g/cc) on HGBs/bamboo fibre/PP composites and observed an 8.29% weight reduction using 10 wt% HGBs loading. The different density reduction performance may be attributed to the different fractional HGB fracture during the sample preparation process especially the twin-screw process. The density of HGBs (iM30K and S60HS) used in this study is 30.4% higher than the HGBs (iM16K). The difference value between experimental density and theoretical density is also caused by the HGBs breakage. This can be verified from the morphological study in section 7.2.3.

The density results of the HGBs (iM30K) filled RPP composites were shown in Table 7-2.

Table 7-2 Density results of RPP and HGB filled RPP composites

Sample code	Experimental Density (g/cm ³)	Theoretical value (g/cm ³)
RPP3	0.916±0.004	0.910
RPP3-2.5iM30K	0.905±0.003	0.898
RPP3-5iM30K	0.897±0.005	0.887
RPP3-10iM30K	0.879±0.005	0.865
RPP4	0.907±0.004	0.890
RPP4-2.5iM30K	0.893±0.005	0.879
RPP4-5iM30K	0.884±0.004	0.869
RPP4-10iM30K	0.868±0.004	0.848

The density of the HGBs filled RPP was effectively reduced with the increasing of the HGBs content, as compared to the neat RPP. The density of 10 wt% HGBs (iM30K) filled RPP3 and RPP4 was found to decrease by 4.0% and 4.3%, respectively. The results of the experimental density were slightly higher than the theoretical value, which was likely because of the breakage of the HGBs during the processing of twin-screw extrusion and injection moulding.

7.2.2 Mechanical properties

7.2.2.1 Tensile properties

To evaluate the tensile behaviour of the VPP/HGB and VPP/Al(OH)₃ composites, the results were compared with the VPP. Table 7-3 illustrates the tensile test results of the VPP composites filled with different composition (0-10 wt%) of HGB and Al(OH)₃.

Table 7-3 Tensile properties of virgin PP, HGB filled and Al(OH)₃ filled composites

Sample code	Tensile strength (MPa)	ΔTensile strength ^a (MPa)	Tensile modulus (MPa)	ΔTensile modulus ^b (MPa)
PP	32.7	0.0	1705.8	0.00
PP-2.5iM30K	31.4	-1.3	1843.3	137.45
PP-5iM30K	29.0	-3.7	1913.1	207.26
PP-10iM30K	25.1	-7.6	2015.9	310.03
PP-10iM30K-5MAPP	27.1	-5.6	2087.9	382.10
PP-2.5S60HS	30.8	-1.8	1843.1	137.28
PP-5S60HS	29.4	-3.3	1863.0	157.13
PP-10S60HS	25.5	-7.2	1996.1	290.27
PP-10S60HS-5MAPP	27.5	-5.2	2141.0	435.13
PP-2.5Al(OH) ₃	34.8	2.1	1776.7	70.85
PP-5Al(OH) ₃	34.0	1.3	1808.6	102.72
PP-10Al(OH) ₃	33.0	0.3	1852.5	146.61
^a ΔTensile strength is the difference to neat PP				
^b ΔTensile modulus is the difference to neat PP				

It is shown in Figure 7-1 that the tensile modulus increased with the addition of HGBs content.

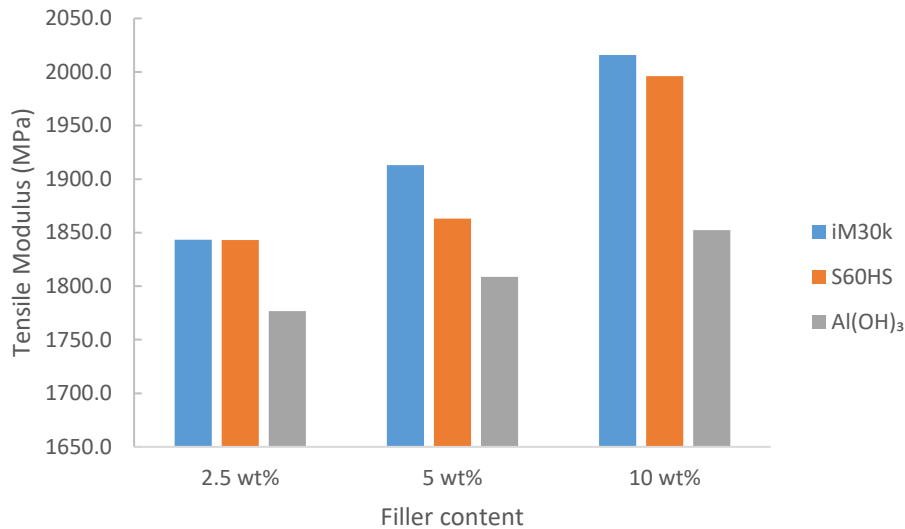


Figure 7-1 Correlations of tensile modulus of VPP based composites at different iM30K, S60HS, Al(OH)₃ loading

For the tensile modulus, Al(OH)₃ and two kinds of HGBs fillers showed a significant reinforcement effect while PP-10iM30K obtained the highest value (2015.88 MPa). Therefore, it could be concluded that HGBs have better improvement on tensile modulus than aluminium hydroxide. The existing rigid inorganic particles can hinder the displacement of the macromolecular chain of the composite, which contributes to the improvement of tensile stiffness (Liang et al., 2015a).

Liang (2005) studied the effect of HGBs addition on the tensile modulus of ABS composites and they observed a similar trend in tensile modulus with increasing HGBs addition from 0% vol to 20% vol. They suggested that the increase in tensile modulus with HGBs addition was because the inherent Young's modulus of HGBs is much higher than the base resin (Liang, 2005).

The effects of different filler loading on the tensile strength of the composites are shown in Figure 7-2.

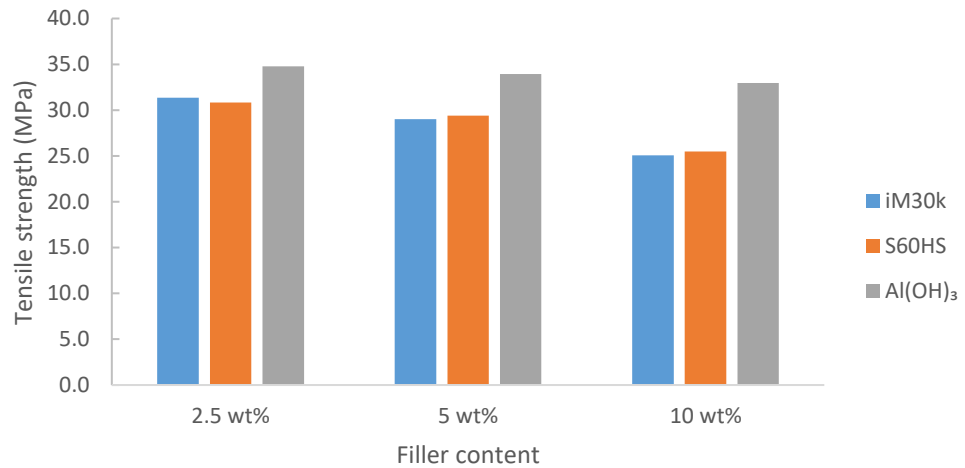


Figure 7-2 Correlations of the tensile strength of VPP based composites at different iM30K, S60HS, Al(OH)₃ loading

In this study, with the addition of 10 wt% of HGB (iM30K), the tensile strength of the composites reduced by 23.3%. Kumar et al. (2017) investigated the impacts of HGBs on the mechanical properties of HGB/MAPP/PP composites and reported that the tensile strength reduced by 8% with 10 wt% of HGBs addition. They suggested that the reduction in tensile strength was possibly attributed to the weak interfacial adhesion that exists between the polymer matrix and the spherical particles. As is shown in Table 7-3, compared to PP-10iM30K, the tensile strength of PP-10iM30K-5MAPP improved by 8% via the addition of 5 wt% of MAPP into the matrix. For tensile modulus and tensile strength, there was not any significant difference in results with the particle size when the HGB loading is the same. Therefore, it was shown that the effects of the HGB particle size on the tensile properties are

insignificant in this experimental range. Liang (2005) observed a similar tendency in the HGBs/ABS composite systems.

An enhancement of tensile strength was observed with the addition of aluminium hydroxide. The tensile strength of composites at 2.5 wt% Al(OH)₃ addition reaches the peak and increased by 6.36%, as compared to virgin PP. Further addition of aluminium hydroxide up to 10 wt% will decrease the tensile strength by 5.1%.

The tensile strength and tensile modulus of the HGBs filled RPP composites are presented in Table 7-4.

Table 7-4 Tensile properties of HGBs filled RPP composites

	Tensile strength (MPa)	ΔTensile strength ^a (MPa)	Tensile modulus (MPa)	ΔTensile modulus ^b (MPa)
RPP3	24.0	0.0	1479.8	0.0
RPP3-2.5iM30K	22.8	-1.2	1588.3	108.5
RPP3-5iM30K	21.2	-2.7	1625.2	145.3
RPP3-10iM30K	18.5	-5.5	1767.1	287.2
RPP3-10iM30K-5MAPP	22.2	-1.7	1804.3	324.5
RPP4	22.6	0.0	990.1	0.0
RPP4-2.5iM30K	21.3	-1.2	1004.7	14.6
RPP4-5iM30K	20.2	-2.4	1047.7	57.6
RPP4-10iM30K	18.0	-4.6	1070.3	80.2
RPP4-10iM30K-5MAPP	20.4	-2.2	1300.1	310.0
^a ΔTensile strength is the difference to 100% recycled PP				
^b ΔTensile modulus is the difference to 100% recycled PP				

The tensile properties of the RPP/HGBs composites are similar to the VPP/HGBs composites. The effect of iM30K content of the tensile modulus of RPP3 and RPP4 is shown in Figure 7-3.

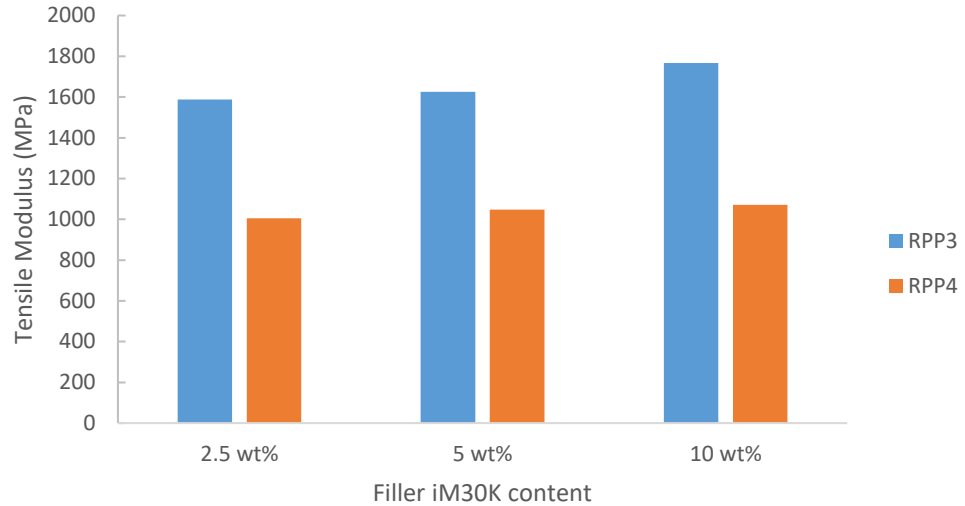


Figure 7-3 Correlations of iM30K content of the tensile modulus of RPP3 and RPP4 based composites

The addition of HGBs as filler can improve the tensile modulus of the RPP composites slightly. With the addition of 10 wt% iM30K, the tensile strength of RPP4-10iM30K increased 80.2 MPa as compare to pure RPP4, and the tensile strength of RPP3-10iM30K increased 287.2 MPa as compare to pure RPP3. The results were consistent with the findings in Kumar et al. (2017). As is shown in Table 7-4, the coupling agent can also increase the tensile modulus, especially for RPP4, with 5 wt% of MAPP, the tensile modulus of 10iM30K filled RPP4 increased from 1070 MPa to 1300 MPa. The improved interaction of RPP and HGBs hence increase the tensile modulus of the composites.

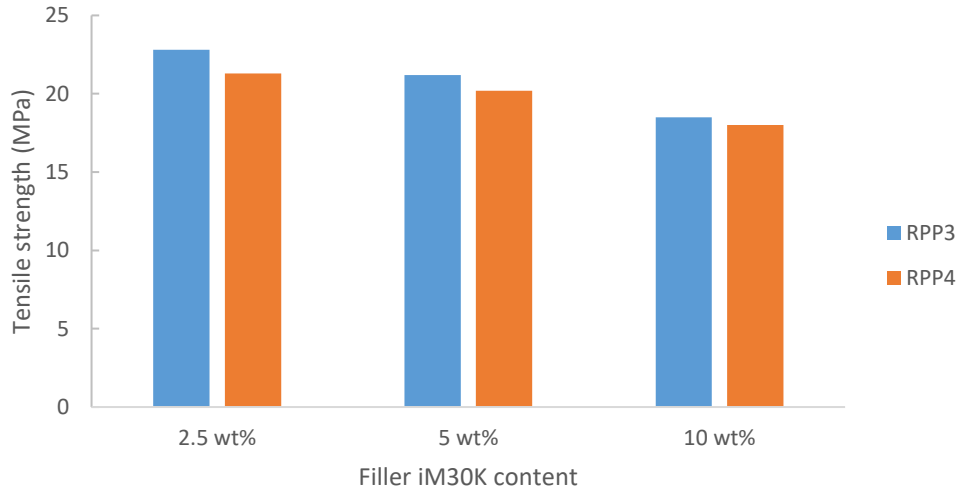


Figure 7-4 Correlations of iM30K content of the tensile modulus of RPP3 and RPP4 based composites

Figure 7-4 indicates the effects of Im30k content on the tensile strength of the RPP3 and RPP4 based composites. The tensile strength of the RPP based composites decreases with the increase of HGBs content. With 10 wt% addition of iM30K, the tensile strength of RPP3-10iM30K and RPP4-10iM30K deteriorated 23% and 20% as compared to neat RPP3 and RPP4. These results of tensile strength have much in common with the VPP/HGBs composites. Liang (2007) observed the increase of the tensile strength of PP/HGBs when the volume fraction of the HGBs is less than 5%, then the tensile strength reduced with the further addition of HGBs. The possible reason is that in the study of Liang (2007), the HGBs was pretreated by the silane coupling agent.

In this study, the incorporation of the coupling agent MAPP can improve the tensile strength. As compared to RPP3-10iM30K and RPP4-iM30K, the sample with the addition of 5 wt% MAPP (RPP3-10iM30K-5MAPP and RPP4-10iM30K-5MAPP) improved the tensile strength by 20% and 13%. The explanation is that

MAPP improves the interactions between PP matrix and the fillers (Gu et al., 2016b).

7.2.2.2 Flexural properties

Based on the previous study, flexural properties are important properties which limit the use of RPP for some automobile applications such as dashboard and column board. To investigate the effects of HGBs on flexural properties composites, VPP/HGB and RPP/HGB composites were both studied. The results of VPP/HGB and VPP/ $\text{Al}(\text{OH})_3$ composites are presented in Table 7-5.

Table 7-5 Flexural properties of virgin PP, HGB filled and Al(OH)₃ filled composites

Sample code	Flexural strength (MPa)	ΔFlexural strength ^a (MPa)	Flexural modulus (MPa)	ΔFlexural modulus ^b (MPa)
PP	40.82	0.0	1334.0	0.0
PP-2.5iM30K	41.98	1.2	1498.3	164.3
PP-5iM30K	41.00	0.2	1632.2	298.1
PP-10iM30K	40.09	-0.7	1733.1	399.1
PP-10iM30K-5MAPP	43.57	2.8	1851.0	516.9
PP-2.5S60HS	41.09	0.3	1437.6	103.6
PP-5S60HS	40.85	0.0	1603.0	269.0
PP-10S60HS	39.36	-1.5	1602.5	268.5
PP-10S60HS-5MAPP	43.26	2.4	1819.8	485.8
PP-2.5Al(OH) ₃	42.95	2.1	1627.9	293.9
PP-5Al(OH) ₃	42.61	1.8	1694.1	360.1
PP-10Al(OH) ₃	42.31	1.5	1707.8	373.8
^a ΔFlexural strength is the difference to neat PP				
^b ΔFlexural modulus is the difference to neat PP				

The correlations between flexural modulus and filler content is shown in Figure 7-5.

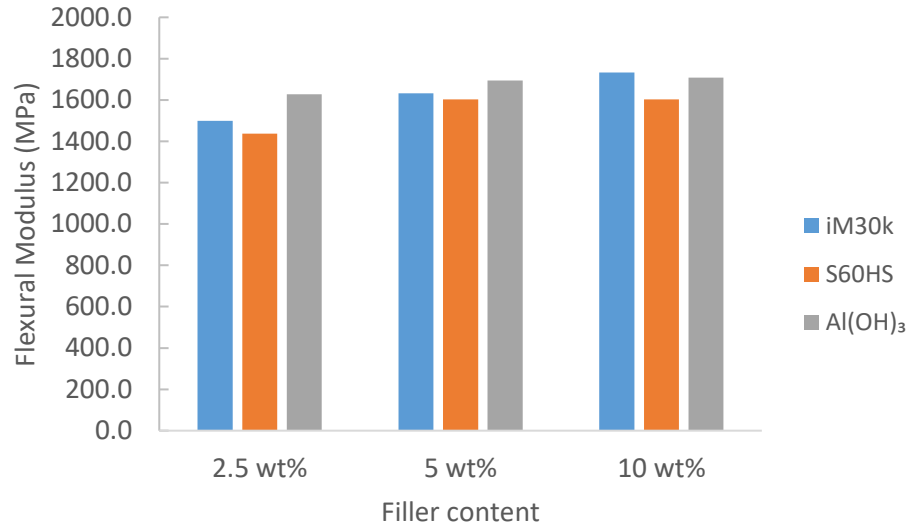


Figure 7-5 Correlations of the flexural modulus of VPP based composites at different iM30K, S60HS, Al(OH)₃ loading

It can be observed that 10 wt% of HGBs (iM30K) added VPP composite has the best performance and achieved 29.9% of improvement with respect to the neat PP. When the HGB (S60HS) and aluminium hydroxide loading is higher than 5 wt%, the enhancement of flexural modulus is very limited.

The results in Figure 7-6 show that for HGBs filled composites, the flexural strength reached a peak when the filler loading is 2.5 wt%.

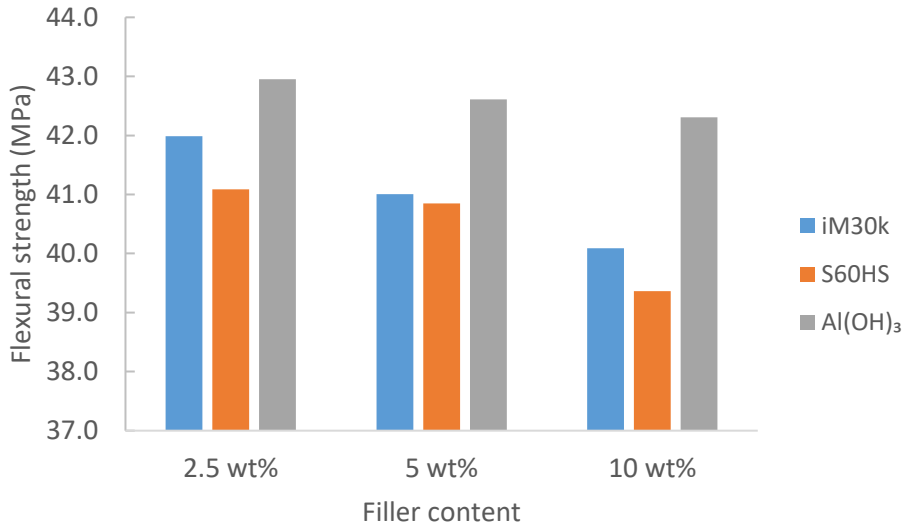


Figure 7-6 Correlations of flexural strength of VPP based composites at different iM30K, S60HS, Al(OH)₃ loading

With the further addition of HGBs up to 10 wt% iM30k the flexural strength of PP composite decreased from 31.35 MPa to 25.08 MPa. Liang (2005) studied the flexural properties of ABS/HGBs composites and reported that the highest flexural strength was observed with 5 wt% HGBs loadings. The difference in flexural strength shown in Table 7-5 between PP-10iM30K and PP-10iM30K-5MAPP suggests the coupling agent plays a vital role in improving the interfacial adhesion between the PP matrix and HGBs. It is evident from Table 7-5 that with a similar amount of filler loading, same HGB loading, iM30K has an average 5% higher flexural modulus and 1% higher flexural strength than S60HS filled composites. This improvement may be attributed to the high crush strength of the smaller size HGBs. Up to 2.5 wt% Al(OH)₃ addition the flexural strength increased by 5.2%. However, with the further addition of Al(OH)₃ up to 10 wt% the flexural strength decreased to 42.31 MPa. Liang (2017) observed that the flexural strength of

Mg(OH)₂/PP matrix reached the maximum value when the filler weight fraction is 30%, then the value keeps decrease but still higher than the unfilled PP composite.

Table 7-6 illustrated the flexural properties of the HGBs filled RPP composites.

Table 7-6 Flexural properties of HGBs filled RPP composites

Sample code	Flexural strength (MPa)	ΔFlexural strength ^a (MPa)	Flexural modulus (MPa)	ΔFlexural modulus ^b (MPa)
RPP3	32.9	0.0	1267.4	0.0
RPP3-2.5iM30K	32.5	-0.4	1297.7	30.3
RPP3-5iM30K	32.8	-0.1	1399.7	132.2
RPP3-10iM30K	30.3	-2.6	1416.7	149.3
RPP3-10iM30K-5MAPP	34.9	2.0	1477.5	210.1
RPP4	23.1	0.0	754.8	0.0
RPP4-2.5iM30K	23.3	0.2	770.4	15.6
RPP4-5iM30K	22.7	-0.4	790.5	35.7
RPP4-10iM30K	22.5	-0.6	856.8	102.0
RPP4-10iM30K-5MAPP	26.6	3.5	913.3	158.5
^a ΔFlexural strength is the difference to 100% recycled PP.				
^b ΔFlexural modulus is the difference to 100% recycled PP.				

Figure 7-7 indicates that the addition of HGBs can improve the flexural modulus of the RPP based composites.

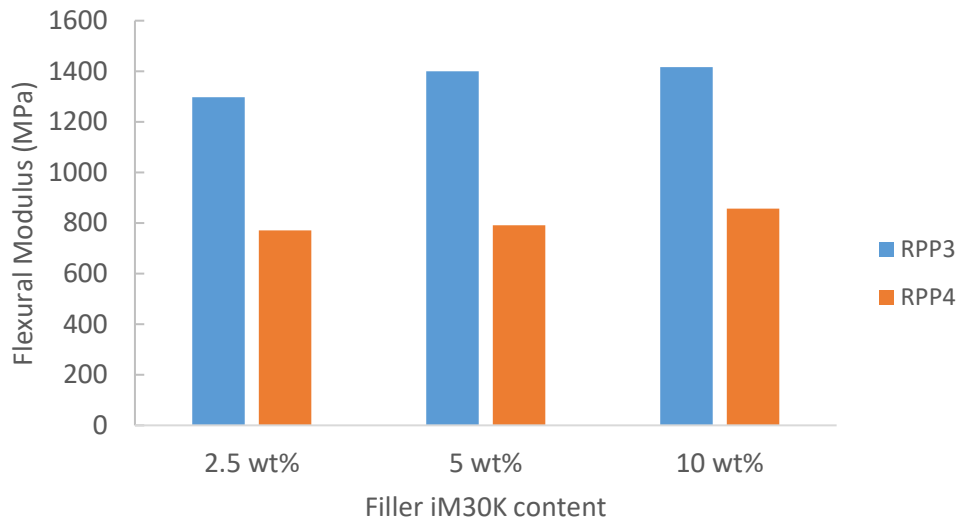


Figure 7-7 Correlations of iM30K content of the flexural modulus of RPP3 and RPP4 based composites

As compared to pure RPP3 and RPP4 in Table 7-6, the flexural modulus of 10 wt% added RPP3 and RPP4 improved 11.8% and 13.5%, respectively. The enhanced flexural modulus was due to the added HGBs increase the stiffness of the composites, which is further attributed to the increase in the interfacial area of contact (Herrera-Franco and Valadez-González, 2005).

However, as is shown in Figure 7-8, the incorporation of HGBs will slightly reduce the flexural strength performance of the composites.

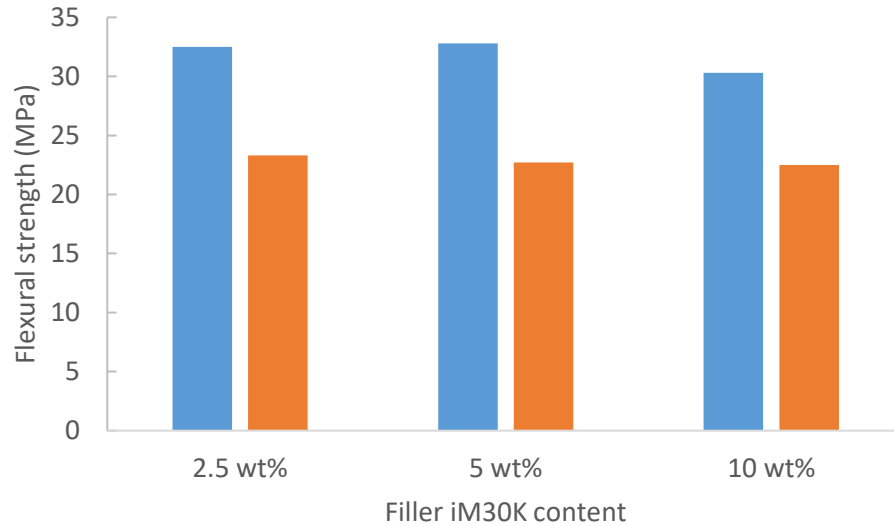


Figure 7-8 Correlations of iM30K content of the strength of RPP3 and RPP4 based composites

A significant improvement of flexural strength was observed by adding the coupling agent MAPP (in Table 7-6), two samples with 5 wt% MAPP and 10 wt% iM30K achieved the highest flexural modulus and strength in the RPP3 and RPP4 based composites, respectively. The improved interfacial adhesion contributes to both stronger flexural modulus and flexural strength.

7.2.2.3 Impact strength

Table 7-7 shows the results of un-notched impact strength of PP composites at 2.5 wt%, 5 wt% and 10 wt% filler loading.

Table 7-7 Impact properties of virgin PP, HGB filled and Al(OH)₃ filled composites

Sample code	Impact strength (kJ/m ²)	ΔImpact strength ^a (kJ/m ²)
PP	56.72	0.0
PP-2.5iM30K	34.06	-22.7
PP-5iM30K	27.74	-29.0
PP-10iM30K	21.56	-35.2
PP-10iM30K-5MAPP	20.99	-35.7
PP-2.5S60HS	29.96	-26.8
PP-5S60HS	24.77	-31.9
PP-10S60HS	21.70	-35.0
PP-10S60HS-5MAPP	20.99	-35.7
PP-2.5Al(OH) ₃	43.28	-13.4
PP-5Al(OH) ₃	36.57	-20.1
PP-10Al(OH) ₃	33.26	-23.5
^a ΔImpact strength is the difference to neat PP		

It can be observed in Figure 7-9 that the increase of all of these three filler content will contribute to the reduction of unnotched impact strength. And Al(OH)₃ filled VPP composites maintained the highest impact resistance.

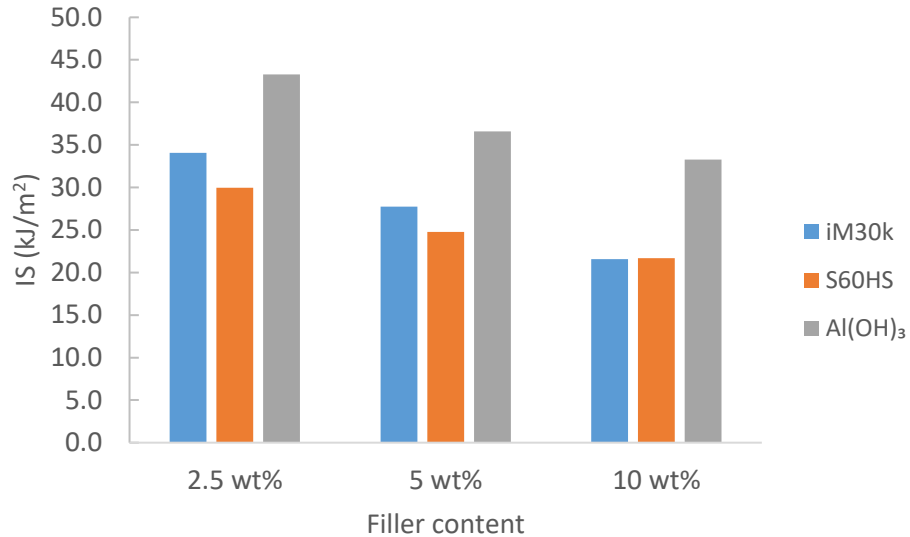


Figure 7-9 Correlations of un-notched impact strength of VPP based composites at different iM30K, S60HS, Al(OH)₃ loading

The IS helps to characterise the energy of crack initiation and crack propagation (Franco-Marquès et al., 2011). Compared to VPP (in Table 7-7), a sharp decrease in the IS was observed for the composites filled with HGBs and Al(OH)₃. One of the explanations is that the impact properties of composites are extensively correlated with filler and matrix adhesion (Leong et al., 2004). Some researchers used the hydroxylation and silane treatment to improve the adhesion of the base matrix and hollow glass beads, however, in some cases the interaction was still not strong enough (Kumar et al., 2017). In this study, the addition of MAPP slightly reduced the IS of 10 wt% HGBs filled PP composites.

The decrease of the IS with HGBs addition may also be attributed to the brittle nature of the HGBs themselves and to the fact that they cannot generate deformation when exerted force on them (Kumar et al., 2017, Wang et al., 2010). The smaller size HGBs filled composites showed a higher value of

IS. 2.5 wt% iM30K added PP composites has increased the notched impact strength by 4.1 kJ/m² compare to 2.5 wt% S60HS filled composites. The NIS of PP/HGBs composites observed a slight increase when the volume fraction of HGB is less than 15% (Liang, 2006). The main cause of the difference may be the pre-treatment with a silane coupling agent. It improved the interfacial adhesion of PP and HGBs, thus help to absorb impact deformation energy.

The un-notched impact strength of the RPP/HGB composites was presented in Table 7-8.

Table 7-8 Un-notched impact strength of HGB filled RPP composites

Sample code	Impact strength (kJ/m ²)	ΔImpact strength ^a (kJ/m ²)
RPP3	108.7	0.0
RPP3-2.5iM30K	105.0	-3.7
RPP3-5iM30K	85.2	-23.5
RPP3-10iM30K	49.9	-58.8
RPP3-10iM30K-5MAPP	22.4	-86.3
RPP4	95.5	0.0
RPP4-2.5iM30K	94.6	-0.9
RPP4-5iM30K	88.8	-6.7
RPP4-10iM30K	49.2	-46.3
RPP4-10iM30K-5MAPP	39.0	-56.6
^a ΔImpact strength is the difference to neat RPPs		

One of the major drawbacks of HGB is the deterioration of the impact performance of the composites. As is shown in Figure 7-10 the un-notched impact strength of the composites dramatically decreased when the HGB loading is 5 wt% or greater.

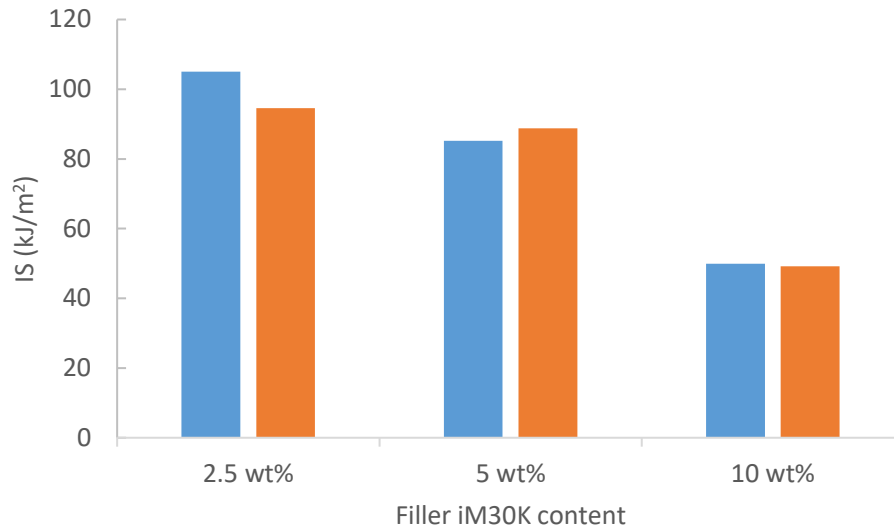


Figure 7-10 Correlations of iM30K content of the strength of RPP3 and RPP4 based composites

It is observed that when the iM30K loading is 10 wt%, the IS of RPP3-10iM30K and RPP4-10iM30K reduced by 54.1% and 48.5% as compared to pure RPP3 and RPP4. One explanation is that at high content of HGB agglomeration occurs, which initiates crack forming and facilitated crack propagation (Ayaz et al., 2016). The results in Table 7-8 show that MAPP has negative effects on the IS of the PP/HGBs composites. For RPP3-10iM30K, the addition of 5 wt% of the MAPP deteriorated 55%. Kumar et al. (2017) also expect the impact strength will be increased because of the improved filler-matrix interfacial adhesion, however, the interaction is not sufficient enough.

7.2.3 Morphological studies

The scanning electron microscopy (SEM) images of the fracture surface of the HGB (S60HS) filled VPP composites are presented in Figure 7-11.

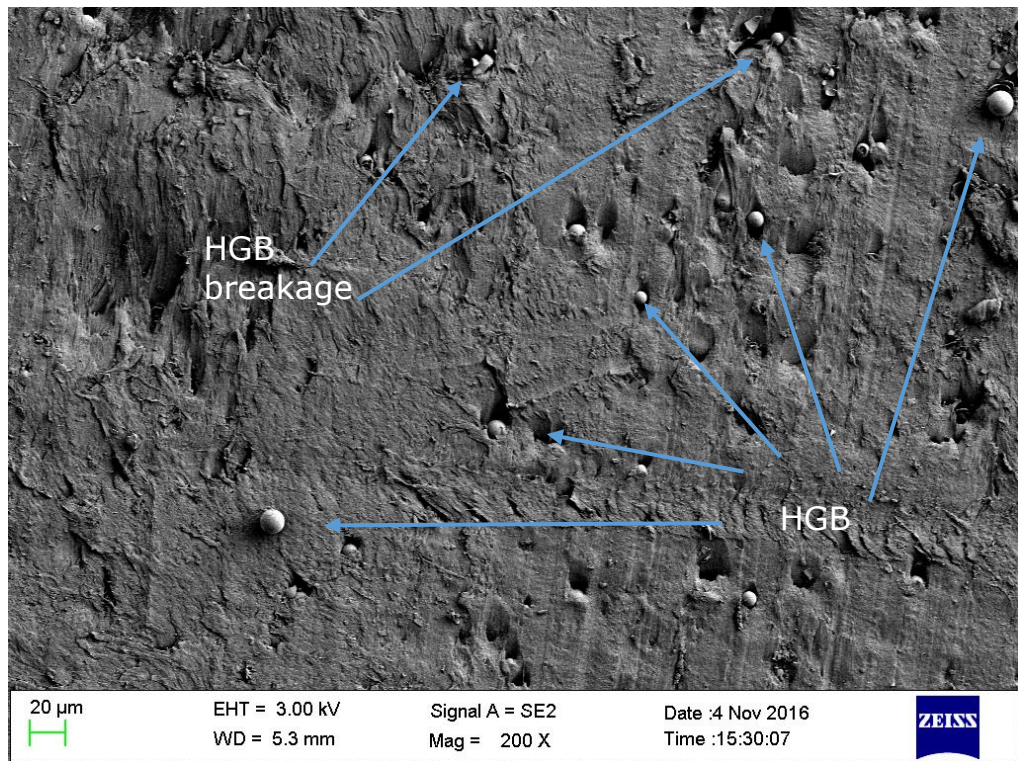


Figure 7-11 SEM images of the fracture surface of PP-5S60HS

It can be found from Figure 7-11 that HGB is uniformly dispersed in the PP matrix, and the HGB breakage was observed. Figure 7-13 shows HGBs filled PP composites without the addition of coupling agent and it can be seen that there was poor surface adhesion between HGBs and matrix.

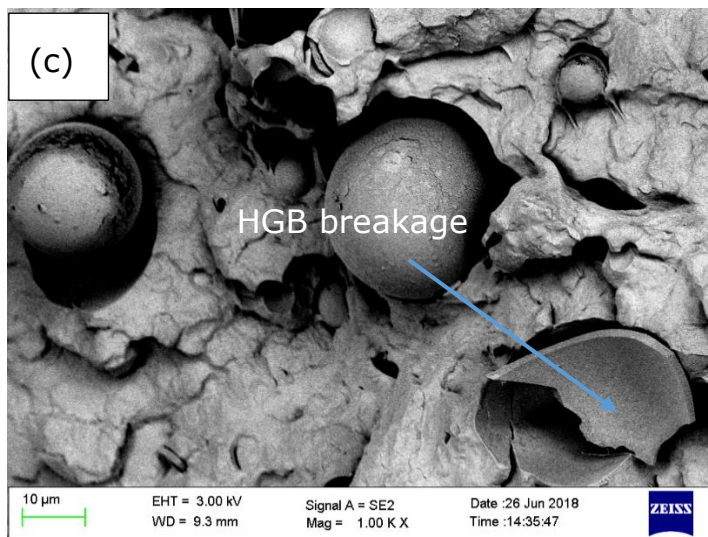
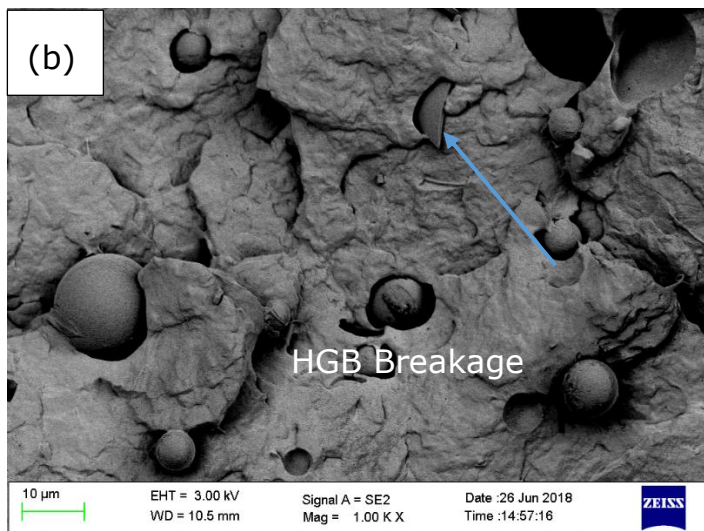
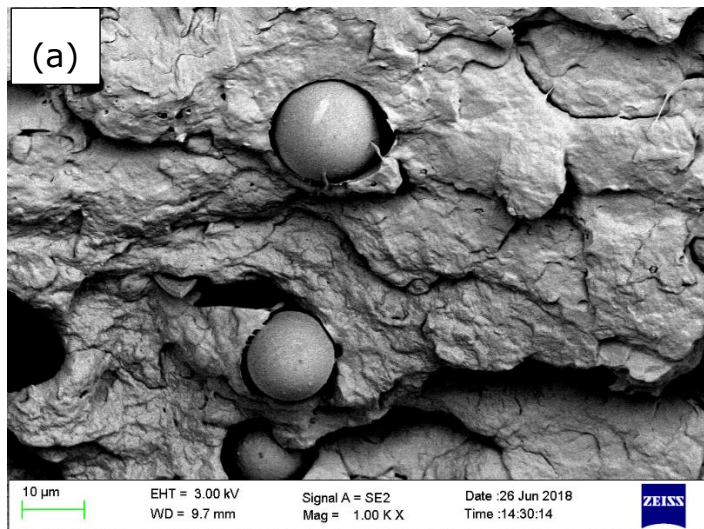


Figure 7-12 SEM images of the fracture surface of (a) PP-2.5S60HS (b) PP-5S60HS (c) PP-10S60HS

Liang (2014) observed the microstructure of the 20 vol% HGBs filled PP composites and find the distribution of the HGBs in the PP matrix is roughly homogeneous. Moreover, it can be inferred that more cracks were seen to form with the increase of HGBs content. The interfacial adhesion between HGBs and PP is vital in controlling the mechanical properties of the composites. Figure 7-13 is the photograph of the 10 wt% HGBs filled PP composite with the addition of 5 wt% MAPP and it can be seen that the interfacial adhesion between HGBs and PP matrix is significantly improved.

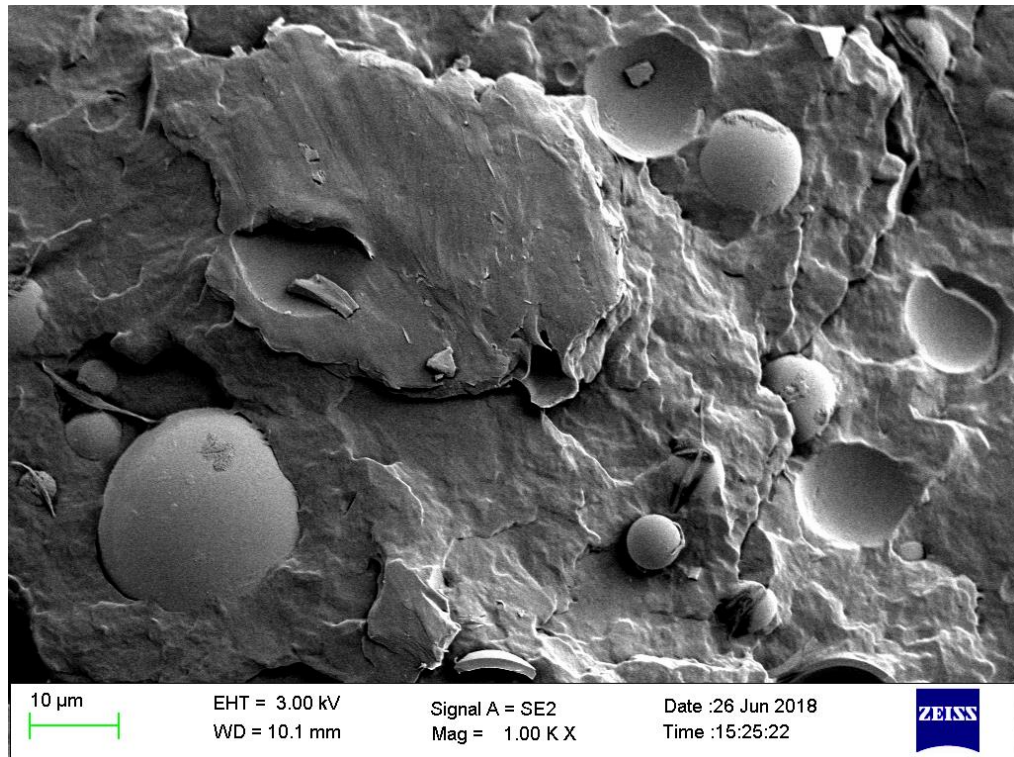


Figure 7-13 SEM images of the fracture surface of PP-10S60HS+5MAPP

Kumar et al. (2017) showed that the chemical treatment of HGBs surface and incorporation of MAPP can successfully support the good dispersion of HGBs and appropriate matrix wetting. By comparing the mechanical results between PP-

10S60HS and PP-10S60HS-5MAPP, both tensile and flexural properties gain remarkable improvement. Tensile modulus, tensile strength, flexural modulus and flexural strength of 5 wt% MAPP filled PP-10S60HS composites were increased by 7.9%, 7.3%, 9.9%, 10.9%, respectively as compared to PP-10S60HS without coupling agent.

7.2.4 Conclusions

The weight reduction and mechanical performance of HGBs filled VPP and RPP composites were tested and analysed. The results of the VPP/HGBs composites were further compared with VPP/ $\text{Al}(\text{OH})_3$ composites.

The content of the HGBs in the PP or RPP matrix affects the density reduction. At 10 wt% filler loading, the sample PP-10S60HS obtained a 3.5% weight reduction, while the sample PP-10 $\text{Al}(\text{OH})_3$ has a 5.4% increment of density. The density of sample RPP3-10iM30K and RPP4-10iM30K reduced 4.0% and 4.2% as compared to pure RPP3 and pure RPP4. The experimental results of the composite density are higher than the theoretical value, which is caused by the HGB breakage during the processing.

At the same filler content, $\text{Al}(\text{OH})_3$ filled VPP composites obtained a slightly higher tensile strength, flexural modulus and flexural strength than the HGB filled VPP composites. It was found that although all of these fillers will reduce the un-notched impact properties, $\text{Al}(\text{OH})_3$ filled VPP composites showed superior performance in maintaining the impact resistance.

In general, the effects of HGBs filler on the RPP on the mechanical properties are the same as the virgin PP-based

composites. And have the following findings:

- The HGBs enhanced the tensile modulus but the tensile strength will slightly reduce with the further addition of HGBs. The coupling agent MAPP can increase the tensile modulus and overcome the tensile strength loss due to high HGBs content.
- HGBs also have positive effects on flexural modulus. The flexural strength slightly reduced with increasing HGBs content. The addition of MAPP also dramatically improve both flexural modulus and strength.
- The un-notched Izod impact strength degraded with increased HGBs loadings, especially when the HGBs loading is higher than 5 wt%. The presence of the MAPP is not sufficient to improve the interfacial adhesion of the filler-PP matrix, the un-notched impact strength reduced with the addition of MAPP in the 10 wt% HGB filled composites.

7.3 Flammability tests for VPP/HGB composites

The outsourced cone calorimeter test was processed for investigating the effects of HGB on the flame retardancy of PP composites. As the flame retardancy of HGB was not fully investigated in the literature, to avoid the impurities in RPP affect the analysis of HGB flame retardancy, the RPP/HGB composites were not studied in this section. And it may be further studied in future work.

7.3.1 Cone calorimeter test

7.3.1.1 Heat release rate (HRR)

Heat release rate (HRR) is an important factor which represents the intensity of the combustion in the cone calorimeter test. Figure 7-14 shows the HRR results of the HGB and $\text{Al}(\text{OH})_3$ filled PP composites.

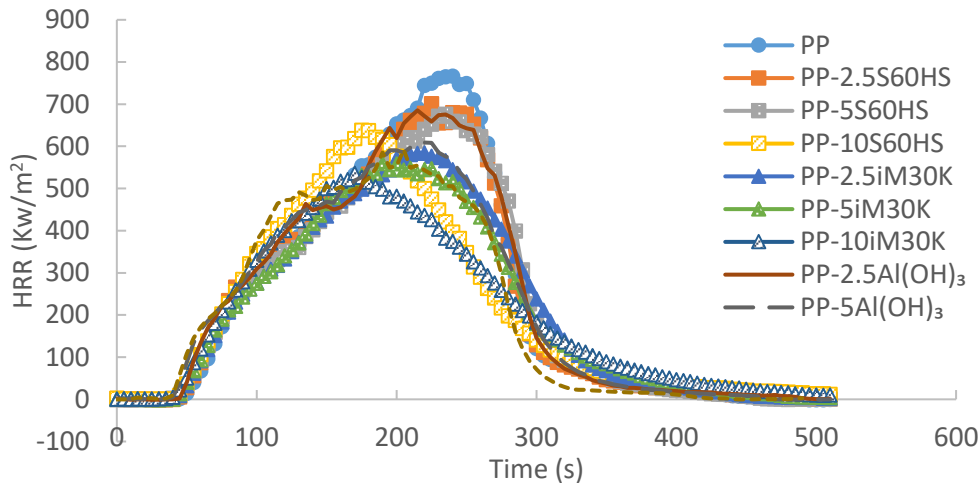


Figure 7-14 HRR results of the hollow glass beads and $\text{Al}(\text{OH})_3$ filled PP composites

The peak HRR (PHRR) is a commonly used factor to describe the fire hazard (Liu et al., 2014). In Figure 7-14, it can be observed that pure PP has the highest PHRR among the test samples. The PHRR of pure PP was 766.6 kW/m^2 occurred at 240s. For the HGBs filled PP composites, the PHRR reduced with the increase of HGBs content. When the content of S60HS in the composite increased from 2.5 wt% to 10 wt%, compared to pure PP, the PHRR reduced 11.3% and 16.8%, which occurred at 240s and 175s, respectively. iM30K filled PP also presented a similar tendency. The PHRR of PP-2.5iM30K was 584.6 kW/m^2 at 220s, and for PP-10iM30K, it was 536.6 kW/m^2 at 170s. For 2.5 wt%, 5 wt% and 10 wt% $\text{Al}(\text{OH})_3$ filled PP, the PHRR were 685.3, 608.9, 591.9 kW/m^2 , respectively. With the

addition of HGB, especially the smaller size HGBs (iM30K), the PHRR was reduced. 10 wt% iM30K filled PP composites showed the lowest PHRR, which indicated that HGBs act as a flame retardant in the PP matrix. The small size HGBs iM30K showed superior flame retardant properties compared to S60HS, which has the same density. The possible explanation is that at the same filler content, the small size HGBs has a much higher surface area, due to the low density of the HGBs, it formed a protective layer above the molten surface of the molten polymer. This protective layer reduced the heat transfer and contact of the degraded PP with the underlying PP matrix, thus the HRR of the HGBs filled PP reduced. Liang and Zhang (2010) studied the flame retardant mechanism of $\text{Al}(\text{OH})_3$, the hydroxides of $\text{Al}(\text{OH})_3$ may release water during heating, Al_2O_3 will form an insulation layer and the combustible material content was reduced with the addition of $\text{Al}(\text{OH})_3$. In this study, the iM30K is a more effective flame retardant than $\text{Al}(\text{OH})_3$, the density of iM30K is 75% lower than $\text{Al}(\text{OH})_3$, which means at same weight fraction, iM30K has much higher volume fraction. On the other hand, although S60HS also has low density, but the median particle size of S60HS is 172.7% higher than $\text{Al}(\text{OH})_3$, which is closely correlated to the specific surface area. It is confirmed that both low density and small size contributes to the flame retardant performance of HGB iM30K.

7.3.1.2 Smoke production rate (SPR)

Figure 7-15 illustrates the SPR curves of the hollow glass bubble and $\text{Al}(\text{OH})_3$ filled PP composites.

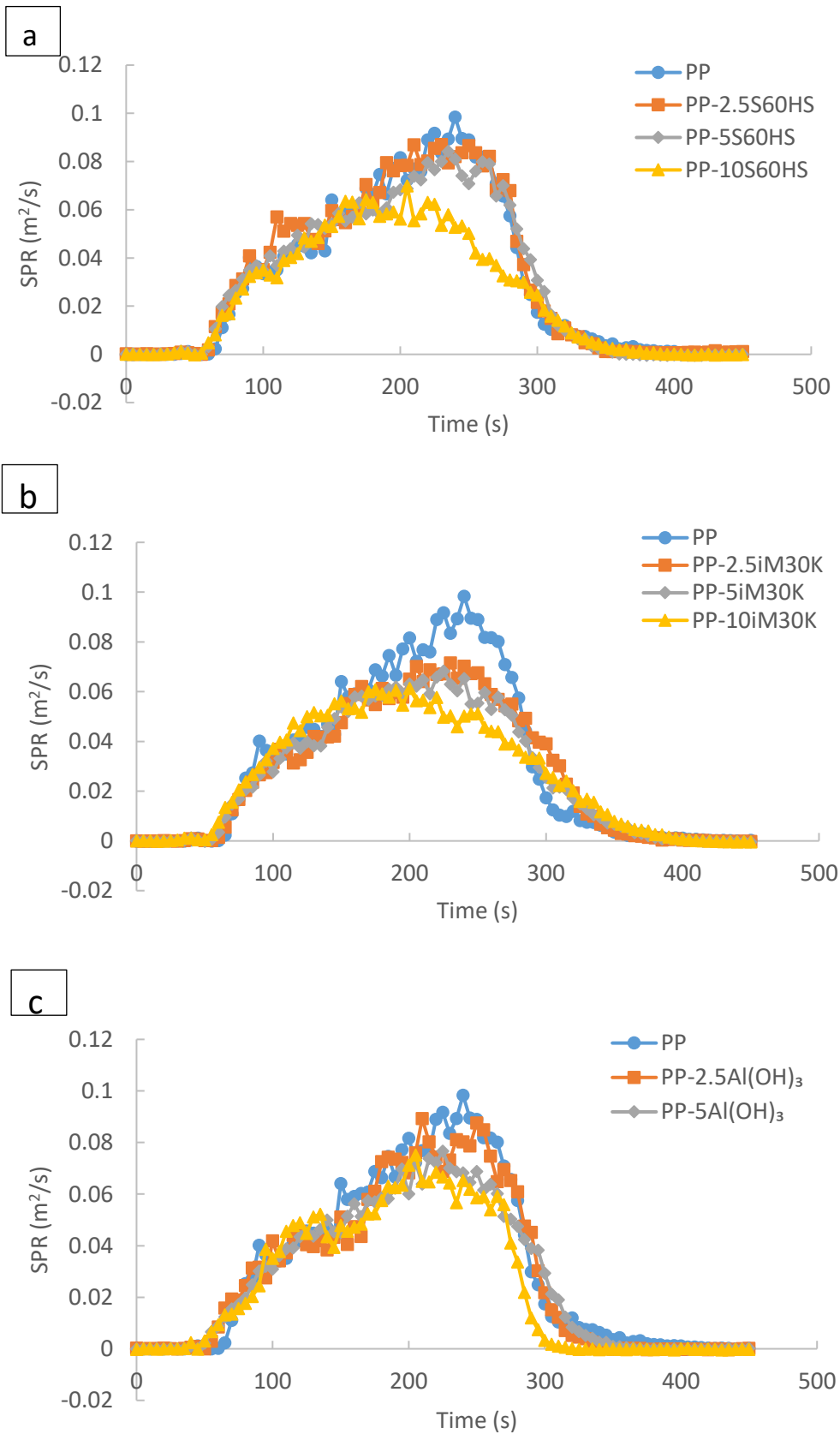


Figure 7-15 SPR results of (a) S60HS filled PP composites (b) iM30k filled PP composites (c) Al(OH)₃ filled composites

Among these samples, it can be observed that the pure PP has the highest peak SPR of 0.098 m²/s at 240s. For HGBs and Al(OH)₃ filled PP composites, the value of SPR reduced with the increase of filler content. PP-10iM30K has the lowest peak SPR of 0.061m²/s at 200s among all the test samples. For 10 wt%S60HS and 10 wt% Al(OH)₃ filled PP, the peak SPR were reduced by 28.9% and 23.6% as compared to pure PP. The reduced smoke production may be explained by the formation of HGBs/Al(OH)₃ rich char layer, which hindered the release of the smoke-forming materials to be released during the combustion. The smoke suppression tendency is consistent with the HGB filled thermoplastic polyurethane composites studied by Jiao et al. (2017). One interesting finding is that the size of the HGBs has significant impacts on the peak SPR at low concentration. The peak SPR of PP-2.5iM30k was 19.4% lower than PP-2.5S60HS. One possible reason is that for the same weight fraction of iM30K and S60HS, both HGBs had the same density, the smaller size iM30k has a higher specific surface area and it can be more effective in forming a protective layer.

7.3.1.3 Mass of the composites in cone calorimeter test

The mass curves of the HGBs and $\text{Al}(\text{OH})_3$ filled PP composites are illustrated in Figure 7-16.

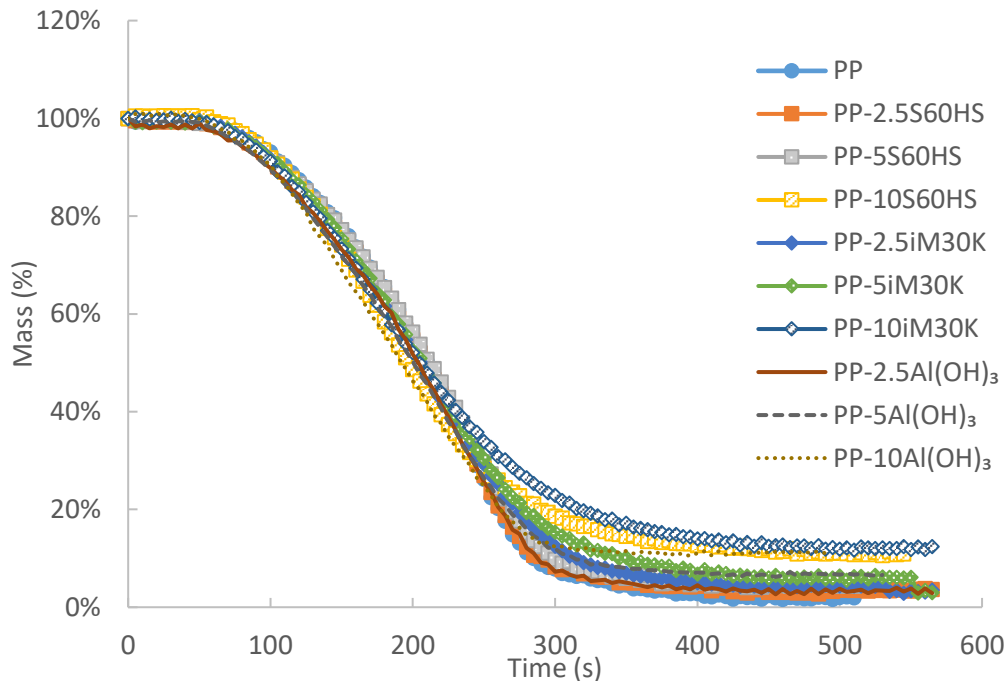


Figure 7-16 Mass curves of the hollow glass beads and $\text{Al}(\text{OH})_3$ filled PP composites in cone calorimeter test

It was found that at the first 200s, the mass loss of the HGBs and $\text{Al}(\text{OH})_3$ filled PP composites were faster than pure PP. And the rate of mass loss was increased with the addition of the filler content. The time of 40% mass loss of pure PP, PP-10S60HS, PP-10iM30K and PP- $\text{Al}(\text{OH})_3$ were 192s, 178s, 182s and 170s, respectively. Jiao et al. (2017) observed the addition of HGB accelerated the mass loss of thermoplastic polyurethane (TPU) composites, the main reason is that HGB catalysed TPU to decompose at a lower temperature. The decomposition of the PP composites formed varies of smoke particulates, flammable gases and inflammable glasses. As is shown in Figure 7-15, compared to VPP, less smoke formed during the

combustion, however, the produced flammable gases accelerated the mass loss.

7.3.1.4 Total heat release (THR)

Figure 7-17. represents the THR results of HGBs and $\text{Al}(\text{OH})_3$ filled PP composites.

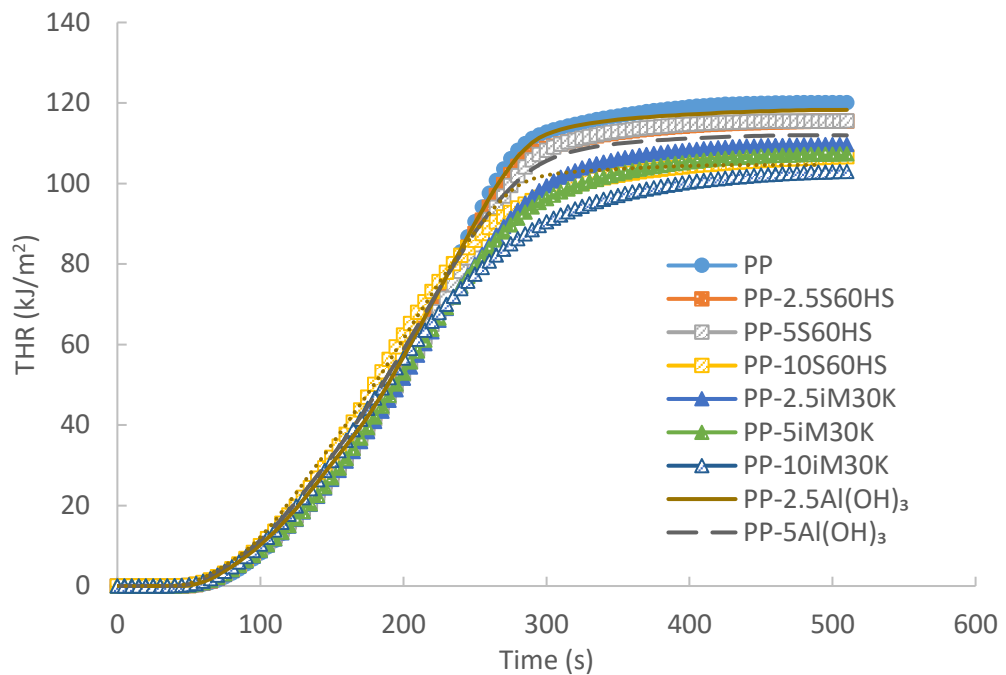


Figure 7-17 THR results of the hollow glass beads and $\text{Al}(\text{OH})_3$ filled PP composites

The highest THR 120.1 kJ/m^2 was observed in pure PP. When the weight fraction increase from 2.5 wt% to 10 wt%, THR for S60HS filled PP reduced from 115.5 to 106.7 kJ/m^2 , and for iM30K and $\text{Al}(\text{OH})_3$, this value reduces from 109.7 to 103.0 kJ/m^2 and 118.3 to 104.6 kJ/m^2 . The reduction of THR is attributed to the fact that the flammable contents in HGBs and $\text{Al}(\text{OH})_3$ filled PP composites are lower than the pure PP. At 2.5 wt% filler loading, an 8.7% reduction of THR was observed in PP-2.5iM30K, which is more effective than S60HS and $\text{Al}(\text{OH})_3$. The explanation is that at the same weight fraction, HGBs have

much higher volume fraction than $\text{Al}(\text{OH})_3$, besides, the high specific surface area of iM30K contributes to the formation of an effective protective layer even at a low weight fraction. Due to the low density of HGB, the protective layer is above the molten surface of the polymer, which hindered the flammable gases to the flame zone and protects the underlying polymers.

7.3.1.5 Time to ignition (TTI)

The time to ignition (TTI) results of the HGBs and $\text{Al}(\text{OH})_3$ filled PP composites are shown in Figure 7-18.

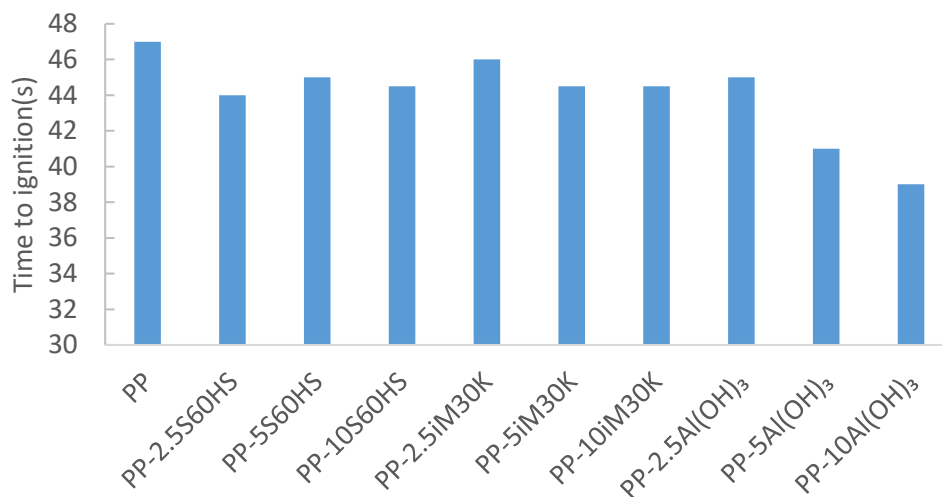


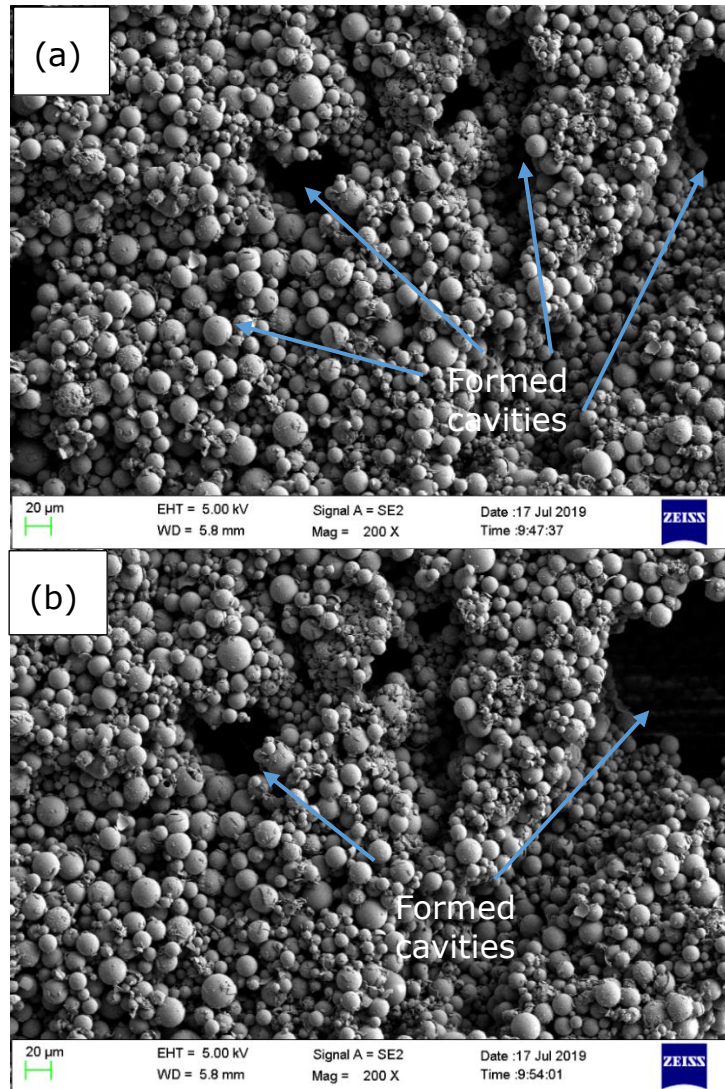
Figure 7-18 TTI results of the HGBs and $\text{Al}(\text{OH})_3$ filled PP composites

The pure PP took the longest TTI (47s). With the addition of HGBs, TTI was slightly decreased by 1 to 3 seconds as compared to pure PP, which implies that the presents of HGBs accelerated the degradation of HGBs filled PP composites. The result is consistent with the findings in the mass curves in Figure 7-16. The addition of $\text{Al}(\text{OH})_3$ also makes the PP composites easier to be ignited. The TTI of $\text{Al}(\text{OH})_3$ filled PP continued to drop from 45s to 39s as the weight fraction of $\text{Al}(\text{OH})_3$ increase from 2.5 wt% to 10 wt%. The possible reason

is that the presence of $\text{Al}(\text{OH})_3$ at the surface of the composites hindered the heat transfer, thus the surface temperature rises quickly to the decomposition temperature.

7.3.2 Morphological study of char residue

The morphology of the PP-10S60HS, PP-10iM30K and PP-10 $\text{Al}(\text{OH})_3$ char residue is presented in Figure 7-19.



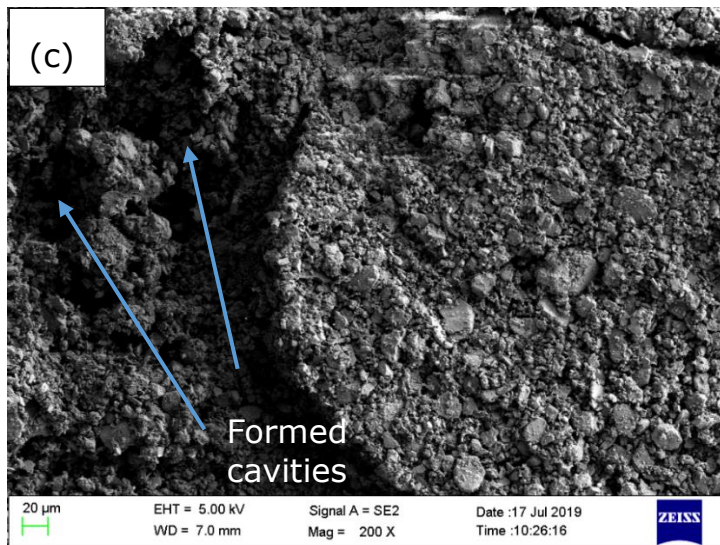


Figure 7-19. SEM images of the char residue of (a) PP-10S60HS (b) PP-10iM30K (c) PP-10Al(OH)₃

From the observation of the char residue, both S60HS and iM30K filled PP composites formed a layer that is tightly stacked by HGBs. This layer can reduce the heat transfer between the flame zone and the underlying PP matrix. As is shown in Figure 7-19(a) and (b), the flammable and non-flammable gases go through the HGBs layer and formed some cavities. It can be seen that the HGBs (iM30K) formed a more compact protection layer than HGBs (S60HS), which is more effective in heat insulation and mass transfer. Figure 7-19(c) shows the structure of the PP/Al(OH)₃ char residue, the Al(OH)₃ or Al₂O₃ powder formed a thin non-flammable layer. The presence of this non-flammable layer reduces the mass transfer and burning rate. The above results are consistent with the mechanism mentioned in the discussion of HRR, SPR and other results in the cone calorimeter test. It proves the HGBs and Al(OH)₃ protection layer are responsible for improving the flame retardant performance of PP.

7.3.3 UL94 horizontal burning

The UL94 horizontal burning results are divided into three groups according to the filler iM30K, S60HS and Al(OH)₃. Figure 7-20 presents the UL94 results of composites at the filler content of 2.5 wt%, 5 wt% and 10 wt%.

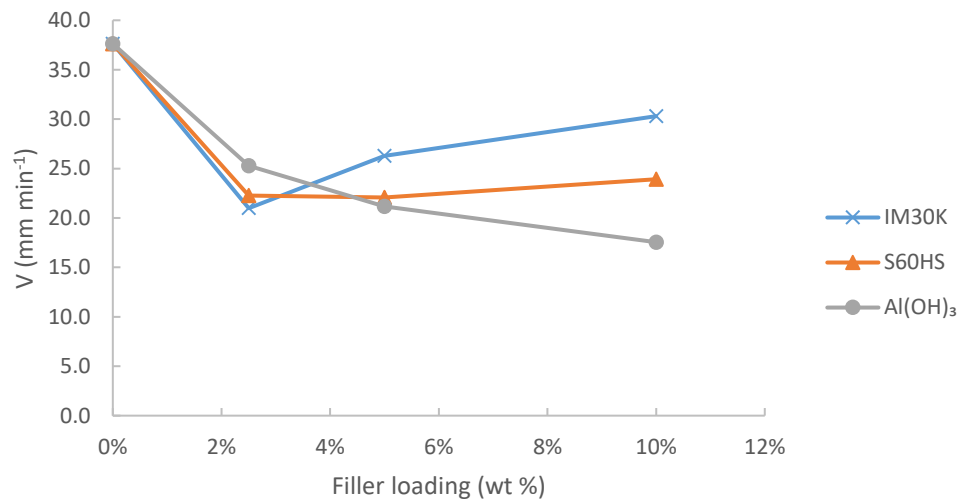


Figure 7-20 Relationship between burning velocity and filler loading

The results illustrate that aluminium hydroxide can reinforce the flame-retardant performance of the composites. The burning rate the aluminium hydroxide filled composites steadily decrease with increasing content. And when the filler loading is 10 wt%, the burning rate of the composites showed a 53.4% reduction. These findings are consistent with the experiment results by Liang et al (Liang and Zhang, 2010).

For HGBs filled composites, the minimum burning rate occurs when the HGBs loading is 2.5 wt%. When the HGBs loading higher than 2.5 wt%, the burning rate increase. One of the explanation is that the density of the HGBs is lower than the molten plastics, and it forms a protective layer above the

underlying plastics. However, unlike the cone calorimeter test, there is no holder under the plastics, as a result, when the composite is burning, it forms molten drops and easy flame propagation which accelerates the burning. For $\text{Al}(\text{OH})_3$ filled PP composites, the density of $\text{Al}(\text{OH})_3$ particles is much higher than the PP matrix,

As for the effects of particle size on the burning rate, the addition of smaller size HGBs resulted in a higher increase in the burning velocity when the filler loading is higher than 2.5 wt%. With the increase of the HGB content, the protective layer loses with the molten drops and propagation the flame. The same phenomenon was also reported that when the particle size is more than 5 μm , the burning rate will decrease with the increase of particle diameter (Liang and Zhang, 2010). The smaller size particle is easier to aggregate in the matrix and form a non-uniform dispersion which leads to the reduced burning velocity (Liang and Zhang, 2010). It was found HGBs has better flame-resistant properties than $\text{Al}(\text{OH})_3$ when the filler loading is less than 3 wt%. This study also showed that an appropriate amount of HGBs contributes to the flame retardancy effects.

7.3.4 Thermal properties

The TGA curves of PP/HGB and PP/ $\text{Al}(\text{OH})_3$ composites are illustrated in Figure 7-21.

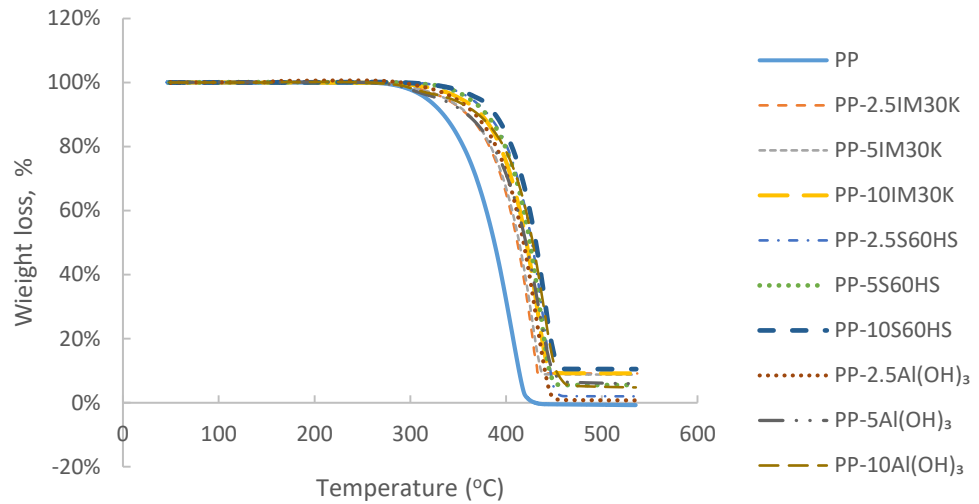


Figure 7-21 TGA curves of PP/HGB, PP/Al(OH)₃ composites, containing different wt% filler content

The temperature at 5% weight loss and the corresponding maximum degradation rate of the composites are given in Table 7-9.

Table 7-9 Temperature at 5% weight loss, the temperature at the maximum degradation rate of PP/HGBs, PP/Al(OH)₃ composites

Sample code	Temperature (°C) at 5 wt% loss	$\Delta T_{5 \text{ wt}\%}^a$	Temperature (°C) at maximum degradation rate	ΔT_{max}^b
PP	315	0	406	0
PP-2.5iM30K	333	19	427	20
PP-5iM30K	333	19	429	22
PP-10iM30K	349	34	433	27
PP-2.5S60HS	361	46	441	34
PP-5S60HS	359	45	437	31
PP-10S60HS	368	53	441	35
PP-2.5Al(OH) ₃	344	29	433	26
PP-5Al(OH) ₃	325	10	434	28
PP-10Al(OH) ₃	336	21	441	34
<p>^a $\Delta T_{5 \text{ wt}\%}$ is the difference of temperature at 5 wt% loss to neat PP.</p> <p>^b ΔT_{max} is the difference of temperature at the maximum degradation rate to neat PP.</p>				

From the results of temperature at 5% weight loss, it shows that the thermal stability of the PP/HGBs and PP/Al(OH)₃ composites have been improved as compared to neat PP.

Among these fillers, S60HS has the best performance because of the thermal insulation properties, which was in accordance with the works carried out by Wang et al. (2010). The initial degradation temperature of PP-10S60HS improved by 53.13°C and T_{\max} greater than 34.75°C with respect to neat PP. The temperature at 5% weight loss increase with increasing the filler weight fraction. The improvement may be attributed to the fact that the existence of the inorganic fillers hindered the movement of the macromolecular chains of the polymer, which can improve the thermal stability and heat resistance of the composites Liang et al. (2015b). Therefore, it could be concluded that the HGBs and $\text{Al}(\text{OH})_3$ can not only improve the mechanical properties of the composites but also improve the overall thermal stability.

7.3.5 Conclusion

The cone calorimeter test (CCT) results illustrated that the addition of $\text{Al}(\text{OH})_3$ and HGBs, especially HGBs (iM30K), can significantly reduce the heat release rate (HRR) and smoke production. Due to the low density and small size of iM30K, it can form an effective protection layer to suppress the flame. The results of the UL94 horizontal burning test demonstrated that the burning velocity of the $\text{Al}(\text{OH})_3$ filled-PP composites gradually decreased with an increase of the filler loading. The flame retardant of the HGB filled composites were optimised when 2.5 wt% HGBs were filled in the matrix. $\text{Al}(\text{OH})_3$ filled composites showed superiority when the filler loading is higher than 3 wt%. HGBs and $\text{Al}(\text{OH})_3$ dramatically promote the thermal stability of the composites. Among these fillers, high particle size HGBs (S60HS) shows the best thermal stability performance. It is observed that the initial degradation

temperature of PP-10S60HS increased 53.13°C with respect to pure PP.

7.4 Summary

This chapter investigated the mechanical, thermal and flammability performance of the HGBs filled PP composites. This study consists of the study of HGBs filled VPP-based and RPP-based composites.

In VPP-based composites, two different sizes HGBs (iM30K, S60HS) were selected. $\text{Al}(\text{OH})_3$ was also selected as a traditional mineral filler, which is expected to have a high density (as compared to plastics) and flame retardant properties. The study showed that the HGBs filler demonstrated superior density reduction performance than $\text{Al}(\text{OH})_3$ filler. However, the tensile strength, flexural strength and un-notched impact strength of the HGBs filled PP composites were lower than the $\text{Al}(\text{OH})_3$ filled PP composites at the same filler loading.

The small size HGB (iM30K) was selected as the filler for RPP-based composites. The effects of HGBs and coupling agent on the mechanical properties of the composites are consistent with the findings in VPP-based study. The HGBs will contribute to the increase of the tensile and flexural modulus. And the reduction of the tensile strength and flexural strength can be compensated by adding the coupling agent MAPP. The impact strength reduction is the major problem of the application of HGB. When the HGB loading is higher than 5 wt%, the un-notched impact strength of the composites significantly reduced due to the agglomeration of HGBs and poor interfacial adhesion.

In the flammability study, the CCT results showed that the heat release rate (HRR) reduced with the addition of HGBs and $\text{Al}(\text{OH})_3$ content, the lowest HRR 536.6 kW/m^2 was observed in 10 wt% iM30K filled PP. For the UL94 horizontal burning test, at the 2.5 wt% loadings, HGBs (iM30K) filled PP composites showed the lowest burning rate. The above results proved that the addition HGB improved the flame retardant properties of the PP composites. In the thermal study, the addition of $\text{Al}(\text{OH})_3$ and HGB also showed a promising improvement in thermal stability, the sample PP-10S60HS obtained the 53.13°C increase in the initial degradation temperature as compared to neat pp.

This page is intentionally left blank.

Chapter 8 Conclusion and further work

8.1 Conclusion

PP has high flexibility and has applied in many automobile plastic parts and it occupies the highest weight fraction among all plastics used in a vehicle. Therefore this study focuses on PP composites because of more options in parts selection. For improving the quality of the RPP products, researchers have studied various methods. However, very few of the studies cooperated with the industry, and the production of a real automobile part has been rarely reported. To understand the knowledge gap between the improving techniques and industrial requirements, the following types of PP composites are studied.

8.1.1 Plastic characterisation and Talc-filled RPP composites

The selected RPPs and VPPs were characterised and compared to find the potentially applicable automobile parts. For RPP/talc/MAPP/VPP composites, Taguchi L9 (3^3) orthogonal array (OA) was applied as an experimental design tool. The effects of the weight fraction of talc, MAPP and VPP on the mechanical performance of the composites were measured and expressed in signal to noise (S/N) ratio. The results showed that talc is the most influential factor in controlling the tensile modulus and flexural modulus. VPP has the most significant effects in the tensile strength and flexural strength. The interaction between MAPP and VPP has the most significant effect on the tensile and flexural modulus, while talc and MAPP

have the most observable effects on the tensile and flexural strength. The multi-dimensional data was reduced to a single array of scores using PCA, and the optimal composition was hence obtained by analysing the PCA scores.

The effectiveness of the Taguchi-ANOVA optimising approach has been successfully proven by confirmation tests on the composite of the optimal formula. Based on the results of this study, armrest boxes were produced in the industrial trial. Comparison of the RPP-based armrest box and the VPP-based armrest box (provided by our industrial partner) indicates VPP-based armrest box has a consistent appearance (without a visible colour difference) and better thermal ageing performance. The economic evaluation showed the RPP-based armrest box can have 35.2% of cost-saving as compared to the cost of the VPP-based pellets provided by our partner.

8.1.2 RPP/PE and RPP/Elastomer blended composites

To further overcome the low impact properties of the talc-filled RPP composites and extend the applicable fields to automobile bumpers, the selected RPP was blended with LLDPE, LLDPE-g-MA and SEBS-g-MA.

The results prove that the addition of LLDPE, LLDPE-g-MA and SEBS-g-MA successfully improved the impact properties of the RPP composites. The addition of SEBS-g-MA to RPP has the most significant improvement in notched impact strength at room temperature and -30°C, where 361.6% (53.6 kJ/m²) and 115.2% (6.8 kJ/m²) improvement was observed, respectively. However, the reported tensile strength, flexural strength, and flexural modulus were reduced with the increasing content of LLDPE, LLDPE-g-MA and SEBS-g-MA. By comparing the

mechanical results of the prepared composites with the bumper requirements, the sample 90 wt% RPP3 blended with 10 wt% LLDPE-g-MA meets all of the mechanical requirements for the middle-end bumpers. And the RPP3 can be partially (20 wt%-40 wt%) replaced by VPP3 to maintain a more balanced performance. However, due to the lack of suitable moulds, the industrial trial for producing the automobile bumper was not processed.

The effects of SEBS-g-MA was further assessed in the RPP/Al(OH)₃/SEBS-g-MA and RPP/Talc/SEBS-g-MA composites. The result proves SEBS-g-MA can significantly improve the notched impact properties. Sample 10 wt% Al(OH)₃ 20 wt% SEBS-g-MA 70 wt% RPP obtained the highest notched impact strength (37.8 kJ/m²), which exceed the requirements of the high-end bumpers (>35 kJ/m²). However, the flexural strength (681.3 MPa) of this sample was significantly lower than the required value (1300-1700 MPa). It was found that the addition of both mineral fillers was insufficient to compensate for the flexural properties loss due to the addition of SEBS-g-MA.

8.1.3 Recycled short carbon fibre filled PP/RPP composites.

A novel procedure was developed to utilise recycled short carbon fibre as the filler in PP composites. The recycled carbon fibre was milled to a smaller size, followed by the process of 1) dispersion in surfactant added water, 2) drying in the oven, 3) hot compressing with VPP or RPP pellets, 4) milling into plastic pellets, 5) twin-screw extrusion and 6) injection moulding to obtain the standard specimens for testing. The effects of the content of recycled short milled carbon fibre (rSMCF) and MAPP

on the mechanical performance of the composites were the primary focus. Both of the rSMCF filled VPP and RPP composites showed a significant increase in tensile modulus and flexural modulus, confirming a low concentration of rSMCF (1 wt% to 5 wt%) is effective in improving the stiffness of the composite. The addition of MAPP to the VPP and RPP matrix effectively improved the fibre-matrix interfacial adhesion. In rSMCF filled RPP composites, the tensile modulus, tensile strength, flexural modulus and flexural strength were significantly improved with the increment of MAPP contents. However, the high content of MAPP contributes to the reduction of impact strength due to the low molecular weight of MAPP. DSC and FTIR technique prove the existence of PE contamination in the RPP. The microscale morphological study confirmed the bonding between fibre and VPP or RPP matrix was improved with increasing MAPP content. While the interfacial adhesion performance of MAPP in VPP is better than in RPP, since the existence of partially miscible PE in RPP. This study confirmed that the small content of recycled short carbon fibre has the potential to significantly improve the mechanical performance of both VPP and RPP based composites. However, the contaminations in the RPP may affect the performance of the composites. In the future, more recycled plastics from difference sources should be studied, and establish the correlations and interactions between all the compositions and properties.

8.1.4 Hollow glass beads filled PP/RPP composites

The mechanical, thermal and flammability performance of the hollow glass beads (HGB) filled VPP and RPP composites were characterised. HGB filled VPP or RPP composites were expected to have a lower density, $\text{Al}(\text{OH})_3$ was selected as the high-

density mineral filler for the comparison. The results prove that the HGB has superior density reduction performance than $\text{Al}(\text{OH})_3$. However, at the same filler loading, the tensile strength, flexural strength and un-notched impact strength of the HGB filled PP composites were lower than the $\text{Al}(\text{OH})_3$ filled PP composites. But the reduction of the tensile strength and flexural strength can be compensated by adding the coupling agent MAPP. The impact strength reduction is the major problem of the application of HGB. When the HGB loading is higher than 5 wt%, the un-notched impact strength of the composites significantly reduced due to the agglomeration of HGB and poor interfacial adhesion.

The flammability results of HGB filled VPP composites were compared to the $\text{Al}(\text{OH})_3$ filled VPP composites. The CCT results indicated the heat release rate reduced with both additions of $\text{Al}(\text{OH})_3$ and HGB, the smaller sized HGB (iM30K) has the lowest HRR at 10 wt% loading. And at 2.5 wt% loading, HGB (iM30K) filled VPP also showed the lowest burning rate. In the thermal study, the HGB also improve the thermal stability, because the existence of the HGB hindered the movement of the macromolecular chains of the polymer. And higher sized HGB (S60HS) at 10 wt% showed the best thermal stability performance by increasing the initial degradation temperature of the composites by 53.13°C as compared to the neat PP.

8.2 Further work

The work presented in this thesis has already assessed the feasibility of utilising the RPP for two typical automobile parts: armrest boxes and bumpers. The mechanical properties of the prepared formula successfully meet the mechanical

requirements of the selected parts. However, there is still a lot of work that need to do. This work can be categorised as the following aspects:

1) The recycled plastics focused in this study is RPP, the further study can be extended to other commonly used plastics, such as ABS, PUR, LDPE/HDPE, PA, PS.

2) In the current study, the mechanical properties are the major concern of the prepared samples. In the future, deeper cooperation with the industry should be established to have a better understanding of automobile production. The criteria of the evaluation of the RPP-based composites should be extended to more aspects, such as flammability, durability, degradation effects and cost. It is better if the industrial partner can provide the full detailed requirements during the study and the evaluation after an industrial trial.

3) During the whole period of the study, some of the recycled plastics were in shortage. And the purity of the RPP should be improved. During this study, it was found that the purchased RPP usually contains some unexpected "impurities", such as the PET in RPP3 in Chapter 5, and PE in RPP5 in Chapter 6. These kinds of impurities are not recognized by the supplier, and it will influence the material properties' stability and the effectiveness of reinforcing techniques. In the future, a better understanding of plastic recycling is required because the automobile industry requires a high capability of material supply and quality assurance.

4) The processing of the recycled short carbon fibre can be improved. The current process can only be used at lab-scale production. The process, especially the drying is both energy and time-consuming. The tests of the recycled short carbon

fibre filled composites should also be extended to fulfil the industrial requirements.

5) The main advantages of hollow glass beads (HGBs) are low density and flame retardancy. To improve the competitiveness of HGB, other fillers may be incorporated into the HGB filled composites, and to gain a more balanced performance. Besides, the processing of the HGBs composites should also be improved to reduce the HGBs breakage.

This page is intentionally left blank.

Reference

- 3M. 2013. *The powder to do more* [Online]. Available: <https://multimedia.3m.com/mws/media/7895050/3m-glass-bubbles-im16k-an-introductory-presentation.pdf> [Accessed 17 March 2021].
- ABDI, H. & WILLIAMS, L. J. 2010. Principal component analysis. *Wiley Interdisciplinary Reviews: Computational Statistics*, 2, 433-459.
- ABREU, F. O. M. S., FORTE, M. M. C. & LIBERMAN, S. A. 2005. SBS and SEBS block copolymers as impact modifiers for polypropylene compounds. *Journal of Applied Polymer Science*, 95, 254-263.
- ADHIKARY, K. B., PANG, S. & STAIGER, M. P. 2009. Accelerated Ultraviolet Weathering of Recycled Polypropylene—Sawdust Composites. *Journal of Thermoplastic Composite Materials*, 22, 661-679.
- ADRECO PLASTIC. 2018. *ABS plastic properties* [Online]. Available: <https://www.adrecoplastics.co.uk/abs-plastic-properties-and-application/> [Accessed 11 September 2019].
- AKONDA, M. H., LAWRENCE, C. A. & WEAGER, B. M. 2012. Recycled carbon fibre-reinforced polypropylene thermoplastic composites. *Composites Part A: Applied Science and Manufacturing*, 43, 79-86.
- AL-MAADEED, M. A., SHABANA, Y. M. & KHANAM, P. N. 2014. Processing, characterization and modeling of recycled polypropylene/glass fibre/wood flour composites. *Materials & Design*, 58, 374-380.
- AL-SALEM, S. M., LETTIERI, P. & BAEYENS, J. 2009. Recycling and recovery routes of plastic solid waste (PSW): a review. *Waste Manag*, 29, 2625-43.
- SERIA TRADING. n.d. *What exactly is talc* [Online]. Available: <https://kaolin.co.za/articles/what-exactly-is-talc.html> [Accessed 17 March 2021].
- ALTAN, M. 2010. Reducing shrinkage in injection moldings via the Taguchi, ANOVA and neural network methods. *Materials & Design*, 31, 599-604.
- ARUTCHELVI, J., SUDHAKAR, M., ARKATKAR, A., DOBLE, M., BHADURI, S. & UPPARA, P. V. 2008. Biodegradation of

polyethylene and polypropylene.

- ASHENAI GHASEMI, F., GHASEMI, I., MENBARI, S., AYAZ, M. & ASHORI, A. 2016. Optimization of mechanical properties of polypropylene/talc/graphene composites using response surface methodology. *Polymer Testing*, 53, 283-292.
- AUMNATE, C., RUDOLPH, N. & SARMADI, M. 2019. Recycling of Polypropylene/Polyethylene Blends: Effect of Chain Structure on the Crystallization Behaviors. *Polymers*, 11, 1456.
- AYAZ, M., DANESHPAYEH, S. & NOROOZI, A. 2016. Enhancing the impact and flexural strength of PP/LLDPE/TiO₂/SEBS nano-composites by using Taguchi methodology. *Composites Science and Technology*, 129, 61-69.
- BAJRACHARYA, R. M., MANALO, A. C., KARUNASENA, W. & LAU, K.-T. 2017. Durability characteristics and property prediction of glass fibre reinforced mixed plastics composites. *Composites Part B: Engineering*, 116, 16-29.
- BECHTOLD, K. 2006. How to Meet Increased Quality Performances of Plastic OEM Interior Trims. *Material Testing Product and Technology News*, 36, 1-11.
- BERTINI, F., CANETTI, M., AUDISIO, G., COSTA, G. & FALQUI, L. 2006. Characterization and thermal degradation of polypropylene–montmorillonite nanocomposites. *Polymer Degradation and Stability*, 91, 600-605.
- BHATTACHARYA, D. & BEPARI, B. 2014. Feasibility study of recycled polypropylene through multi response optimization of injection moulding parameters using grey relational analysis. *Procedia Engineering*, 97, 186-196.
- BILLINGHAM, N. C. 2002. Degradation. *Encyclopedia of Polymer Science and Technology*.
- BRO, R. & SMILDE, A. K. 2014. Principal component analysis. *Analytical Methods*, 6, 2812-2831.
- CAI, G., WADA, M., OHSAWA, I., KITAOKA, S. & TAKAHASHI, J. 2019. Interfacial adhesion of recycled carbon fibers to polypropylene resin: Effect of superheated steam on the surface chemical state of carbon fiber. *Composites Part A: Applied Science and Manufacturing*, 120, 33-40.
- CANETTI, M., BERTINI, F., DE CHIRICO, A. & AUDISIO, G. 2006. Thermal degradation behaviour of isotactic polypropylene blended with lignin. *Polymer Degradation and Stability*, 91, 494-498.

- CAPONE, C., DI LANDRO, L., INZOLI, F., PENCO, M. & SARTORE, L. 2007. Thermal and mechanical degradation during polymer extrusion processing. *Polymer Engineering & Science*, 47, 1813-1819.
- CELINA, M. C. 2013. Review of polymer oxidation and its relationship with materials performance and lifetime prediction. *Polymer Degradation and Stability*, 98, 2419-2429.
- CHAN, C.-M., WU, J., LI, J.-X. & CHEUNG, Y.-K. 2002. Polypropylene/calcium carbonate nanocomposites. *Polymer*, 43, 2981-2992.
- CHINA PLASTICS PROCESSING INDUSTRY ASSOCIATION 2017. *China plastics industry yearbook*, China light industry press.
- CHINAIRN. 2018. *2006-2016 National plastic production data* [Online]. Available: <http://www.chinairn.com/news/20181009/115727765.shtml> [Accessed 7 September 2019].
- CHIU, F.-C., YEN, H.-Z. & LEE, C.-E. 2010. Characterization of PP/HDPE blend-based nanocomposites using different maleated polyolefins as compatibilizers. *Polymer Testing*, 29, 397-406.
- CLEMONS, C. 2010. Elastomer modified polypropylene-polyethylene blends as matrices for wood flour-plastic composites. *Composites Part A: Applied Science and Manufacturing*, 41, 1559-1569.
- DA COSTA, H. M., RAMOS, V. D. & DE OLIVEIRA, M. G. 2007. Degradation of polypropylene (PP) during multiple extrusions: Thermal analysis, mechanical properties and analysis of variance. *Polymer Testing*, 26, 676-684.
- DANESHAYEH, S., ASHENAI GHASEMI, F., GHASEMI, I. & AYAZ, M. 2016. Predicting of mechanical properties of PP/LLDPE/TiO₂ nano-composites by response surface methodology. *Composites Part B: Engineering*, 84, 109-120.
- DAS, S. 2011. Life cycle assessment of carbon fiber-reinforced polymer composites. *The International Journal of Life Cycle Assessment*, 16, 268-282.
- DENAC, M., MUSIL, V. & ŠMIT, I. 2005. Polypropylene/talc/SEBS (SEBS-g-MA) composites. Part 2. Mechanical properties. *Composites Part A: Applied Science and Manufacturing*, 36, 1282-1290.

- EIRAS, D. & PESSAN, L. A. 2009. Mechanical properties of polypropylene/calcium carbonate nanocomposites. *Materials Research*, 12, 517-522.
- EPA 2019. The 2018 EPA Automotive Trends Report: Greenhouse Gas Emissions, Fuel Economy, and Technology since 1975.
- ETCHEVERRY, M. & BARBOSA, S. E. 2012. Glass Fiber Reinforced Polypropylene Mechanical Properties Enhancement by Adhesion Improvement. *Materials*, 5, 1084-1113.
- FANG, C., NIE, L., LIU, S., YU, R., AN, N. & LI, S. 2013. Characterization of polypropylene–polyethylene blends made of waste materials with compatibilizer and nano-filler. *Composites Part B: Engineering*, 55, 498-505.
- FCA 2019. 2019 Sustainability report.
- FELDMAN, D. 2002. Polymer Weathering: Photo-Oxidation. *Journal of Polymers and the Environment*, 10, 163-173.
- FRANCO-MARQU S, E., M NDEZ, J. A., P LACH, M. A., VILASECA, F., BAYER, J. & MUTJ , P. 2011. Influence of coupling agents in the preparation of polypropylene composites reinforced with recycled fibers. *Chemical Engineering Journal*, 166, 1170-1178.
- FRED. 2019. *Producer Price Indexes* [Online]. Available: <https://fred.stlouisfed.org/series/PCU325211325211#0> [Accessed 25 March 2019].
- FU, S.-Y. & LAUKE, B. 1996. Effects of fiber length and fiber orientation distributions on the tensile strength of short-fiber-reinforced polymers. *Composites Science and Technology*, 56, 1179-1190.
- FU, S. Y., LAUKE, B., M DER, E., YUE, C. Y. & HU, X. 2000. Tensile properties of short-glass-fiber- and short-carbon-fiber-reinforced polypropylene composites. *Composites Part A: Applied Science and Manufacturing*, 31, 1117-1125.
- FUNG, C.-P. & KANG, P.-C. 2005. Multi-response optimization in friction properties of PBT composites using Taguchi method and principle component analysis. *Journal of Materials Processing Technology*, 170, 602-610.
- GALLONE, T. & ZENI-GUIDO, A. 2019. Closed-loop polypropylene, an opportunity for the automotive sector. *Field Actions Science Reports. The journal of field actions*, 48-53.

- GAMZE KARSLI, N., YESIL, S. & AYTAC, A. 2014. Effect of hybrid carbon nanotube/short glass fiber reinforcement on the properties of polypropylene composites. *Composites Part B: Engineering*, 63, 154-160.
- GAO, H., XIE, Y., OU, R. & WANG, Q. 2012. Grafting effects of polypropylene/polyethylene blends with maleic anhydride on the properties of the resulting wood-plastic composites. *Composites Part A: Applied Science and Manufacturing*, 43, 150-157.
- GARDINER, G. 2014. *Recycled carbon fiber: Comparing cost and properties* [Online]. Available: <https://www.compositesworld.com/articles/recycled-carbon-fiber-comparing-cost-and-properties> [Accessed 18 November 2019].
- GEORGE, S., VARUGHESE, K. T. & THOMAS, S. 2000. Thermal and crystallisation behaviour of isotactic polypropylene/nitrile rubber blends. *Polymer*, 41, 5485-5503.
- GIANNADAKIS, K., SZPIEG, M. & VARNA, J. 2011. Mechanical Performance of a Recycled Carbon Fibre/PP Composite. *Experimental Mechanics*, 51, 767-777.
- GIJSMAN, P. 2008. Review on the thermo-oxidative degradation of polymers during processing and in service. *e-Polymers*.
- GOBI KANNAN, T., WU, C. M. & CHENG, K. B. 2014. Influence of laminate lay-up, hole size and coupling agent on the open hole tensile properties of flax yarn reinforced polypropylene laminates. *Composites Part B: Engineering*, 57, 80-85.
- GONZ LEZ-GONZ LEZ, V. A., NEIRA-VEL ZQUEZ, G. & ANGULO-S NCHEZ, J. L. 1998. Polypropylene chain scissions and molecular weight changes in multiple extrusion. *Polymer Degradation and Stability*, 60, 33-42.
- GU, F., HALL, P. & MILES, N. J. 2016a. Development of composites based on recycled polypropylene for injection moulding automobile parts using hierarchical clustering analysis and principal component estimate. *Journal of Cleaner Production*, 137, 632-643.
- GU, F., HALL, P. & MILES, N. J. 2016b. Performance evaluation for composites based on recycled polypropylene using principal component analysis and cluster analysis. *Journal of Cleaner Production*, 115, 343-353.
- GU, F., HALL, P., MILES, N. J., DING, Q. & WU, T. 2014.

- Improvement of mechanical properties of recycled plastic blends via optimizing processing parameters using the Taguchi method and principal component analysis. *Materials & Design*, 62, 189-198.
- GULMINE, J. V., JANISSEK, P. R., HEISE, H. M. & AKCELRUD, L. 2002. Polyethylene characterization by FTIR. *Polymer Testing*, 21, 557-563.
- HAN, H., WANG, X. & WU, D. 2012. Preparation, crystallization behaviors, and mechanical properties of biodegradable composites based on poly(L-lactic acid) and recycled carbon fiber. *Composites Part A: Applied Science and Manufacturing*, 43, 1947-1958.
- HASHEMI, S. 2008. Tensile and flexural properties of injection-moulded short glass fibre and glass bead ABS composites in the presence of weldlines. *Journal of Materials Science*, 43, 721-731.
- HAWKINS, W. L. 1984. Polymer Degradation. *Polymer Degradation and Stabilization*. Berlin, Heidelberg: Springer Berlin Heidelberg.
- HENRY, F. & GREGORIE, E. T. 1942. Automobile chassis construction. Google Patents.
- HERRERA-FRANCO, P. J. & VALADEZ-GONZ LEZ, A. 2005. A study of the mechanical properties of short natural-fiber reinforced composites. *Composites Part B: Engineering*, 36, 597-608.
- HESS, A. S. & HESS, J. R. 2018. Analysis of variance. *Transfusion*, 58, 2255-2256.
- HONDA. 2020. *Plastics and Resin Business* [Online]. Available: https://www.hondatrading.com/en/business/plastics_and_resin/ [Accessed 20 May 2020].
- HOR K, Z., FORTELN , I., KOLAŘ K, J., HLAVAT , D. & SIKORA, A. 2005. Polymer Blends. *Encyclopedia of Polymer Science and Technology*.
- HOTELLING, H. 1933. Analysis of a complex of statistical variables into principal components. *Journal of educational psychology*, 24, 417.
- HOMKHIW, C., RATANAWILAI, T. & THONGRUANG, W. 2014. The optimal formulation of recycled polypropylene/rubberwood flour composites from experiments with mixture design. *Composites Part B: Engineering*, 56, 350-357.

- HOWARTH, J., MAREDDY, S. S. R. & MATIVENGA, P. T. 2014. Energy intensity and environmental analysis of mechanical recycling of carbon fibre composite. *Journal of Cleaner Production*, 81, 46-50.
- HP, S. 2019. *The significance of Interaction Plots in Statistics* [Online]. Available: <https://medium.com/@hpsuresh12345/the-significance-of-interaction-plots-in-statistics-6f2d3a6f77a3> [Accessed 16 August 2020].
- HUFENBACH, W., BHM, R., THIEME, M., WINKLER, A., MDER, E., RAUSCH, J. & SCHADE, M. 2011. Polypropylene/glass fibre 3D-textile reinforced composites for automotive applications. *Materials & Design*, 32, 1468-1476.
- HUSSEIN, R. M. 2018. Modeling and characterization of thermo-oxidative behavior of bismaleimide composites.
- HU, Y.-H. & CHEN, C.-Y. 2003. Study of the thermal behaviour of poly(methyl methacrylate) initiated by lactams and thiols. *Polymer Degradation and Stability*, 80, 1-10.
- IN CIO, A. L. N., NONATO, R. C. & BONSE, B. C. 2017. Recycled PP/EPDM/talc reinforced with bamboo fiber: Assessment of fiber and compatibilizer content on properties using factorial design. *Polymer Testing*, 61, 214-222.
- INUWA, I. M., HASSAN, A., SAMSUDIN, S. A., HAAFIZ, M. K. M. & JAWAID, M. 2017. Interface modification of compatibilized polyethylene terephthalate/polypropylene blends: Effect of compatibilization on thermomechanical properties and thermal stability. *Journal of Vinyl and Additive Technology*, 23, 45-54.
- JACOB, A. 2019. *Building confidence in recycled carbon fiber* [Online]. Available: <https://www.compositesworld.com/blog/post/building-confidence-in-recycled-carbon-fiber> [Accessed 18 November 2019].
- JIANG, X. L. & ZHANG, Y. X. 2009. Study of the structure and the mechanical properties of dynamically cured PP/MAH-g-SEBS/epoxy blends. *Chinese Chemical Letters*, 20, 877-880.
- JIAO, C., WANG, H., LI, S. & CHEN, X. 2017. Fire hazard reduction of hollow glass microspheres in thermoplastic polyurethane composites. *J Hazard Mater*, 332, 176-184.
- JOLLIFFE, I. 2003. Principal component analysis. *Technometrics*, 45, 276.

- KARSLI, N. G. & AYTAC, A. 2011. Effects of maleated polypropylene on the morphology, thermal and mechanical properties of short carbon fiber reinforced polypropylene composites. *Materials & Design*, 32, 4069-4073.
- KARSLI, N. G. & AYTAC, A. 2013. Tensile and thermomechanical properties of short carbon fiber reinforced polyamide 6 composites. *Composites Part B: Engineering*, 51, 270-275.
- KATIE, M. & SCOTT, L. 2000. *ROBUST DESIGN* [Online]. Available: <https://vardeman.public.iastate.edu/IE361/s00mini/maurer.htm> [Accessed March 25 2020].
- KAYNAK, E., UREYEN, M. E. & KOPARAL, A. S. 2017. Thermal characterization and flammability of polypropylene containing sepiolite-APP combinations. 17, 341.
- KAZEMI NAJAFI, S. 2013. Use of recycled plastics in wood plastic composites – A review. *Waste Management*, 33, 1898-1905.
- KELEN, T. 1983. *Polymer degradation*.
- KHANAM, P. N. & ALMAADEED, M. A. A. 2015. Processing and characterization of polyethylene-based composites. *Advanced Manufacturing: Polymer & Composites Science*, 1, 63-79.
- KILIARIS, P. & PAPASPYRIDES, C. D. 2010. Polymer/layered silicate (clay) nanocomposites: An overview of flame retardancy. *Progress in Polymer Science*, 35, 902-958.
- KIM, H.-S., LEE, B.-H., CHOI, S.-W., KIM, S. & KIM, H.-J. 2007. The effect of types of maleic anhydride-grafted polypropylene (MAPP) on the interfacial adhesion properties of bio-flour-filled polypropylene composites. *Composites Part A: Applied Science and Manufacturing*, 38, 1473-1482.
- KONEVSKIKH, T., LUKACS, R., BL MEL, R., PONOSSOV, A. & KOHLER, A. 2016. Mie scatter corrections in single cell infrared microspectroscopy. *Faraday Discussions*, 187, 235-257.
- KRAUS, T., KHNEL, M. & WITTEN, E. 2014. Composites Market Report 2014 Market developments, trends, challenges and opportunities. *Federation of Reinforced Plastics, Frankfurt, Germany*.
- KUMAR, N., MIREJA, S., KHANDELWAL, V., ARUN, B. & MANIK,

- G. 2017. Light-weight high-strength hollow glass microspheres and bamboo fiber based hybrid polypropylene composite: A strength analysis and morphological study. *Composites Part B: Engineering*, 109, 277-285.
- KUMAR, N. R., RAO, C. H. R., SRIKANT, P. & RAO, B. R. 2015. Mechanical properties of corn fiber reinforced polypropylene composites using Taguchi method. *Materials Today: Proceedings*, 2, 3084-3092.
- KUMAR, S., PANDA, A. K. & SINGH, R. K. 2011. A review on tertiary recycling of high-density polyethylene to fuel. *Resources, Conservation and Recycling*, 55, 893-910.
- KUTZ, M. 2012. *Handbook of Environmental Degradation of Materials*, Burlington, UNITED STATES, William Andrew.
- LA MANTIA, F. P., MORREALE, M., BOTTA, L., MISTRETTA, M. C., CERAULO, M. & SCAFFARO, R. 2017. Degradation of polymer blends: A brief review. *Polymer Degradation and Stability*, 145, 79-92.
- LAPCIK JR., L., JINDROVA, P., LAPCIKOVA, B., TAMBLYN, R., GREENWOOD, R. & ROWSON, N. 2008. Effect of the talc filler content on the mechanical properties of polypropylene composites. *Journal of Applied Polymer Science*, 110, 2742-2747.
- LEE, H., OHSAWA, I. & TAKAHASHI, J. 2015. Effect of plasma surface treatment of recycled carbon fiber on carbon fiber-reinforced plastics (CFRP) interfacial properties. *Applied Surface Science*, 328, 241-246.
- LEJA, K. & LEWANDOWICZ, G. 2010. Polymer Biodegradation and Biodegradable Polymers-a Review. *Polish Journal of Environmental Studies*, 19.
- LEONG, Y. W., ABU BAKAR, M. B., ISHAK, Z. A. M., ARIFFIN, A. & PUKANSZKY, B. 2004. Comparison of the mechanical properties and interfacial interactions between talc, kaolin, and calcium carbonate filled polypropylene composites. *Journal of Applied Polymer Science*, 91, 3315-3326.
- LI, J., LUO, X. & LIN, X. 2013. Preparation and characterization of hollow glass microsphere reinforced poly(butylene succinate) composites. *Materials & Design*, 46, 902-909.
- LIANG, J.-Z. 2006. Impact fracture toughness of hollow glass bead-filled polypropylene composites. *Journal of Materials Science*, 42, 841-846.

- LIANG, J.-Z. 2007. Tensile properties of hollow glass bead-filled polypropylene composites. *Journal of Applied Polymer Science*, 104, 1697-1701.
- LIANG, J.-Z. 2014. Estimation of thermal conductivity for polypropylene/hollow glass bead composites. *Composites Part B: Engineering*, 56, 431-434.
- LIANG, J.-Z. 2017. Tensile and flexural properties of polypropylene composites filled with highly effective flame retardant magnesium hydroxide. *Polymer Testing*, 60, 110-116.
- LIANG, J. & ZHANG, Y. 2010. A study of the flame-retardant properties of polypropylene/ $\text{Al}(\text{OH})_3/\text{Mg}(\text{OH})_2$ composites. *Polymer International*, 59, 539-542.
- LIANG, J. Z. 2005. Mechanical Properties of Hollow Glass Bead-filled ABS Composites. *Journal of Thermoplastic Composite Materials*, 18, 407-416.
- LIANG, J. Z., FENG, J. Q., TSUI, C. P., TANG, C. Y., LIU, D. F., ZHANG, S. D. & HUANG, W. F. 2015a. Mechanical properties and flame-retardant of PP/MRP/ $\text{Mg}(\text{OH})_2/\text{Al}(\text{OH})_3$ composites. *Composites Part B: Engineering*, 71, 74-81.
- LIANG, J. Z., LI, B. & RUAN, J. Q. 2015b. Crystallization properties and thermal stability of polypropylene composites filled with wollastonite. *Polymer Testing*, 42, 185-191.
- LIANG, J. Z. & LI, F. H. 2006. Measurement of thermal conductivity of hollow glass-bead-filled polypropylene composites. *Polymer Testing*, 25, 527-531.
- LIANG, J. Z. & LI, F. H. 2007. Simulation of heat transfer in hollow-glass-bead-filled polypropylene composites by finite element method. *Polymer Testing*, 26, 419-424.
- LIANG, J. Z., ZHANG, Y. J. & JIANG, X. H. 2010. Heat resistant properties of PP/ $\text{Al}(\text{OH})_3/\text{Mg}(\text{OH})_2$ flame retardant composites. *Polymer Bulletin*, 66, 289-299.
- LIAO, C. Z. & TJONG, S. C. 2011. Effects of carbon nanofibers on the fracture, mechanical, and thermal properties of PP/SEBS-g-MA blends. *Polymer Engineering & Science*, 51, 948-958.
- LIN, J. H., HUANG, C. L., LIU, C. F., CHEN, C. K., LIN, Z. I. & LOU, C. W. 2015a. Polypropylene/Short Glass Fibers Composites: Effects of Coupling Agents on Mechanical Properties, Thermal Behaviors, and Morphology.

- Materials (Basel)*, 8, 8279-8291.
- LIN, J. H., PAN, Y. J., LIU, C. F., HUANG, C. L., HSIEH, C. T., CHEN, C. K., LIN, Z. I. & LOU, C. W. 2015b. Preparation and Compatibility Evaluation of Polypropylene/High Density Polyethylene Polyblends. *Materials (Basel)*, 8, 8850-8859.
- LIU, L., HU, J., ZHUO, J., JIAO, C., CHEN, X. & LI, S. 2014. Synergistic flame retardant effects between hollow glass microspheres and magnesium hydroxide in ethylene-vinyl acetate composites. *Polymer Degradation and Stability*, 104, 87-94.
- LIU, S.-P., YING, J.-R., ZHOU, X.-P., XIE, X.-L. & MAI, Y.-W. 2009. Dispersion, thermal and mechanical properties of polypropylene/magnesium hydroxide nanocomposites compatibilized by SEBS-g-MA. *Composites Science and Technology*, 69, 1873-1879.
- LIU, Y., ZHANG, X., SONG, C., ZHANG, Y., FANG, Y., YANG, B. & WANG, X. 2015. An effective surface modification of carbon fiber for improving the interfacial adhesion of polypropylene composites. *Materials & Design*, 88, 810-819.
- LOCOCK, K. 2017. *The Recycled Plastics Market: Global Analysis and Trends*. CSIRO, Australia.
- LOVIE, P. 2005. Interaction Plot. *Encyclopedia of Statistics in Behavioral Science*.
- LOVINGER, A. J. & WILLIAMS, M. 1980. Tensile properties and morphology of blends of polyethylene and polypropylene. *Journal of Applied Polymer Science*, 25, 1703-1713.
- LYU, M.-Y. & CHOI, T. G. 2015. Research trends in polymer materials for use in lightweight vehicles. *International Journal of Precision Engineering and Manufacturing*, 16, 213-220.
- MACCARRONE, S. 2018. *Daimler's approach to sustainable vehicles: recover, reuse, renew* [Online]. Available: <https://matmatch.com/blog/daimlers-approach-sustainable-vehicles-recover-reuse-renew/> [Accessed 22 March 2019].
- MADI, N. K. 2013. Thermal and mechanical properties of injection molded recycled high density polyethylene blends with virgin isotactic polypropylene. *Materials & Design*, 46, 435-441.
- MAI, K., LI, Z., QIU, Y. & ZENG, H. 2001. Mechanical properties

and fracture morphology of Al(OH)₃/polypropylene composites modified by PP grafting with acrylic acid. *Journal of Applied Polymer Science*, 80, 2617-2623.

- MBA POLYMERS. 2014. *Closing the loop on automotive plastics waste* [Online]. Available: <https://mbapolymers.com/news/news-closing-loop-automotive-plastics/> [Accessed 17 June 2019].
- MCGENITY, P. M., HOOPER, J. J., PAYNTER, C. D., RILEY, A. M., NUTBEEM, C., ELTON, N. J. & ADAMS, J. M. 1992. Nucleation and crystallization of polypropylene by mineral fillers: relationship to impact strength. *Polymer*, 33, 5215-5224.
- MCKINNON, D., BAKAS, I., HERCZEG, M., VEA, E. B., BUSCH, N., CHRISTENSEN, L. H., CHRISTENSEN, C., DAMGAARD, C. K., MILIOS, L. & PUNKKINEN, H. 2018. *Plastic Waste Markets: Overcoming barriers to better resource utilisation*, Nordic Council of Ministers.
- MCNALLY, T., BOYD, P., MCCLORY, C., BIEN, D., MOORE, I., MILLAR, B., DAVIDSON, J. & CARROLL, T. 2008. Recycled carbon fiber filled polyethylene composites. *Journal of Applied Polymer Science*, 107, 2015-2021.
- MEHAT, N. M. & KAMARUDDIN, S. 2011. Optimization of mechanical properties of recycled plastic products via optimal processing parameters using the Taguchi method. *Journal of Materials Processing Technology*, 211, 1989-1994.
- MENDES, A. A., CUNHA, A. M. & BERNARDO, C. A. 2011. Study of the degradation mechanisms of polyethylene during reprocessing. *Polymer Degradation and Stability*, 96, 1125-1133.
- MENG, F., MCKECHNIE, J. & PICKERING, S. J. 2018. An assessment of financial viability of recycled carbon fibre in automotive applications. *Composites Part A: Applied Science and Manufacturing*, 109, 207-220.
- MENG, F., MCKECHNIE, J., TURNER, T., WONG, K. H. & PICKERING, S. J. 2017. Environmental Aspects of Use of Recycled Carbon Fiber Composites in Automotive Applications. *Environmental Science & Technology*, 51, 12727-12736.
- MINISTRY OF COMMERCE P.R.C. 2018. The development of renewable resources recycling industry in China (2018).
- MINITAB.COM. 2019a. *Catalogue of Taguchi designs* [Online].

Available: <https://support.minitab.com/en-us/minitab/18/help-and-how-to/modeling-statistics/doe/supporting-topics/taguchi-designs/catalogue-of-taguchi-designs/> [Accessed 20 March 2019].

MINITAB.COM. 2019b. *What is the signal-to-noise ratio in a Taguchi design?* [Online]. Available: <https://support.minitab.com/en-us/minitab/18/help-and-how-to/modeling-statistics/doe/supporting-topics/taguchi-designs/what-is-the-signal-to-noise-ratio/> [Accessed 20 March 2019].

MITTE. 2018. *The truth about recycling plastic* [Online]. Available: <https://mitte.co/2018/07/18/truth-recycling-plastic/> [Accessed 11 September 2019].

MONTI, M., SCRIVANI, M. T. & GIANOTTI, V. 2020. Effect of SEBS and OBC on the Impact Strength of Recycled Polypropylene/Talc Composites. *Recycling*, 5, 9.

MOURAD, A.-H., AKKAD, R., SOLIMAN, A. & MADKOUR, T. 2009. Characterisation of thermally treated and untreated polyethylene-polypropylene blends using DSC, TGA and IR techniques. *Plastics, Rubber and Composites*, 38, 265-278.

MOURAD, A.-H. I. 2010. Thermo-mechanical characteristics of thermally aged polyethylene/polypropylene blends. *Materials & Design*, 31, 918-929.

MRAZ, S. 2018. *Carbon Fiber Composite Market to Hit \$31 Billion by 2024* [Online]. Available: <https://www.machinedesign.com/materials/article/21836686/carbon-fiber-composite-market-to-hit-31-billion-by-2024> [Accessed 23 March 2020].

NASIR, A., YASIN, T. & ISLAM, A. 2011. Thermo-oxidative degradation behavior of recycled polypropylene. *Journal of Applied Polymer Science*, 119, 3315-3320.

NEKHLAOU, S., ESSABIR, H., KUNAL, D., SONAKSHI, M., BENSALAH, M. O., BOUHFID, R. & QAISS, A. 2015. Comparative study for the talc and two kinds of moroccan clay as reinforcements in polypropylene-SEBS-g-MA matrix. *Polymer Composites*, 36, 675-684.

NIST. 2012a. *Engineering statistics handbook* [Online]. Available: <https://www.itl.nist.gov/div898/handbook/pri/section3/pri333.htm> [Accessed 25 March 2020].

- NIST. 2012b. *Multi-factor Analysis of Variance* [Online]. Available: <https://www.itl.nist.gov/div898/handbook/eda/section3/eda355.htm> [Accessed 25 March 2020].
- OICA. 2018. *2018 Production statistics* [Online]. Available: <http://www.oica.net/category/production-statistics/2018-statistics/> [Accessed 22 March 2019].
- OKTEM, H., ERZURUMLU, T. & UZMAN, I. 2007. Application of Taguchi optimization technique in determining plastic injection molding process parameters for a thin-shell part. *Materials & Design*, 28, 1271-1278.
- OZCELIK, B. 2011. Optimization of injection parameters for mechanical properties of specimens with weld line of polypropylene using Taguchi method. *International Communications in Heat and Mass Transfer*, 38, 1067-1072.
- PAPADOPOULOU, C. P. & KALFOGLOU, N. K. 2000. Comparison of compatibilizer effectiveness for PET/PP blends: their mechanical, thermal and morphology characterization. *Polymer*, 41, 2543-2555.
- PARIDA, A. K., ROUTARA, B. C. & BHUYAN, R. K. 2015. Surface roughness model and parametric optimization in machining of GFRP composite: Taguchi and Response surface methodology approach. *Materials Today: Proceedings*, 2, 3065-3074.
- PATIL, A., PATEL, A. & PUROHIT, R. 2017. An overview of Polymeric Materials for Automotive Applications. *Materials Today: Proceedings*, 4, 3807-3815.
- PEARSON, K. 1901. LIII. On lines and planes of closest fit to systems of points in space. *The London, Edinburgh, and Dublin Philosophical Magazine and Journal of Science*, 2, 559-572.
- PICKERING, S. J. 2006. Recycling technologies for thermoset composite materials—current status. *Composites Part A: Applied Science and Manufacturing*, 37, 1206-1215.
- PIMENTA, S. & PINHO, S. T. 2011. Recycling carbon fibre reinforced polymers for structural applications: Technology review and market outlook. *Waste Management*, 31, 378-392.
- PLASTICSEUROPE 2013. *Automotive-The world moves with plastics*. Brussels, Belgium: PlasticsEurope.
- PLASTICSEUROPE 2018. *Plastics-the facts 2018*. Brussels,

Belgium: PlasticsEurope.

- PLASTICSTODAY. 2015. *Plastics use in vehicles to grow 75% by 2020, says industry watcher* [Online]. Available: <https://www.plasticstoday.com/automotive-and-mobility/plastics-use-vehicles-grow-75-2020-says-industry-watcher/63791493722019> [Accessed 22 March 2019].
- PLAWKY, U., SCHLABS, M. & WENIG, W. 1996. The role of styrene-ethylene/butylene-styrene triblock copolymer as impact modifier in polypropylene-polyethylene blends. *Journal of Applied Polymer Science*, 59, 1891-1896.
- POLYMER PROPERTIES DATABASE. n.d.-a. *DEPOLYMERIZATION* [Online]. Available: <http://polymerdatabase.com/polymer%20chemistry/Depolymerization.html> [Accessed 20 August 2020].
- POLYMER PROPERTIES DATABASE. n.d.-b. *MELTING POINTS OF POLYMERS* [Online]. Available: <http://polymerdatabase.com/polymer%20physics/Polym er%20Tm%20C.html> [Accessed 20 August 2020].
- POLYMER PROPERTIES DATABASE. n.d.-c. *PHOTODEGRADATION OF POLYMERS* [Online]. Available: <http://polymerdatabase.com/polymer%20chemistry/Photo%20Oxidation.html> [Accessed 12 March 2021].
- POWER PLASTIC RECYCLING. N.A. *13 high performance plastics used in the automotive industry* [Online]. Available: <https://powerplasticrecycling.com/high-performance-plastics-used-in-the-automotive-industry/> [Accessed 17 March 2021].
- PRADEEP, S. A., IYER, R. K., KAZAN, H. & PILLA, S. 2017. Automotive Applications of Plastics: Past, Present, and Future. 651-673.
- PREMALAL, H. G. B., ISMAIL, H. & BAHARIN, A. 2002. Comparison of the mechanical properties of rice husk powder filled polypropylene composites with talc filled polypropylene composites. *Polymer Testing*, 21, 833-839.
- QIAN, S., IGARASHI, T. & NITTA, K.-H. 2011. Thermal degradation behavior of polypropylene in the melt state: molecular weight distribution changes and chain scission mechanism. *Polymer Bulletin*, 67, 1661-1670.
- QIU, W., ENDO, T. & HIROTSU, T. 2006. Structure and properties of composites of highly crystalline cellulose with polypropylene: Effects of polypropylene molecular

- weight. *European Polymer Journal*, 42, 1059-1068.
- QIU, W., ZHANG, F., ENDO, T. & HIROTSU, T. 2003. Preparation and characteristics of composites of high-crystalline cellulose with polypropylene: Effects of maleated polypropylene and cellulose content. *Journal of Applied Polymer Science*, 87, 337-345.
- RABELLO, M. S. & WHITE, J. R. 1996. Photodegradation of talc-filled polypropylene. *Polymer Composites*, 17, 691-704.
- RAJANDAS, H., PARIMANNAN, S., SATHASIVAM, K., RAVICHANDRAN, M. & SU YIN, L. 2012. A novel FTIR-ATR spectroscopy based technique for the estimation of low-density polyethylene biodegradation. *Polymer Testing*, 31, 1094-1099.
- RAMAZANI, S. A. A., RAHIMI, A., FROUNCHI, M. & RADMAN, S. 2008. Investigation of flame retardancy and physical-mechanical properties of zinc borate and aluminum hydroxide propylene composites. *Materials & Design*, 29, 1051-1056.
- RAVI KUMAR, N., SRIKANT, P., RANGA RAO, C. H. & MEERA SAHEB, K. 2017. Statistical analysis of mechanical properties of vakka fiber reinforced polypropylene composites using Taguchi method. *Materials Today: Proceedings*, 4, 3361-3370.
- RECYCLING TODAY. 2017. *Recycled plastics make inroads in automotive applications* [Online]. Available: <https://www.recyclingtoday.com/article/recycled-plastics-make-inroads-in-automotive-applications/> [Accessed 15 May 2020].
- REN, X., WANG, X. Q., SUI, G., ZHONG, W. H., FUQUA, M. A. & ULVEN, C. A. 2008. Effects of carbon nanofibers on crystalline structures and properties of ultrahigh molecular weight polyethylene blend fabricated using twin-screw extrusion. *Journal of Applied Polymer Science*, 107, 2837-2845.
- ROBESON, L. M. 2007. Polymer blends. *A Comprehensive Review*.
- ROSA, J. L., ROBIN, A., SILVA, M. B., BALDAN, C. A. & PERES, M. P. 2009. Electrodeposition of copper on titanium wires: Taguchi experimental design approach. *Journal of Materials Processing Technology*, 209, 1181-1188.
- ROY, D. & GUPTA, B. R. 1993. Rheological behavior of short carbon fiber-filled thermoplastic elastomer based on

- styrene–isoprene–styrene block copolymer. *Journal of Applied Polymer Science*, 49, 1475-1482.
- RYDZ, J., SIKORSKA, W., KYULAVSKA, M. & CHRISTOVA, D. 2015. Polyester-Based (Bio)degradable Polymers as Environmentally Friendly Materials for Sustainable Development. *International Journal of Molecular Sciences*, 16, 564-596.
- SADAT-SHOJAI, M. & BAKHSHANDEH, G.-R. 2011. Recycling of PVC wastes. *Polymer Degradation and Stability*, 96, 404-415.
- ŞAHIN, Y., SAHIN, S. & İNAL, M. 2018. Modelling of the Tensile Properties of Calcium Carbonate Filled Polypropylene Composite Materials with Taguchi and Artificial Neural Networks. *IFAC-PapersOnLine*, 51, 282-286.
- SAMPERI, F., PUGLISI, C., ALICATA, R. & MONTAUDO, G. 2004. Thermal degradation of poly(ethylene terephthalate) at the processing temperature. *Polymer Degradation and Stability*, 83, 3-10.
- SANTOS, A. S. F., AGNELLI, J. A. M., TREVISAN, D. W. & MANRICH, S. 2002. Degradation and stabilization of polyolefins from municipal plastic waste during multiple extrusions under different reprocessing conditions. *Polymer Degradation and Stability*, 77, 441-447.
- SATTLER, S. 2019. *Can luxury be sustainable?* [Online]. Available: <https://www.daimler.com/magazine/sustainability/mercedes-environmental-protection-luxury-sustainable.html> [Accessed 23 May 2020].
- SCHIRP, A. & SU, S. 2016. Effectiveness of pre-treated wood particles and halogen-free flame retardants used in wood-plastic composites. *Polymer Degradation and Stability*, 126, 81-92.
- SCHMIDT, E. 2018. *Manufacturing Electric Vehicles with Recycled Materials* [Online]. Available: <https://www.fleetcarma.com/manufacturing-electric-vehicles-recycled-materials/> [Accessed 20 May 2020].
- SCIENCEDAILY. 2018. *Cheap, small carbon nanotubes* [Online]. Available: <https://www.sciencedaily.com/releases/2018/05/180523160148.htm> [Accessed 23 May 2020].
- SCOTT, G. 2000. 'Green' polymers. *Polymer Degradation and Stability*, 68, 1-7.

- SHAH, A. A., HASAN, F., HAMEED, A. & AHMED, S. 2008. Biological degradation of plastics: A comprehensive review. *Biotechnology Advances*, 26, 246-265.
- SHAH, A. U. R., LEE, D.-W., WANG, Y.-Q., WASY, A., HAM, K. C., JAYARAMAN, K., KIM, B.-S. & SONG, J.-I. 2014. Effect of concentration of ATH on mechanical properties of polypropylene/aluminium trihydrate (PP/ATH) composite. *Transactions of Nonferrous Metals Society of China*, 24, s81-s89.
- SHAH, D. & J. SCHUBEL, P. 2015. *On recycled carbon fibre composites manufactured through a liquid composite moulding process*.
- SHAMA RAO, N., SIMHA, T., RAO, K. & RAVI KUMAR, G. 2015. Carbon composites are becoming competitive and cost effective.
- SHANKS, R. A., LI, J. & YU, L. 2000. Polypropylene-polyethylene blend morphology controlled by time-temperature-miscibility. *Polymer*, 41, 2133-2139.
- SHAW, M. T. & TUMINELLO, W. H. 1994. A closer look at the MWD-viscosity transform. *Polymer Engineering & Science*, 34, 159-165.
- SHAZED, M. A., SURAYA, A. R., RAHMANIAN, S. & MOHD SALLEH, M. A. 2014. Effect of fibre coating and geometry on the tensile properties of hybrid carbon nanotube coated carbon fibre reinforced composite. *Materials & Design (1980-2015)*, 54, 660-669.
- SHIMADZU. 2017. *Measuring Polyethylene (PE)-Polypropylene (PP) Blend Samples* [Online]. Available: <https://www.ssi.shimadzu.com/sites/ssi.shimadzu.com/files/Industry/Literature/T153-Measuring-Polyethylene-PE-Polypropylene-PP-Blend-Samples.pdf> [Accessed 17 March 2021].
- SIDDIQUE, R., KHATIB, J. & KAUR, I. 2008. Use of recycled plastic in concrete: A review. *Waste Management*, 28, 1835-1852.
- SIMS, G. D. & BROUGHTON, W. R. 2000. 2.05 - Glass Fiber Reinforced Plastics—Properties. In: KELLY, A. & ZWEBEN, C. (eds.) *Comprehensive Composite Materials*. Oxford: Pergamon.
- SINGH, B. & SHARMA, N. 2008. Mechanistic implications of plastic degradation. *Polymer Degradation and Stability*, 93, 561-584.

- SINGH, N., HUI, D., SINGH, R., AHUJA, I. P. S., FEO, L. & FRATERNALI, F. 2017. Recycling of plastic solid waste: A state of art review and future applications. *Composites Part B: Engineering*, 115, 409-422.
- SLĂTINEANU, L., STORM, B. K., NAGIT, G., DODUN, O., MERTICARU, V., COTEATA, M., RIPANU, M. I., MIHALACHE, A. M., BOCA, M., IBANESCU, R., PANAIT, C. E., OANCEA, G. & KYRATSI, P. 2017. Production of recyclates – compared with virgin Plastics – a LCA Study. *MATEC Web of Conferences*, 112, 04024.
- SOCALINGAME, L., PERRIN, D., B N ZET, J. C., MANI, S., COIFFIER, F., RICHAUD, E. & BERGERET, A. 2015. Reprocessing of artificial UV-weathered wood flour reinforced polypropylene composites. *Polymer Degradation and Stability*, 120, 313-327.
- SONG, D., GAO, J., LI, X. & LU, L. 2014. Evaluation of aging behavior of polypropylene in natural environment by principal component analysis. *Polymer Testing*, 33, 131-137.
- SONG, Y.-M., WANG, Q.-W., HAN, G.-P., WANG, H.-G. & GAO, H. 2010. Effects of two modification methods on the mechanical properties of wood flour/recycled plastic blends composites: addition of thermoplastic elastomer SEBS-g-MAH and in-situ grafting MAH. *Journal of Forestry Research*, 21, 373-378.
- SPI. 2016. *Automotive recycling devalued is now revalued* [Online]. The Plastics Industry Trade Association Available: <https://www.plasticsindustry.org/sites/default/files/2016-03256-SPI-PMW-Auto-Recycle-web.pdf> [Accessed 16 June 2019].
- STR MBERG, E. & KARLSSON, S. 2009. The effect of biodegradation on surface and bulk property changes of polypropylene, recycled polypropylene and polylactide biocomposites. *International Biodeterioration & Biodegradation*, 63, 1045-1053.
- STRAIN, I. N., WU, Q., POURRAHIMI, A. M., HEDENQVIST, M. S., OLSSON, R. T. & ANDERSSON, R. L. 2015. Electrospinning of recycled PET to generate tough mesomorphic fibre membranes for smoke filtration. *Journal of Materials Chemistry A*, 3, 1632-1640.
- STRAPASSON, R., AMICO, S. C., PEREIRA, M. F. R. & SYDENSTRICKER, T. H. D. 2005. Tensile and impact

- behavior of polypropylene/low density polyethylene blends. *Polymer Testing*, 24, 468-473.
- STRICKER, F., BRUCH, M. & M LHAUPT, R. 1997. Mechanical and thermal properties of syndiotactic polypropene filled with glass beads and talcum. *Polymer*, 38, 5347-5353.
- SU, Z., JIANG, P., LI, Q., WEI, P. & ZHANG, Y. 2005. Toughening of polypropylene highly filled with aluminum hydroxide. *Polymers and Polymer Composites*, 13, 139-150.
- SUBRAMANIAN, P. M. 2000. Plastics recycling and waste management in the US. *Resources, Conservation and Recycling*, 28, 253-263.
- TAGUCHI, G., CHOWDHURY, S. & WU, Y. 2007. Quality Engineering: The Taguchi Method. *Taguchi's Quality Engineering Handbook*.
- TAI, C. M., LI, R. K. Y. & NG, C. N. 2000. Impact behaviour of polypropylene/polyethylene blends. *Polymer Testing*, 19, 143-154.
- TAN, J. K., KITANO, T. & HATAKEYAMA, T. 1990. Crystallization of carbon fibre reinforced polypropylene. *Journal of Materials Science*, 25, 3380-3384.
- THOMASON, J. L. 2002. The influence of fibre length and concentration on the properties of glass fibre reinforced polypropylene: 5. Injection moulded long and short fibre PP. *Composites Part A: Applied Science and Manufacturing*, 33, 1641-1652.
- THOMASON, J. L. & VLUG, M. A. 1997. Influence of fibre length and concentration on the properties of glass fibre-reinforced polypropylene: 4. Impact properties. *Composites Part A: Applied Science and Manufacturing*, 28, 277-288.
- TJONG, S. C., BAO, S. P. & LIANG, G. D. 2005. Polypropylene/montmorillonite nanocomposites toughened with SEBS-g-MA: Structure-property relationship. *Journal of Polymer Science Part B: Polymer Physics*, 43, 3112-3126.
- UNTERWEGER, C., DUCHOSLAV, J., STIFTER, D. & F RST, C. 2015. Characterization of carbon fiber surfaces and their impact on the mechanical properties of short carbon fiber reinforced polypropylene composites. *Composites Science and Technology*, 108, 41-47.
- UTRACKI, L. A. 1999. Polymer blends: fundamentals. In: KARGER-KOCSIS, J. (ed.) *Polypropylene: An A-Z*

reference. Dordrecht: Springer Netherlands.

- VALENTE, M., SARASINI, F., MARRA, F., TIRILL, J. & PULCI, G. 2011. Hybrid recycled glass fiber/wood flour thermoplastic composites: Manufacturing and mechanical characterization. *Composites Part A: Applied Science and Manufacturing*, 42, 649-657.
- VARSAVAS, S. D. & KAYNAK, C. 2018. Effects of glass fiber reinforcement and thermoplastic elastomer blending on the mechanical performance of polylactide. *Composites Communications*, 8, 24-30.
- VEEJAY PLASTIC. 2016. *Top 3 High-Performance Plastics Used in Auto Manufacturing* [Online]. Available: <http://www.veejayplastic.com/blog/top-3-high-performance-plastics-used-in-auto-manufacturing/> [Accessed 11 September 2019].
- VELIS, C. 2014. Plastic waste: A story for one player – China. . Vienna: International Solid Waste Association.
- VERMA, S., BALASUBRAMANIAM, B. & GUPTA, R. K. 2018. Recycling, reclamation and re-manufacturing of carbon fibres. *Current Opinion in Green and Sustainable Chemistry*, 13, 86-90.
- VOLKSWAGEN. 2019. *Recycling* [Online]. Available: <https://www.volkswagenag.com/en/sustainability/environment/recycling.html#> [Accessed 22 March 2019].
- VOLVO. 2018. *Volvo Cars aims for 25 per cent recycled plastics in every new car from 2025* [Online]. Available: <https://www.media.volvocars.com/global/en-gb/media/pressreleases/230703/volvo-cars-aims-for-25-per-cent-recycled-plastics-in-every-new-car-from-2025> [Accessed 22 March 2019].
- WALDMAN, W. R. & DE PAOLI, M.-A. 2008. Photodegradation of polypropylene/polystyrene blends: Styrene-butadiene-styrene compatibilisation effect. *Polymer Degradation and Stability*, 93, 273-280.
- WAMBUA, P., IVENS, J. & VERPOEST, I. 2003. Natural fibres: can they replace glass in fibre reinforced plastics? *Composites Science and Technology*, 63, 1259-1264.
- WANG, K., ADDIEGO, F., BAHLOULI, N., AHZI, S., R MOND, Y. & TONIAZZO, V. 2014. Impact response of recycled polypropylene-based composites under a wide range of temperature: Effect of filler content and recycling. *Composites Science and Technology*, 95, 89-99.

- WANG, K., BAHLOULI, N., ADDIEGO, F., AHZI, S., R MOND, Y., RUCH, D. & MULLER, R. 2013. Effect of talc content on the degradation of re-extruded polypropylene/talc composites. *Polymer Degradation and Stability*, 98, 1275-1286.
- WANG, T., CHEN, S., WANG, Q. & PEI, X. 2010. Damping analysis of polyurethane/epoxy graft interpenetrating polymer network composites filled with short carbon fiber and micro hollow glass bead. *Materials & Design*, 31, 3810-3815.
- WEON, J. I. & SUE, H. J. 2006. Mechanical properties of talc- and CaCO₃-reinforced high-crystallinity polypropylene composites. *Journal of Materials Science*, 41, 2291-2300.
- WITIK, R. A., TEUSCHER, R., MICHAUD, V., LUDWIG, C. & M NSON, J.-A. E. 2013. Carbon fibre reinforced composite waste: An environmental assessment of recycling, energy recovery and landfilling. *Composites Part A: Applied Science and Manufacturing*, 49, 89-99.
- WONG, K. H., SYED MOHAMMED, D., PICKERING, S. J. & BROOKS, R. 2012. Effect of coupling agents on reinforcing potential of recycled carbon fibre for polypropylene composite. *Composites Science and Technology*, 72, 835-844.
- WRAP. 2010. China market sentiment survey.
- WRAP. 2014. *End market applications for household polyethylene film pellets* [Online]. Available: <https://wrap.org.uk/resources/report/end-markets-recycled-household-plastic-film> [Accessed 17 March 2021].
- WRAP 2016. Plastics market situation report.
- XIAO, B., ZAIMA, T., SHINDO, K., KOHIRA, T., MORISAWA, J., WAN, Y., YIN, G., OHSAWA, I. & TAKAHASHI, J. 2019. Characterization and elastic property modeling of discontinuous carbon fiber reinforced thermoplastics prepared by a carding and stretching system using treated carbon fibers. *Composites Part A: Applied Science and Manufacturing*, 126, 105598.
- XIAO, S., DONG, H., GENG, Y. & BRANDER, M. 2018. An overview of China's recyclable waste recycling and recommendations for integrated solutions. *Resources, Conservation and Recycling*, 134, 112-120.
- YAN, X., IMAI, Y., SHIMAMOTO, D. & HOTTA, Y. 2014.

Relationship study between crystal structure and thermal/mechanical properties of polyamide 6 reinforced and unreinforced by carbon fiber from macro and local view. *Polymer*, 55, 6186-6194.

- YANG, M., WANG, K., YE, L., MAI, Y.-W. & WU, J. 2003. Low density polyethylene-polypropylene blends: Part 1- Ductility and tensile properties. *Plastics, rubber and composites*, 32, 21-26.
- YANG, W. H. & TARNG, Y. S. 1998. Design optimization of cutting parameters for turning operations based on the Taguchi method. *Journal of Materials Processing Technology*, 84, 122-129.
- YOUNESI, M. & BAHROLOLOOM, M. E. 2009. Producing toughened PP/HA-LLDPE ternary bio-composite using a two-step blending method. *Materials & Design*, 30, 4253-4259.
- YOUSIF, E. & HADDAD, R. 2013a. Photodegradation and photostabilization of polymers, especially polystyrene. *SpringerPlus*, 2, 398.
- YOUSIF, E. & HADDAD, R. 2013b. Photodegradation and photostabilization of polymers, especially polystyrene: review. *SpringerPlus*, 2, 398-398.
- YU, J., SUN, L., MA, C., QIAO, Y. & YAO, H. 2016. Thermal degradation of PVC: A review. *Waste Management*, 48, 300-314.
- ZEUS. 2005. *Thermal Degradation of Plastics* [Online]. Available: http://www.appstate.edu/~clementsjs/polymerproperties/zeus_thermal_degradation.pdf [Accessed 15 August 2019].
- ZHENG, Y., GU, F., REN, Y., HALL, P. & MILES, N. J. 2017. Improving Mechanical Properties of Recycled Polypropylene-based Composites Using TAGuchi and ANOVA Techniques. *Procedia CIRP*, 61, 287-292.
- ZHOU, Z., TANG, Y., DONG, J., CHI, Y., NI, M., LI, N. & ZHANG, Y. 2018. Environmental performance evolution of municipal solid waste management by life cycle assessment in Hangzhou, China. *Journal of Environmental Management*, 227, 23-33.
- ZHU, Y. D., ALLEN, G. C., JONES, P. G., ADAMS, J. M., GITTINS, D. I., HEARD, P. J. & SKUSE, D. R. 2014. Dispersion characterisation of CaCO₃ particles in PP/CaCO₃

composites. *Composites Part A: Applied Science and Manufacturing*, 60, 38-43.

ZUIDERDUIN, W. C. J., WESTZAAN, C., HU TINK, J. & GAYMANS, R. J. 2003. Toughening of polypropylene with calcium carbonate particles. *Polymer*, 44, 261-275.